Synthesis and Structural Studies of a Dimeric Bis(oxamate) Copper(II) Complex

Marta Martinez Belmonte

Submitted in fulfilment of the requirements for the Degree of Doctor of Philosophy

Department of Chemistry
Faculty of Sciences
University of Glasgow

September 2009

For my parents and my sister

Without your love and unconditional support
I would had never arrived to the end of this trip

Abstract

A new series of a dimeric bis(oxamato) copper(II) complex of formula $M_4[Cu(oeo)]_2$ (where $Et_2H_2(oeo)$ is diethyl ethylene-1,2-dioxamate and M = alkali metal) is described. The complex is formed by two copper(II) atoms and two ligand molecules of which each oxamato group is coordinating towards two different copper(II) ions leading to a distorted square planar environment. Due to the *trans*-bis(*N*,*O*) arrangement around the copper(II) ion, the dimer displays a helicoidal structure.

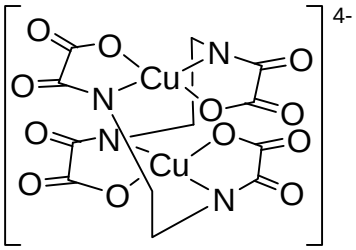

We present here detailed structural studies of this complex with a number of counter ions. Many polymorphs and hydrates are observed and their synthesis and structures are described.

A sequential strategy has been developed in which starting from the ligand precursor, Et_2H_2oeo, the addition of alkali metal hydroxides affords the hydrolysis of the ester leading to the formation of the salt of the ester, M_2H_2oeo. Then, transmetallation of the alkali metal salt is carried out with the addition of a copper(II) salt. The dimeric copper(II) complex, $M_4[Cu(oeo)]_2$, is finally achieved with the addition of the corresponding alkali metal hydroxide. Structural studies of the intermediate compounds are also described.

The partial occupancy in the copper(II) site is a common feature in $M_4[Cu(oeo)]_2$. Surprisingly, the copper(II) site can be left vacant and the compound still remain with the same helicoidal structure as the non-coordinated ligand, when the amide is protonated, adopting a structurally similar H-bond arrangement. A wide range of copper(II) occupancies have been observed in the different obtained compounds: from compounds with a fully occupied site to compounds with only 10% of copper(II)

present in the complex . These differences in the amount of copper(II) present in the complex has consequences in its packing in the crystal structure.

The synthesis and characterisation of the copper(II) complex using tetrabutylammonium hydroxide as the counterion is also reported. As a result of the bulky nature of the cation, the mononuclear structure is observed, $(n\text{-}Bu_4N)_4[Cu(oeoH)_2]$. Initial transmetallation reactions are reported with Co(II), in which partial and complete exchange from Cu(II) is observed.

Contents

Accompanying material: CIF files of the obtained crystal structures

Acknowledgments

I would specially like to thank my parents and my sister for their love, for their guidance and unconditional support over my time in Glasgow; for believing in me and giving me the strength to continue all the way until achieving this. Without them, this work would had never been written. I would also like to thank my aunt Silvia, for being such a good listener and adviser.

I would also like to thank my supervisor, Dr. Daniel J. Price, for having given me the opportunity to work with him. He introduced me into the fascinating world of Crystallography and made me realise what I really enjoy working on.

I am in debt to Dr. Mark Murrie and his entire group, Stoff, Kyle, Pascal and Alan. Firstly, for allowing me to use his chemicals and equipment. Secondly, for keeping me company in the lab and in the research office; and finally, for listening, helping and giving me advise during all my research.

I would also like to thank the people of the Chemistry department, Dr. Andy Parkin, Prof. Chick Wilson and Mark Schmidtmann; as well as all the technical support, especially Jim Gallagher and Kim Wilson.

I would also like to thank all the people who have kept me company in the glaswegian rainy days and made me enjoy this city, specially Martina, Pau, Gavin, Sergio, Pedro and many, many more. Particularly, I would like to thank my two flatmates Olaya and Martí, who always made feel like at home.

I would also like to thank Louis, my friend and love. He has made the writing of this thesis easier than expected; with his love, his support and his common sense he has helped me to not get crazy over this time.

I will always be grateful to all my hometown friends. Even being so far away, they have always given me their friendship and their love; specially Ariadna and Laura, who helped me in the most difficult times.

And finally, I also want to name in my friend Mireia. So many things to say and so many changes after that. I have never been the same person. She gave me the strength and the courage to leave and go to Glasgow. Without her, it would have never happened.

Author’s declaration

The work contained in this thesis, submitted for the Degree of Doctor of Philosophy, is my original work except where referenced to others. No materials within have been previously submitted for a degree at this or any other university.

Abbreviations

Å - angstrom

^{o}C - degrees centigrade

CI - chemical ionization

d - doublet

DMSO - dimethylsulphoxide

EI - electron impact

equiv - equivalents

Et - ethyl

EtOH - ethanol

FAB - fast atom bombardment

hrs - hours

Hz - hertz

IR - infrared

m - multiplet

Me - methyl

MeOH - methanol

min - minutes

NMR - nuclear magnetic resonance

ox - oxalate

q - quartet

RT - room temperature

s - singlet

t - triplet

w - wide

Experimental

Chemicals

All starting compounds were obtained from commercial sources and used without purification. Solvent for all synthetic operations and all crystal growing techniques were used from commercial sources, except water which was purified from running water of the chemistry department of University of Glasgow.

Physical Measurements

^{1}H and ^{13}C NMR spectra were recorded on a Bruker DPX/400 spectrometer operating at 400 and 100 MHz respectively. All coupling constants are measured in Hz. Mass spectra (MS) were recorded on a Jeol JMS700 (MStation) spectrometer. Infra-red (IR) measurements were recorded on a Jasco FT/IR-4100 equipped with a Pike Technologies MIRacle ATR, unless otherwise stated. Electronic spectra were recorded on a Shimadzu UV-3101PC. When the compound was solid, samples were dispersed in a KBr disk. A baseline correction has been applied to the absorption spectrum. Elemental analyses were performed by the Microanalytical service of the University of Glasgow. Scanning Electron Microscopy (SEM) associated with energy dispersive X-ray spectroscopy (EDX) was performed on FEI (Philips) XL30 ESEM (Environmental Scanning Electron Microscope). Powder diffraction analyses were performed using a Siemens D5000 instrument operating with a Cu*K*α X-ray tube. Samples were prepared by compaction into a Si sample holder.

Crystallographic Data Collection and Structure Determination

Single-crystal collections were performed on a Bruker APEX II CCD Diffractometer by using graphite-monochromated Mo-Kα radiation (λ = 0.71073 Å) at 100(2)K and an Oxford Cryosystems low temperature device, unless otherwise stated. All crystals were of suitable dimensions and mounted on glass fibres or cotton glass.

Unless otherwise stated, all structures were solved using Direct Methods[1] and refined by full-matrix least-squares technique on F^2,[2] in the WinGX environment.[3] Graphical manipulations were carried out with Diamond.[4]

[1] G.M. Sheldrick, *Acta Crystagraphr., Sect. A*, **1990**, *46*, 467; A. Altomare, G. Cascarano, C. Giacovazzo, A. Guagliardi, *J. Appl. Crystallogr*. **1993**, *26*, 343-350.
[2] G. M. Sheldrick, SHELX97, Programs for Crystal Structure Analysis (Release 97-2), University of Göttingen, Germany, 1998.
[3] L. J. Farrugia, *J. Appl. Cryst*., **1999**, *32*, 837
[4] Brandenburg, K. (2005). DIAMOND, Version 3.1, Crystal Impact GbR, Bonn, Germany.

Chapter 1: Introduction

1. 1 Molecular-based Magnets

"Molecular Magnetism is a relatively recent scientific field which originated from the transformation of Magnetochemistry in an interdisciplinary area, where chemists and physicists started to collaborate very closely with the stated goal of designing, synthesizing, and characterising the magnetic properties of molecular based materials".[1] This area of research owes its common frontiers with supramolecular chemistry, theoretical chemistry and physics, material sciences and molecular electronics.

The first molecular-based magnets were discovered in 1986 when both Kahn and Miller groups found that some materials could exhibit spontaneous magnetization (the appearance of an ordered spin state) below a critical temperature, *Tc*, in ferromagnetic or ferrimagentic compounds.[2,3,4,5] The Kahn group reported the first molecular ferrimagnet based on copper(II)-manganese(II) derivatives whereas the Miller group described the first molecular ferromagnets containing organic building blocks (Scheme 1.1). Since then, the field of molecular magnetism has emerged as a novel area in research and has developed a great deal, thanks in large part to the use of heterobimetalic systems.[6]

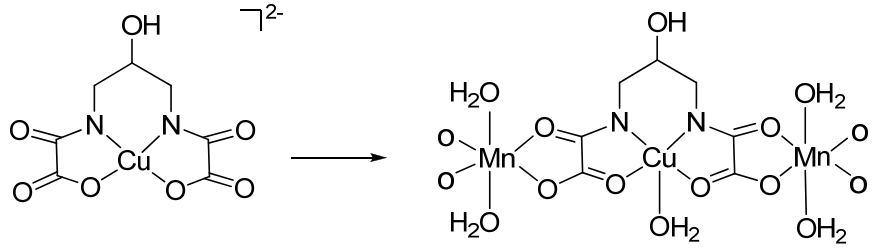

[Cu(pbaOH)]$^{2-}$ Mn[Cu(pbaOH)]

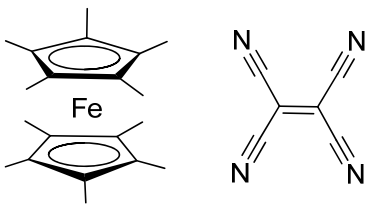

$[Fe(C_5Me_5)_2)]^{\cdot+}$ $[TCNE]^{\cdot-}$

Scheme 1. 1 At top copper(II)-manganese(II) derivatives molecular ferrimagnets and at the bottom the first molecular ferromagnets TCNE = tetracyanoethylene.

The main goal of the synthesis molecular-based magnets is the rational design of new materials with predictable magnetic properties, specifically spontaneous magnetisation below a critical temperature, *Tc* or Curie temperature. Then, for a given family of compounds, the shift of the *Tc* towards higher temperatures is desired. This requires increasing interactions between spin carriers along three directions of the space as magnetic ordering is most generally a three-dimensional phenomenon. Moreover, the increase of both coercive field (the intensity of the applied magnetic field needed to bring the magnetisation of the material to zero after the saturation of the magnetisation) and remnant magnetization (the magnetisation left after the external field has been removed) for the given family of compounds is also desired. These features could provide a memory effect to the magnetic materials and for this to happen it seems necessary to use spin carriers presenting a large magnetic anisotropy in which the magnetic moments of the material will align its magnetic moments to an energetically favourable direction (easy axis). Finally, the study of other physical properties such as the optical properties or the processability is also desired.[7]

The type of approach in which the magnetic properties of a family of compounds are studied was initially carried out by Kahn's group who designed series of oxamato-bridged $M^{II}Cu^{II}$ complexes using different types of ligands. A series of oxamato-bridged $M^{II}Cu^{II}$ chains (M = Mn, Fe, Co and Ni) were prepared from mononuclear copper(II) complex $[Cu(pbaOH)]^{2-}$ [H_4pbaOH = *N, N'*-2-hydroxy-1,3-propylenebis(oxamid acid)] (Figure 1.1). Some members of these series show long range 3D ferromagnetic order of the ferromagnetic chains (*Tc* = 4.6 - 9.5 K) while others can order antiferromagentically (T_N = 2.4 - 3.4K) depending on the nature of the interchain hydrogen bonds involving crystallisation water molecules.[8] This shows how subtle differences in the crystal packing of the chains can influence in the 3D magnetic behaviour and it also points out the limitations to obtain 1D molecule-based magnets due to the difficulty to control the interchain interactions.

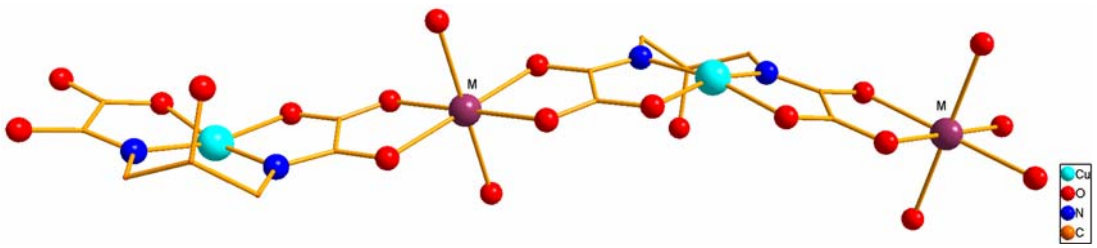

Figure 1. 1 View of the heterobimetallic $M^{II}Cu^{II}$ chain using the $Cu(opbaOH)]^{2-}$ building block.

On the other hand, series of $M^{II}Cu^{II}$ chains (M = Mn and Co) were prepared using the $[Cu(opba)]^{2-}$ [H_4opba = *N, N'*-1,2-phenylenebis(oxamid acid)] complex. This type of compounds generally behaves as almost ideal 1D ferrimagnets with no long-range magnetic order above 2.0 K, suggesting that the chains are well isolated in the crystal lattice. Then, Kahn and Stumpf prepared the oxamato-bridged $M^{II}_2Cu^{II}_3$ planes (M = Mn, Fe, Co and Ni) using the same copper(II) complex and these ferrimagnetic planes show higher ordering temperatures than their chain analogues (37 K). These results suggest that the increase of the dimensionality in the interactions could give high-*Tc* molecule-based magnets (Figure 1.2).

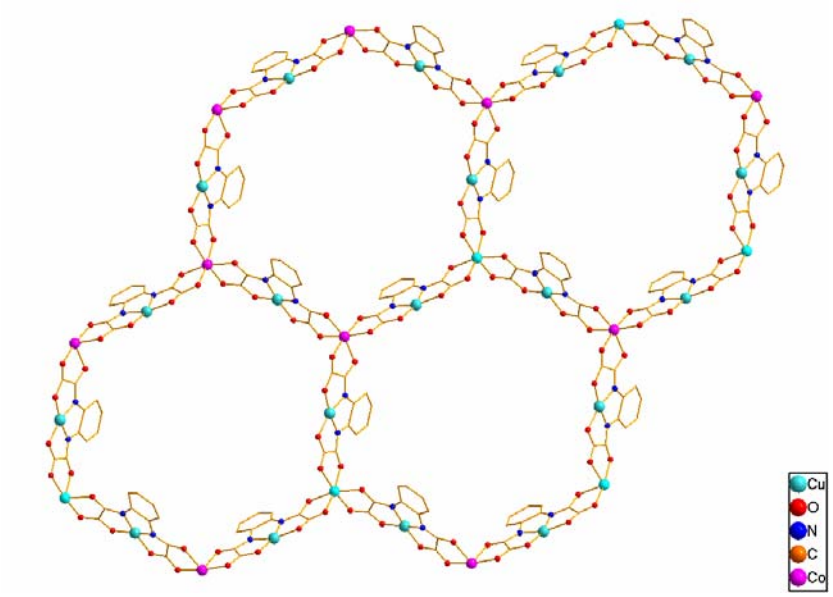

Figure 1. 2 Structure of the 2D coordination polymers Co[Cu(opba)] where the $Co^{II}_2Cu^{II}_3$ planes can be observed.

Magnetism is a consequence of unpaired electrons in materials and depending on the origin of the unpaired electrons three different types of molecular-based magnets might arise.[9] In the purely organic magnets the unpaired electrons arise entirely from the *p* orbitals (Scheme 1.2),[10] whereas in the metal-containing magnetic units such as $Ba_4(C_2O_4)Cl_2[\{Fe(C_2O_4)(OH)\}_4]$ (Figure 1.3),[11] the unpaired electrons arise from the *d* orbitals. Finally, in the metal-organic radical compounds some electrons can arise from the *p* orbitals and some others from the *d* orbitals (Scheme 1.3).[12]

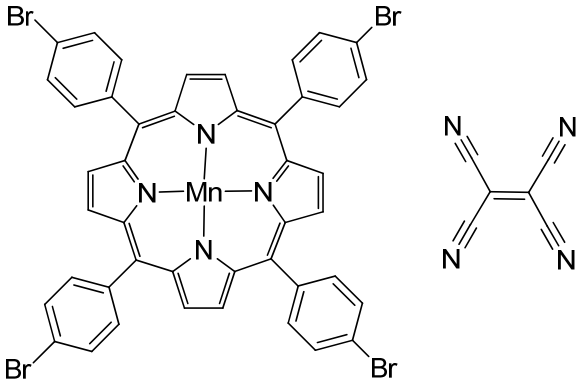

Scheme 1. 2 Molecular structure of $Mn^{III}TClPP]^{+}[TCNE]^{-}$

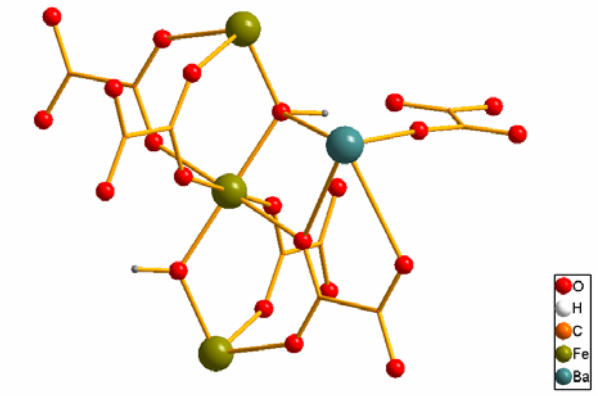

Figure 1. 3 Part of an iron hydroxide oxalate chain of $Ba_4(C_2O_4)Cl_2[\{Fe(C_2O_4)(OH)\}_4]$.

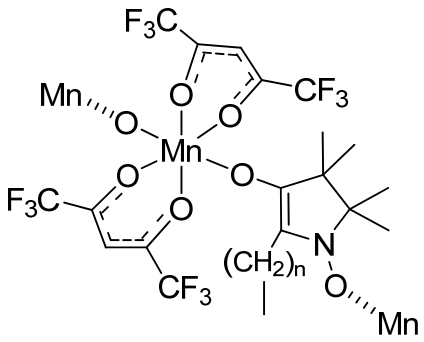

Scheme 1. 3 Segment of a chain of $Mn(hfac)_2NITEt$ when n = 1 and $Mn(hfac)_2NIT$-*n*-Pr when n = 2.

As stated above, long-range magnetic ordering is essentially a 3D phenomenon and it only occurs in three dimensional polymers, although it may also occur in two dimensional systems in the case of uniaxial magnetic anisotropy. There is no long-range magnetic ordering in one dimension at a finite temperature but it is expected to occur at absolute zero for a chain in the lack of interchain interactions. However, the low dimensional 0D and 1D coordination polymers can exhibit slow relaxation of the magnetization accompanied by magnetic hysteresis effects below a blocking temperature.[8] This magnetic behaviour has no analogy in the world of classical

magnetic materials and it is not a consequence of a three dimensional phenomenon. Instead, it is has a pure molecular origin that is associated with the magnetic anisotropy of the polynuclear species or the chain, respectively. These are so-called SMMs (single-molecule magnets) and SCMs (single-chain magnets) (Figure and Scheme 1.4). The $[Mn_{12}O_{12}(O_2CR)_{16}(H_2O)_4]$ (R = Me, Et, Ph, etc) family compounds was the first SMMs family discovered and it has been the most widely studied (Figure 1.5).[13,14] In this type of compounds the intermolecular interactions are minimal and therefore it shows a magnetic behaviour of a single-molecule, otherwise 1-, 2- or 3-D molecule-based magnetism is observed.[15]

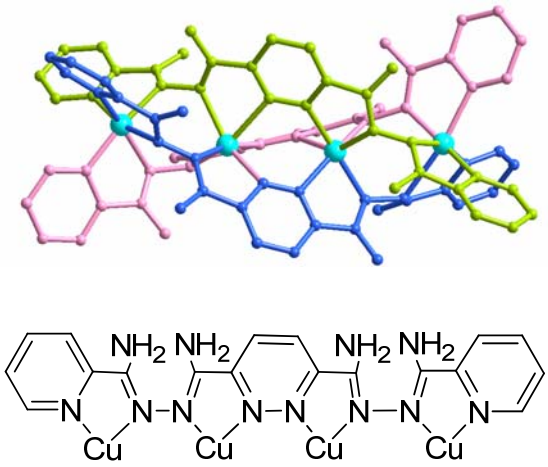

Figure and Scheme 1. 4 Example of a finite 1-D magnetic chain (SCM).[16]
The metal complex is a triple-stranded helicate containing four metal centres (Cu^{2+}).
Each strand, whose structure can be seen below, is represented in one colour for clarity.

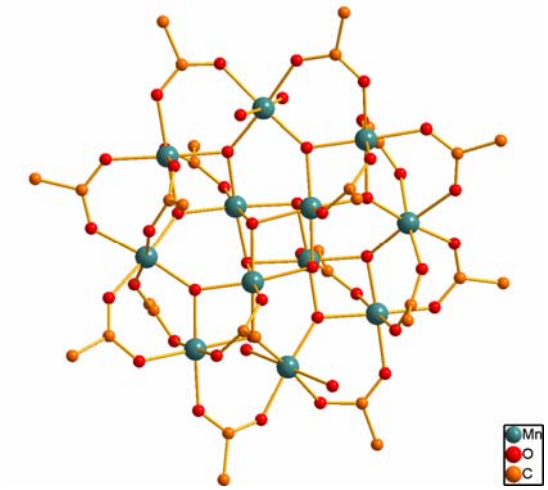

Figure 1. 5 View of the structure of the $[Mn_{12}O_{12}(O_2CR)_{16}(H_2O)_4]$ (R = Me, Et, Ph, etc) family compounds.

Since Kahn's group first produced his polymetallic coordination network based on the oxamato-bridged ligand, there has been a significant effort directed towards the preparation of bimetallic species, in which metal ions are bridged by extended bis(bidentate) ligands such as oxamate, oxamide, oxalate, dithiooxalate or oximate. Among this group,[17] bis(oxamato) type transition metal complexes have been extensively used as versatile building blocks for magnetic homo- and hetero-polymetallic systems for the exploration of magnetic molecular properties,[18] since it allows the control of the overall structure and the magnetic properties of the final multidimensional *n*D (*n* = 0-3) products. The magnetic properties of polymetallic systems derive from the cooperative exchange interactions between the paramagnetic metal ions through the bridging ligands. Therefore, they depend on the nature of the metal and the ligand constituents and also on the particular level of organization created by the metal-ligand coordinative interactions. As such, ligand design is crucial to achieve the desired organization of the paramagnetic metal ions and to efficiently transmit exchange interactions between the metal ions in a controlled manner.[8]

Oxamato-bridged polymetallic complexes exhibit a high diversity of molecular architectures and magnetic properties. The synthesis of these compounds relies on the use of aliphatic and aromatic group-substituted oxamato-containing metal complexes as ligands (building blocks) interacting with other metal ions through the two adjacent *cis* carbonyl oxygen atoms of the oxamato groups (Scheme 1.5).[19]

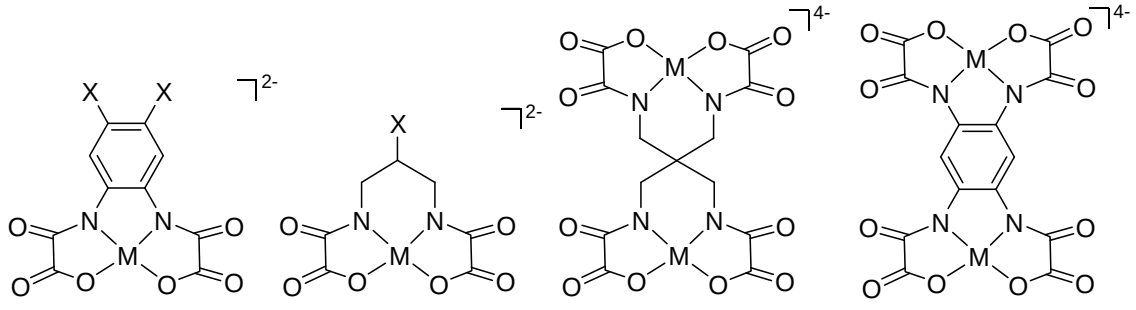

1a $[M(opbaX_2)]^{2-}$ M = Cu^{2+}, Ni^{2+} (X = H, Cl, Me

1b $[M(pbaX)]^{2-}$ M = Cu^{2+}, Ni^{2+} (X = H, OH, Me)

2a $[M(bpbaX)]^{4-}$ M = Cu^{2+}

2b $[M(bopbaX)]^{4-}$ M = Ni^{2+}

Scheme 1. 4 Metal oxamato mono- (**1**) and dinuclear (**2**) complexes (M = Cu and Ni).

The M^{II} ions (M = Cu, Ni, Co) are initially coordinated thorough the bidentate *N,O*-oxamato donor set to give mono- or oligonuclear complexes thanks to their potential binding ability toward middle and late 3d divalent metals ions. Then, thanks to the free carbonyl oxygen atoms of the oxamato groups, these molecular complexes can be used as ligands towards other M^{II} ions (M = Fe, Co, Cu, Ni, Mn, Gd, etc.) and coordinate these other metal ions. This molecular-programmed approach based on the ligand design allows the rational design of coordination polymers of variable dimensionality.[8] Also, it allows designing polynuclear compounds with variable nuclearity when blocking ligands are used in the coordination sphere on the latter coordination ion in order to avoid polymerization. Lastly, this polynuclear complexes are used for the construction of the *n*D (*n* = 1-3) coordination polymers.

There are also examples of the rational design of high-spin homo- and hetero-polymetallic complexes for the study of the magnetism of 0D compounds based on the use of mono- and dinuclear oxamato copper(II) complexes as bis- and tetrakis(bidentate) ligands, respectively. This type of approach was also initiated by Kahn and coworkers who prepared a series of oxamato-bridged $Cu^{II}M^{II}_4$ trimers using the **1b** building block where X = H. The metals that were initially used were Cu, Ni and Mn (Figure 1.6a),[20] although other metals such as La or Sm have also been subsequently used. These complexes exhibit S = 1/2 for Cu, S = 3/2 for Ni and S = 9/2 for Mn ground states as a consequence of the antiferromagnetic coupling between the Cu ion and the peripheral M^{II} metal ions through the oxamato bridge. On the other hand, a series of oxamato-bridged $Cu^{II}_2M^{II}_4$ hexamers from the type of complex **2a** using Cu and Ni were prepared by Journaux and coworkers. In these case, the weak interferromagentic interaction between the central Cu^{II} ions though the tetramethylenemethanetetraamidate bridge is masked by the intermolecular antiferromagnetic interactions (Figure 1.6b).[21] However, the typical slow magnetic relaxation phenomenon of the SMMs has not been observed in this family of oxamato-bridged trinuclear and hexanuclear species.

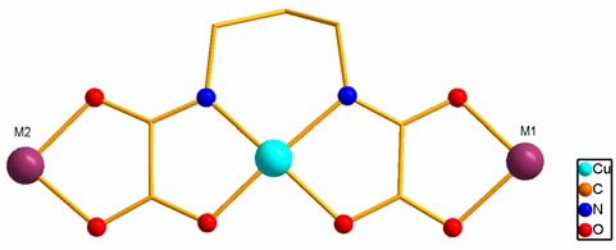

a. $[Cu(pba)]^{2-}$

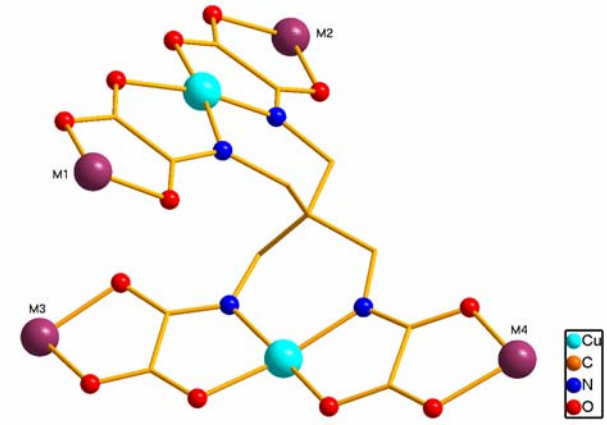

b. $[Cu(bpba)]^{2-}$

Figure 1. 6 Structures of the 0D coordination compounds prepared by using the copper(II) building trinuclear blocks $Cu^{II}M^{II}_4$, $[Cu(pba)]^{2-}$ **(a)**, and hexanuclear $Cu^{II}_2M^{II}_4$ building blocks, $[Cu_2(bpba)]^{4-}$ **(b)**.

As we can see, these ligands can form mono- and dinuclear metal complexes. This is a consequence of the structurally well organised ligand and thus, the self- assembly is structurally trivial. However, Julve and coworkers designed a family of aromatic polyoxamato ligands with which they could show that the nuclearity and the topology of the complexes resulting from the interaction between ligands and the first-row transition metal ions depend mainly on the topology of the ligand and on the preferred coordination geometry of the metal ion.[8] These ligands are polymethyl-substituted benzene rings with multiple oxamato binding sites which provide a variety of binding modes and depending on the number of oxamato binding sites, they can act as mono-, di- and trinucleating ligands. For instance, the *N*-phenyloxamato (H_2pma) can act as a mononucleating ligand when coordinating the late 3d divalent metal ions through the amide nitrogen and the carboxylate oxygens atoms of the oxamato groups. This type of ligand can either afford a four coordinate square-planar or a six coordinating octahedral geometry in a *cis* or *trans* environment. The dinucleating ligand *N*, *N'*-1,3-phenylenebis(oxamato) (H_4mpba) can afford four and six coordinating geometries,[22]

whereas *N*, *N*', *N''*-1,3,5-benzenetriyltris(oxamato) (H_6mpta) can afford tri- or tetranuclear metal complexes (Scheme 1.6).[23]

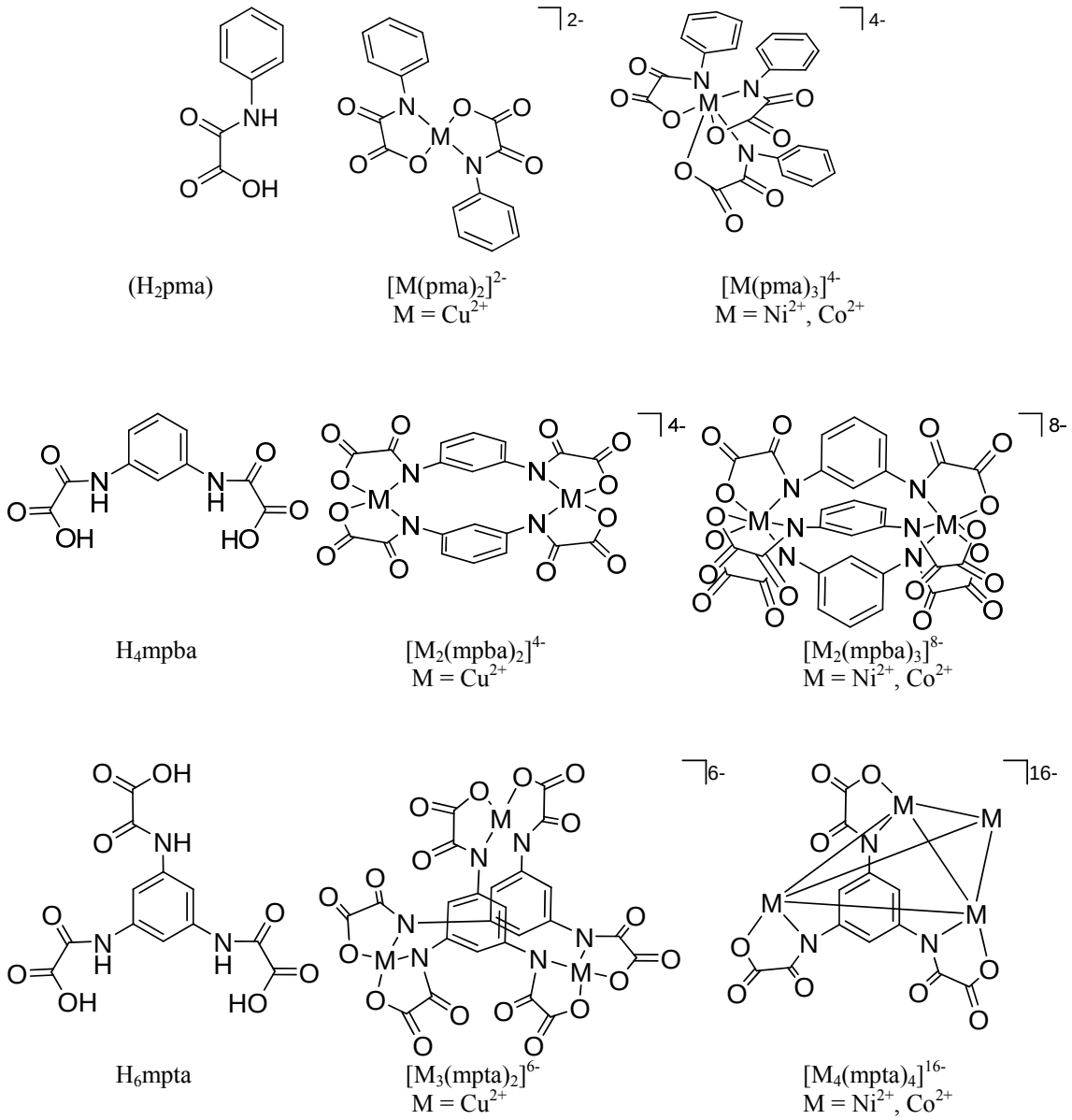

Scheme 1. 6 Family of aromatic polyoxamato complexes showing the different nuclearity and topology of the ligands.

Then, depending on the oxamato metal building block and the nuclearity of the complexes that are formed, *n*D (*n* = 0-3) coordination polymers can be obtained. This can be noted in the series of H_2pma ligands where the benzyl ring is di- or trimethyl-substituted (H_2pmaMe_2 and H_2pmaMe_3, respectively). The metal oxamato complexes can form heterobimetallic single chain magnets with different topologies. They can assemble oxamato-bridged heterobimetallic chains in which two copper oxamato building block coordinates an octahedral Co^{2+} ion displaying either a *cis* or a *trans*

environment of the solvent molecules. $CoCu(pmaMe_2)_2(H_2O)_2$ shows a zigzag architecture in which the solvent molecules are in *cis* environment around the Co ion (Figure 1.7), whereas $CoCu(pmaMe_3)_2(H_2O)_2{\cdot}4H_2O$ shows a linear 1D chain where the solvent molecules are in *trans* (Figure 1.8).[24]

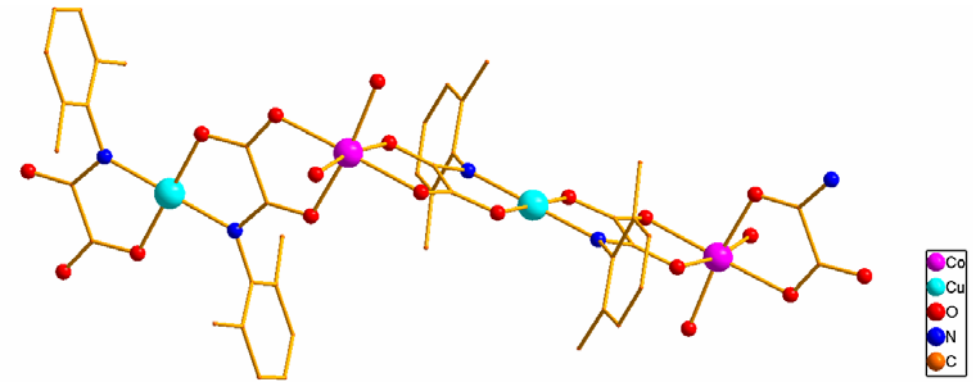

Figure 1. 7 View of the zigzag structure of $CoCu(pmaMe_2)_2(H_2O)_2$.

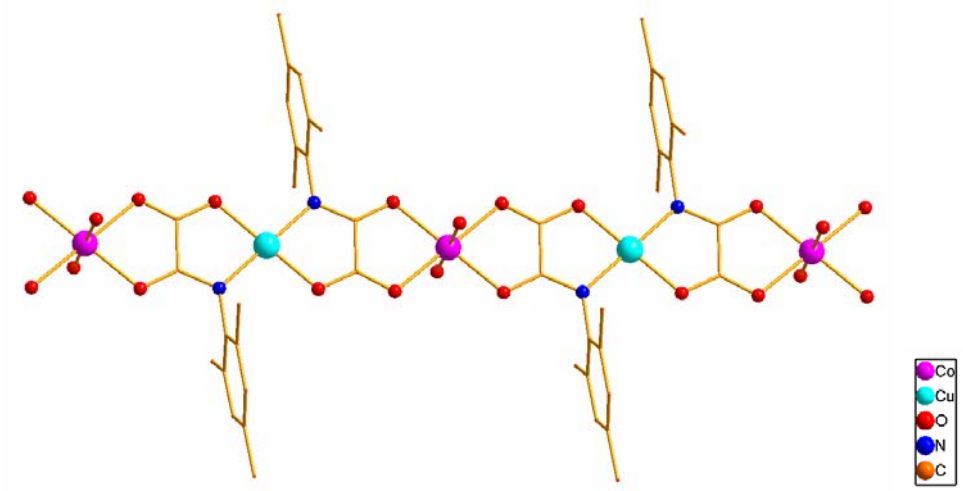

Figure 1. 8 View of the heterobimetallic chain of $CoCu(pmaMe_3)_2(H_2O)_2{\cdot}4H_2O$

Moreover, two linear 1D chains can be linked to build 2D networks such as in bimetallic complex $Co_2Cu_2(mpba)_2(H_2O)_6$ (Figure 1.9). The complex forms $Co^{II}Cu^{II}$ chains which are linked through the meta phenylene diamine of the H_4mpba ligand. The Co^{2+} is also coordinated by two metal oxamato building blocks and two water molecules in a *trans* environment.[25]

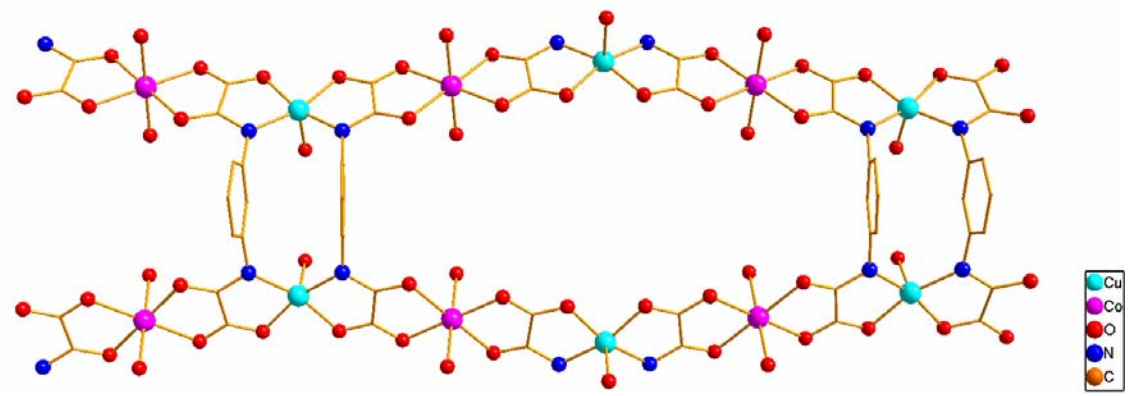

Figure 1. 9 View of the two dimentional network of $Co_2Cu_2(mpba)_2(H_2O)_6$.

On the other hand, 3D arquitectures can be observed when the H_4mpba ligand forms the triple-stranded dinuclear $[M^{II}_2(mpba)_3]^{8-}$ complex where the metal units display a 3D "honeycomb" architecture such as in $Li_5[Li_3M_2(mpba)_3(H_2O)_6]\cdot 31H_2O$ (M = Ni, Co) (Figure 1.10).[26]

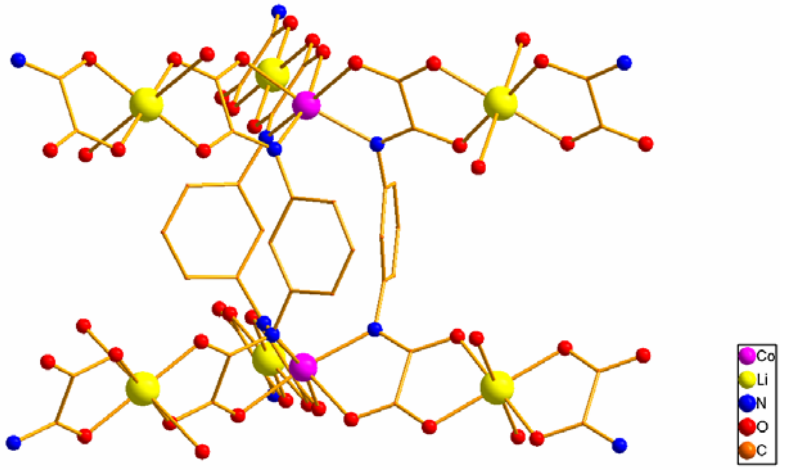

Figure 1. 10 View of the three dimetional network of $Li_5[Li_3Co_2(mpba)_3(H_2O)_6]\cdot 31H_2O$.

In the future, the properties of molecular magnetic materials may be quite similar to the robust, inert and cheap non-molecular materials such as transition metal oxides or intermetallics, like samarium cobalt.[27] However, at present, it is difficult to see how molecular systems will surpass their useful properties. Among others, they may find applications in molecular electronics and nanotechnology, magneto-optical devices, storage media or read/write devices which necessitate the fabrication of thin films although it is clear that the existing knowledge and development in thin film technologies will continue to develop using simple atomic/ionic materials. Even so, molecular systems can offer advantages over conventional magnetic materials: the

structures that can be formed are more complex and more diverse than the structures of inorganic and organic materials and, thus, they often permit scope for the incorporation of other useful functionalities. Moreover, they can offer advantageous physical properties compared with classical magnets such as transparency, lightness and ease processability.

1. 2 Initial aims of the project

Inspired by Kahn's work, some changes have been done to the original structure using mono-, di- or trinuclear complexes of the first-row transition metal ions with related aliphatic or aromatic-substitued mono-, di- and tri (oxamato) ligands as building blocks and their consequences have been investigated. However, when this project begun, to the best of our knowledge, the variation to the Kahn´s structure using the simplest aliphatic group-substituted (ethylene)oxamato-containing metal complexes had never been reported. Thus, the synthesis and the investigation of the consequences in the change of the original structure using diethyl ethylene-1,2-dioxamate as the ligand precursor were the aim of this project.

Through this thesis, for simplicity and clarity, a simple nomenclature will be used when naming the proligand and its derivates. Diethyl ethylene-1,2-dioxamate is represented by Et_2H_2(oeo) where "o" and "e" refer to oxamate and ethylenediamine, respectively. Under appropriate conditions the ethyl groups of the proligand can be cleaved to give first $EtH_2(oeo)^-$ and then $H_2(oeo)^{2-}$. Afterwards, the amide protons can also be removed when the ligand is coordinating a metal to give $(oeo)^{4-}$ (Scheme 1.9). In other work,[28] diethyl ethylene-1,2-dioxamate was abbreviated as (enda)H_2Et_2. However, our nomenclature will be maintained throughout this work since it seems to be a clear way of describing the actual composition of the organic molecule in every complex that will be discussed.

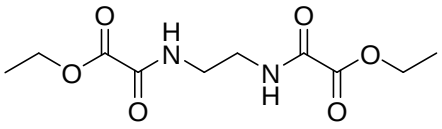

$Et_2H_2(oeo)$

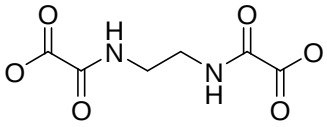

$[H_2(oeo)]^{2-}$

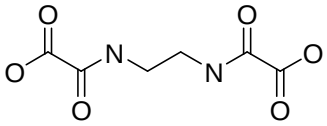

$(oeo)^{4-}$

Scheme 1. 5 The ligand precursor and its related ligands

Furthermore, this nomenclature can be easily extended to related ligands, like the ligand precursor bis(ethylamine)oxamide, $H_2(eoe)$, of which the mononuclear and binuclear copper(II) complex have been already reported (Scheme 1.3).[29] The chemistry of the compound will be discussed in the following chapters.

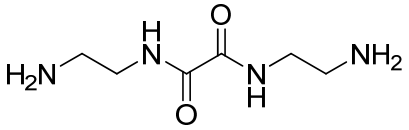

a

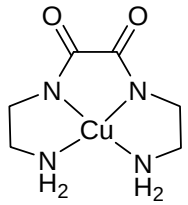

b

Scheme 1. 6 Bis(ethylamine)oxamide, $H_2(eoe)$ (**a**) and its mononuclear complex $[Cu(L^1)]$ (H_2L^1 = 1,8-diamino-3,6-diazaoctane-4,5-dione) (**b**). Using our notation the complex would be named [Cu(eoe)].

On the other hand, the synthesis and the chemistry of related polynuclear bis(oxamato) complexes of $Et_2H_2(oeo)$ is more complicated than similar and larger previously reported complexes. The stability of the ligand and the structure of the "oeo" compounds were quite different than expected. Consequently, a great proportion of the work was invested in understanding the chemistry and the structures formed with this ligand.

1. 3 The ligand

Diethyl ethylene-1,2-dioxamate, $Et_2H_2(oeo)$, is a flexidentate ligand which can chelate as well as bridge metal ions to build polynuclear and low-molecular weight molecules.

It has several Lewis-basic donor atoms which allow the step-wise incorporation of several transition metal ions to give polymetallic complexes with well-defined physical properties. As discussed above, one of the current challenges for inorganic chemists is the design and synthesis of high nuclearity complexes with transition metal ions in a controlled fashion and this ligand, Et_2H_2(oeo), was a promising example for this challenge.

Following to the previous preparations of bis(oxamato) ligands,[30,31,32] the synthesis of diethyl ethylene-1,2-dioxamate, Et_2H_2(oeo), was optimized by adding a solution of ethylendiamine to a solution of about five equivalents of diethyloxalate, both reagents dissolved in ethanol, and then heating the mixture in a steam bath for few hours. This new approach improved the previous ones achieving high yields in a cheap and easy synthesis method.

When the oxamate group acts as a bidentate ligand, it is capable, like oxamide and oxalate groups, of coordinate as a bridging ligand to give many types of binuclear complexes. However, the binuclear copper(II) complexes formed by the oxamate are more stable than those formed by the oxalate but less stable than those formed with oxamides, allowing the extent of magnetic interaction between two metal ions.[33] This is a result of the strong electron-donating capability of the two deprotonated amido nitrogens of the oxamide which gives a greater stability of its metal complexes when comparing with the oxalate or oxamato ones. This greater basicity is also responsible for the occasional stabilization of high oxidation states such as Cu(III) and Ni(III). Moreover, the lower electronegativity of the nitrogen atoms relative to the oxygen atoms allows stronger magnetic interactions between metal centres through the oxamato when comparing to the same situation with oxalato-bridged compounds, but weaker when comparing with oxamidato-bridged compounds.[34]

In general, the preparation of polymetallic complexes, such as molecular extended systems or even molecules containing an increasing number of metallic centres with predetermined physical properties, follows a step-by-step strategy.[35] We will see that the hydrolysis of the esters of diethyl ethylene-1,2-dioxamate, Et_2H_2(oeo), is carried out with the addition of two equivalents of hydroxide affording the salt of the ester, M_2H_2(oeo) M = alkali metal or *n*-Bu_4N. Afterwards, the addition of a transition metal

such as copper(II), and two more equivalents of base (OH^-), affords the metalation of the amide by the hydrogen amide dissociation. Similarly to the compounds mentioned above (Scheme 1.1), a mononuclear bis(oxamato) copper(II) complex $[Cu(oeo)]^{2-}$ was expected to be obtained where the tetradentate chelating ligand coordinates the copper atom though the oxalate oxygens and the amide nitrogens giving a square planar environment around the metal ion (Scheme 1.11).

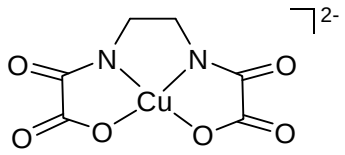

Scheme 1. 7 Mononuclear bis(oxamato) copper(II) complex $[Cu(oeo)]^{2-}$

Then, once the building block would be achieved, we hoped to prepare polymetallic complexes by adding further transition metal ions into the $[Cu(oeo)]^{2-}$ building block, which would might give rise to the formation of extended bimetallic magnetic chains (Scheme 1.12).

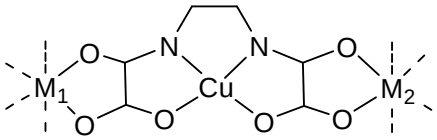

Scheme 1. 8 Hypothetical bimetallic magnetic chain

1. 4 Acid – base properties of the amides

Through most of the range of pH, in absence of metal ions, the amide group is neutral because of the electron withdrawing character of the adjoining carbonyl oxygen atom. However, the amido nitrogen atom can behave as a very weak acid in aqueous solution by hydrogen dissociation (pK_a~13-15) of the nitrogen to give a negatively charged species. As far as the (substituent)oxamatos are concerned, the following acid-base equilibriums are involved (Scheme 1.13).[36]

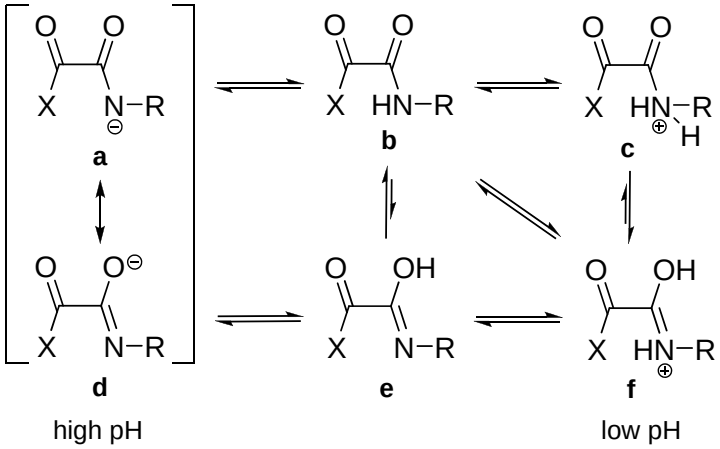

Scheme 1. 9 Protonic equilibria in the amide group. The major species in basic solution is at the top left (**a**) while in neutral solution it is at the top centre (**b**) and in acid solutions at the bottom right (**f**). The bottom centre (**e**) and the top right (**c**) are the tautomers of their relative forms. In our case, X = O.

When the amide is anionic (**a**), protonation and metalation occur at the nitrogen atom, whereas when the amide is neutral (**b**), protonation occurs at the amide oxygen as well as metalation of most metal ions. Moreover, in metalation and protonation at neutral amide, the C-O bond becomes longer and weaker while the C-N becomes shorter and stronger, thus it increases the double character of the C-N bond and its barrier to rotation (Scheme 1.14).

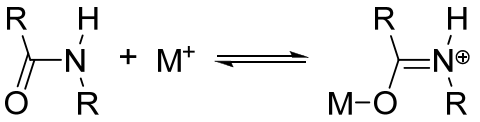

Scheme 1. 10 Metalation of the amide oxygen in neutral pH

Following to the previously stated, displacement of the hydrogen bound to the nitrogen by a metal ion can occur when a strong M-N bond is formed. This is seen for transition metals but not for alkali and alkaline earth metals, which will not affect the removal of the hydrogen in water. However, the hydrolysis and precipitation of the metal ion in neutral and basic conditions, and the insolubility of the amides in common solvents, makes the metalation of the amide difficult.

Nevertheless, if the amide possesses a coordinated substituted group, the hydrolysis of the amide is less favourable and choosing the right substituent, its solubility can be increased. Furthermore, if the coordinating group is at a position which can form a 5- or 6-membered chelate ring with the amide nitrogen, and a heavy metal ion is also present, the amide dissociates and coordinates simultaneously in an unexpectedly low pH

range.[37] This is because the metal needs a primary ligating site or anchor in order to chelate the nitrogen by substitution of the hydrogen bound to the nitrogen. Therefore, by providing an anchor for the metal ion and the possibility of chelation with the amide, the primary binding site reduces the possibility of the hydrolysis of the metal ion and permits the achievement of the hydrogen substitution by the metal.

1. 5 Metalation

The synthesis of bis(oxamato) transition metal complexes usually starts by the treatment with four equivalents of base (OH^-) to diethyl *N-N'*-bis(oxamates) and then gentle heating of the reaction mixtures until the total dissolution.[38,39] When the reaction mixture is cooled down to room temperature, the solution of a transition metal ion is then added. The colour change that proceeds in our case, from colourless to deep blue, indicates the formation of the metal complex.

However, the mechanism and the nature of the intermediate compounds in the formation of bis(oxamato) complexes has been not studied so far, although it has been for oxamides.[34] Nevertheless, the formation of the tetraanionic species due to the saponification of the esters and the deprotonation of the hydrogen amides, by the addition of four equivalens of base to diethyl *N-N'*-bis(oxamate), is assumed. Also, the formation of a dianionic, trianionic and tetraanionic species of diethyl *N*,*N*'-4,5-dinitro-*o*-phenylene-bis(oxamate) ($niboH_2Et_2$) by treatment of the compound with NaOH at room temperature, have been recently reported.[40]

Based upon the mechanism proposed by Ojima,[41] the metalation mechanism of an amide is shown (Scheme 1.15). Species **1** can coordinate a metal ion as shown in species **2,** which has some electron density at the nitrogen atom and promotes the hydrogen dissociation of the amide to give species **3**. Then, the resonance in species **4** stabilizes the chelate ring. This tendency in a *N-N'*-bis(coordinating group substitued) oxamato is promoted by the strong chelate effect.

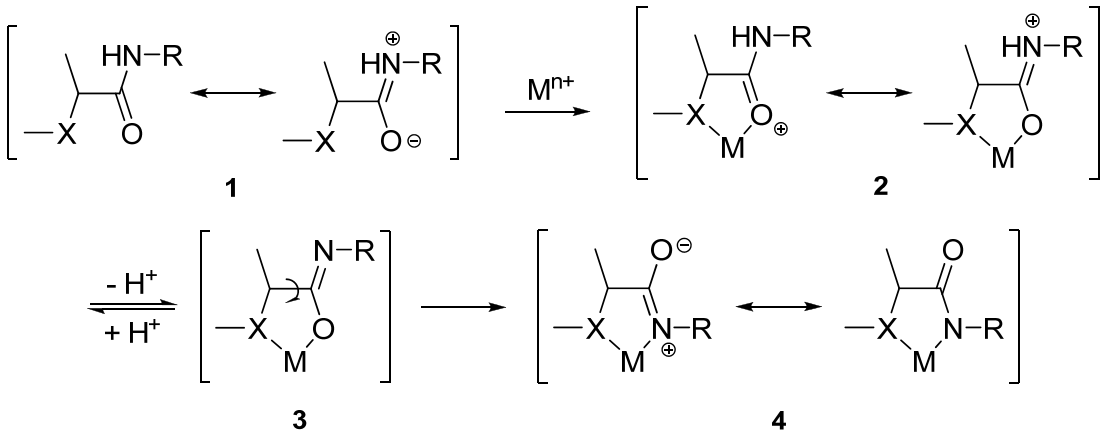

Scheme 1. 11 Metalation mechanism of an amide with a coordinating substituted group at a position that it can form a 5-membered ring. R: H, C. X: coordinating group, in our case, oxygen atom.

1. 6 Magnetic interactions

The amido nitrogen is coordinated to a metal ion, it is sp^2 hybridized to conjugate with $p\pi$ electrons of the carbonyl group. In the case of an oxamide, oxalate or oxamate dianion, the carbonyl oxygens can coordinate to another metal ion to form a binuclear system. The presence of an effective π-path between the two metal ions is the reason why the complexes formed shows such strong magnetic interaction although the two metal ions are separated by three "non-magnetic" atoms.

That is to say that, for instance in our case, where oxamato groups are coordinated to copper(II), the metal ion is surrounded by two nitrogen and two oxygen atoms belonging to oxamato groups. The unpaired electrons arising from the copper(II) ion in such planar surroundings occupies the $d_{x^2-y^2}$ type orbital pointing toward the Cu-N and Cu-O directions. Moreover, the N-C-O and O-C-O linkages are conjugated and consequently, the spin density is delocalized not only toward the four atoms bound to Cu(II), but also along the N-C-O and O-C-O bonds. The delocalization is a bit more pronounced along the N-C-O than along the O-C-O linkages since the 2p valence orbitals in the nitrogen are more diffuse than the 2p valence orbitals of oxygen, so that the $3d_{x^2-y^2}$(Cu)-2p(N) overlaps are more pronounced than the $3d_{x^2-y^2}$(Cu)-2p(O) overlaps.[6] Therefore, the extent of magnetic interaction follows the order oxamidato>oxamato>oxalato complexes.

Hence oxamato groups are efficient in propagating strong antiferromagnetic interaction between two like metal centres. This is most easily seen in the case of Cu(II) in elongated tetragonal surroundings with almost coplanar basal planes (Figure 1.11).[42] The magnetic orbitals of the copper(II) point from the metal toward the four nearest neighbours and overlap either side of the bridge, which favours strong antiferromagnetic interactions. The direct overlap of the magnetic orbitals of the two neighbouring copper ions is negligible. However, the oxamato bridge between metals mediate a very significant superexchange interaction

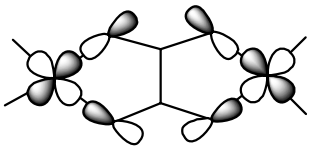

Figure 1. 11 Magnetic orbitals centred in the copper(II) ions.

1. 7 The chemistry of Copper (II)

Although copper can form compounds with +1 and +2 oxidation states, the aqueous chemistry of the copper(II) is dominated by the oxidation state +2. In aqueous solutions, almost all copper(II) salts are blue due to the presence of $[Cu(OH_2)_6]^{2+}$, except in concentrated solutions of copper(II) chloride. In these solutions, due to the formation of $[CuCl_4]^{2-}$, the solutions are light blue. Moreover, the addition of hydroxide into a copper(II) solution forms a blue-greenish gelatinous solid $Cu(OH)_2$. If the solution is heated, the hydroxide decomposes to form the copper(II) oxide, CuO, which is black and if there is chlorine in solution, the copper(II) hydroxide and oxide that is formed it is likely to contain chlorine.

All these changes in the chemistry of the copper(II) have been observed in the preparation of our complexes and they have been used to study the reactions. For instance, one of the impurities that has been widely observed in the synthesis of the copper(II) complexes has been the dark green copper(II) chloride hydroxide due to the addition of base to the copper(II) solution and which became a method of knowing when to stop the addition of base into the reaction mixture.

The copper(II) complexes that have been obtained have an octahedral, distorted square pyramid or distorted square planar environment. The Jahn-Teller effect is observed in

the copper(II) octahedral complexes obtained, where the ligands that are in *trans* suffer an elongation of the bond lengths. These complexes are coordinated towards oxygen atoms and they have a turquoise colour. Nevertheless, the coordination preference of mostly of the copper(II) complexes obtained display a distorted square-planar or distorted square-based pyramid geometry and they are coordinated by nitrogen and oxygen atoms having a very characteristic deep blue colour.

1. 8 X-ray Crystallography

1. 8. 1 Introduction

Characterisation of compounds obtained in this work was mainly carried out using X-ray diffraction analysis. This technique is widely used in chemistry, biology, physics and biomedicine, and most chemistry departments have a diffractometer to analyse crystals using X-ray crystallography. It is the most powerful and unambiguous technique for the structure elucidation of crystalline solids available to modern scientists and it has grown steadily since Max von Laue discovered in 1912 that a copper sulphate crystal could act as a three-dimensional diffraction grating on irradiation with X-rays.[43] Since then, the advent of modern high speed computers, automated diffractometers and powerful structure solution programs have allowed X-ray diffraction to become widely accepted as necessary standard technique. However, it is limited by the necessity of growing high quality single crystals of the compound that wants to be studied, which most of the times is not obvious and straightforward.

The interaction of X-rays with single crystals leads to a diffraction pattern from which a three-dimensional crystal structure can be determined precisely as well as the distance and angle between atoms. It is a consequence of the constructive interference of waves scattered by the cell's contents. When light is scattered by an object it leads to interference effects in which the waves suffer constructive or destructive interference. The interaction of waves with the same amplitudes leads to destructive interference where they cancel out if they have a phase difference of 180^{o}. They are *out-of-phase*. In contrast, the waves in the constructive interference have no phase difference and it results in the reinforcement of the waves and in the *in-phase* scattering. The intermediate between these two situations is the partial interference.

A qualitatively simple method for obtaining the conditions for diffraction was expressed by W. L. Bragg in 1912 who described the diffraction of X-rays from a crystal as a reflection caused by various lattice planes belonging to the same family.[44] Due to the repetitive nature of the crystal, the atomic planes in the crystal are separated by a distance *d* (Figure 1.12).

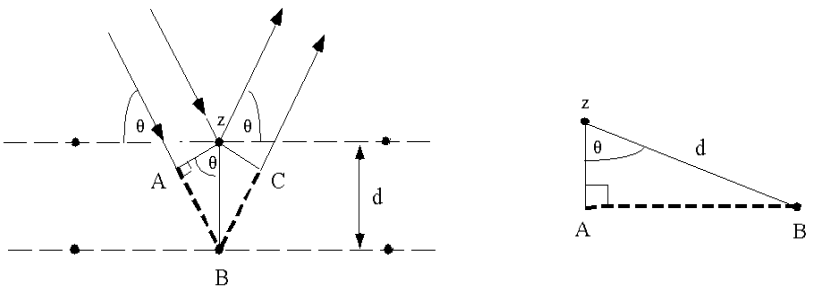

Figure 1. 12 The figure geometrically describes the direction of the diffraction beam due to the constructive interference between atoms located on planes with interplanar spacing *d*.[45]

The angle created by the X-ray beams and the family of planes (with indices hkl) is the angle θ and the path difference between the waves scattered in z and B is equal to AB+BC = $2d \sin \theta$. The Bragg's law provides the condition for these two waves to combine themselves with maximum positive interference:

$$n\lambda = 2d \sin \theta \qquad (1)$$

Only if this difference in path is a multiple of λ (the wavelength of the radiation) the reflected waves will interfere constructively. If this equation is not verified, the reflected waves will interfere destructively. The crystal is formed by number of family planes which will reflect the X-ray beams and interfere constructively.

The interference of the scattered X-rays by the electrons in the crystal produces the diffraction pattern in which the constructively interfered waves appear as spots in the pattern, which are the so-called "reflections". The geometry of the spots is related to the lattice and the unit cell geometry, and the symmetry of the pattern is related to the symmetry of the crystal. The former provides information about the repeated distances in the lattice and the later about the symmetry relations between units in the lattice. The intensity of the reflections depends on the nature and arrangement of the atoms in the unit cell, thus the amount of electrons. The reflections observed are composed by the interference of waves scattered from different atoms at different positions in the unit cell and all atoms, thus all electrons, contribute to the intensities of all reflections. This

means that to solve the structure measurement of these individual intensities must be carried out.

The department's diffractometer that has been used for recording X-ray data is a Bruker APEX II CCD Diffractometer (Figure 1.13.a). The diffractometer uses the 4-circle Kappa goniometer and a CCD detector (Figure 1.13.b), and it is equipped with an Oxford Cryostream unit which cools to 100K.

a **b**

Figure 1. 13. a. The department's Bruker APEX II CCD Diffractometer.
b. Close up picture of the APEX II detector (right), KAPPA goniometer (middle below), the X-ray tube (left) and a camera for positioning the crystal in the beam (left on top).

The 4-circle Kappa Goniometer allows the crystal to be brought to any orientation in space by means of a three rotation axes. Then, once the crystal is oriented, a fourth axis is afforded by the rotation of the detector which is positioned to collect the diffracted beams. CCD (Charge Coupled Device) detectors possess a fast read-out time that allows quick evaluation of the crystal suitability for a full data collection permitting to save time in the experiment. This technology is particularly useful for any material that can deteriorate over its exposure to X-rays, since the detection of every collected image, with several hundreds of reflections, is done in a minimum time (in the order of minutes). Finally, in order to get the best collections of diffraction data, the crystals are usually kept at a very low temperature (~100 K) using a dry nitrogen stream. At these

temperatures the crystals are more stable and resist the effects of X-ray radiation much better.

1. 8. 2 Experimental methods in X-ray crystallography

Once the crystal of the compound has been obtained, the procedure to carry out for the structure determination follows a sequential method. First, the data collection of the crystal is performed using a diffractometer. Afterwards, the data is extracted and processed, and the structure is solved where the whole or the partial structure is found. Finally, when all atoms have been found, the structure is refined is order to get the contributions of the atoms correctly represented in the structure model.

Data collection

A single crystal diffractometer consists of a X-ray source, a X-ray detector, a goniometer that orients the crystal so that a chosen X-ray diffracted beam can be received by the detector, and a computer. The computer controls the goniometer and the detector movements, and performs the mathematical operations required to position the crystal and the detector in the desired orientations.[44]

As stated above, the detector used has a CCD (Charge Coupled Device) area detector, which is the most commonly used area detector. Any particle or kind of electromagnetic radiation can be detected through its interaction with matter. In the case of area detectors, they are semiconductors that measure the number of photons arriving per unit time as a function of the position within the detector's surface. In this type of detectors, the incident radiation produces electron-hole pairs in the semiconductor and the electrons are trapped in potential wells that are then read out with phosphor coupled through fibre optics to the CCD chip.[46] The nature of these devices allows the detection of many diffraction beams simultaneously and thereby saving time in the experiment. Also, less movement of the crystals is required to access to all reflections thanks its two-dimensional nature. Efficient recording, high dynamic range, low noise level and fast read-out time give the CCD some clear advantages as a rapid area detector.

The detector needs to be combined with a goniometer for mounting and moving the crystal. The goniometer that was used is a Four-circle goniometer with Kappa geometry. These types of goniometers have very precise mechanics and their main advantage is the wide accessibility to the crystal as it can be brought to any orientation in space by means of three rotation axes. The first axis, κ axis, is represented by the rotation of the arm where the goniometer head that carries the crystal is mounted. The instrument has a main axis which passes through the crystal and it is normal to the equatorial plane and to the incident and diffracted X-rays beam. The rotation of the cradle about this axis is defined by the ω angle. Lastly, the rotation axis around the goniometer head is represented by φ. In addition, the detector is mounted on a horizontal arm that can be moved about an axis passing through the crystal as well as back and forth, providing another degree of freedom: the crystal detector distance. The rotation of the detector about the main axis is described by 2θ.

The conventional generators used in crystallographic laboratories to produce X-rays are of the sealed tubes or the rotating anode chambers. In these generators, a high voltage is supplied as a potential difference between an incandesce filament (cathode) and a pure metal (anode) generating an electrical current of free electrons between them. In this process, electrons jump form the incandescent filament to the anode causing the reorganization of the electronic energy levels of the atoms of the latter. The energetic restoration of the excited anodic electrons is carried out with an X-ray emission whose frequency corresponds exactly to the energy gap that the electron needs to return to its original state. Therefore, X-rays show a specific wavelength, the characteristic wavelength of the anode. Copper and molybdenum are the most frequently used anodes. In the rotating anode generators the anode is in the form of a cylinder that is maintained in a continuous rotation so that the incidence of electrons is distributed over its cylindrical surface and a higher X-ray intensity can be produced.

The process of X-ray production is done under vacuum because the presence of gas molecules decreases its efficiency by collations with the electrons in the beam. Also, this process generates a lot of heat and the X-ray generators need to be chilled.

Data processing

The electronic pictures generated by the detector are called frames and the individual elements of each picture are called pixels. The intensities from the area detector data are extracted via integrations. The computer that controls the goniometer and the detector also stores the raw frames which are then used to calculate the integrated intensities. This involves that the computer sequentially scans through each frame to build-up a 3-D image of each reflection putting a box around this constructed 3-D spot, while it tries to ensure that a minimal amount of background is contained within the box and not windowing out the reflection intensity. For each reflection, the summation of the detector counts registered in each pixel of the box yields the intensity of that reflection.

Diffraction intensity for a given hkl reflection is directly proportional with the square of the modulus of the structure factor, *F*, which is what we calculate in order to solve a structure. There are various factors that allow us to correct the measured intensities and thereby obtaining the modulus of *F*. Among these corrections, some are geometric and instrument specific corrections (Lorentz and polarization corrections) and some others are effects that depend on the material content and quality of the crystal (absorption and extinction). Lorentz correction is a consequence of the diffraction from some lattice planes can be measured for a longer time than others whereas polarization correction depends on the partial polarization of the incident X-ray beam and on the scattered angle of the diffracted beam. On the other hand, a sample can absorb some of the X-ray beam. This absorbance depends on the wavelength as well as the elemental make-up of the crystal and the path length of the X-rays through the crystal. Extinction correction takes into account that the lattice planes that are first encountered by the primary beam will reflect a significant fraction of the primary intensity so that deeper planes will receive less primary radiation. Also, it takes into account the loss of intensity due to dynamic effects inside the crystal.

1. 8. 3 Structure solution

The goal of the structural analysis of a single crystal is to obtain from the diffraction data the distribution of the atomic electron density in the unit cell. Since X-ray are scattered by the electrons of the crystal, what we are able to determine is the electron density distribution and from here we can then obtain the atomic positions in the

electron density map. However, we only need to determine the contents of one unit cell as the crystal structure is periodic and the presence of symmetry in the unit cell reduces this even further.

The electron density is a smoothly varying continuous function with a single numerical value (in units of electrons per cubic Angstrom) at each point in the structure. However, this is not a convenient function to work with and thus the structure is described in terms of atomic positions and atomic displacements (vibrations), each with its own electron density distribution about its centre. Moreover, the individual contributions of atoms to X-ray scattering are known as atomic scattering factors and are calculated from electron densities derived from quantum mechanics. These atomic scattering factors are known mathematical functions, varying with Bragg angle θ, available in published tables and incorporated in standard crystallography computer programs.

Each symmetry independent atom in the asymmetric unit of a crystal is described by its atomic scattering factor, the displacement parameters and three coordinates specifying its positions relative to the unit cell axes. The atomic displacements modify the diffraction pattern and cause the electron density to be spread out over a larger volume, usually unequally in different directions (anisotropic). This effect is described by a set of anisotropic displacement parameters for each atom, being expressed in the most commonly mathematical model by six anisotropic displacement parameters and represented graphically as an ellipsoid.

The crystal structure and its X-ray diffraction pattern are related to each other by the mathematical process of Fourier transformation so that each one is the Fourier transform of the other.[47] The diffraction pattern is a set of discrete reflections, each a wave with its own amplitude and relative phase. As stated above, the goal of crystals structure analysis is the determination of the distribution of atomic electron density in the unit cell starting from the diffraction data. However, this is not possible to reach in a unique and automatic way because from the experimental data only the amplitudes and not the phases of the structure factors can be obtained. The diffraction pattern is the Fourier transform of the electron density and its mathematical relationship is given by:

$$F(hkl) = \sum_{j=1}^{N} f_j \exp[2\pi i(hx_j + ky_j + lz_j)] \qquad (2)$$

where f_j is the atomic scattering factor for the jth atom in the unit cell, which has coordinates x_j, y_j, z_j. Here f_j incorporates the effect of atomic displacements in this equation. The integers h, k, and l are the indices of a family of planes for one particular reflection. What we can see in equation (2) is that each reflection in the diffraction pattern is a wave that is made up as a sum of the waves scattered by the individual atoms, each atom in accordance with its electron density distribution (f_j). As stated above, the relative phases of the waves scattered by the atoms in a particular direction have to be *in-phase* for diffraction to occur. Therefore, F(hkl) is a complex number with an amplitude and a phase with which, in order to obtain the diffraction pattern, the equation is applied for each reflection (each direction in which a discrete diffracted beam occurs) involving the sum of the N terms (the number of atoms in the unit cell). Equation (2) can also be used to calculate expected diffraction pattern and it is used at various stages during the crystal determination.

On the other hand, the electron density is the inverse Fourier transform of the structure factor:

$$\rho(x,y,z) = \frac{1}{V}\sum_{hkl} F(hkl)\exp[-2\pi i(hx + ky + lz)] \qquad (3)$$

Here the crystal structure is expressed as its electron density (e $Å^{-3}$) instead of being described by discrete atomic scattering factors and therefore the unit cell volume is included in the equation. In order to find the electron density at a particular point in the structure, all scattered X-ray waves (thus, reflections F) have to be added together. This equation is the basis that is used in Fourier synthesis calculations in crystallography.

As a result, if the modulus and phases of the structure factors are known, the atomic positions can be determined. Unfortunately, this is not possible to obtain directly from the diffraction intensities because only their amplitudes ($|F|^2$) and not their intrinsic phases can be known. This is the so-called crystallographic phase problem: how to identify the atomic positions starting only from the moduli of the structure factors. A general solution of the problem cannot be found although the problem can have a

solution since the measured intensities are proportional to the squares of the structure factors. There are methods that can solve the problem where the possibility of solving a system of non-linear equations relies on obtaining a first approximation solution, the initial structural model, and then this can be refined until the best agreement with experimental data is be achieved.

The modified versions of the electron density equation are used in the crystal structure determination and these are referred as Fourier synthesis or Fourier maps. They are variations of equation (3) which can be written in a different but equivalent way:

$$\rho(xyz) = \frac{1}{V}\sum_{hkl}|F(hkl)|\exp[i\phi(hkl)]\exp[-2\pi i(hx+ky+lz)] \qquad (4)$$

where the structure factor F has been separated into its amplitude$|F|$ and its phase. ϕ is the intrinsic phase of the wave itself (i.e. the structure factor) and (hx+ky+lz) is an extra phase shift for the position relative to the origin. The phase problem arises because the former is lost in the experiment. The different kinds of Fourier synthesis use a different coefficient instead of the amplitudes $|F|$. They are referred to the different methods used to solve the phase problem, being the Patterson Synthesis and Direct Methods the two most important. The former uses the coefficient $|F_o|^2$ instead of $|F_o|$, where F_o are the observed structure factors. This method also sets all phases equal to zero. The later uses $|E_o|$ which is the normalised observed structure factor amplitudes. They represent the diffraction pattern expected for point atoms of equal size with their electron density concentrated into a single point instead of spread out over a finite volume.

1. 8. 4 Patterson synthesis and Direct Methods

Patterson synthesis

In the Patterson synthesis the complex structure factors F(hkl) are replaced by the product of each one with its complex conjugate F^*(hkl) cancelling out the imaginary terms and giving a real number. This is to say that the amplitudes of equation (4) are replaced by their squares and the unknown phases are omitted (effectively, all set equal to zero).

$$P(uvw) = \frac{1}{V}\sum_{hkl}\left|F(hkl)^2\right|\cos[2\pi(hu + kv + lw)] \qquad (5)$$

By doing this replacement the result is that the function will not longer be the electron density distribution but it is closely related to it. From the available experimental data, the Patterson function can be immediately calculated. This function introduces a new space: the Patterson map where the peaks are not the position of individual atoms but vectors between pairs of atoms in the structure, the height of its maxima is proportional to the number of electrons of the atom implied. For every pair of atoms in the structure with coordinates (x_1,y_1,z_1) and (x_2,y_2,z_2) there will be a peak in the Patterson map at the position (x_1-x_2,y_1-y_2,z_1-z_2) and also one at the position (x_2-x_1,y_2-y_1,z_2-z_1), each one giving a vector to each other. Therefore a Patterson peak at (u,v,w) is a vector between two atoms whose x coordinates differ by u, z coordinates differ by v and y coordinates differ by w. Once the Patterson map is calculated then the absolute positions of the atoms (x,y,z) within the unit cell can be obtained and these positions can be used to obtain the unknown phases of the diffracted beams and finally calculate the electron density function.

The Patterson synthesis is usually used when the structure contains a few heavy atoms among many light atoms although it is also used when a significant proportion of the structure is expected to have a well defined rigid internal geometry, such as condensed aromatic rings, which will have several interatomic vectors with almost the same length and direction.

Direct Methods

On the other hand, the phase problem for small and medium size molecules can be solved by using the Direct Methods. The phase and the amplitude of the wave are independent quantities but Direct Methods assumes that there is information about the phases contained in the structure factor amplitudes.[48] These methods try to derive the structure factor phases directly from the observed amplitudes through mathematical relationships using constrains or statistical correlations between the phases of different Fourier components. Thereby, two important properties of the electron density function have been considered in order to develop these mathematical relationships: firstly, the

structure is composed of discrete atoms and secondly, the electron density must be positive or equal to zero at any point of the unit cell. These properties create some limitations in the distribution of phases associated with the structure factors and direct methods establish systems of equations that describe these limitations.

The most important relationship that Direct Methods uses is the structure invariants. The amplitudes of the structure factors are independent on the chosen origin and thus they only depend on the structure, whereas the phases depend on it. Because of that, structure factor amplitudes are called structure invariants. The product of structure factors will be invariant to an origin if the sum of their phases is zero and therefore with the combination of structure factors that satisfies this relationship new invariants can be obtained. Direct methods generate phases starting from a random phase set in order to satisfy the stated relationship.

Moreover, Direct Methods work with structure factors that have been modified in order to behave as showing the scattering from point atoms located at the same positions as the original atoms and the amplitudes of the structure factors of the electron density function are changed by the normalised observed structure factors, $|E_o|$. In addition, only the strongest E values of the whole data set are used to find the initial model of the structure since this data contains the most information about the locations of the atoms.

1. 8. 5 Completing and refining the structure

The structural models obtained from the first electron density map, in both by Patterson and direct methods, are often incomplete and in all cases they only represent a first approximation of the real structure. However, this set of atoms usually contains sufficient phase information to locate the remaining atoms. From the atoms and relative positions of the initial model (the calculated phase angles and the observed structure factors) a set of structure factors are calculated and an electron density map is obtained. Difference maps are calculated using ($|F_o|$ - $|F_c|$) coefficients and the result is an electron density map where the features of the previous model are removed, peaks where not enough amount of electron density has been placed will appear as well as negative electron density holes where too much electron density has been modelled. New atoms are then included in the model and this cycling process is repeated until all non-hydrogen atoms are located.

Once all atoms have been located the model is then refined in order to adjust the values of the parameterised model. The parameters being refined in a crystal structure are the positional and the vibrational parameters for each atom. As above mentioned, atoms are described by their positional coordinates in the unit cell (x,y,z) and their atomic displacements. Atomic displacement parameters are a consequence of the thermal motion which makes the electron density around the atom to become wider. When atoms are described as an isotropic (spherical) structural model they are represented by four variables (three positional and one thermal variable). Moreover, when atoms are expressed in an anisotropic structural model where the different directions of the vibrations are described in the form of an ellipsoid; librational variables are added and thus six thermal variables are associated to each atom. This model affords very precise geometrical parameters of the structure (interatomic distances, angles, etc.). In addition to these atomic parameters, an overall scale factor is refined. This scale factors account for several items from the size of the crystal to intensity of the radiation source.

The most widely used model to carry out the refinement is the Least-squared method. In order to minimise the differences between the calculated and the observed structure factors the minimisation of the following function (6) is carried out using several cycles of refinement until convergence is achieved.

$$\Sigma\, w\, (|F_o| - |F_c|)^2 \rightarrow 0 \qquad (6)$$

The weight, *w*, represents the relative influence that an observation should have in the results. The observations that are believed to be unreliable or less precise, such as high-angle weak reflections, get very small weights compared with more accurate ones and consequently possible systematic errors in the experimental observations can be avoided. Several weighting functions (*w*) have been proposed but in our case the following weighting scheme was employed:

$$w = \frac{1}{\sigma^2(F_o^{\,2}) + (aP)^2 + bP} \qquad (7)$$

where $P=(F_o^2+2F_c^2)/3$ and a and b are adjustable parameters that are chosen to give an even distribution of the variances across all groups of data based on the relative intensities.

During the refinement process, the calculated diffraction pattern model (F_c) with the positional and vibrating parameters included, will show increasing similarity to the observed pattern (F_o). One way to know how good the former model fits with the observed data is to following calculate discrepancy factors:

$$R_1 = \sum \frac{\left(|F_o| - |F_c|\right)}{\sum F_o} \qquad (8) \qquad \text{and} \qquad wR_2 = \left\{ \frac{\sum \left[w\left(F_o^2 - F_c^2\right)\right]^2}{\sum w\left[F_o^2\right]^2} \right\}^{1/2} \qquad (9)$$

The R_1 defines the disagreement factor of a structural model in terms of differences between the calculated and the observed diffraction pattern. The wR_2 is a weighted R factor based on all data and R_1 is based only on the observed data, $F_o > 2\sigma(F_o)$. For small or medium size structure giving good quality crystals we would expect values of 0.03-0.07 for the former and 0.10-0.19 for the later. In addition, the *goodness of fit*, S, gives an indication on how reliable the standard deviations of the positional and displacement parameters of the atoms really are

$$Goff = S = \left\{ \frac{\sum \left[w\left(F_o^2 - F_c^2\right)\right]^2}{n - p} \right\}^{1/2} \qquad (10)$$

where n is the number of reflections and p is the total number of parameters refined.

[1] MAGMANet (Molecular Approach to Nanomagnets and Multifunctional Materials): network of excellence. http://www.magmanet-eu.net. *Date of access*: *April 10, 2010.*
[2] J. S. Miller, J. C. Calabrese, A. J. Epstein, R. W. Bigelow, J. H. Zang, W. M. Reiff, *J. Chem. Soc. Chem. Commun,.,* **1986**, 1026.
[3] J. S. Miller, J. C. Calabrese, H. Rommelman, S. R. Chittipedi, J. H. Zang, W. M. Reiff, A. J. Epstein, *J. Am. Chem. Soc.,* **1987**, *109*, 769.
[4] Y. Pei, M. Verdaguer, O. Kahn, J. Sletten, J.-P. Renard*, J. Am. Chem. Soc.,* **1986**, *108*, 428.
[5] O. Kahn, Y. Pei, M. Verdaguer, J.-P. Renard, J. Sletten, *J. Am. Chem. Soc.,*. **1988**, *110*, 782.
[6] O. Kahn, *Adv. Inorg. Chem*., **1995**, *43*, 179
[7] H. O. Stumpf, J L. Ouahab, Y. Pei, P. Bergerat, O. Kahn, *J. Am. Chem. Soc*., **1994**, *116,* 3866

[8] E. Pardo, R. Ruiz-García, J. Cano, X. Ottenwaelder, R. Lescouëzec, Y. Journaux, F. Lloret, M.Julve, *Dalton Trans.* **2008**, 2780; and references therein.
[9] H. O. Stumpf, Y. Pei, O. Kahn, J. Sletten, J. P. Renard, *J. Am. Chem. Soc.,* **1993**, *115*, 6738
[10] D. K. Rittenberg, K-I Sugiura, Y. Sakata, S.i Mikami, A. J. Epstein, J. S. Miller, *Adv. Mater*., **2000**, *12*, 126; (b) J. S. Miller, *Adv. Mater*., **2002**, *12*, 1105
[11] D. J. Price, S. Tripp, A. K. Powell, P. T. Wood*, Chem. Eur. J*., **2001**, *7*, 1
[12] A.Caneschi, D.Gatteschi, J.P.Renard, P.Rey, R.Sessoli, *Inorg. Chem*., **1989**, *28*, 3314
[13] R. Sessoli, D. Gatteschi, A. Caneschi and M. A. Novak, *Nature,* **1993**, *365*, 141.
[14] R. Sessoli, H. L. Tsai, A. R. Schake, S. Y. Wang, J. B. Vincent, K. Folting, D. Gatteschi, G. Christou, D. N. Hendrickson*, J. Am. Chem. Soc.,* **1993**, *115*, 1804
[15] R. Bagai and G. Christou*, Chem. Soc. Rev.,* **2009**, *38*, 1011
[16] C. J. Matthews, S. T. Onions, G. Morata, L. J. Davis, S. L. Heath, D. J. Price*, Angew. Chem. Int. Ed.,* **2003**, 42, 3166
[17] (a) O. Kahn, *Molecular Magnetism*, VCH, Weinheim, **1993**; (b) A. Aukauloo, X. Ottenwaelder, R. Ruiz, Y. Journaux, Y. Pei, E. Revière, M. Muñoz, *Eur. J. Inorg. Chem*., **2000**, 951; (c) T. Rüffer, B. Bräuer, A. K. Powell, I. Hewitt, G. Salvan, *Inorg. Chim. Acta,* **2007**, *360*, 3475; (d) Y. Pei, Y. Journaux, O. Kahn, *Inorg. Chem.,* **1988**, *27*, 399; (e) Y. Pei, Y. Journaux, O. Kahn, *Inorg. Chem,*. **1989**, *28*, 100. M. Mitsumi, H. Okawa, H. Sakiyama, M. Ohba, N. Matsumoto, T. Kurisaki, H. Wakita, *J. Chem. Soc., Dalton Trans.,* **1993**, 2991; (f) Y. Pei, Y. Journaux, O. Kahn, A. Dei, D. Gatteschi, *J. Chem. Soc., Chem. Commun.,* **1986**, 1300; (g) J. Ribas, C. Diaz, R. Costa, Y. Journaux, C. Mathonière, O. Kahn, A. Gleizes, *Inorg. Chem.,* **1990**, *29*, 2042
[18] I. Unamuno, J. M. Gutiérrez-Zorrilla, A. Luque, P. Román, L. Lezama, R. Calvo, T. Rojo, *Inorg. Chem.,* **1988**, *37*, 6452
[19] (a) B. Cervera, J. L. Sanz, M. J. Ibañez, G. Vila, F. Lloret, M. Julve, R. Ruiz, X. Ottenwaelder, A. Aukauloo, S. Poussereau, Y. Journaux, M.C.Muñoz, *J. Chem. Soc., Dalton Trans.,* **1998**, 781; (b) A. Aukauloo, X. Ottenwaelder, R. Ruiz, Y. Journaux, Y. Pei, E. Rivière, B. Cervera, M. C. Muñoz, *Eur. J. Inorg. Chem.,* **1999**, 209; (c) A. Aukauloo, X. Ottenwaelder, R. Ruiz, S. Poussereau, Y. Pei, Y. Journaux, P. Fleurat, F. Volatron, B. Cervera, M. C. Muñoz, *Eur. J. Inorg. Chem.,* **1999**, 1067; (d) K. E. Berg, Y. Pellegrin, G. Blondin, X. Ottenwaelder, Y. Journaux, M. M. Canovas, T. Mallah, S. Parsons, A. Aukauloo, *Eur. J. Inorg. Chem.,* **2002**, 323; (e) X. Ottenwaelder, R. Ruiz-García, G. Blondin, R. Carrasco, J. Cano, D. Lexa, Y. Journaux and A. Aukauloo, Chem. Commun., **2004**, 504
[20] (a)Y. Pei,, Y. Journaux, O. Kahn. A. Dei, D. Gatteschi, *J. Chem. Soc., Chem. Commun.* **1986**, *16*, 1300. b) Y. Pei, Y. Journaux and O.Kahn, *Inorg. Chem.*, **1988**, *27*, 399; (c) J. Ribas, C. Díaz, R. Costa, Y. Journaux, C.Mathonière, O. Kahn, A. Gleizes, *Inorg. Chem.*, **1990**, *29*, 2042; (d) R. Vicente, A. Escuer, J. Ribas, *Polyhedron*, **1992**, *11*, 857; (e) R. Costa, A. García, J. Ribas, T.Mallah, Y. Journaux, J. Sletten, X. Solans, *Inorg. Chem.*, **1993**, *32*, 3733; (f) O. Guillou, R. L. Oushoorn, O. Kahn, K. Boubekeur, P. Batailm, *Angew. Chem. Int. Ed.,* **1992**, *31*, 626; (g) O. Guillou, C. Daiguebonne, M. Camara, N. Kerbellec, *Inorg.Chem.,* **2006**, *45*, 8468
[21] A. Aukauloo, X. Ottenwaelder, R. Ruiz, Y. Journaux, Y. Pei, E. Rivière, M. C. Muñoz, *Eur. J. Inorg. Chem*., **2000**, 951
[22] C. L. M. Pereira, E. Pedroso, H. O. Stumpf, M. A. Novak, L. Ricard, R. Ruiz-Garcia, E. Rivière, Y. Journaux, *Angew. Chem., Int. Ed,*. **2004**, *43*, 956
[23] X. Ottenwaelder, J. Cano, Y. Journaux, E. Rivière, C. Brennan, M. Nierlich, R. Ruiz-García, *Angew. Chem., Int. Ed,*. **2004**, *43*, 850
[24] E. Pardo, R. Ruiz-García, F. Lloret, J. Faus, M. Julve, Y. Journaux, M. A. Novak, F. S. Delgado, C. Ruiz-Pérez, *Chem. Eur. J.*, **2007**, *13*, 2054
[25] C. L. M. Pereira, E. Pedroso, H. O. Stumpf, M. A. Novak, L. Ricard, R. Ruiz-García, E. Rivière, Y. Journaux, *Angew. Chem., Int. Ed.,* **2004**, *43*, 956
[26] E. Pardo, D. Cangassu, M.-C. Dul, R. Lescouëzec, P. Herson, Y. Journaux, E. F. Pedroso, C. L. M. Pereira, M. C. Muñoz, R. Ruiz-García, J. Cano, P. Amorós, M. Julve, F. Lloret, *Angew. Chem., Int. Ed.,* **2008**, *47*, 4211
[27] M. Murrie and D. J. Price, *Annu. Rep. Prog. Chem., Sect. A,* **2007**, *103*, 20
[28] T. Rüffer, B. Bräuer, B. Walfort*, Inorg. Chem. Commun.,* **2006**, *9*, 1111
[29] P. Comba, S. P. Gavrish, Y. D. Lampeka, P. Lightfoot, A.Peters, *J. Chem. Soc*., *Dalton Trans*., **1999**, 4099
[30] W. Gaade, *Recl. Trav. Chim. Pay-B*, **1936**, *55*, 325.
[31] K. Nonoyama, H. Ojima, M. Nonoyama, *Inorg. Chim. Acta***, 1976**, *20*, 127
[32] B. Cervera, J.L. Sanz, M.J. Ibañez, G. Vila, F. Lloret, M. Julve, R. Ruiz, X. Ottenwaelder, A. Aukauloo, S. Poussereau, Y. Journaux, M.C. Muñoz, *J. Chem. Soc*., *Dalton Trans.*, **1998**, 781
[33] H. Ojima, K. Nonoyama, *Coord. Chem. Rev.,* **1988,** *92,* 85

[34] R. Ruiz, J. Faus, F. Lloret, M.Julve, Y. Journaux, *Coord. Chem. Rev.,* **1999**, *193–195*, 1069
[35] K. E. Berg, Y. Pellegrin, G. Blondin, X. Ottenwaelder, Y. Journaux, M. Moragues Canovas, T. Mallah, S. Parsons, A. Aukauloo, *Eur. J. Inorg. Chem.,* **2002**, *323-325*, 1434
[36] H. Sigel and R. B. Martin, *Chem. Rev.*, **1982**, 82 (4), 385
[37] K. Nonoyama, H. Ojima, M. Nonoyama, *Inorg. Chim. Acta***, 1976**, *20*, 127
[38] B. Cervera, J.L. Sanz, M.J. Ibañez, G. Vila, F. Lloret, M. Julve, R. Ruiz, X. Ottenwaelder, A. Aukauloo, S. Poussereau, Y. Journaux, M.C. Muñoz, *J. Chem. Soc*., *Dalton Trans.*, **1998**, 781
[39] K. Nonoyama, H. Ojima, M. Nonoyama, *Inorg. Chim. Acta***, 1976**, *20*, 127
[40] T. Rüffer, B. Bräuer, F. E. Meva, B. Walfort, *Dalton Trans.*, **2008**, 5089
[41] H. Ojima, K. Nonoyama, *Coord. Chem. Rev.,* **1988**, *92,* 85
[42] Z.N. Chen, S. X. Liu, J. Qiu, Z. M. Wang, J. L. Huang, W. X.Tang**,** *J. Chem. Soc., Dalton Trans.***, 1994**, 2989
[43] J. W. Ziller and A.L. Rheingold, **1992**, "X-ray Crystallography". In: Russell S Drago, *Physical Methods for chemists*, 2nd ed. Orlando: Harcourt Brace Jovanovich college Publishing. 689-712
[44] C. Giacovazzo (editor), **2002**, *Fundamentals of Crystallography,* 2nd ed. Oxford University Press.
[45] P. J. Schields. Bragg's Law and Diffraction: How waves reveal the atomic structure of crystals. Department of Earth & Space Sciences, State University of New York at Stony Brook. http://www.eserc.stonybrook.edu/ProjectJava/Bragg. *Last modified: December 4, 2007*.
[46] Crystallography. Department of Crystallography, Instituto de Química-Física Rocasolano (CSIC), Madrid. http://www.xtal.iqfr.csic.es/Cristalografia. *Last modified: February 10, 2010*.
[47] The 10th BCA/CCG Intensive Teaching School in X-ray Structure Analysis, 2005, Durham
[48] Crystallography, Notes and Manuals. Chemical Crystallography Laboratory, University of Oklahoma. http://xrayweb.chem.ou.edu/index.html. *Last modified: December 10, 2010*

Chapter 2: Ligands and Precursors

2. 1 Introduction

2. 1. 1 Diethyl ethylene–1,2–dioxomate, Et_2H_2(oeo) (1)

The synthesis of diethyl ethylene-1,2-dioxamate ligand, Et_2H_2(oeo) **(1)**, was optimized from the reported bis(oxamato) synthesis.[1,2] Gaade already synthesised the compound in 1936 using ethylendiamine and seven equivalents of diethyloxalate at low temperatures.[3] However, the addition and five and six equivalents of diethyloxalate to an ethanol solution of ethylendiamine and the later warming of the mixture in a water bath for several hours afforded an easier and cheaper synthesis method maintaining good yields (Scheme 2.1). Afterwards, when the solution was cooled down to room temperature, the white solid that formed was filtered and washed several times in ethanol. Recrystallisation of the product using different organic solvents was also carried out but very low yields were obtained due to the solubility of the product in the solvents and thus better results were obtained when the solid was washed with ethanol.

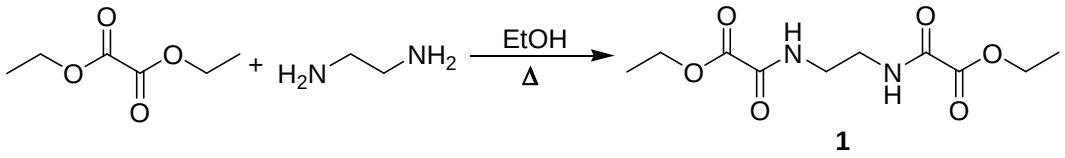

1

Scheme 2. 1

Several crystallisation techniques were attempted to grow crystals of **1** in common organic solvents at room temperature but no big crystals were obtained. This is probably a consequence of the intermolecular hydrogen bonding between the amide hydrogen and the carbonyl oxygen atoms that also makes **1** be soluble in common organic solvents only at high temperatures. Eventually, crystals of **1** were formed from the filtrate of one of the synthesis of the compound after several days.

2. 1. 2 Saponification of Et_2H_2(oeo). Synthesis of M_2H_2(oeo) M=alkali metals

Hydrolysis of the esters of **1** was attained when two equivalent of the corresponding base were added to a solution of **1** that was dissolved in ethanol and heated in a water

bath (Scheme 2.2). The white solid that was then formed was collected by filtration and dried in air.

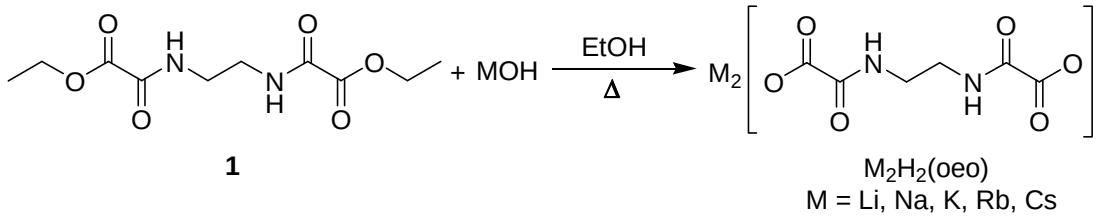

1

M_2H_2(oeo)
M = Li, Na, K, Rb, Cs

Scheme 2. 2

The same procedure was followed to obtain salts of all stable alkali metals of **1.** Full characterisation was carried out on the initial synthesis of the salts. However, the purity of the final compounds was only checked by NMR measurements since the alkali metal that was used on the base was the only component that was changed from one synthesis to another.

It has been noted that a slight of excess of base (~5%) must be added to **1** to avoid the formation of a coproduct as a result of the single cleavage of the ester linkage of the starting material. For instance, potassium ethyl ethylene-1,2-dioxamate, $KEtH_2$(oeo) **(4b)**, can be achieved by the partial hydrolysis of **1** and can be isolated since it has a lower solubility in water than the dianion. Moreover, **4b** can be fully characterised by NMR measurements (^{1}H-NMR and ^{13}C-NMR) and can be seen as an impurity in the synthesis of dipotassium ethylene-1,2-dioxamate salt, K_2H_2(oeo) **(4a)**. In the case presented here, the final product was obtained as a mixture of **4a** and **4b** existing as 4:1. The impurity is not an obstacle for using the sample as reagent for the synthesis of the copper dimer since more base will be added and the full cleavage of the mono salt will be achieved. Single crystals of **4a** (**4a**·H_2O) were achieved by slow solvent diffusion of methanol into an aqueous solution of **4a**.

The species formed due to the single cleavage of **1** was also observed in the NMR measurement of the final product of the synthesis of dilithium ethylene-1,2-dioxamate, Li_2H_2(oeo) **(2a)**, as a result of the addition of only two equivalents of base. In this case, the amount of base added was higher than the amount added in the synthesis of **4b** and therefore, less amount of lithium ethyl ethylene-1,2-dioxamate, $LiEtH_2$(oeo) **(2b)**, was obtained (50:1). On the other hand, single crystals of **2a** (**2a**·$2H_2O$) were grown as a by-

product of the synthesis of the microcrystalline solid of $Li_4[Cu(oeo)]_2 \cdot nH_2O$ in methanol and water (See Chapter 4).

Crystal structures of **2a**$\cdot 2H_2O$ and **4a**$\cdot H_2O$ have similar crystal lattices. They are built by one doubly deprotonated ligand molecule, $[H_2(oeo)]^{2-}$, two cations, and two or one water molecules, respectively. They both display a layered structure where cationic layers of the metal are alternated with anionic organic layers. As in compound **1**, the ethylenediamine fragment displays an *anti* conformation. The cyclic hydrogen bond $R^2_2(10)$ motif that connects two oxamato groups of two neighbouring ligands leading to the formation of the organic layer can be observed in both structures.[4] The main difference between the two species is the environment of the cations in the crystal lattice since the lithium atoms have a distorted squared-pyramid coordination and the potassium cations have a pentagonal bypiramidal or a square antiprismatic geometry. However, lithium and potassium ions are both coordinated to oxygen atoms of the water molecules or the carbonyl oxygen atoms of the ligand.

In the synthesis of disodium ethylene-1,2-dioxamate, $Na_2H_2(oeo)$ **(3)**, and the synthesis of dicaesium ethylene-1,2-dioxamate, $Cs_2H_2(oeo)$ **(6)**, the product obtained did not contain the by-product as a result of the single hydrolysis of **1.** In both syntheses an excess of base (4%) was added to the starting material. Several attempts of growing single crystal of $Na_2H_2(oeo)$ were attempted but the crystals obtained were too small for X-ray analysis.

Finally, in the preparation of dirubidium ethylene-1,2-dioxamate, $Rb_2H_2(oeo)$ **(5a)**, the formation of rubidium ethyl ethylene-1,2-dioxamate, $RbEtH_2(oeo)$ **(5b)**, was also observed in the ^{1}H-NMR measurement of the final product existing as 3:1, respectively. The attempt of crystal growing of **5a** was also carried out but no suitable single crystals for X-ray analysis were obtained.

2. 1. 3 Transmetallation of $M_2H_2(oeo)$ with transition metals. Synthesis of $M'H_2(oeo)$ M'=Cu(II), Co(II), Ni(II)

Once the alkali metal salt of diethyl ethylene-1,2-dioxamate, $M_2H_2(oeo)$, was obtained, transmetallation of the salt was attained by addition of an aqueous solution of

$CuCl_2 \cdot 2H_2O$ to a solution of $M_2H_2(oeo)$ in water giving rise to the precipitation of a turquoise solid with a $CuH_2(oeo) \cdot n(H_2O)$ composition.

Depending on the synthetic conditions of $CuH_2(oeo) \cdot n(H_2O)$, three structurally distinct phases have been observed. Rapid addition of concentrate $CuCl_2 \cdot 2H_2O$ solution to the reaction solution gives rise to the formation of an amorphous solid, **(7a)**, with no Bragg peaks in the PXRD measurements but four broad bands. According to microanalysis measurements **7a** precipitates with three water molecules. On the other hand, slower addition rates of a $CuCl_2 \cdot 2H_2O$ solution to a less concentrated solution of the alkali metal salt of diethyl ethylene-1,2-dioxamate, $M_2H_2(oeo)$, resulted on a microcrystalline phase, **(7b)**, which while showing an similar IR spectra to **7a** but with more marked peaks, it shows distinct Braggs peaks in the PXRD measurements. According to microanalysis measurements **7b** also precipitates with three water molecules.

In very slow reactions in which components come together under conditions of slow diffusion, such as in gel tubes, afforded a crystalline phase, copper ethylene-1,2-dioxamate dihydrate, $CuH_2(oeo) \cdot 2H_2O$ **(7c)**. Simulation of the powder diffractogram from the single crystal data of **7c**, showed that the reflections positions and intensities matched well with the powder diffraction recorded for **7b**. The conditions in which suitable crystals for X-ray analysis are grown are very narrow. Quite a lot of attempts to obtain crystals of **7c** were carried out changing the proportions of the reagents in the gel tubes or in the H-shaped tubes, most of them resulting in the formation of a partial crystalline solid. Big enough crystals of **7c** were eventually obtained when equal proportions of reagents came together in gel tube conditions after six months (Figure 2.1).

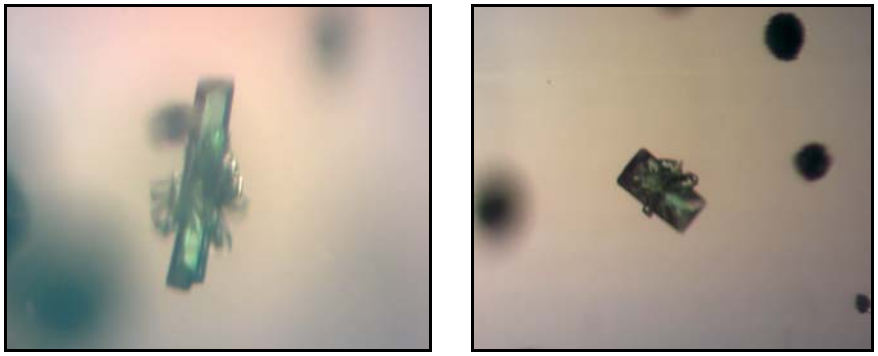

Figure 2. 1 Pictures of the turquoise crystals of **7c** in the gel tubes.
Approximate scale: width of image 1mm.

Crystals of the cobalt salt of ethylene-1,2-dioxamate, CoH_2(oeo), were also obtained. However, they were grown with one DMSO molecule of crystallisation, CoH_2(oeo)·DMSO **(8)**, since they were obtained from a different procedure. Slow solvent diffusion into a mixture solution of $(n\text{Bu}_4\text{N})_x[\text{Cu(oeo)}_y]$ in water and $CoCl_2 \cdot 6H_2O$ in DMSO afforded single crystals of **8**. The aim of this synthesis was the preparation of transition bimetallic bis(oxamato) complexes using the copper(II) ethylene-1,2-dioxamato as building block. On the other hand, the attempt of CoH_2(oeo) crystal growing using gel tubes was carried out with no success.

Crystal structures of **7c** and **8** are neutral dimeric species of the metal and the ligand molecule. They both contain in the asymmetric unit one metal ion, one doubly deprotonated ligand molecule $[H_2(\text{oeo})]^{2-}$ and one solvent molecule. The whole dimer is generated by the inversion centre present in the mid-point of the dimeric units. The two oxamato groups of the ligand molecules are in both structures chelating towards the metal ion through the carboxylate oxygen and the carbonyl amide giving rise to a *trans* conformation of the oxamato group.

Each metal ion is hexacoordinated with four oxygen atoms arising from the two oxamate groups, one solvent molecule and one carbonyl oxygen from a neighbouring dimer. The latter connects the dimeric units into a 3-D network. However, while **7c** displays a *trans* conformation through the two oxamato units in the copper environment, **8** adopts a *cis* environment around the cobalt. The inversion centre present in the middle point of the dimer in **8** relates the two enatiomers (Λ and Δ) present in the dimer by symmetry. Moreover, the conformation that ethylendiamine group adopts in each structure is different. In **7c**, the group adopts an *anti* conformation whereas in **8**, displays a *gauche* configuration. Consequently, the different conformations around the metal ion as well as in the ethylendiamine groups result in dimers with two different morphologies.

The interaction between dimers in the crystal lattice through hydrogen-bonding is also different as a result of the distinct morphologies of the dimers and the different crystallisation solvents used. However, the classical interaction between two oxamato groups of two different dimers involving N2-H2 and O5 forming the cyclic $R^2_2(10)$ motif,[4] is present in both crystal lattices.

It has been noted that the type of cyclic motif $R^2_2(10)$ is very common in the salts of diethyl ethylene-1,2-dioxamate when connecting ligand molecules in the crystal lattice. It can also link dimeric units of the salt in three dimensions as in previously mentioned species. In addition, we will see in future chapters, that this type of motif can link the two organic molecules present in the $[Cu(oeo)]_2^{4-}$ complex.

Finally, the transmetallation of the alkali salt of diethyl ethylene-1,2-dioxamate using Ni(II) was also carried out. The crystalline phase of $NiH_2(oeo)\cdot 3H_2O$ **(9)**, was obtained although the attempt of crystal growing using gel tubes failed.

2. 2 Results

2. 2. 1 Description of structure of $Et_2H_2(oeo)$ (1)

Compound **1** forms monoclinic centrosymmetric crystals which crystallise in the space group $P2_1/c$ containing two molecules per unit cell. Thus, only one half of the molecule is found in the asymmetric unit and the other half is generated by symmetry through an inversion centre in the mid-point of the ethylenediamine C-C bond. The ethylendiamine group displays an *anti* conformation (Figure 2.2).

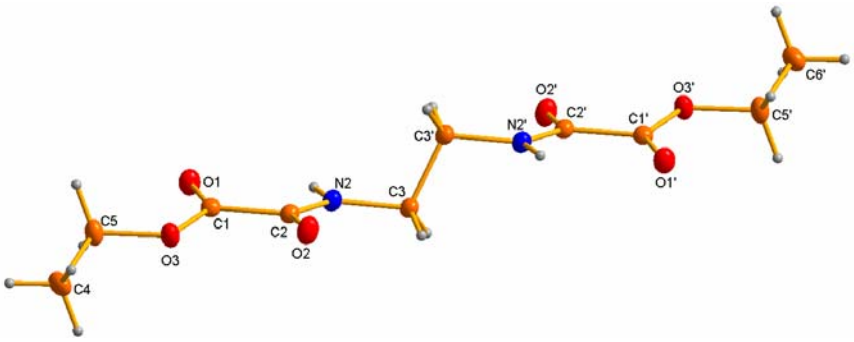

Figure 2. 2 Diamond-plot (50% of probability level) of the molecular structure of **1** with atom numbering scheme. Prime denotes symmetry operation 1-x, -y, 1-z.

Each molecule is linked to four neighbouring molecules through hydrogen bonds between the amide nitrogen and the amide carbonyl oxygen of the neighbouring molecule forming a D motif (Figure 2.3).[4]

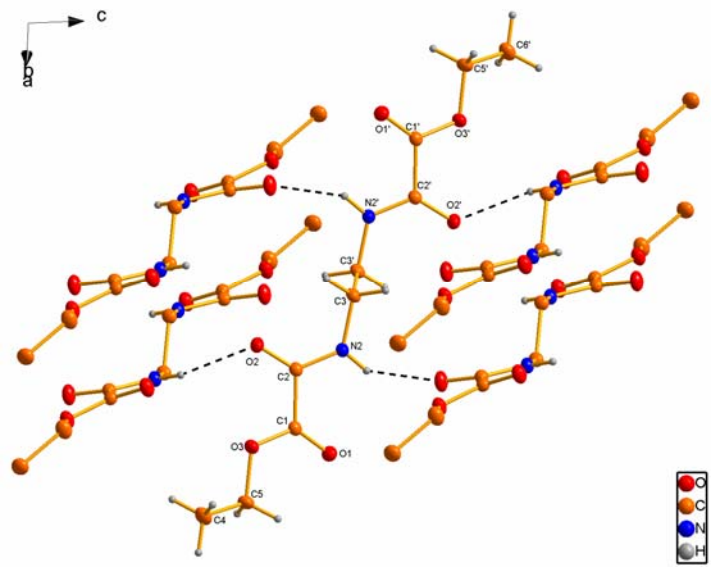

Figure 2. 3 Perspective view of the crystal packing of **1** showing hydrogen bonds (dashed lines) between neighbouring molecules. Alkyl hydrogen atoms of the neighbouring molecules are omitted for clarity.

This hydrogen bonding gives a 2-D layered pattern along the *ac*-plane. The outer surface of the layer is made of the hydrophobic ethyl groups, resulting from the weak interlayer interactions and the platy morphology of the crystals (Figure 2.4).

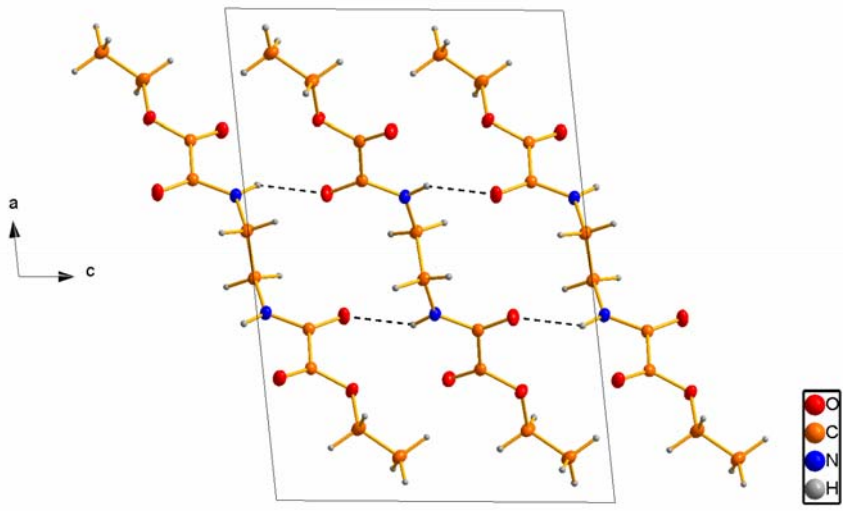

Figure 2. 4 Perspective view of structure **1** along the *b*-axis showing the hydrogen bonging (dashed lines) between neighbouring molecules.

2. 2. 2 Description of structure of $Li_2H_2(oeo)\cdot 2H_2O$ ($2a\cdot 2H_2O$)

Compound $\mathbf{2a}\cdot 2H_2O$ crystallises in the monoclinic space group $P2_1/c$. The asymmetric unit is formed by half of the ligand molecule, $[H_2(oeo)]^{2-}$, one lithium ion and one water molecule. As in compound **1**, the other half of the ligand is generated by symmetry through the inversion centre in the mid-point of the ethylenediamine C-C bond of the

organic molecule, leading to an *anti* conformation of the diamine (Figure 2.5). The lithium atom has a distorted square-pyramidal geometry having a chelating oxamate group coordinated through two carbonyl oxygens, one carboxylate oxygen of a neighbouring ligand and two water molecules.

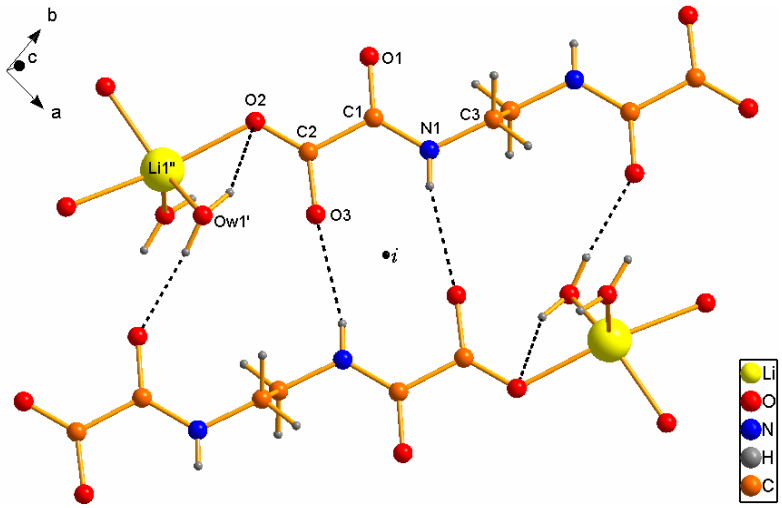

Figure 2. 5 Schematic view of **2a·2H$_2$O** with atom numbering scheme showing the hydrogen bonds network (dashed lines). Atoms are drawn using isotropic thermal parameters. Prime denotes -1+x, 0.5-y, -0.5+z and double prime denotes -1+x, -1+x, -1+z.

The packing in the *ac*-plane can be described as alternating layers of lithium ions and organic ligands along the *a*-axis (Figure 2.6). The molecules of the organic layer are linked through H-bonds between two oxamato groups of neighbouring molecules leading to an organic chain along the *b*-axis (Figure 2.5). This pattern of hydrogen bonging displays a cyclic $R^2_2(10)$ motif which has an inversion centre in the middle point of the motif relating the hydrogen-bonds by symmetry.[4]

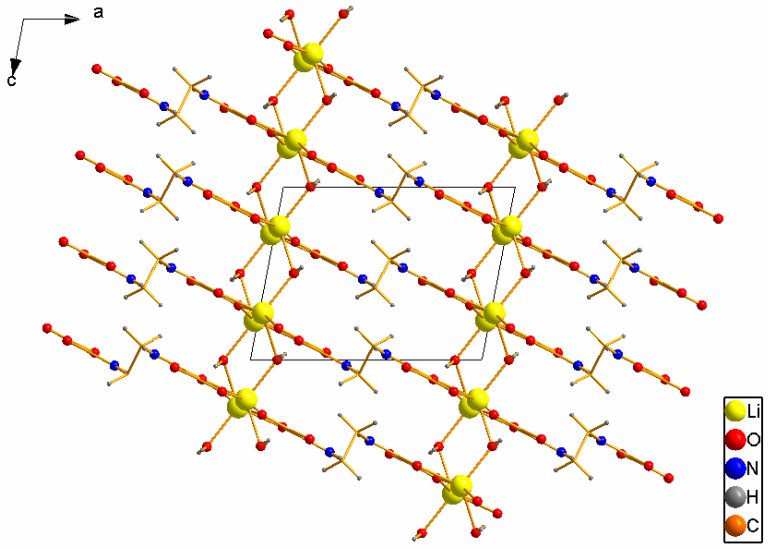

Figure 2. 6 Crystal packing of **2a·2H$_2$O** along the *ac*-plane.

Due to the *anti* conformation of the ethylenediamine fragment the organic layer displays a ladder shaped organic chain. The water molecule Ow1 connects lithium cations and organic layers along the *c*-direction. The directional hydrogen bonds between Hw1A and the carbonyl amide oxygen (O2) of the above neighbouring ligand and Hw1B and the carboxylate oxygen of the below close ligand (O1) connect these organic layers.

2. 2. 3 Description of structure $K_2H_2(oeo)\cdot H_2O$ (4a·H_2O)

The potassium salt of diethyl ethylene–1,2–dioxamate, $K_2H_2(oeo)\cdot H_2O$ **(4a**·H_2O**)**, crystallises in the non-centrosymmetric monoclinic space group *Cc*. The crystal, as common in such polar space groups, has a merohedral twinning having a 38(3)% of inverted structure. The asymmetric unit contains one doubly hydrolised ligand molecule, $[H_2(oeo)]^{2-}$, two potassium ions and one water molecule. Both potassium ions are only coordinated by oxygen atoms in different geometries. K1 is coordinated by four oxamate groups from different nearby organic molecules providing a square antiprismatic environment. On the other hand, K2 has pentagonal bypiramidal geometry where the ion is coordinated by four different organic molecules which all provide a monodentate coordination to the cation, except one that is chelating through a carboxylate group. The two remaining sites are occupied by crystallisation waters (Figure 2.7).

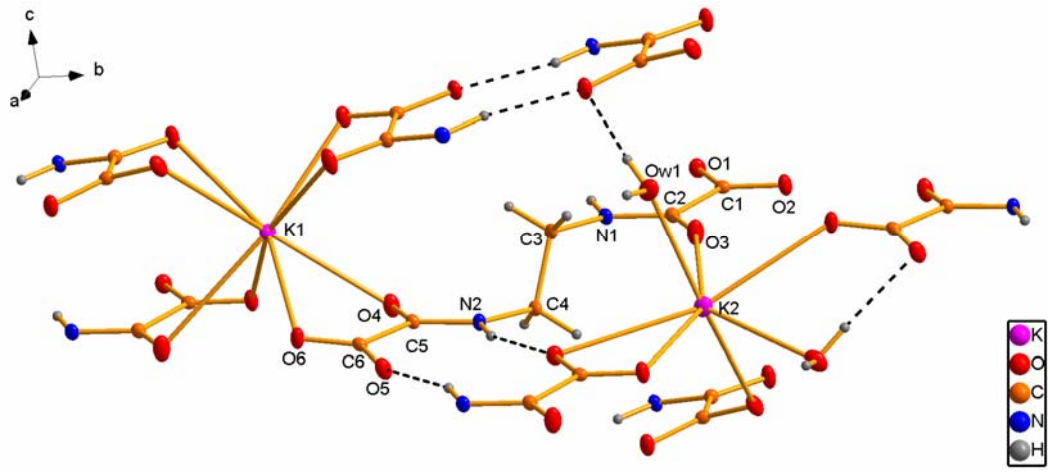

Figure 2. 7 Schematic view of the potassium environments with atom numbering scheme. Thermal ellipsoids are drawn at the 50% of probability level.

The packing in the *bc*-plane can the described as alternating layers of potassium ions and organic ligands in which, as in the lithium salt crystal structure, the ligands are

linked through H-bonds between oxamato groups of two neighbouring molecules forming an organic chain in the *a*-axis direction (Figure 2.8). In this organic pattern, the hydrogen bonding forms a cyclic $R^2_2(10)$ motif (Figure 2.9).[4] The ethylenediamine is in an *anti* conformation which, in addition with the hydrogen bond motif, forms a ladder shaped-organic chain. The water molecule has two directional hydrogen bonds to two carbonyl oxygens forming a $R^2_1(11)$ motif. Hw1B is hydrogen bonded to a carboxylate carbonyl oxygen and Hw1A is hydrogen bonded to a carbonyl oxamate oxygen of two neighbouring ligands.

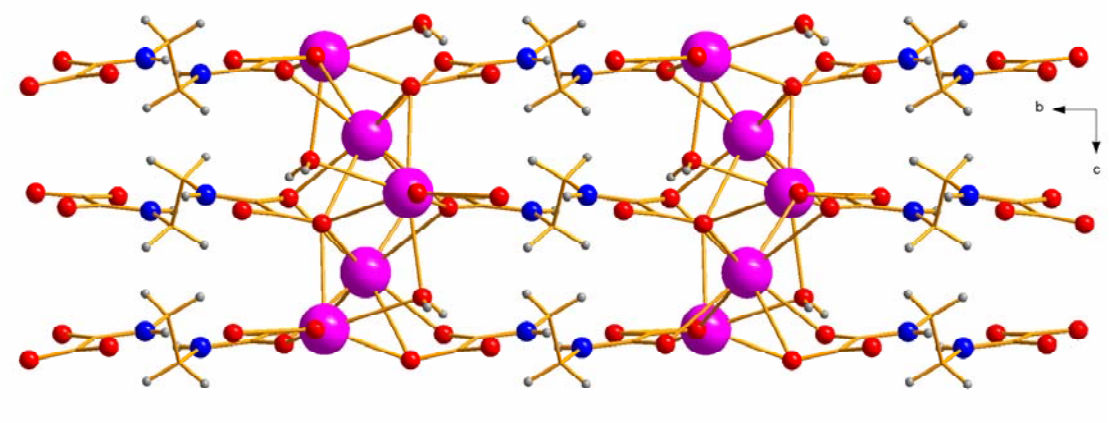

Figure 2. 8 Crystal packing of **4a**·H_2O in the *bc*-plane.

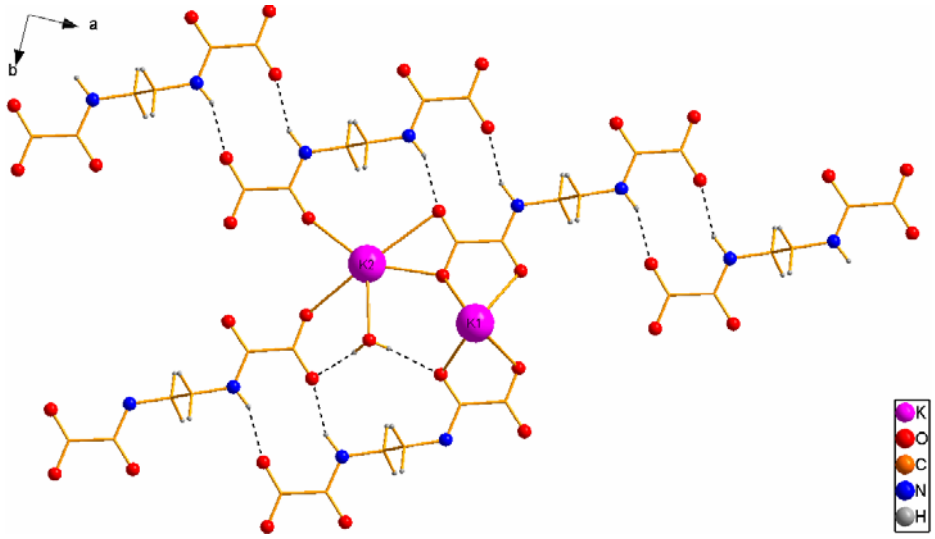

Figure 2. 9 Representation of the hydrogen bonds (dashed lines) between ligand molecules and the water molecules Ow1 along the [1 -1 0] direction.

2. 2. 4 Description of structure $CuH_2(oeo)\cdot 2H_2O$ (7c)

The copper salt of diethyl ethylene–1,2–dioxomate, $CuH_2(oeo)\cdot 2H_2O$ **(7c)**, crystallises in the monoclinic centrosymmetric $P2_1/c$ space group. The asymmetric unit contains

one copper atom, one doubly deprotonated ligand molecule $[H_2(oeo)]^{2-}$ and two crystallisation water molecules.

Each end of the ligand chelates one cooper atom through the carbonyl amide oxygen and the carboxylate oxygen atom of the oxamato group with the ethylenediamine unit adopting an *anti* conformation (Figure 2.10). The two oxamato groups of the organic molecule are close to be parallel as the dihedral angle between the mean planes of the two oxamato groups of the ligand molecule, measuring the mean planes by taking all the atoms that form the group, is 18.75(5)°. Thus, each copper atom is coordinated to two oxamato groups of two different molecules in the basal plane giving rise to the formation of the chair-like dimer $[CuH_2(oeo)]_2$ which has an inversion centre in the middle point of dimeric unit. The dihedral angle between O1-Cu1-O2 and O3'-Cu1-O4' mean planes, where prime denotes the symmetry related operation, is 5.23(5)°.

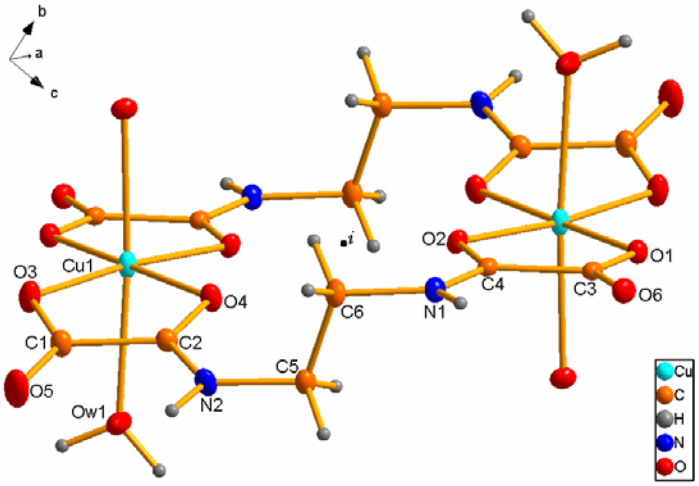

Figure 2. 10 Perspective view of the copper dimer with the atom numbering scheme showing the inversion centre in the middle of the dimer. Thermal ellipsoids are drawn at 50% of probability level.

The copper(II) atom shows the Jahn-Teller tetragonal distortion in which the axial distances are between 1.940(1)-1.970(1) Å and the equatorial distances are roughly 2.38 Å. One of the axial sites is filled with one water molecule (Ow1) and the other one is filled with a carboxylate carbonyl oxygen (O6) of a nearby ligand connecting two different dimeric units into a 3-D network in the *bc*-plane (Figure 2.11).

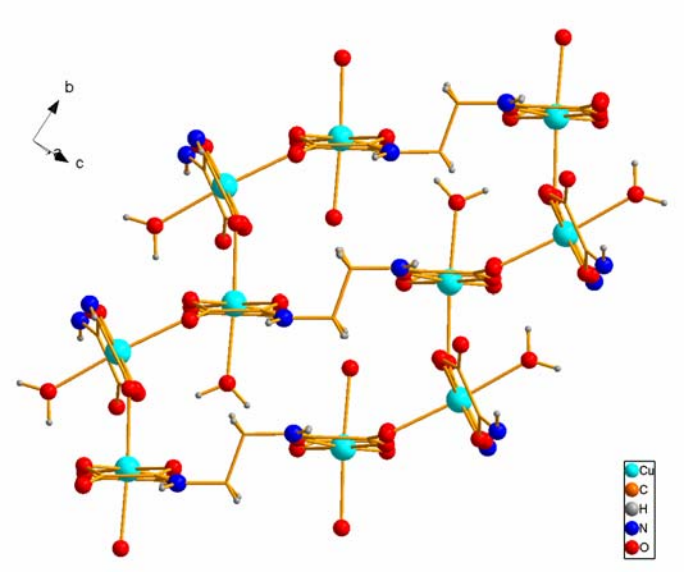

Figure 2. 11 Crystal packing of **7c** showing the connections between dimers.

Dimeric units are also connected through hydrogen bondings between two oxamato units, involving N2-H2 and O5 of each oxamato group, and forming the cyclic $R^2_2(10)$ motif.[4] This type of motif is also noted in the lithium and potassium salts. Moreover, the other amide group of the ligand molecules, N1-H1, is hydrogen bonded to the water of crystallisation Ow2 (2.338(29)Å), which at the same time is hydrogen bonded to another oxamato group through Hw2b. Hw2a is involved in weak hydrogen-bonding with the symmetry related Ow2. Finally, Ow1 is hydrogen-bonded to the carbonyl amide (O2) and the carbonyl acetate (O6) of two close ligands but forming a second order $R^4_4(12)$ hydrogen-bond motif within the dimeric unit (Figure 2.12).

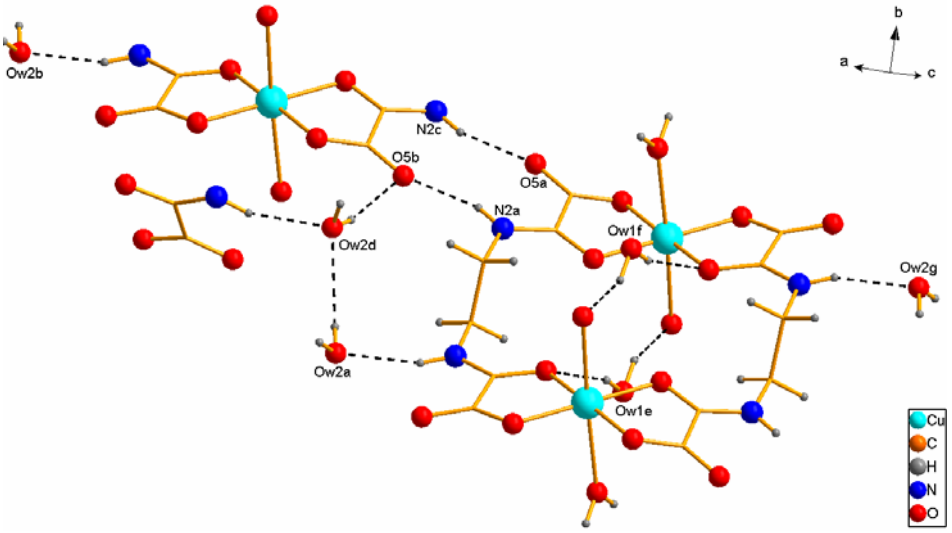

Figure 2. 12 Schematic view of the representation of the hydrogen bonds (dashed lines) between dimers. Symmetry codes: a = x, y, z; b = 1+x, 1+y, z; c = 3-x, 2-y, 1-z; d = 3-, 2-y, 1-z; e = 2-x, -y, 1-z; f = x, 1+y, z; g = 2-x, 1-y, 1-z.

2. 2. 5 Description of structure $CoH_2(oeo)\cdot DMSO$ (8)

The cobalt salt of diethyl ethylene–1,2–dioxomate crystallises in the monoclinic space group $P2_1/n$ containing in the asymmetric unit one cobalt ion, one doubly deprotonated ligand molecule $[H_2(oeo)]^{2-}$ and one DMSO molecule.

Similarly to the copper(II) salt, each end of the organic molecule is chelating to one cobalt atom through the carbonyl amide oxygen and the carboxylate oxygen atom of the oxamato group to form a dimer built using two cobalt atoms and two ligand molecules, $[CoH_2(oeo)]_2$ (Figure 2.13). In this case, the oxamato groups adopt a *cis* environment around the cobalt atom and through the inversion centre present in the middle of the dimer; the two enantiomers (Λ and Δ) are related by symmetry. Moreover, the ethylenediamine displays a *gauche* configuration which gives a different morphology to the metal-ligand dimer. The two possible enantiomeric conformations of the ethylendiamine (λ and δ) are present in the dimer, also symmetry related by the inversion centre. The two oxamato groups of the organic molecule are close to be perpendicular to each other, as the dihedral angle between the mean planes of the two oxamato groups of the ligand molecule, measuring the mean planes by taking all the atoms that form the group, is 79.15(7)°.

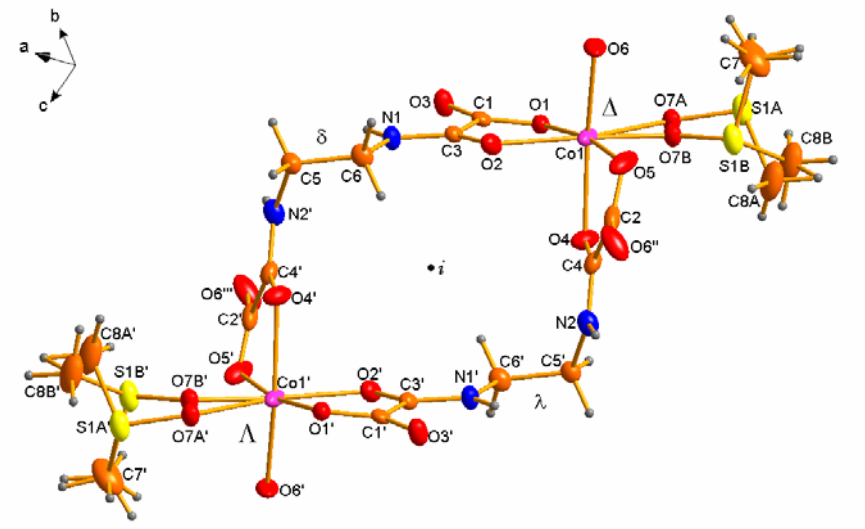

Figure 2. 13 Perspective view of the cobalt dimer with atom numbering scheme and showing the inversion centre in the middle of the dimer. Thermal ellipsoids are drawn at the 50% of probability level. Prime denotes symmetry operation 1-x, 1-y, 1-z, double prime 0.5-x, -0.5+y, 0.5-z and triple prime 0.5+x, 1.5-y. 0.5+z.

The cobalt(II) atom has a CoO_6 octahedral geometry with distances between 1.933(4) Å and 2.214(5) Å. Four of the oxygens arise from two oxamato groups provided by the two different ligands of the dimer, another from the DMSO molecule, and the sixth site is filled by an oxamato carbonyl oxygen (O6) of a neighbouring dimer. This carbonyl oxygen atom (O6) connects nearby dimeric units in the crystal structure in a 3-D network (Figure 2.14). This type of linkage between neighbouring dimers is also noted in **7c**, leading to the shortest distance between cobalt atoms (5.432(5) Å).

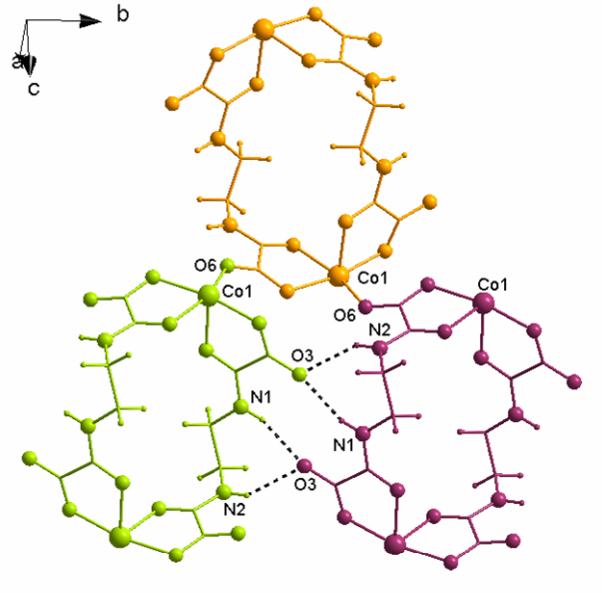

Figure 2. 14 Schematic perspective view of the connection between dimers through the carbonyl carboxylate oxygen and the hydrogen-bonds. Hydrogen bonds are represented by dashed lines. DMSO molecules are omitted for clarity.

In addition, the union between dimers through O6 atom relates the alternating Λ and Δ coordination environments of the metal ions along the *b*-axis in a zig-zag pattern. The structure presents a perfect alternation of Λ and Δ chiral sites (Figure 2.15).

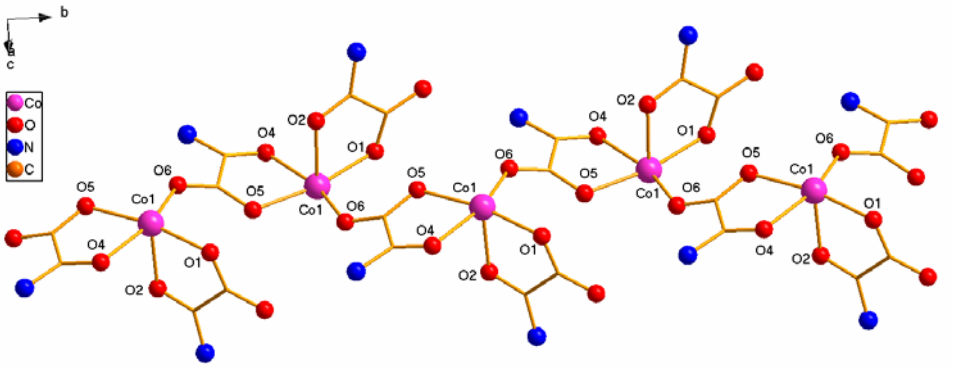

Figure 2. 145 Schematic view of the zig-zag pattern between metal ions which relates the Λ and Δ environment of the cobalt ions along the *b*-axis direction. DMSO molecules are omitted for clarity and the oxamate group is a fragment of the $[H_2(oeo)]^{2-}$.

The dimeric units are also connected through a hydrogen-bond network between amines and carbonyl oxygen atoms of oxamato groups from nearby ligands (Figure 2.15). In this case, two different motifs are displayed in the crystal structure. As in all the previous ionic structures, the cyclic $R_2^2(10)$ motif is formed between the amine groups N1-H1 and the carbonyl oxygen O3 of two neighbouring dimers.[4] Due to the ethylenediamine conformation in the ligand, two amines of the same molecule chemically equivalent but crystallographically different (N1 and N2), are hydrogen-bonded to the one oxamato carbonyl oxygen (O3) of the neighbouring dimer forming a $R_2^1(7)$ motif. The inversion centre in the middle of the cyclic $R_2^2(10)$ motif relates by symmetry the two hydrogen-bonding $R_2^1(7)$ motifs present in the connection between two dimers.

2. 3 Experimental Section

2. 3. 1 Diethyl ethylene–1,2–dioxomate, Et_2H_2(oeo) (1)

Synthesis

A solution of ethylenediamine (4.40 ml, 1.00 equivalents, 65.16 mmols) in absolute ethanol (10 ml) was added to diethyloxalate (100 ml, 5.6 equivalents, 729 mmol) and stirred for 8 hours at 45 ^oC. The yellow pale mixture was left to cool down to room temperature. The white solid that formed was filtered off, washed several times with ethanol and dried in air to give a shiny flat solid (Yield 15.7 g; 93%). $C_{10}H_{16}O_6N_2$ requires: C, 46.15; H, 6.20; N, 10.76%. Found: C, 44.80; H, 6.02; N, 10.42 %. ^{1}H-NMR (400 MHz, $CDCl_3$, δ in ppm): 7.60 (s, 2H, *NH*), 4.38 (q, 4H, J = 6.8Hz, *CH_2*), 3.60 (m, 4H, CH_2(*NH*)), 1.42 (t, 6H, J = 6.8Hz, *CH_3*). ^{13}C-NMR (400 MHz, $CDCl_3$, δ in ppm): 160.39 (*CO*-O), 157.47(*CO*-NH), 63.96(*C*H_2-CH_3), 39.43(*CH_2*-NH), 13.96(*CH_3*). IR (KBr, cm^{-1}): ν 3313 (w), 2998-2866 (vs), 1747 (s), 1735 (s), 1677 (w), 1547 (s) (See Appendix A1). MS (CI) m/z = 261.2 ($[C_{10}H_{17}O_6N_2]^+$). Suitable single crystals of **1** for X-Ray structural analysis were collected from the filtrate after several days. Infra-red (IR) spectra were obtained on a Perkin-Elmer 983 spectrophotometer on samples dispersed on a KBr disc.

Crystallographic Data Collection and Structure Determination

All non-hydrogen atoms were refined anisotropically. Hydrogen atoms positions have been assigned to calculated positions and refined using a riding model.

Crystal data and selected details of the refinement are listed in Table 2.1.

Table 2. 1 Crystallographic data for **1**

Empirical formula	$C_{10}H_{16}N_2O_6$
Formula weight	260.25
Crystal system	monoclinic
Space group	$P2_1/c$
a (Å)	14.1668(7)
b (Å)	4.5207(2)
c (Å)	9.7208(5)
α (°)	90.00
β (°)	96.362(3)
γ (°)	90.00
V (Å^3)	618.72(5)
T(K)	100(2)
ρ_{calc} (g/cm^3)	1.397
Z	2
F (000)	276
Reflections collected	10627
Unique reflections	1871
Reflections observed [I>2σ(I)]	1571
R_{int}	0.0339
Parameters refined	82
Number of restraints	0
λ (Å); Mo Kα	0.71073
μ (mm^{-1})	0.116
θ Range (°)	1.45-30.43
Goodness-of-fit (GOF) on F^2	1.043
[a]R_1 [I>2σ(I)]	0.0358
[b]wR_2 (all data)	0.0979
Largest difference in peak and hole (e Å^{-3})	0.53 and -0.15
Crystal size (mm)	0.01x0.4x0.6
Crystal morphology	Flat colourless

[a]$R_1 = \Sigma(|F_o| - |F_c|)/ \Sigma|F_o|$

[b]$wR_2 = [\Sigma w(F_o^2 - F_c^2)^2]/\Sigma w(F_o^2)^2]^{1/2}$ where $w = 1/[\sigma^2(F_o^2) + (0.2P)^2$ and $P = [F_o^2 + 2F_c^2]/3$

2. 3. 2 Dilithium ethylene–1,2–dioxomate, Li_2H_2(oeo) (2)

Synthesis

A mixture of **1** (5.70 g, 21.90 mmols) and ethanol (120 ml) was heated until the solid was dissolved. A solution of LiOH (1.07 g, 43.80 mmols) in water (16 ml) was then added drop-wise and a white solid was formed. The mixture was left to cool down to room temperature and stirring overnight. The white precipitate formed was collected by

vacuum filtration, washed with ethanol and dried in air. The final product was obtained as a mixture of dilithium ethylene-1,2-dioxamate (Li_2H_2oeo, **2a**) and lithium ethyl ethylene-1,2-dioxamate (LiEtH_2oeo, **2b**), existing as 50:1. ^{1}H-NMR (400 MHz, D_2O, δ in ppm): **2a,** 3.27 (s, 4H, *CH_2*NH); **2b,** 3.30 (m, *NH*). ^{13}C-NMR (400 MHz, D_2O, δ in ppm): **2a,** 166.02 (*CO*-O), 165.47 (*CO*-NH), 38.57 (CH_2-NH). IR (ATR, cm^{-1}): ν 3415 (w), 3308 (s), 3195 (w), 3073 (w), 2964 (w), 1670 (s), 1635 (s), 1548 (s), 1390 (s), 1273 (s), 1228 (s), 1050 (s) (See Appendix A1). MS (FAB^-) **2a,** *m*/*z* = 209.2 ($[C_6H_6O_6N_2Li]^-$). Small single crystals of **2a**·$2H_2O$ suitable for X-Ray analysis were obtained as a by-product in the synthesis of the microcrystalline solid of $Li_4[Cu(oeo)]_2 \cdot nH_2O$ in methanol and water (See Chapter 3).

Crystallographic Data Collection and Structure Determination

Due to the weak diffraction and the small size of the crystal, the amount of data collected was very low. Consequently, in order to avoid the overparametization of the model, all atoms were refined isotropically. The hydrogen atoms positions were placed in calculated positions and refined using a riding model, except those from the crystallisation water molecule. These hydrogen atoms were located in difference-Fourier maps, refined with three restraints (O-H and H···H distances) and given isotropic thermal parameters [$U_{iso}(H) = 1.2U_{eq}(Ow1)$.

Crystal data and selected details of the refinement are listed in Table 2.2.

Table 2. 2 Crystallographic data for **2**

Empirical formula	$C_3H_5NO_4Li$
Formula weight	126.02
Crystal system	monoclinic
Space group	$P2_1/c$
a (Å)	9.2721(72)
b (Å)	7.6342(49)
c (Å)	7.0381(42)
α (°)	90.00
β (°)	100.849(30)
γ (°)	90.00
V (Å^3)	489.3(5)
T(K)	100(2)
ρ_{calc} (g/cm^3)	1.711
Z	4
F (000)	260
Reflections collected	4666
Unique reflections	485
Reflections observed [I>2σ(I)]	403
R_{int}	0.0414
Parameters refined	46
Number of restraints	3
λ (Å); Mo Kα	0.71073
μ (mm^{-1})	0.155
θ Range (°)	2.24-20.35
Goodness-of-fit (GOF) on F^2	4.389
[a]R_1 [I>2σ(I)]	0.1746
[b]wR_2 (all data)	0.5243
Largest difference in peak and hole (e Å^{-3})	1.09 and -0.88
Crystal size (mm)	0.05x0.05x0.1
Crystal morphology	flat colourless

[a]$R_1 = \Sigma(|F_o| - |F_c|)/ \Sigma|F_o|$
[b]$wR_2 = [\Sigma w(F_o^2 - F_c^2)^2]/\Sigma w(F_o^2)^2]^{1/2}$ where $w = 1/[\sigma^2(F_o^2) + (0.2P)^2$ and $P = [F_o^2 + 2F_c^2]/3$

2. 3. 3 Disodium ethylene–1,2–dioxomate, Na_2H_2(oeo) (3)

Synthesis

To a stirring solution of **1** (5.00 g, 19.21 mmols) in absolute ethanol (60 ml) at approx. 78 °C, a solution of NaOH (1.64 g, 2.1 equiv, 40.0 mmols) dissolved in water (5 ml) was added drop-wise and stirred at this temperature for one hour. The mixture was left to cool down to room temperature and stirring overnight. The white solid that formed was collected by filtration, washed with ethanol and dried in air (Yield: 4.02 g, 84,28%).[5] ^{1}H-NMR (400 MHz, D_2O, *δ* in ppm): 3.30 (s, 4H, CH_2NH).

2. 3. 4 Dipotasium ethylene–1,2–dioxomate, K_2H_2(oeo) (4)

Synthesis

To a stirring solution of **1** (8.95 g, 34.39 mmols) in 100 ml of ethanol at 65 °C an aqueous solution (7 ml) of KOH (3.86 g, 59.16 mmols) was added drop-wise and stirred at this temperature for 3hrs. The white solid that formed was collected by filtration, washed with ethanol and acetone, and dried in air. The final product was obtained as a mixture of dipotassium ethylene-1,2-dioxamate (K_2H_2oeo, **4a**) and potassium ethyl ethylene-1,2-dioxamate (KEtH_2oeo, **4b**), existing as 4:1. ^{1}H-NMR (400 MHz, D_2O, δ in ppm): **4a,** 3.31 (s, 4H, *CH*$_2$NH); **4b,** 4,23 (q, 4H, J = 6.8Hz, *CH*$_2$), 3.35 (m, 4H, *CH*$_2$NH), 1.22 (t, 6H, J = 6.8 Hz, *CH*$_3$). ^{13}C-NMR (400 MHz, D_2O, δ in ppm): **4a,** 166.99 (*CO*-O), 165.38 (*CO*-NH), 38.56 (*C*H$_2$-NH); **4b,** 165.90 (*C*^{1}*O*-O), 160.27 (*C*^{6}*O*-O), 158.87 (*C*^{5}*H*-NH), 64.00 (*C*^{7}*H*$_2$-CH$_3$), 38.88 (*C*^{4}*H*$_2$-NH), 38.22 (*C*^{3}*H*$_2$-NH), 13.07 (*C*^{8}*H*$_3$). MS (FAB) **4a** m/z = 279.1 ([$C_6H_5O_6N_2K_2$]$^-$).

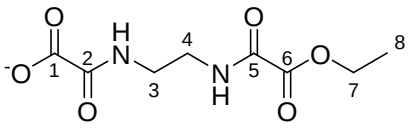

Scheme 2. 3 KEtH_2oeo **(4b)**

Needle shaped single crystals of **4a**·H_2O were obtained by slow solvent diffusion of methanol into an aqueous solution of K_2H_2(oeo). IR (ATR, cm^{-1}): ν 3453(w), 3303(s), 3262(s), 2983 (w), 1639 (w), 1620 (s), 1538 (s), 1538 (s), 1456 (s), 1373(s), 1265 (s), 1224 (s), 1050 (s) (See Appendix A1).

Crystallographic Data Collection and Structure Determination

The Flack parameter value,[6] 0.38(3), indicates that inversion twinning is present, though due to the twinning. All non-hydrogen atoms were refined anisotropically. The hydrogen atoms were placed in calculated positions and refined with a riding model, except those from the crystallisation water molecule which were located in difference-Fourier maps, refined with two restraints (O-H distances) and given isotropic thermal parameters [U_{iso}(H) = 1.2U_{eq}(Ow1)].

Crystal data and selected details of the refinement are listed in Table 2.3.

Table 2. 3 Crystallographic data for **4a**·H_2O

Empirical formula	$C_6H_8K_2N_2O_7$
Formula weight	298.34
Crystal system	monoclinic
Space group	*Cc*
a (Å)	7.6734(2)
b (Å)	19.7430(5)
c (Å)	7.2112(2)
α (°)	90.00
β (°)	100.6710(10)
γ (°)	90.00
V (Å^3)	1073.57(5)
T(K)	100(2)
ρ_{calc} (g/cm^3)	1.846
Z	4
F (000)	608
Reflections collected	6781
Unique reflections	2359
Reflections observed [I>2σ(I)]	2335
R_{int}	0.0212
Parameters refined	161
Number of restraints	4
λ (Å); Mo Kα	0.71073
μ (mm^{-1})	0.909
θ Range (°)	2.06-30.44
Goodness-of-fit (GOF) on F^2	1.058
[a]R_1 [I>2σ(I)]	0.0192
[b]wR_2 (all data)	0.0534
Largest difference in peak and hole (e Å^{-3})	0.35 and -0.27
Crystal size (mm)	0.4x0.5x0.9
Crystal morphology	Colourless block

[a]$R_1 = \Sigma(|F_o| - |F_c|)/ \Sigma|F_o|$

[b]$wR_2 = [\Sigma w(F_o^2 - F_c^2)^2]/\Sigma w(F_o^2)^2]^{1/2}$ where $w = 1/[\sigma^2(F_o^2) + (0.2P)^2$ and $P = [F_o^2 + 2F_c^2]/3$

2. 3. 5 Dirubidium ethylene–1,2–dioxomate, Rb_2H_2(oeo) (5)

Synthesis

To a stirring solution of **1** (1.00 g, 3.84 mmols) in absolute ethanol (60 ml) at approx. 76 °C, an aqueous solution of RbOH (0.45 ml, 3.82 mmols, 50 wt.% in water) was added drop-wise. The mixture was left to cool down to room temperature and stirring overnight. The white solid precipitated was collected by filtration, washed with ethanol and acetone, and dried in air. The final product was obtained as a mixture of dirubidium ethylene-1,2-dioxamate (Rb_2H_2oeo, **5a**) and rubidium ethyl ethylene-1,2-dioxamate ($RbEtH_2$oeo, **5b**), existing as 3:1. ^{1}H-NMR (400 MHz, D_2O, *δ* in ppm): **5a**, 3.30 (s, 4H, CH_2NH). **5b**, 4.22 (q, 4H, *J* = 6.8Hz, CH_2), 3.33 (m, 4H, CH_2NH), 1.22 (t, 6H, *J* =

6.8Hz, *CH*$_3$). $C_6H_8O_7N_2Rb_2$, **5a**·H_2O requires: C, 18.42; H, 2.05; N, 7.16%. Found: C, 18.32; H, 1.69; N, 7.57 %.

2. 3. 6 Dicesium ethylene–1,2–dioxomate [Cs_2H_2(oeo)] (6)

Synthesis

To a stirring solution of **1** (0.74g, 2.83mmols) in absolute ethanol (10ml) at approx. 68°C, a solution of CsOH (1.04g, 5.88mmols, 95.0%) in water (1.5ml) was added drop-wise. The mixture was left stirring for 90min while cooling down to room temperature. The white solid precipitated was collected by filtration, washed with ethanol and dried in air (Yield 1.18g, 85.96%).[7] ^{1}H-NMR (400 MHz, D_2O, δ in ppm): 3.30 (s, 4H, *CH*$_2$NH).

2. 3. 7 Copper ethylene–1,2–dioxomate, CuH_2(oeo)·nH_2O (7)

Synthesis of CuH_2(oeo)·3H_2O (7a)

To an aqueous solution (3.5 ml) of **4** (1.00 g, 3.35 mmols) a solution of $CuCl_2$·2H_2O (0.84 g, 4.78 mmols) dissolved with the minimum amount of water, was added drop-wise. The solution was stirred for one hour and the turquoise solid filtered off, washed several times in water and dried in air. $CuC_6H_{12}O_9N_2$ (Mw: 319.71) requires: C, 22.95; H, 1.91; N, 8.93. Found: C, 23.52; H, 2.52; N, 8.20%. IR (ATR, cm^{-1}): ν 3484(w), 3426(w), 3261 (w), 3100(w), 2957 (w), 1683 (s), 1631 (w), 1563 (s), 1468(s), 1362(s) (See Appendix A1).

Synthesis of CuH_2(oeo)·3H_2O (7b)

To a stirring suspention of **1** (1.59 g, 6.11 mmols) and water (10 ml) at aprox 78 °C, an aqueous solution (5 ml) of NaOH (0.60 g, 14.62 mmols) was added dropwise. The solution was stirred for an hour at this temperature, cooled down to room temperature and filtered by gravity to eliminate impurities. An aqueous solution (5 ml) of $CuCl_2$·2H_2O (1.00 g, 6.10 mmol) was then added and the mixture was stirred for another hour. The light turquoise solid that formed was filtered off, washed several

times with water and dried in air (Yield: 1.16 g, 58.00%). $CuC_6H_{12}O_9N_2$ (Mw: 319.71) requires: C, 22.95; H, 1.91; N, 8.93%. Found: C, 22.52; H, 2.77; N, 8.67%. IR (ATR, cm^{-1}): ν 3609(s), 3519(w), 3410(w), 3260 (s), 3093(w), 2957-2907 (w), 1680 (s), 1639 (w), 1604 (w), 1590(w), 1557 (s), 1438(s), 1368(w).

Synthesis of $CuH_2(oeo)\cdot 2H_2O$ (7c)

Well shaped turquoise prismatic crystals of compound **7c** suitable for X-Ray analysis were obtained by gel-tube method. An aqueous solution (3 ml) of $CuCl_2\cdot 2H_2O$ (0.17 g, 1 mmol) was allowed to diffuse indisturbed into a gel containing $Na_2H_2(oeo)$ (0.24 g, 1 mmol). After six months, big turquoise crystals formed in the gel. The gel was formed as follows: 2ml of tetramethyl orthosilicate (TMOS, 98%) were added to a solution of 18ml of water containing $Na_2H_2(oeo)$ and stirred vigorously until the mixture becomes monophasic. The mixture is added immediately to a gel tube which was left to solidify overnight. The next day, the solution of $CuCl_2\cdot 2H_2O$ was added and allowed to diffuse into the gel.

Crystallographic Data Collection and Structure Determination of 7c

The difference-Fourier map revealed disorder in one of the water molecules. A disorder model involving two positions for the oxygen atom was used, the occupation factors converging at 0.90 and 0.20 for Ow2 and Ow3, respectively. The short interatomic distance between sites (2.078(13) Å) ensures a mutually exclusive occupancy. Due to the low occupancy factor of Ow3, the oxygen atom was refined with isotropic thermal parameters and hydrogen atoms were not located. The rest of all non-hydrogen atoms were refined anisotropically.

The hydrogen atom positions of the organic ligand were assigned to calculated positions and refined using a riding mode. The hydrogen atoms of the water molecules Ow1 and Ow2 were located on a ΔF map, refined with three restraints for each molecule (O-H and H···H distances) and given isotropic thermal parameters [$U_{iso}(H) = 1.2U_{eq}(Ow)$].

Crystal data and selected details of the refinement are listed in Table 2.4.

Table 2. 4 Crystallographic data for **7c**

Empirical formula	$C_6H_{10}CuN_2O_8$
Formula weight	301.50
Crystal system	monoclinic
Space group	$P2_1/c$
a (Å)	10.7513(6)
b (Å)	5.8042(3)
c (Å)	16.4521(9)
α (°)	90.00
β (°)	93.514(3)
γ (°)	90.00
V (Å^3)	1024.73(10)
T(K)	100(2)
ρ_{calc} (g/cm^3)	1.954
Z	4
F (000)	611
Reflections collected	11899
Unique reflections	3116
Reflections observed [I>2σ(I)]	2696
R_{int}	0.0244
Parameters refined	171
Number of restraints	6
λ (Å); Mo Kα	0.71073
μ (mm^{-1})	2.168
θ Range (°)	1.90-30.48
Goodness-of-fit (GOF) on F^2	1.065
[a]R_1 [I>2σ(I)]	0.0294
[b]wR_2 (all data)	0.0786
Largest difference in peak and hole (e Å^{-3})	1.05 and -0.75
Crystal size (mm)	0.05x0.1x0.4
Crystal morphology	turquoise prism

[a]$R_1 = \Sigma(|F_o| - |F_c|)/ \Sigma|F_o|$

[b]$wR_2 = [\Sigma w(F_o^2 - F_c^2)^2]/\Sigma w(F_o^2)^2]^{1/2}$ where $w = 1/[\sigma^2(F_o^2) + (0.2P)^2$ and $P = [F_o^2 + 2F_c^2]/3$

2. 3. 8 Cobalt ethylene–1,2–dioxomate [CoH_2(oeo)·DMSO] (8)

Synthesis

To a suspension of Et_2H_2(oeo) (2.60 g, 9.99 mmols) in water (10 ml) was added dropwise a 40% aqueous solution (26.2 ml) of tetrabutylammonium hydroxide (40.0 mmols). The resulting mixture was stirred at room temperature for 1 hr and then an aqueous solution of $CuCl_2·2H_2O$ (1.30 g, 7.40 mmols) dissolved with the minimum amount of water was added. The deep blue solution was left stirring overnight and then it was filtered to eliminate the solid that formed. 3ml of the final solution were added dropwise to a stirring solution of $CoCl_2·6H_2O$ (1.00 g, 4.11 mmols) in DMSO (4 ml) and the mixture was stirred overnight. Slow solvent diffusion of ethanol into the final solution gave small purple crystals of **8** suitable for X-ray analysis. IR (ATR, cm^{-1}): ν 3286(w), 2926-2960(w), 1696 (s), 1926 (w), 1536 (s), 1467 (s) (See Appendix A1).

After a several weaks, the purple solid that formed in the reaction mixture was collected by filtration and dried in air **(29)** (See Chapter 11).

Crystallographic Data Collection and Structure Determination

All non-hydrogen atoms were refined anisotropically. The hydrogen atom positions of the organic molecule were assigned to calculated positions and refined with fixed individual displacement parameters [$U_{iso}(H) = 1.2U_{eq}(C_{ethyl})$ or $1.2U_{eq}(N_{amine})$] using a riding mode.

The difference-Fourier map revealed disorder in the DMSO crystallisation molecule. Two sets of atoms were found and refined with occupancy factors of 0.47 and 0.53, respectively. The same atom types of the two atom sets were constrained to have the same displacement parameters and the bond lengths of pairs chemically equivalent were restrained to be equal with a 0.01 esd, except pairs C7-S1A and C7-S1B which were refined with 0.1 esd. Bonds angles were restrained by an application of similar distance restraints to next nearest atoms. The hydrogen atoms of the methyl groups of the DMSO molecules were located on the difference-Fourier map and refined with fixed individual displacement parameters [$U_{iso}(H) = 1.5U_{eq}(C_{methyl})$].

Crystal data and selected details of the refinement are listed in Table 2.5.

Table 2. 5 Crystallographic data for **8**

Empirical formula	$C_8H_{12}CoN_2O_7S$
Formula weight	339.19
Crystal system	monoclinic
Space group	$P2_1/n$
a (Å)	7.5838(4)
b (Å)	9.3320(5)
c (Å)	18.0194(9)
α (°)	90.00
β (°)	96.161(3)
γ (°)	90.00
V (Å^3)	1267.90(11)
T(K)	100(2)
ρ_{calc} (g/cm^3)	1.777
Z	4
F (000)	692
Reflections collected	11896
Unique reflections	3961
Reflections observed [I>2σ(I)]	2503
R_{int}	0.0418
Parameters refined	185
Number of restraints	5
λ (Å); Mo Kα	0.71073
μ (mm^{-1})	1.548
θ Range (°)	2.27-30.81
Goodness-of-fit (GOF) on F^2	1.023
[a]R_1 [I>2σ(I)]	0.0511
[b]wR_2 (all data)	0.1294
Largest difference in peak and hole (e Å^{-3})	0.89 and -0.79
Crystal size (mm)	0.02×0.2×0.1
Crystal morphology	pink

[a]$R_1 = \Sigma(|F_o| - |F_c|)/ \Sigma|F_o|$

[b]$wR_2 = [\Sigma w(F_o^2 - F_c^2)^2]/\Sigma w(F_o^2)^2]^{1/2}$ where $w = 1/[\sigma^2(F_o^2) + (0.2P)^2$ and $P = [F_o^2 + 2F_c^2]/3$

2. 3. 9 Nickel ethylene–1,2–dioxomate [NiH_2(oeo)·$3H_2O$] (9)

Synthesis

To an stirring aqueous solution (6ml) of **9** (1.00 g, 3.57 mmols) a solution of $NiCl_2·6H_2O$ (0.87 g, 3.57 mmols) in water (2 ml) was added drop-wise. The mixture was left stirring for one hour and the light green solid was collected by filtrations and washed with water (Yield: 0.89 g, 96.4%). $C_6H_{16}O_{11}N_2Ni$ requires: C, 20.54; H, 4.56; N, 7.98. Found: C, 20.48; H, 4.28; N, 7.77%. IR (ATR, cm^{-1}): ν 3453(s), 3298(s), 3269(s), 3098 (w), 2962(w), 1644 (vs), 1556 (vs), 1442 (s).

[1] K. Nonoyama, H. Ojima, M. Nonoyama, *Inorganica Chimica Acta*, **1976**, *20*, 127
[2] B. Cervera, J.L. Sanz, M.J. Ibañez, G. Vila, F. Lloret, M. Julve, R. Ruiz, X. Ottenwaelder, A. Aukauloo, S. Poussereau, Y. Journaux, M.C. Muñoz, *J. Chem. Soc*., *Dalton Trans.*, **1998**, 781
[3] W. Gaade, *Recl. Trav. Chim. Pay-B*, **1936**, *55*, 325
[4] M. C. Etter, J. C. MacDonald. *Acta Cryst*. **1990**, *B46*, 256
[5] The degree of hydratation of the salt is unknown. However, we believe the salt exists as the monohydrate and thus the percent yield is calculated based on this molecular weight.
[6] Flack, H. D., Acta Cryst. *A39*, **1983**, 876.
[7] The degree of hydratation of the salt is unknown. However, we believe the salt exists as the monohydrate and thus the percent yield is calculated based on this molecular weight.

Chapter 3: The dimer

3. 1 Structure of the dimer

The dimeric $[Cu(oeo)]_2^{4-}$ structure is made up of two ligands of the hydrolysed and deprotonated proligand diethyl ethylene-1,2-dioxamate **(1)**, $(oeo)^{4-}$, and two copper(II) atoms (Scheme 3.1). Each end of the flexidentate ligand contains one double deprotonated oxamato substituent which is coordinating towards a copper(II) atom to form the dimeric metal complex $[Cu(oeo)]_2^{4-}$. The two deprotonated amido nitrogens and the two carboxylate oxygen atoms adopt a $\eta^4(\kappa^2N{:}\kappa^2O)$ distorted square-planar environment around the metal.

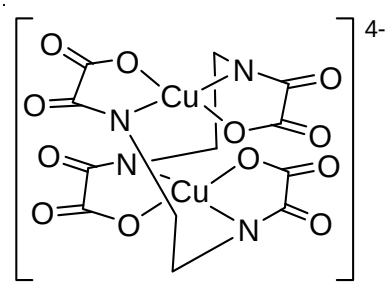

Scheme 3. 1 The dimeric $[Cu(oeo)]_2^{4-}$ complex

The dimer displays a helicoidal structure with a *trans*-bis(*N*,*O*) arrangement around the metal and with the two ethylendiamine fragments adopting a *gauche* configuration. The two possible enatiomeric conformations (δ,λ) of the *gauche* configuration of the ethylenediamine are present in the dimer, one in each ligand molecule. Due to steric impediments of the ethylenediamine fragments, the helicoidal structure with a *cis*-bis(*N*,*O*) environment is excluded although this coordination type is usually observed in related bis(oxamato) complexes. However, some *trans*-bis(*N*,*O*) environments have been reported.[1,2,3]

Each $(oeo)^{4-}$ ligand adopts a tetradentate coordination mode around the metal ion forming two five-membered chelated rings towards the copper(II) atoms with each oxamato unit. In addition, a fused ten-membered ring built by the two ethylenediamines and the copper(II) ions is formed leading to a 5^2-10-5^2 pattern. This pattern imposes a severe distortion of the metal environment from the ideal square planar arrangement. The average distance between the two copper sites within the dimer is 3 Å.

Furthermore, the copper(II) dimer contains several additional potential coordination sites which could allow the step-wise incorporation of further transition metals to give polymetallic bis(oxamato) transition metal complexes.

Two comparable patterns of 5^n-10-5^n fused chelate rings (n = 2, 3) have been noticed in structurally similar copper(II) dimeric systems in which the ligand is built by *N,N'*-ethyl bis(oxamide) ligands. In these compounds, which were previously discussed in Chapter 1, two alike octadentate ligand systems are known to produce the dicopper(II) compounds $[Cu_2(L^1)_2]$ where H_2L^1 =1,8-diamino-3,6-diazaoctane-4,5-dione,[4] and $[Cu_2(L^2)]$ where L^2 = 7,16-bis(2-aminoethyl)-1,4,7,10,13,16-hexaazacyclooctadecane-2,3,11,12-tetraonate(4-)) (Scheme 3.2).[5] $[Cu_2(L^1)_2]$ has a distorted square-planar environment whereas $[Cu_2(L^2)]$ has a 4+1 coordination with the apical position filled by one oxygen atom of the neighbouring molecule within the stack of dimers.

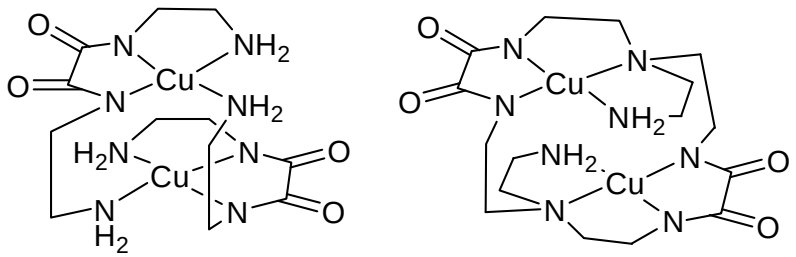

$[Cu_2(L^1)_2]$ $[Cu_2(L^2)]$

Scheme 3. 2

3. 2 Geometry of dimer

To a first approximation, the copper(II) environment in the dimer has a tetragonal distortion in which the metal environment on is in between a tetrahedral and a square-planar geometry. This distortion has been studied by looking at the angles around the metal as well as the dihedral angle formed by the two five-membered rings, which are not coplanar.

The O-Cu-N angle, α, formed by the two chelating donor atoms of each oxamato group is approximately between 82° and 87° (Scheme 3.3). This causes an opening of the O-Cu-N' angle formed by the donor atoms of the two neighbouring oxamato group, β, which is around 95° and 100°. These angles are similar with those reported earlier for distorted square-planar bis(oxamato) copper(II) complexes.[6,7,8]

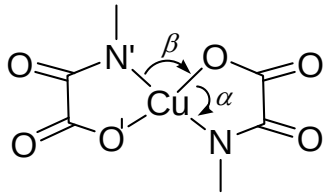

Scheme 3. 3

Furthermore, the angle between formed by the two chelating oxamato groups has also been investigated. Since the nitrogen, oxygen and carbon atoms of the oxamato groups are almost coplanar, the dihedral angle between the two oxamato groups has been measured by the planes formed with the copper and the two donor atoms of each oxamato group (Figure 3.1). Lastly, the displacement of the copper site from the least-squares plane, defined by the atom donor of the two chelating oxamato groups, as well as the displacement of these atoms, has been quantified.

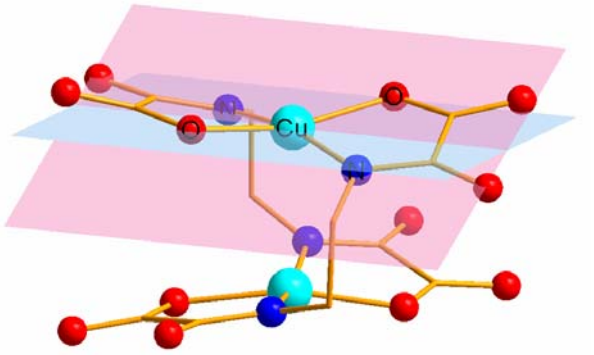

Figure 3. 1 Perspective view of the copper dimer $[Cu(oeo)]_2^{4-}$ showing the planes formed by the atom donors of the oxamato groups and the copper atom. Hydrogen atoms are omitted for clarity.

In some $Li_4[Cu(oeo)]_2$ crystal structures as well as in $Cs_4[Cu(oeo)_2]\cdot 5½H_2O$ **(23)**, the copper(II) ion has a 4+1 coordination with two nitrogens and two oxygen atoms arising from two oxamato groups in the basal plane (See Chapter 4 and Chapter 8, respectively). The square-pyramidal coordination sphere is completed by an apical oxygen atom from the neighbouring unit within the stack of the crystal packing. As a result, the copper atom is slightly displaced from the least-squares plane, defined by the atom donors of the basal plane, towards the apical position. This displacement has been also quantified.

In analogy to related copper(II) bis(oxamato) complexes,[8,9,10,11] in most of the dimeric structures the average distance between Cu-N (amide) sites is significantly shorter than

the average distance between Cu-O (carboxylate) sites. As discussed by Cervera *et al.* this is a consequence of the higher basicity of the former.[5] However, we will see in future chapters that in some cases this trend is not observed due to the dominance of the hydrogen bonded geometry of the dimer in the crystal structure. Moreover, we will see that distance between Cu-O (carboylate) and Cu-N (amide) sites is related to the occupancy in the copper(II) site.

The dimer itself can experience different local symmetries (Figure 3.2). It can have a C_2-axis passing through the two copper atoms sites and another through the mid-point of the C-C bond of the two ethylenediamine fragments. The last axis which does not pass through any atom or bonds is perpendicular to the previous ones and goes through the middle point of the dimer. When all three C_2-axis are present, the dimer has the maximal molecular point symmetry, D_2, and thus only a quarter of the molecule is needed to generate the molecule in three dimensions. Only one crystal structure has been found with this molecular symmetry, $Rb_4[Cu(oeo)_2]\cdot 4H_2O$ **(22)**. It crystallises in the *Cccm* space group and the asymmetric unit contains only a quarter of the molecule. We have noted that the Cu···Cu centroid lies on a 4*a* or 4*b* Wyckoff position which results to be placed in the intersection of the three perpendicular C_2-axes.

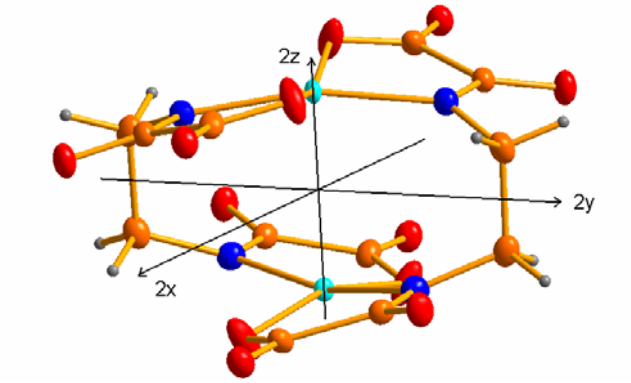

Figure 3. 2 Perspective view of the copper(II) dimer $[Cu(oeo)]_2^{4-}$ with the Cartesian axis (x, y, z) superimposed showing the two-fold symmetry elements that lie on these axis when the molecule has maximal symmetry.

Moreover, the molecule symmetry can be reduced to a C_2 symmetry or a C_1 symmetry. When it is reduced to a C_2 symmetry, the dimer contains one of the two fold axis and only half of the molecule is needed to fully represent the dimer in three dimensions. Thus the asymmetric unit of the crystal structure contains half of the molecule. This molecular symmetry has been observed in several crystal structures which all crystallise

in the *C*2/*c* space group. In these cases, the Cu···Cu centroid lies on a 4*e* Wyckoff position where one of the previously mentioned C_2-axis passes through. Different crystal structures containing one of the three possible two-fold axis have been found. For instance, the two fold axis that is observed in $Na_4[Cu(oeo)_2]\cdot 4H_2O$ **(14)**, goes through the two copper atoms (2z in Figure 3.2). In γ-$Li_4[Cu(oeo)_2]\cdot 6H_2O$ **(10c)**, the axis passes through the mid-point of the C-C bond of the two ethylenediamine fragments (2y in Figure 3.2) and finally, in $Li_4[Cu(oeo)_2]\cdot 5H_2O$ **(12)** it goes though the middle point of the dimer (2x in Figure 3.2).

Finally, when the dimer has the C_1 molecular symmetry, it contains only the identity as symmetry element and the whole molecule is present in the asymmetric unit. We have found examples in a number of crystal structures with the following space groups: $P\bar{1}$, $P6_5$, $P2_1/c$, $P2_1/n$ and $P2/c$.

It is noteworthy how similar two "different" crystal structures can be in this system. Two compounds, $Li_4[Cu(oeo)_2]\cdot 5H_2O$ **(12)** and γ-$Li_4[Cu(oeo)_2]\cdot 6H_2O$ **(10c)**, were analysed using X-ray analysis expecting them to be the same compound, since they were obtained from the same batch and had very similar crystal morphologies and cell parameters. However, the accurate analysis of the data revealed that they are two different compounds crystallising in the same monoclinic space group, *C*2/*c*, with the same crystal packing but with the *a* and *b* cell edges swapped. The number of water molecules in the asymmetric unit apparently seemed to be the same. Nevertheless, in **10c**, one of the oxygen atoms lies on the *c*-axis and consequently only half of the water molecule is present in the asymmetric unit. Therefore, **10c** contains 2½ water molecules in the asymmetric unit whereas **12** has three. Moreover, since the cell edges are swapped, the unique axis changes and the implicit C_2 symmetry that the dimer has also changes. In **12**, the C_2-axis passes through the two C-C bonds of the ethylenediamine whereas in **10c**, it passes through the mid-point of the dimer. The discovery of this structural diversity was serendipitous, as the two different crystals were not initially distinguished by the crystal morphology (See Chapter 4).

In this group of compounds where the molecular point symmetries that the dimer has is C_1 and C_2, the deviations from the maximal D_2 symmetry are minor since the comparison of bond lengths and angles confirm that deviations from D_2 symmetry are

slight. That is to say that when viewing the dimers in isolation they show a good approximation to a pseudo-D_2 symmetry (Figure 3.3). Only when we consider the widen environment of the anion we visually realise the true molecular point symmetry of the dimer (See Chapter 4).

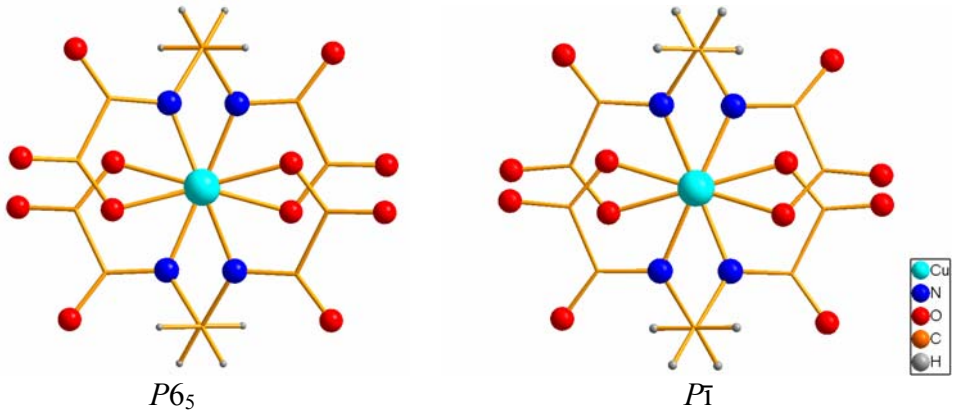

Figure 3. 3 Perspective view of the dimer belonging to two different space groups which both contain the C_1 molecular symmetry group. Looking from above one can easily imagine three pseudo C_2-axis going through the molecule.

3. 3 Chirality

As mentioned above, two $(oeo)^{4-}$ ligands coordinate two copper(II) atoms in a *trans* geometry with the ethylenediamines displaying a *gauche* configuration leading to a helicoidal dimeric copper(II) complex. As a consequence, the dimer shows helicoidal chirality adopting Δ and Λ conformations (Figure 3.4).

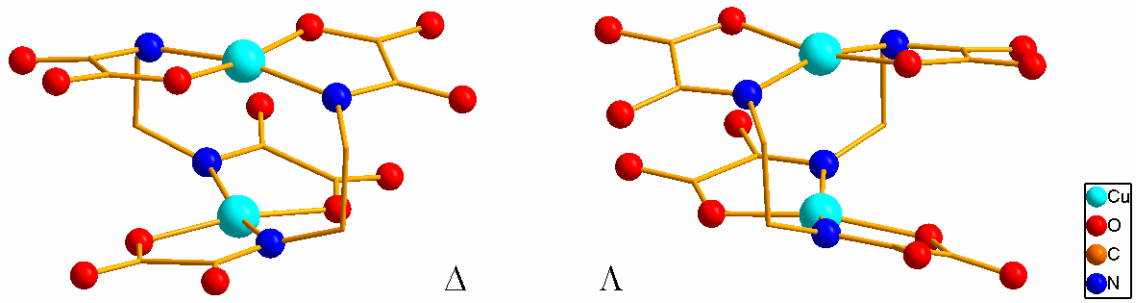

Figure 3. 4 Perspective view of the Δ and Λ enantiomers of the $[Cu(oeo)]_2^{4-}$ complex. Hydrogens atoms have been omitted for clarity.

Almost all crystal structures obtained are racemic being both enantiomers present in the crystal lattice. Since our reactions have been prepared using achiral reagents in an achiral solvent, we expect our reaction solutions to contain equal proportions of each enantiomer and therefore obtain racemic crystal structures. However, one species, *β*-

$Li_4[Cu(oeo)_2]\cdot 6H_2O$ **(10b)**, crystallised in the chiral space group $P6_5$ containing only one enantiomer present in the crystal structure. The crystal was obtained from the same batch where **10c** and **12** were obtained. They crystallised from slow solvent diffusion of an organic solvent into the reactant solution and particularly **10b** was crystallised first at the top of the vial. Nevertheless, the crystal measured is a twin in which the two enantiomers exist in a 88:12 ratio. It is worth noting that one of the aims of this project was to synthesise the chiral compound of the dimer. For that reason, a number of attempts to reproduce the synthesis, in order to study the right conditions to obtain a homochiral sample of the dimer, were carried out but they all were unsuccessful.

The distribution of the two enantiomers in the crystal lattice depends on the space group and on how the dimer packs in lattice. When the dimer packs in stacks in which infinite $[Cu(oeo)]_2^{4-}$ rods are linked to neighbouring $[Cu(oeo)]_2^{4-}$ rods by the counter ions (alkali metals) and crystallisation water molecules, the chirality is alternated within the rod. In some cases, it leads to an alternation of enantiomorphic planes of copper(II) complexes. On the other hand, when the crystal lattice is described as alternated anionic and cationic layers of $[Cu(oeo)]_2^{4-}$ and alkali metal respectively, the chirality of the dimers is alternated within the $[Cu(oeo)]_2^{4-}$ layer or between layers.

3. 4 Partial Copper(II) occupancy

As mentioned in Chapter 1, we observe a partial occupancy in the copper(II) site of the dimer. Due to the structural morphology of the dimeric unit, when the metal site is vacant, it is possible to have hydrogen bonds between the protonated amido nitrogens and the carboxylate oxygens of the two "chelating" oxamato groups, leading to a cyclic $R_2^2(10)$ motif (Figure 3.5).[12] This type of motif is very common in the ethylene-1,2-dioxamate systems. In chapter 2, we have observed we observed this motif in the salts of diethyl ethylene-1,2-dioxamate when connecting ligands molecules or dimeric units in the crystal lattice. Now, we will see this motif when connecting two ligand molecules in the copper(II) dimer.

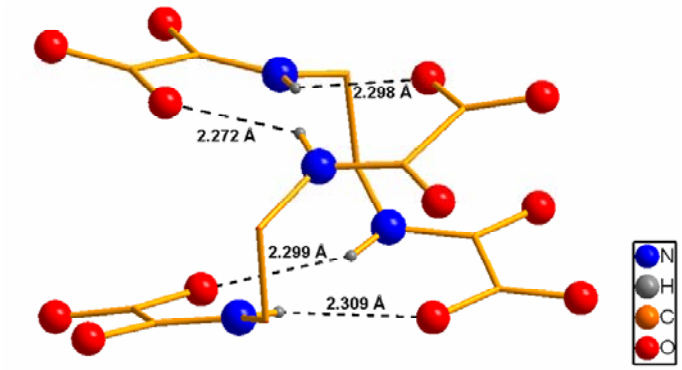

Figure 3. 5 Perspective view of the dimeric unit of **16** with the copper atom site being vacant and showing the hydrogen-bonding between ligand molecules. Hydrogen atoms of the ethylenediamine fragment are omitted for clarity.

In the initial model of the crystal structure in which all non-hydrogen atoms were found and refined using anisotropic thermal parameters, it was noted that the thermal parameter of the copper atom sites was large compared with the thermal parameters of the other atoms present in the asymmetric unit (Figure 3.6).

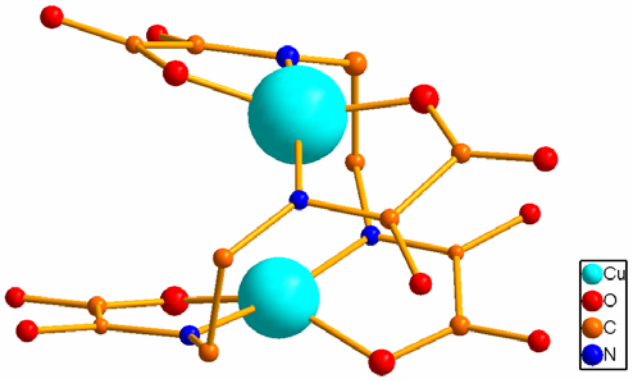

Figure 3. 6 Perspective view of the $[Cu(oeo)]_2^{4-}$ dimeric unit with the copper atom sites fully occupied. Isotropic thermal ellipsoids are drawn in a 50% of probability level showing the different size of the copper atoms when compared with the other atoms in the molecule. Hydrogen atoms are omitted for clarity.

In addition, a large negative electron density in the copper site was observed when looking at the difference Fourier electron density map. It can be noticed that the contour of the map is not flat and homogeneous, like one would expect when the final solution of the crystal structure is found. Instead a rough surface with a large negative hole is observed (Figure 3.7).

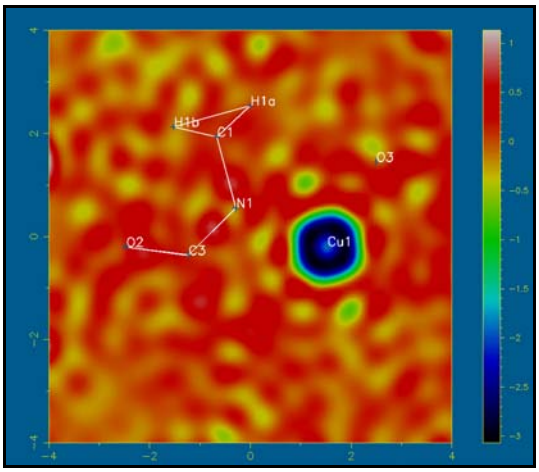

Figure 3. 7 Slant Plane Difference Fourier Electron Density Contour Map of the plane containing N1-Cu1-O3 atoms. In this model, the copper atom is assumed to have a 100% of occupancy. Electron density units: $e^-/Å$. Scale maximum and minimum: 1 and -3 $e^-/Å$, respectively.

As a result of these two facts, it was consistent to think that too much electron density was placed at the copper site. Thus, either the atom chosen for this site is not the right one or the atom site is not always filled. The presence of the copper atom as the only transition metal present in the synthesis was certain and consequently, the occupancy of the metal site was tested refining the copper occupancy free and leading to a copper atom site partially occupied.

By refining the copper occupancy free, the difference Fourier electron density map now showed a pretty flat and homogeneous contour map (Figure 3.8), as well as the atom thermal parameters of the structure showing similar sizes (Figure 3.9).

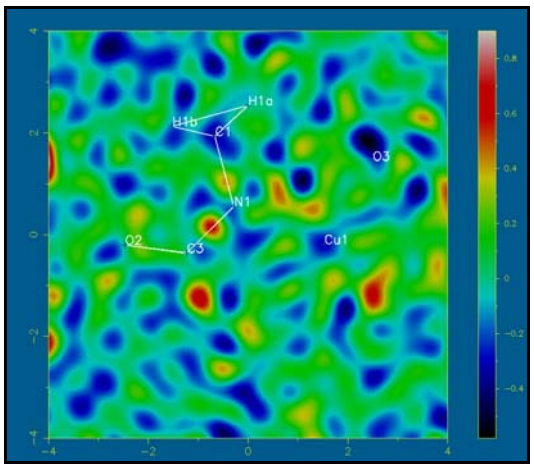

Figure 3. 8 Slant Plane Difference Fourier Electron Density Contour Map of the plane containing N1-Cu1-O3 atoms. In this case, the free refinement of the copper site occupancy lead to 18%. Electron density units: $e^-/Å$. Scale maximum and minimum: 1 and -0.5 $e^-/Å$, respectively.

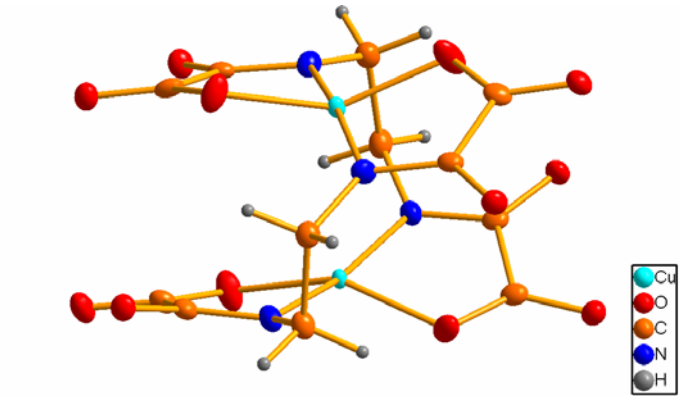

Figure 3. 9 Perspective view of the dimeric unit with partial copper site occupancy. Anisotropic thermal ellipsoids are drawn at 50% of probability level.

A wide range of copper(II) occupancies has been observed within the crystal structures: from structures with a partial copper occupancy of 5%, to structures with a fully occupied copper site. However, over the following chapters it will be discussed in depth the different occupancies that have been found, its relation with the packing of the dimer in the crystal lattice and its relation with the geometry around the copper(II) site.

In addition, when the copper atom is absent, the amide nitrogen must be protonated due to the pK_a of this atom and the pH of the solution, since the copper(II) complex is prepared in water under basic conditions. Thus, when the amide hydrogen atom is present, the amide is hydrogen bonded to the carboxylate oxygen of the neighbouring ligand molecule showing, as previously mentioned, a $R_2^2(10)$ motif. It is surprising that when the copper(II) atom site is vacant the molecule still maintains the same geometry. This is thanks to the intermolecular distance between oxamato groups of the two different organic molecules which is the right one for having hydrogen bonds between the two groups.

Lastly, we have to highlight that in the present and previous chapters, the copper(II) dimeric compounds have been named using the idealised non disordered fully occupied structure, $M_4[Cu(oeo)]_2$, although this is not their real formula in order to cause no confusion and to be as clear as possible. However, the compounds in the following chapters will be named using their real formula.

3. 5 Solid solution

The compositional variation of a crystalline substance due to substitution or omission of various atomic constituents within a crystal structure is a solid solution. As previously mentioned, the copper dimer $[Cu(oeo)]_2^{4-}$ exhibit a wide range of copper occupancies within the dimer due to the substitution by hydrogen bonds maintaining the same geometry.

By representing the occupancy in a graph it can be observed the three different species that can be present in the crystal lattice depending on the amount of copper(II) (Scheme 3.4). Like in aqueous solution (See Chapter 1), the distribution of the species in the crystal lattice is probably essentially an equilibrium between the dimeric and the monomeric structures, $[Cu_2(oeo)_2]^{4-}$ and $[Cu(Hoeo)_2]^{4-}$ respectively, when the percentage of copper(II) is higher than 50%. And between the monomer and the free ligand, $[Cu(Hoeo)_2]^{4-}$ and $[H_2(oeo)_2]^{4-}$ respectively, when the occupancy is below 50%.

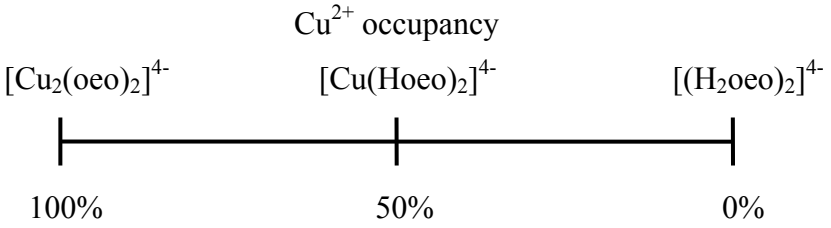

Scheme 3. 4

When dimer is half filled by copper, one of the sites must be filled by the metal and the other site must vacant, giving rise to the formation the hydrogen bonds in the vacancy site (Figure 3.10).

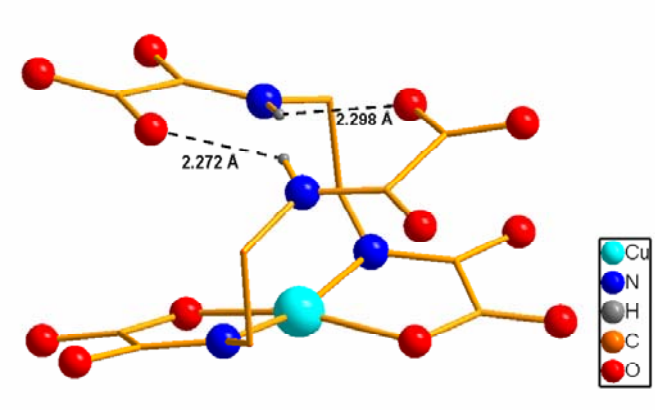

Figure 3. 10 Perspective view of the of the dimeric unit half filled where one of the copper sites is filled by the metal and the other one vacant, leading to the formation of hydrogen bonds between the ligand molecules. Hydrogen atoms of the ethylendiamine fragment have been omitted for clarity.

Therefore, the presence of two possible molecules in the crystal depending on the amount of copper(II), leads to the superposition of two molecules in the model. That is to say that we have a solid solution. When the occupancy is higher than 50% the composition of the solid solution is $M_4\{[Cu(oeo)_2]_x[Cu(Hoeo)_2]_{(1-x)}\}$ while it is lower than a 50%, the composition is $M_4\{[Cu(Hoeo)_2]_x[(H_2oeo)_2]_{(1-x)}\}$.

However, the amount of each molecule present in the crystal is correlated to the amount of copper(II) occupancy but both compounds do not have to be the same value. That is to say that "x" in not equal to the copper(II) occupancy in the dimer. For instance, a copper(II) dimer crystallises containing half of the dimer in the asymmetric unit and 30% of copper(II) occupancy. Therefore, we have a $M_4\{[Cu(Hoeo)_2]_x[(H_2oeo)_2]_{(1-x)}\}$ solid solution. In the $[Cu(Hoeo)_2]^{4-}$ molecule only one copper site can be filled at the time and thus, we can have two possible options: either one of the copper sites in the dimer is filled or the other, leaving the other site of the dimer filled with hydrogen bonds (Scheme 3.5). Consequently, the total percentage of the $[Cu(Hoeo)_2]^{4-}$ molecule in the crystal lattice is 60% and so, the solid solution composition is $M_4\{[Cu(Hoeo)_2]_{0.6}[(H_2oeo)_2]_{0.4}\}$.

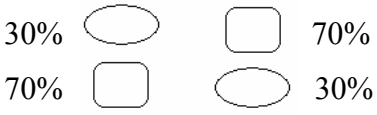

Scheme 3. 5 The ellipsoid represents the copper(II) site being filled and the square represents the hydrogen bonds between oxamato groups.

On the other hand, it has been noted that in general, the thermal ellipsoid of the carboxylate oxygens are rather elongated in one of the directions (Figure 3.9). This is consistent with the superposition of the two molecules in the crystal lattice. Due to the superposition of the two species we would expect two sites for the oxygen atom in the crystal lattice, one for when the atom is coordinated to the copper and another for when it is hydrogen bonded to the amide. However, the sites are not well separated and they appear as an elongated thermal ellipsoid. The possible atom disorder was checked by eliminating the oxygen when the final solution was found and then refining the model. Refinement leaded to only one oxygen site in the difference Fourier map.

3. 6 Diffuse Scattering

Looking at the distribution of the two species in the crystal lattice from a wider perspective, the two molecules can have a random or an ordered distribution within the lattice, or somewhere in between. This could be seen as a type of disorder in the crystal lattice and it could be studied using X-ray diffuse scattering analysis since it is a powerful method for characterizing short range disorder in crystals. However, the problem of the technique is that the diffuse scattering intensities are very weak in comparison to the Bragg peaks. Moreover, the diversity of the different types of disorder and their effect on the diffraction pattern make it vastly time consuming and very difficult to derive a solution.

If the crystal shows an ordered pattern in dimeric molecules, it should be observed in the frames. Therefore, by analyzing a crystal using this technique and studying the intensity of the peaks scattered outside the Bragg reflections, we hoped to be able to determine the distribution of the two species in the crystal. Diffuse scattering was observed in the crystal studied using the Rigaku R-Axis/RAPID single-crystal image-plate detector diffractometer in collaboration with the group specialised in the subject within the Department of Chemistry of the University of Glasgow. However, the structure of the crystal analyzed had implicit some disorder in the counter ions and consequently in the crystallization water molecules, making it difficult to study. Moreover, the dimeric structure contains a large number of atoms which makes the study even more complicated since the molecules usually studied using this technique

are relatively simple. Lastly, these studies are outside of the aim of the project and will be continued in other projects.

[1] T. Rüffer, B. Bräuer, B. Walfort*, Inorg. Chem. Commun.,* **2006**, *9*, 1111
[2] E. Pardo, R. Ruiz-García, J. Cano, X. Ottenwaelder, R. Lescouëzec, Y. Journaux, F. Lloret, M.Julve, *Dalton Trans*.**, 2008**, 2780
[3] T. Rüffer, B. Bräuer, F. E. Meva, B. Walfort, Dalton Trans., **2008**, 5089
[4] P. Comba, S. P. Gavrish, Y. D. Lampeka, P. Lightfoot, A. Peters, *J. Chem. Soc*., *Dalton Trans*., **1999**, 4099
[5] J. C. Colin, T. Mallah, Y. Journaux, F. Lloret, M. Julve, C. Bois, *Inorg. Chem.*, **1996**, *35* (14), 4170
[6] B. Cervera, J.L. Sanz, M.J. Ibañez, G. Vila, F. Lloret, M. Julve, R. Ruiz, X. Ottenwaelder, A. Aukauloo, S. Poussereau, Y. Journaux, M.C. Muñoz, *J. Chem. Soc*., *Dalton Trans.*, **1998**, 781
[7] K. E. Berg, Y. Pellegrin, G. Blondin, X. Ottenwaelder, Y. Journaux, M. Moragues Canovas, T. Mallah, S. Parsons, A. Aukauloo, *Eur. J. Inorg. Chem.*, **2002**, *323-325*, 1434
[8] M. Fettouhi, L. Ouahab, A. Boukhari, O. Cador, C. Mathonière, O. Kahn, *Inorg. Chem.,* **1996***, 35,* 4932
[9] B. Cervera, J.L. Sanz, M.J. Ibañez, G. Vila, F. Lloret, M. Julve, R. Ruiz, X. Ottenwaelder, A. Aukauloo, S. Poussereau, Y. Journaux, M.C. Muñoz, *J. Chem. Soc*., *Dalton Trans.*, **1998**, 781
[10] K. E. Berg, Y. Pellegrin, G. Blondin, X. Ottenwaelder, Y. Journaux, M. Moragues Canovas, T. Mallah, S. Parsons, A. Aukauloo, *Eur. J. Inorg. Chem.,* **2002**, *323-325*, 1434
[11] M. Fettouhi, L. Ouahab, A. Boukhari, O. Cador, C. Mathonière, O. Kahn, *Inorg. Chem.,* **1996***, 35,* 4932
[12] M. C. Etter, J. C. MacDonald. *Acta Cryst*., **1990**, *B46*, 256

Chapter 4: Lithium Compounds

4. 1 Introduction

4. 1. 1 α-$Li_4[Cu_{0.90}H_{0.20}(oeo)]_2 \cdot 6H_2O$ (10a) and $Li_4[Cu_{0.93}H_{0.14}(oeo)]_2 \cdot 10½\ H_2O$ (11)

The first two compounds that were characterised having the $Li_4[Cu(oeo)]_2 \cdot nH_2O$ composition were obtained from an aqueous solution of $(n Bu_4N)_x[Cu(oeo)_y]$ with the later addition of a LiBr solution giving rise, after few days, to two different crystal structures, α- $Li_4[Cu_{0.90}H_{0.20}(oeo)]_2 \cdot 6H_2O$ **(10a)** and $Li_4[Cu_{0.93}H_{0.14}(oeo)]_2 \cdot 10½H_2O$ **(11)**.

They are both formed by the $[Cu(oeo)]_2^{4-}$ dimer which is coordinated towards the lithium cations through the carbonyl oxygen atoms of the ligand. Water molecules fill the coordination sites of the lithium environment. **10a** crystallises in the *C*2/*c* space group containing half molecule in the asymmetric unit whereas **11** crystallises in the $P\bar{1}$ space group having two $[Cu(oeo)]_2^{4-}$ dimers in the asymmetric unit. Moreover, in both crystal lattices, the $[Cu(oeo)]_2^{4-}$ dimer packs in infinite rods which are linked to four and six neighbouring rods though the lithium cations, respectively. Within the rod, each $[Cu(oeo)]_2^{4-}$ dimer is linked to the nearest dimer through a carboxylate oxygen of the later giving rise to square-pyramid environment around the copper atom. Both structures have a partial occupancy in the copper site which in all cases, it is above 89% and therefore the solid solutions have a $Li_4\{[Cu(oeo)_2]_x[Cu(Hoeo)_2]_{(1-x)}\}$ composition where x = 0.80 and 0.83 for **10a** and **11**, respectively.

Nonetheless, **11** decomposes with time in the open air, losing water molecules and crystallinity. Under the microscope, translucent crystals become crazed and opaque indicating some catastrophic structural transition. Probably, the most stable hydrate for $Li_4[Cu(oeo)]_2 \cdot nH_2O$ is the one containing six water molecules since two more $Li_4[Cu(oeo)]_2 \cdot 6H_2O$ polymorphs have been found as well as a crystal structure containing five water molecules, $Li_4[Cu_{0.96}H_{0.08}(oeo)]_2 \cdot 5H_2O$ **(12)**. After a couple of months, the microanalysis of **11** was consistent with $Li_4[Cu(oeo)]_2 \cdot 8H_2O$ (*Anal*. Calc. for $C_6H_{12}Cu_1N_2Li_2O_{10}$ (Mw: 349.6): C, 20.61; H, 3.46; N, 8.01. Found: C, 20.88; H, 3.21; N, 7.89%). On the other hand, in the aqueous synthesis conditions, **10a** and **11** are stable and both probably have similar Gibbs energy of formation since they were formed at similar times.

Due to the high negative charge of the copper(II) complex, **10a** and **11** are only stable in water under basic pH. At neutral conditions they decompose forming a blue solid. However, they are stable during enough time to run a ^{1}H-NMR measurement of the mixture revealing the presence of only one peak at 3.32ppm which is consistent with the formation of the $[Cu(oeo)]_2^{4-}$ dimer. Moreover, the IR measurements of the two species show the same features although, the carbonyl stretchings for **11** are broader, probably due to the larger number of carbonyl environments that **11** has (See Figure 4.11).

Since the formation of **10a** and **11** was carried out adding an unknown amount of LiBr to a $(n\text{Bu}_4\text{N})_x[\text{Cu(oeo)}_y]$ solution, we explored the conditions in which crystals could be afforded again. However, these conditions are very narrow since several unsuccessful attempts were carried out by adding LiBr solutions with different concentrations to a $(n\text{Bu}_4\text{N})_x[\text{Cu(oeo)}_y]$ solution. Insoluble coordination polymers or copper oxides were obtained but no crystals.

4. 1. 2 *β*- $Li_4[Cu_{0.94}H_{0.12}(oeo)]_2{\cdot}6H_2O$ (10b), *γ*-$Li_4[Cu(oeo)]_2{\cdot}6H_2O$ (10c) and $Li_4[Cu_{0.96}H_{0.08}(oeo)]_2{\cdot}5H_2O$ (12)

Compounds **10a** and **11** are the only $Li_4[Cu(oeo)]_2{\cdot}nH_2O$ crystal structures that were formed directly as all other crystals were afforded by slow solvent diffusion of common organic solvents into the reactant solution. They were obtained from an attempt of synthesis of a bis(oxamide) copper(II) complex using $(ebo)H_4$ **(31)** as the chelating ligand.[1,2] However, it is well known that under basic conditions and heat the hydrolysis of the amide gives rise to the formation of the acetate (Scheme 4.1). In our case, pH = 12 and approximately 50 ^{o}C, the hydrolysis resulted to afford our ligand, $(oeo)^{4-}$.

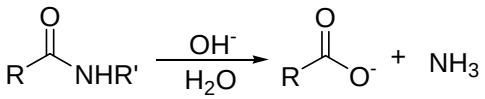

Scheme 4. 1

Thus, from an attempt of synthesis of a copper(II) complex using $(ebo)H_4$ as the ligand, three new crystal structures of $Li_4[Cu(oeo)]_2{\cdot}nH_2O$ were obtained from the same batch and the same crystallisation vial. Surprisingly, one of them crystallises in a chiral space group.

By X-ray analysis it could be revealed that the hydrolysis of the ligand has occured since the refinement values, as well as the thermal parameters, were consistent with the presence of oxygen atoms in the apparent amide nitrogens sites. Moreover, by looking at the Difference Fourier Electron Density Map, it could be observed that not enough electron density was placed in the oxygen sites when the atoms were refined as nitrogens, whereas when they were refined as oxygen a flat surface could be noted in the oxygen sites (Figure 4.1).

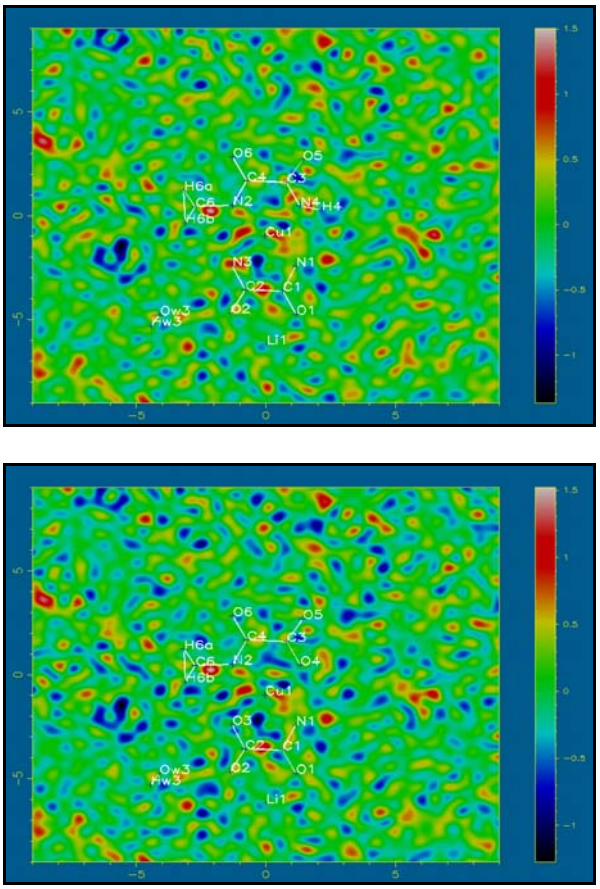

Figure 4. 1 Slant plane difference Fourier electron density contour map of the copper environment (electron density units in e^-/Å. Scale maximum and minimum: 1.5 and -1.25 e^-/Å, respectively.). It can be observed in the top picture some positive electron density in the N3 and N4 sites in the difference Fourier map. However, when the previous sites were refined as oxygen atoms, the surface around the sites was flat (bottom picture).

Slow solvent diffusion of ethanol into the reactant solution afforded two new $Li_4[Cu(oeo)]_2{\cdot}6H_2O$ polymorphs, β-$Li_4[Cu_{0.94}H_{0.12}(oeo)]_2{\cdot}6H_2O$ **(10b)** and γ- $Li_4[Cu(oeo)]_2{\cdot}6H_2O$ **(10c)**; and a new hydrate $Li_4[Cu_{0.96}H_{0.08}(oeo)]_2{\cdot}5H_2O$ **(12)**. **10b** crystallises in the $P6_5$ space group at the top of the vial, being probably the less soluble species. **10c** and **12** crystallises in the monoclinic $C2/c$ space group containing half of the molecule in the asymmetric unit. All three structures, like in compounds **10a** and **11**,

are formed by the $[Cu(oeo)]_2^{4-}$ dimer which is coordinated towards the lithium cations through the carbonyl oxygen atoms of the ligand. Moreover, water molecules fill the coordination sites of the lithium environment and the packing can be described as infinite rods of $[Cu(oeo)]_2^{4-}$ which are linked to four neighbouring rods though the lithium cations.

However, whereas **10b** has a hexagonal crystal packing (Figure 4.15), **10a**, **10c** and **12** have a layered crystal lattice where anionic layers of copper(II) complexes are alternated by cationic layers of lithium ions and water molecules (Figure 4.10 for **10a**; 4.18 for **12** and 4.21 for **10c**). In all three structures a hydrophobic pocket between stacks in present in the anionic layer. The difference between the packing of the structures is how the lithium ions are distributed in the lattice. In **10a**, cations are placed in the diagonal of the *ab*-plane) whereas in **10c** and **12** the lithium atoms make a continuous layer along the *a*-axis and *b*-axis direction, respectively.

The interaction between dimers within the stack of dimers and thus the copper(II) environment, is different between species. In the first two crystal structures obtained, **10a** and **11**, two dimers are linked through the bond between the copper atom of one dimer and the carboxylate oxygen atom of nearest dimer within the rod, leading to square-pyramid environment around the copper atom. This pattern is also seen in **10b**. However, in **10c** and **12**, there is only a weak interaction between dimers though the copper atom and the amide nitrogen of the neighbouring dimer giving a distorted squared-planar coordination to the metal ion. On the other hand, the chirality of the two dimers is alternated within the stack of dimers in all structures, except in **10b**.

In addition, it is noteworthy to emphasize how similar are the crystal lattices for **10c** and **10b**. Actually, the discovery of **10c** species was serendipitous as both compounds had very similar crystal habits and comparable cell parameters and crystal lattices. But, as discussed in Chapter 3 the careful analysis of the crystal data could reveal that a new polymorph was found. The difference between them is that although the cell parameters are the same, *a*-axis and *b*-axis are swapped and therefore the unique axis is exchanged leading to the two fold axis that is implicit in the dimer also being exchanged.

In Chapter 3 we mentioned that in the dimers that have C_1 and C_2 molecular point symmetry, the deviations from the maximal D_2 symmetry are minor and therefore we can say that they have a pseudo-D_2 symmetry. This is to say that, when looking at the dimer for instance, from above, no difference can be noted between different dimers. We need to look at the wider environment of the dimer to realise the real molecular point symmetry. This feature is very clear in the dimer environment of the $Li_4[Cu(oeo)]_2 \cdot nH_2O$ compounds. For instance, in compounds **10b**, **10c** and **12**, even by looking at the interaction between dimers in the crystal lattice though the chetalion of the oxamato groups towards the lithium cations, the real molecular point symmetry it is not obvious (Figures 4.2, 4.3 and 4.4). It is needed to look at the dimers and the lithium cations as a whole to notice the real symmetry in the molecule (Figure 4.5).

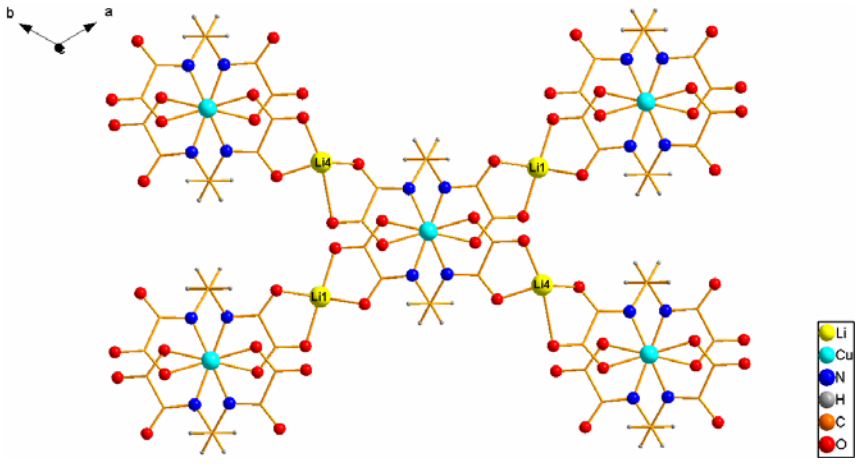

Figure 4. 2 Projection down the *c*-axis of the packing of the dimer in **10b**. It can be observed the lithium atoms Li1 and Li4 connect the dimers in a 2D-network.

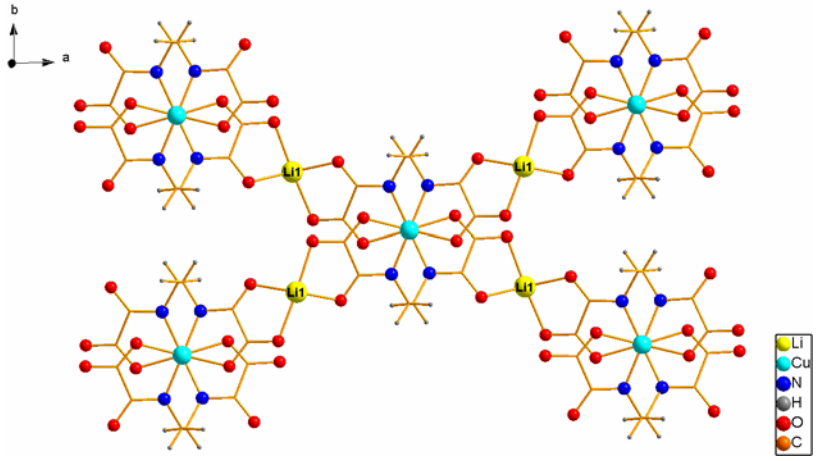

Figure 4. 3 Projection down the *c*-axis of the packing of the dimer in **10c**. It can be observed the lithium atoms Li1 connects the dimers in a 2D-network

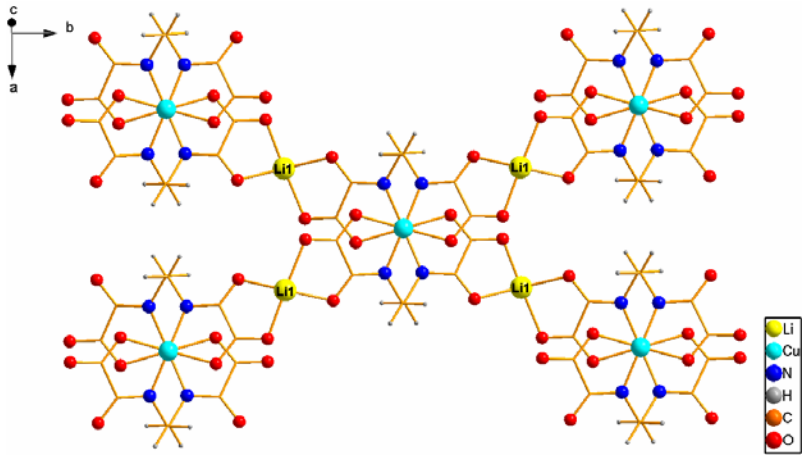

Figure 4. 4 Projection down the *c*-axis of the packing of the dimer in **12**. It can be observed the lithium atoms Li1 connects the dimers in a 2D-network

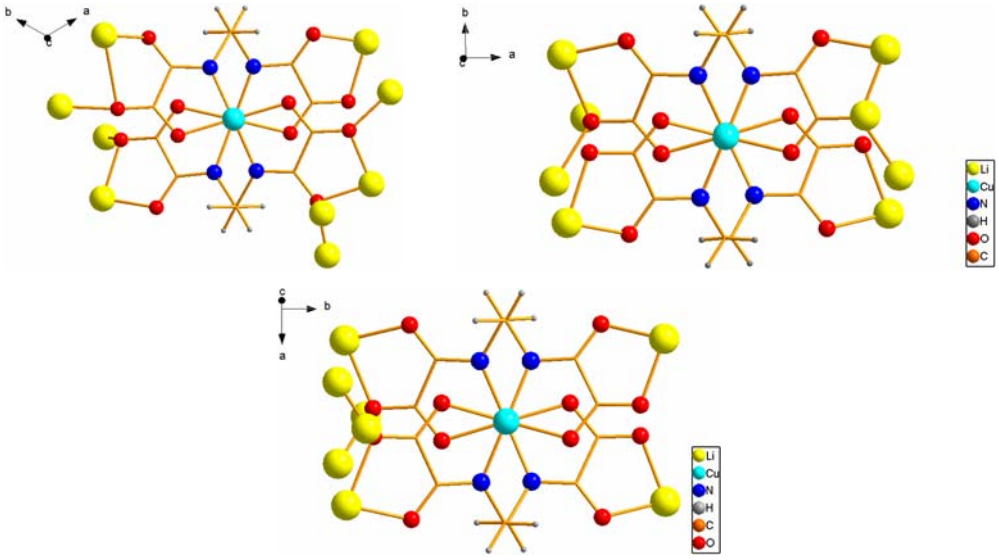

Figure 4. 5 Projection down the *c*-axis of the packing of the dimer for **10b** (top left), **10c** (top right) and **12** (bottom). It can be noticed that when looking down the *c*-axis no obvious difference between dimers is noted in the difference structures. But when looking at the cations it can be observed the difference coordination of the ligand towards the lithium ions. The C_2-axis in **10c** goes through the to two C-C ethylenediamine bonds while in **12** goes through the middle point of the molecule, perpendicular to the two hypothetical C_2-axis that pass through the two copper atoms and through the two ethylendiamine C-C bonds (Figure 3.2). **10b** has no C_2-axis since its molecular point symmetry is C_1.

On the other hand, these three structures have the copper sites fully or almost fully occupied and therefore the solid solutions have a $Li_4\{[Cu(oeo)_2]_x[Cu(Hoeo)_2]_{(1-x)}\}$composition where x = 0.89, 1.00 and 0.83 for **10b**, **10c** and **11**, respectively. Surprisingly, the occupancy in the copper(II) sites of all $Li_4[Cu(oeo)]_2{\cdot}nH_2O$ structures is very high, over 89%, compared with the rest of the copper(II) dimer complexes obtained with other counter ions, $M_4[Cu(oeo)]_2{\cdot}nH_2O$ M =Na, K, Rb. Probably it is related to the morphology of the packing of the dimers. In all structures the dimer packs in stacks in which there is some type of interaction between dimers through the copper

atom, a bond with an oxygen atoms or a weak interaction with the nitrogen of the neighbouring dimer. Therefore, it is needed a large amount of copper in the crystal structure for crystallise forming stacks and be stable. Even more, in some synthesis in which some amount of copper that was in solution was lost due to the precipitation of copper oxide, copper hydroxide, or some coordination polymer, and therefore low presence of copper would be expected in the crystal, a high copper occupancy was also obtained **(10b**, **10c**, **12)**, probably due to the type packing of the dimer.

4. 1. 3 Formation of a microcrystalline solid of $Li_4[Cu(oeo)]_2 \cdot nH_2O$ (13)

As previously mentioned, once $Li_4[Cu(oeo)]_2 \cdot nH_2O$ compound could be characterised, the aim of the project was the preparation of a microcrystalline solid that could be dissolved in water under basic conditions in order to add further transition metals to the compound and form bimetallic copper(II) complexes. The formation of a $Li_4[Cu(oeo)]_2 \cdot nH_2O$ solid from the reactant solution in order to follow with the preparation of bimetallic complexes, was unfeasible since the rotaevaporation of the solvent afforded an insoluble blue solid that was probably a coordination polymer.

Therefore, having in mind that in general $[Cu(oeo)]_2^{4-}$ is soluble in aqueous solutions but insoluble in common organic solvents, a new synthesis approach of a copper(II) crystalline complex was carried out in presence of methanol. In this case, the base that was added was a $(Me_4N)OH$ solution in methanol which probably formed $(Me_4N)_x[Cu(oeo)_y]$. Then by the addition of a solution of LiBr, a microcrystalline solid could be afforded although it co-precipitated other insoluble solids. Purification of the microcrystals from the final mixture could be achieved by using seives. However, this synthesis route was very time consuming and afforded very low yields of the desirable compound, since a lot was lost in the purification process. Hence, another synthesis route was studied.

A pure microcrystalline solid of $Li_4[Cu(oeo)]_2 \cdot nH_2O$ could be achieved using a stepwise method and through the preparation of $Li_2H_2(oeo)$ as intermediate, instead of preparing a $(Me_4N)_x[Cu(oeo)_y]$ solution. To a suspension of $Et_2H_2(oeo)$ in water was added LiOH leading to the formation of $Li_2H_2(oeo)$ and then, the later addition of $CuCl_2 \cdot 2H_2O$ and LiOH gave rise to a $Li_4[Cu(oeo)]_2 \cdot nH_2O$ solution. The addition of 0.9 equivalents of $CuCl_2 \cdot 2H_2O$ could avoid the formation of co-products like copper oxides or hydroxides.

Finally, by charging the final solution with methanol, a deep blue microcrystalline solid was afforded after 24 hrs. The IR and microanalysis of the product was consistent with the formation of $Li_4[Cu(oeo)]_2 \cdot 6H_2O$ solid **(13)**, where the copper(II) copper was assumed to be fully occupied. Moreover, the preparation of **13** could be achieved in other attempts. However, not always a good quality of crystal appearance was obtained, probably due to the ambient conditions as the temperature in the lab varied depending on the time of the year. Compound **13** was analysed using scanning electron microscope (SEM), in which different crystal morphologies were noticed. It could be observed, for instance, hexagonal and diamond shaped prisms, which fit with the expected morphology of **10c** and **10b** crystals, respectively. Also, parallelepipeds shaped crystals were noted which might be assigned to **10a** (Figure 4.6).

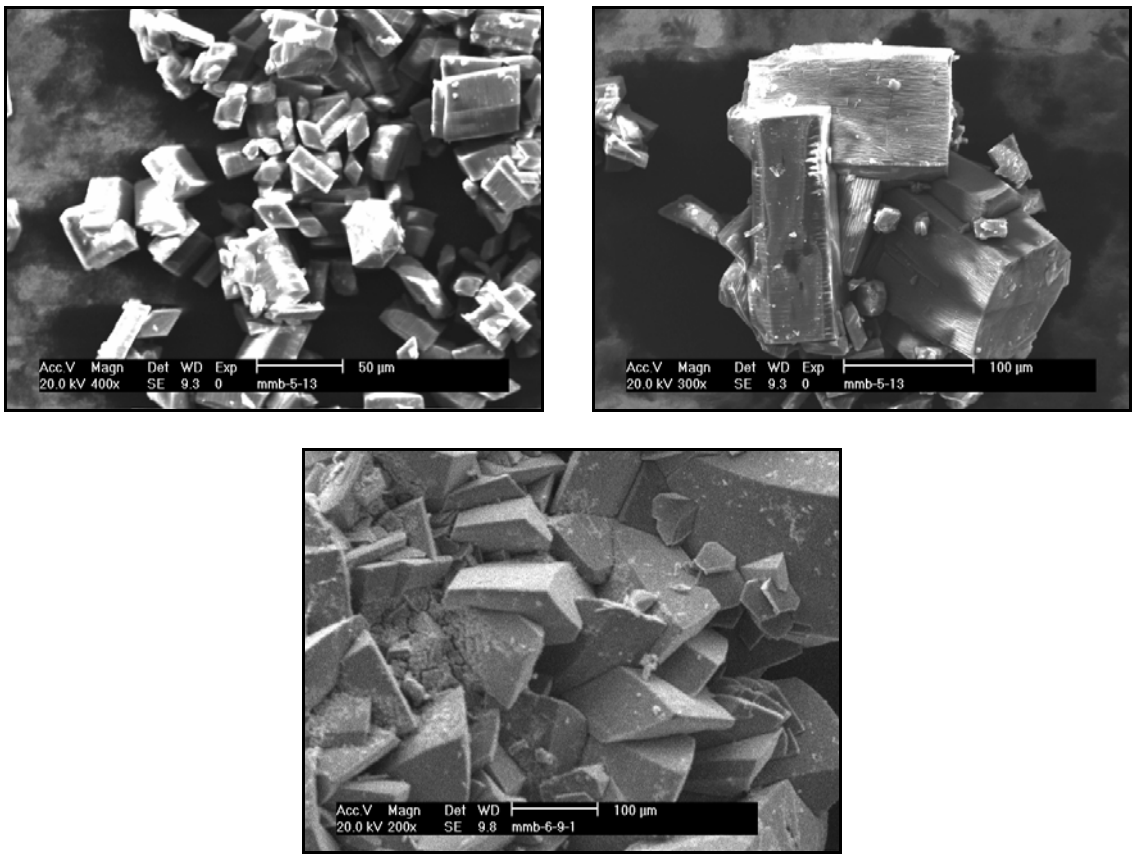

Figure 4. 6 SEM images of **13** from two different syntheses. In the bottom picture, it can be observed that the crystals obtained are not as well defined as the obtained in previous synthesis, top pictures.

The size of the particles of microcrystalline solid could change depending on the ambient conditions in the laboratory and the addition rates of the solvent. In some cases, the morphology of the microcrystals could be clearly observed using a microscope (Figure 4.7).

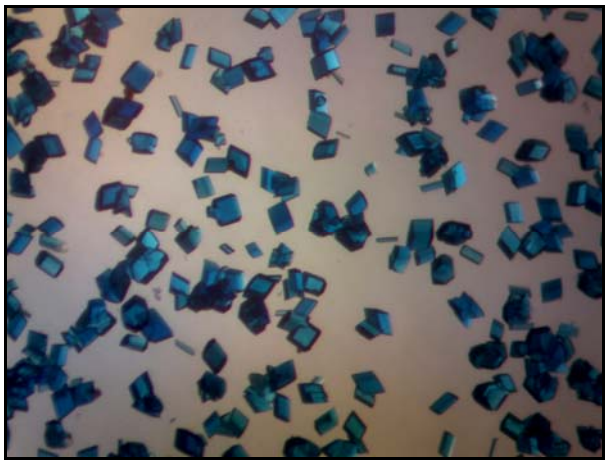

Figure 4. 7 View under the microscope in reflected unpolarized light of the microcrystalline solid of $Li_4[Cu(oeo)]_2 \cdot nH_2O$ showing different crystal habits and morphologies. Approximate scale: width of image 1cm.

In conclusion, even when forming a microcrystalline solid of $Li_4[Cu(oeo)]_2 \cdot nH_2O$ a number of different crystal habits and morphologies could be observed, so different hydrates and polymorphs could be afforded from the same batch. Therefore, the amount of copper present in **13** is unknown as well as the amount of water, leading to the unknown exact composition of the sample.

4. 2 Results

4. 2. 1 Description of structure α-$Li_4[Cu_{0.90}H_{0.20}(oeo)]_2 \cdot 6H_2O$ (10a)

Structure **10a** is made up of chiral anionic dinuclear copper(II) complexes, lithium cations and water molecules of crystallisation. The dinuclear copper complex is formed by two bideprotonated ethylene-1,2-dioxamato ligands, $(oeo)^{4-}$, and two copper(II) atoms leading to the anionic chiral dimeric unit $[Cu(oeo)]_2^{4-}$ (Figure 4.8). The copper(II) site occupancy is 89.7(2)%.

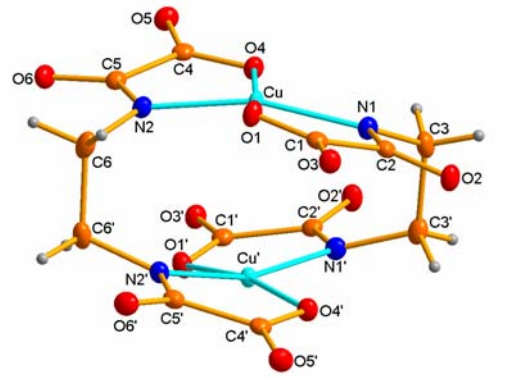

Figure 4. 8 Perspective view of the dinuclear copper (II) complex, $[Cu(oeo)]_2^{4-}$, showing the atom numbering scheme. Anisotropic thermal ellipsoids for non-hydrogen atoms are drawn at the 50% of probability level. Prime denotes symmetry operation -x, -y, 2-z.

The compound crystallises in the centrosymmetric space group *C*2/*c*. Thus, the asymmetric unit contains half of the dimer (one copper (II) atom and one ligand molecule), two lithium ions and three crystallisation water molecules. The other half of the dimer is generated through the C_2 symmetry axis that crosses in the mid-point of the two ethylendiamine C-C bond of the dimer.

The ligand adopts a tetradentate coordination in which each end of the ligand chelates a different copper (II) atom through the carboxylate oxygen and the deprotonated amide nitrogen giving a distorted square-planar geometry. Due to the *gauche* conformation that both ethylenediamine display the two ligands coordinate two different copper atoms giving a chiral copper dimer. These dinuclear units are stacked along the *c*-axis forming a chain in which the chirality of the species is alternated within the chain (Figure 4.9).

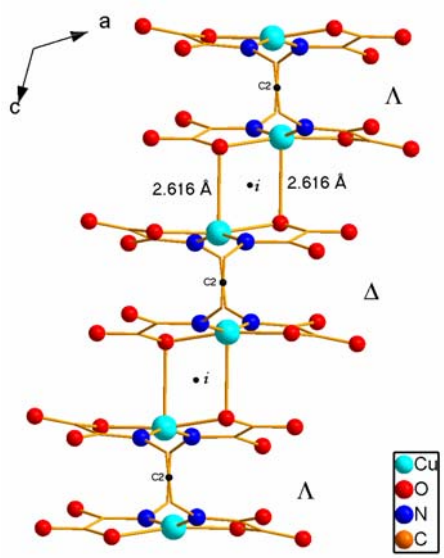

Figure 4. 9 Perspective view down the *b*-axis of the dinuclear copper(II)dimers, $[Cu(oeo)]_2^{4-}$, forming a chain along the *c*-axis. The alternate chirality (Λ and Δ) between dimers can be observed due to the inversion centres. The two fold axis along the C-C is also shown. Hydrogen atoms are omitted for clarity.

The long Cu-O (2.6163(1) Å) bond between two neighbouring molecules within the stack gives a distorted square pyramid coordination environment around the metal. The distance between coppers within the dimer is 3.0225(4) Å and the distance between coppers of neighbouring dimers is 3.5503(5) Å, being the former the longest distance between neighbouring metal atoms in the structure.

The packing of the crystal in the *ab*-plane can be described as rods of dimers growing in the *c*-axis direction surrounded by lithium atoms which due to the morphology of the dimer, they are placed along the diagonal of the *ab*-plane connecting the metal complexes in two dimensions. This pattern leads to a layered structure where metallic sheets are alternated with lithium ion sheets interconnected by water molecule oxygen atoms and carbonyl oxygen atoms of the ligand. In addition, between the rods of dimers there is a hydrophobic region in the metallic layer (Figure 4.10). The distance between dimers along the *b*-axis is 9.6996(4) Å and the distance between rods along the diagonal of the *ab*-plane 12.2659(4) Å.

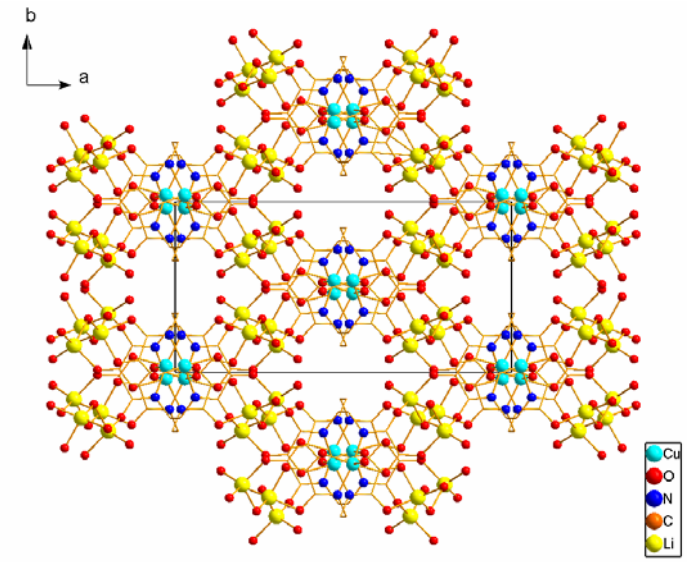

Figure 4. 10 Crystal packing view of **10a** along the *ab*-plane showing the packing of dimers where infinite $[Cu(oeo)]_2^{4-}$ rods running along the *c*-axis direction are linked to four neighbouring rods by lithium cations along the diagonal of the *ab*-plane. Hydrogen atoms are omitted for clarity.

The lithium atoms have a tetrahedral geometry in which the coordination sphere is filled by two water molecules and two oxamato carbonyl oxygens. Li1 has a distorted tetrahedral geometry due to the chelating coordination of the two oxamato carbonyl oxygens (O2 and O3) of the organic ligand. The remaining sites are filled by two water molecules (O7 and O9). On the other hand, Li2 has very small deviations from a tetrahedral geometry. The two oxamato carbonyl oxygens (O5 and O6) are provided by different dimers connecting to neighbouring dimers in the network. The remaining sites are filled by crystallisation waters (O7 and O8). A hydrogen bond network is formed between water molecules and carbonyl oxygens of the ligand.

4. 2. 2 Description of structure $Li_4[Cu_{0.93}H_{0.14}(oeo)]_2 \cdot 10½\ H_2O$ (11)

Compound **11** crystallises in the space group $P\bar{1}$ containing two copper(II) dimeric units $\{[Cu(oeo)]_2^{4-}\}$, eight lithium cations and twenty-one crystallisation water molecules in the asymmetric unit. The molecular symmetry of both dimers is C_1. The occupancy in the copper(II) sites are Cu1 93.0(2)%, Cu2 94.8(2)%, Cu3 93.8(2)%, Cu4 89.5(2)% and therefore, the lowest energetic site to place a copper(II) vacancy is Cu4 and the highest Cu2.

Each copper(II) atom is bonded to two nitrogen atoms and two oxygen atoms arising from two oxamato groups and occupying the vertices of the basal plane of a distorted

square-based pyramid. The apical position for Cu2 is filled by the carboxylate oxygen of the neighbouring dimer (O13) in the asymmetric unit which links the two dimers of the asymmetric unit (Cu2-O13 2.6093(1) Å). The copper atom of the dimer in which O13 is present (Cu3), has a distorted square-planar geometry with a weak interaction with the oxamato amide nitrogen (N4) arising from the other dimer of the asymmetric unit. Due to the long distance between the two atoms (Cu3-N4 2.9353(1) Å) it is considered a weak interaction rather than a bond although the nitrogen is placed in exactly above the copper atom (Figure 4.11).

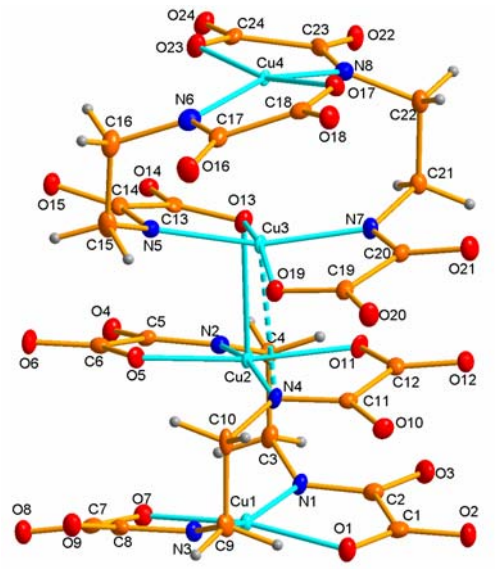

Figure 4. 11 Perspective view of the copper(II)dimers in the asymmetric unit, showing the atom numbering scheme. Anisotropic thermal ellipsoids for non-hydrogen atoms are drawn at the 50% of probability level. The weak interaction between Cu3 and N4 are represented by dashed lines.

The rest of copper(II) atoms present in the asymmetric unit (Cu1 and Cu4) have the apical position occupied by the inversion symmetry related oxamato carboxylate oxygen atom of the neighbouring dimer (O1 and O23 with distances 2.8070(1) Å and 2.5966(1) Å, respectively).

The packing of the dimers can be described as stacks of dimers growing through the diagonal of the unit cell and surrounded by lithium atoms and water molecules (Figure 4.12). The chirality of the dimers is alternated every two dimers along the stack in which the inversion centre in the middle of the unit cell (½, ½, ½) relates the pairs of dimers along the cell (Figure 4.13).

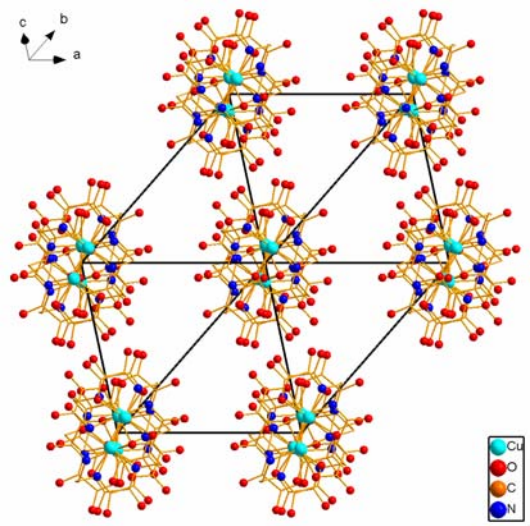

Figure 4. 12 Crystal packing of the dimers along the direction [1, -1, 1]. The dimers are surrounded by lithium atoms and water molecules which are omitted for clarity. Hydrogen atoms are also omitted for clarity.

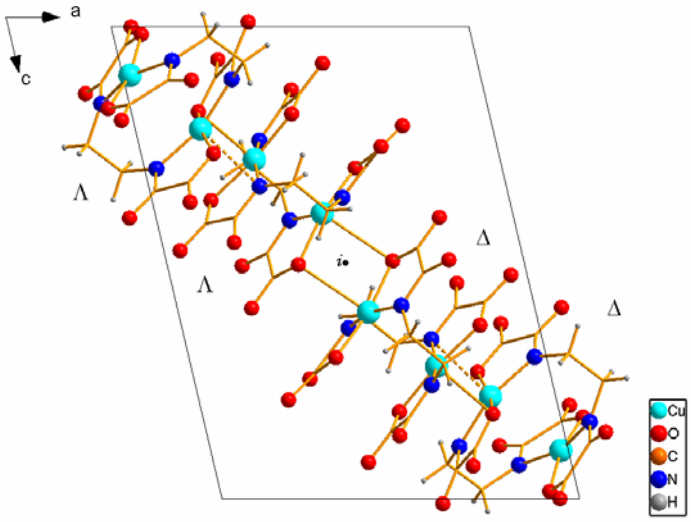

Figure 4. 13 Perspective view along the *b*-axis of the packing of the dimers along the cell diagonal. The dashed lines represent the weak interaction between dimers.

The lithium atoms are coordinated to water of crystallisation, and to carbonyl and carboxylato oxygen atoms, displaying a distorted tetrahedral and squared-based pyramid environment. In addition, the network of hydrogen bonds that involves the carbonyl and carboxylate oxygens, with the water molecules, link the rods of metal complexes into a three dimensional network.

4. 2. 3 Description of structure *β*-$Li_4[Cu_{0.94}H_{0.12}(oeo)]_2 \cdot 6H_2O$ (10b)

Structure **10b** crystallises in the pair of chiral space groups $P6_1$ and $P6_5$ of which, in this case, the crystal determined had the $P6_5$ space group. The asymmetric unit consists of a

dimeric copper(II) complex, $[Cu(oeo)]_2^{4-}$, four lithium cations and six water molecules. As a result of the enantiomorphic $P6_5$ space group, all dimers present in the crystal have the Δ helicoidal conformation. The crystal, as common in chiral space groups, has a merohedral twinning having 88(1)% of inverted structure, thus 88(1)% of $P6_1$ and 22(1)% of $P6_5$. The occupancy of the copper(II) for both atom sites in the dimer is 94.5(2)%.

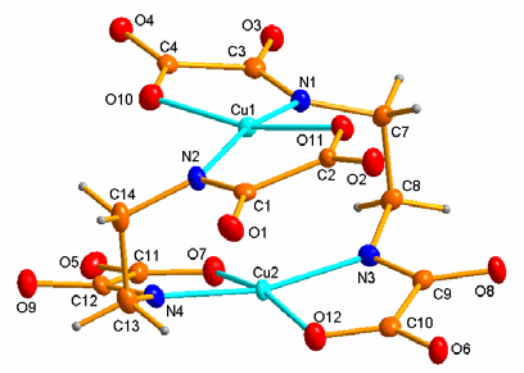

Figure 4. 12 View of the dimeric anion showing the atom labelling. Anisotropic thermal ellipsoids for non-hydrogen atoms are drawn at the 50% of probability level.

Like in all the other crystals the dimer is formed by two ligand molecules $(oeo)^{4-}$ which are coordinated towards two copper(II) atoms to form a dimeric structure (Figure 4.12). The apical position of the square-pyramid based environment of Cu1 is filled by a carboxylate oxygen (O7) of the neighbouring dimer (2.908(3) Å). This bond connects the dimers along the *c*-axis direction leading to the pattern where infinite rods run along this axis. The six-fold screw axis, 6_5, can be observed when looking down the *c*-axis (Figure 4.13).

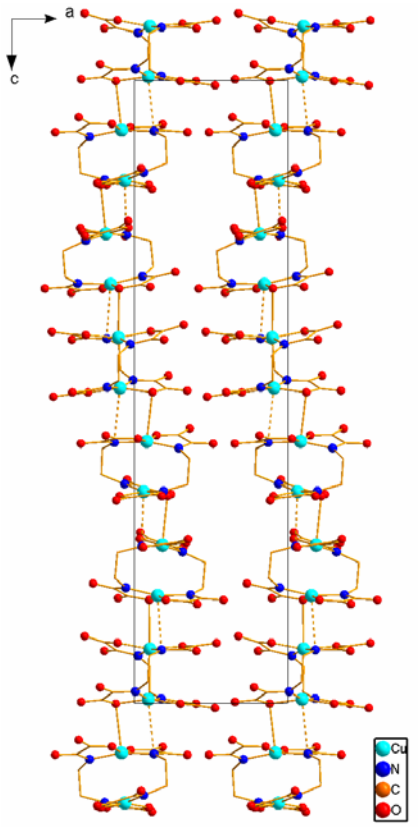

Figure 4. 13 Perspective view of the packing of the copper(II) dimers along the *c*-axis. Hydrogen atoms are omitted for clarity.

Moreover, dimers within the stack are also interconnected by a weak interaction between Cu2 and the nitrogen of the neighbouring dimer (N2), which due to the long distance (3.220(3) Å) it is not considered a bond (Figure 4.14). That leads to the intermolecular distance between copper atoms to be the longest one (3.5285(5) Å) since the intramolecular distance is 2.9673(5) Å.

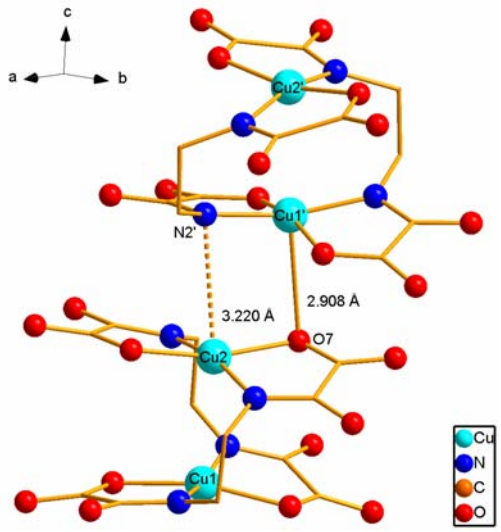

Figure 4. 14 Perspective view of the connection between dimers within the stack. Prime denotes symmetry operation y, 1-x+y, 1/6+z.

Lithium atoms are coordinated to the ligand through carbonyl and carboxylate oxygen atoms connecting the dimeric units in a 3-D network. The whole crystal packing can be viewed as infinite stacks of copper(II) dimers growing along the *c*-axis direction and occupying the vertices of the unit cell (Figure 4.15). They are interconnected by lithium cations and water molecules which surround the copper(II) complexes. The lithium atoms have four and five coordination.

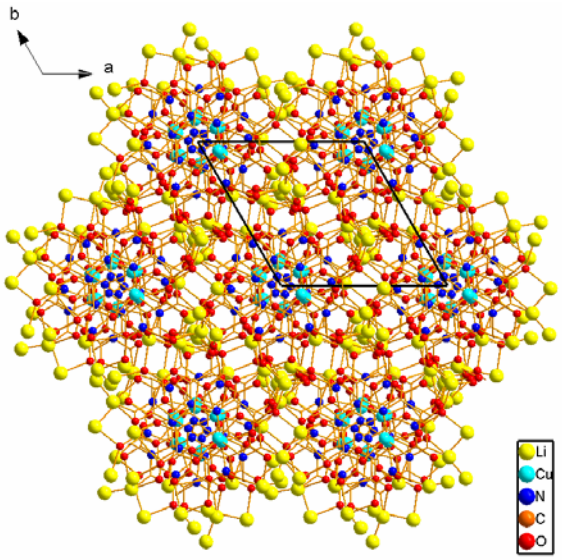

Figure 4. 15 Crystal packing of the dimers along the c direction. Hydrogen atoms are also omitted for clarity.

Two different environments have the lithium atoms. Li1 and Li4 are bichelated by two oxamato groups of two neighbouring dimers linking the stack of dimers network in three dimensions. They both display a square-pyramid geometry and the apical position is filled by a carbonyl oxygen of a neighbouring dimer. Li2 and Li3 have small deviations from a tetrahedral geometry and they are coordinated to three water molecules and to one carbonyl oxygen of an oxamato group of a dimer. Hydrogen bonds are formed between water molecules and carbonyl oxygen atoms of the ligand.

4. 2. 4 Description of structure $Li_4[Cu_{0.96}H_{0.08}(oeo)]_2 \cdot 5H_2O$ (12)

Compound **12** consists of discrete dimeric copper(II) complex anions, $[Cu(oeo)]_2^{4-}$, lithium cations and crystallisation water molecules. It crystallises in the space group *C*2/*c* and the asymmetric unit contains half of the dimeric unit, so one ligand molecule and one copper(II) atom, and 2½ water molecules (Figure 4.16). The other half of the molecule is, in this case, generated by symmetry through the two-fold axis that passes

through the middle point of the dimer which is perpendicular to the two hypothetical C_2-axes that would pass through the two copper atoms and through the two ethylendiamine C-C bonds (See Figure 3.2).

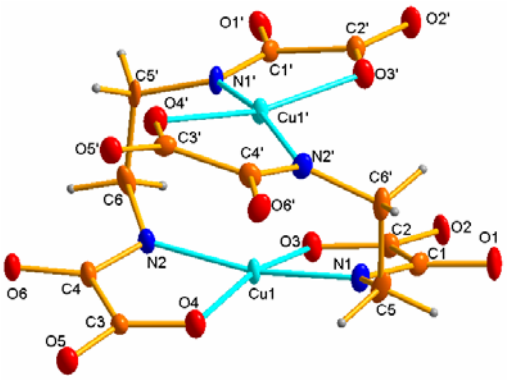

Figure 4. 16 View of the dimeric anion showing the atom labelling. Anisotropic thermal ellipsoids for non-hydrogen atoms are drawn at the 50% of probability level. Prime denotes symmetry operation 1-x, y, ½ -z.

In this compound, copper(II) atom has a distorted square-planar environment with weak interactions between the metal and the nitrogen of the nearest dimeric unit (N1). The inversion centre standing in the middle point of the imaginary parallelogram formed by Cu1-N1 and Cu1'-N1' gives rise to the formation of a stack of copper dimers running parallel to the *c*-axis direction. The distance between the transition metal ion and the nitrogen of the nearest dimer within the stack is 3.305(4) Å making the intramolecular distance between metal ions 3.740(2) Å (Figure 4.17). The intermolecular distance of the copper(II) ions within the dimer is 2.915(2) Å.

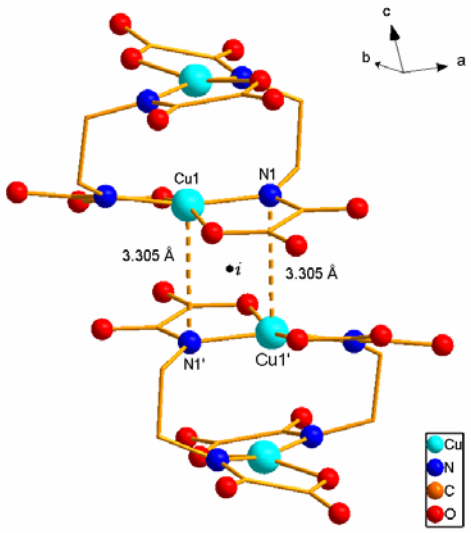

Figure 4. 17 Perspective view of the connection between dimers within the stack. Prime denotes symmetry operation 1-x, 1-y, -z.

The crystal packing can be viewed as alternating layers of copper(II) dimers and lithium ions interconnected by water molecules oxygen atoms and carbonyl oxygen atoms of the ligand molecule. In the cationic layer, there is a hydrophobic pocket between dimers. Thus, looking down the *c*-axis, it can be noted that the stack of dimers occupies the centre of the lattice face and define the vertices, while the centre of the edges are occupied by hydrophobic pockets (Figure 4.18).

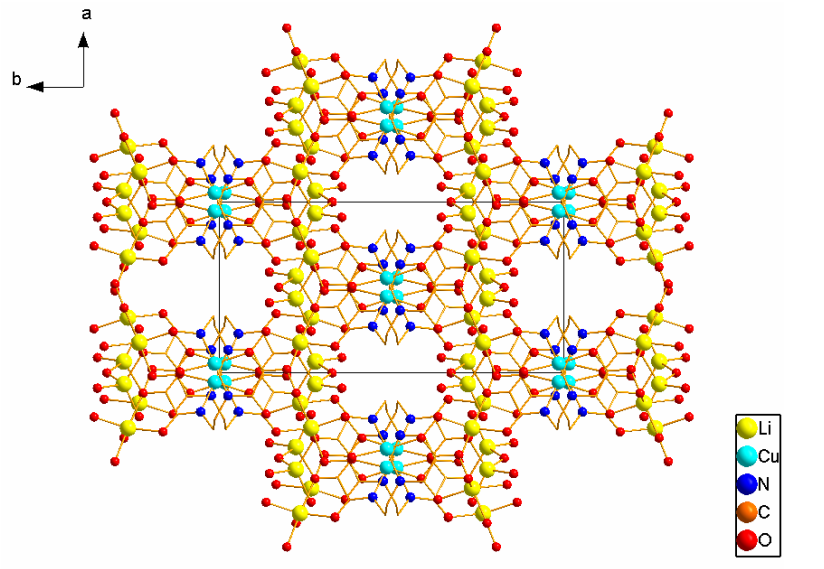

Figure 4. 18 Perspective view of the crystal packing along the *ab*-plane showing the face-centred lattice. Hydrogen atoms are omitted for clarity.

The distribution of the chirality of the dimer in the crystal lattice is displayed in two dimensions in which alternated planes of Δ and Λ enantiomers grow along the *c*-axis direction (Figure 4.19).

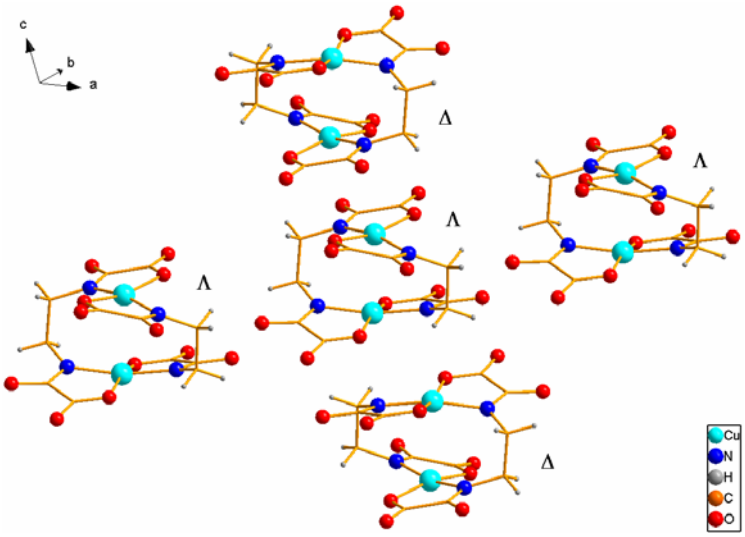

Figure 4. 19 Perspective view of the distribution of the chirality of the dimers in the crystal lattice.

The lithium cations display four and five coordination. Each oxamato group of the dimeric unit is chelating a lithium atom (Li1), linking one dimer to the four neighbouring dimers of the plane in a 2D-network. Li1 has a square-pyramid environment in which the remaining site is filled by a carbonyl oxygen atom of a neighbouring dimer. Li2 has a tetrahedral coordination with three oxygen atoms arising from water molecules and one arising from a carbonyl oxygen.

4. 2. 5 Description of structure γ-$Li_4[Cu(oeo)]_2 \cdot 6H_2O$ (10c)

Compound **10c** crystallises in the space group *C*2/*c*, containing half of the structure in the asymmetric unit: half of the dimer, two lithium ions and three water molecules. The C_2-axis going through the mid-point of the C-C bond of the two ethylenediamine fragments generates the other half of the molecule by symmetry (Figure 4.20). In this case, the copper site is fully occupied.

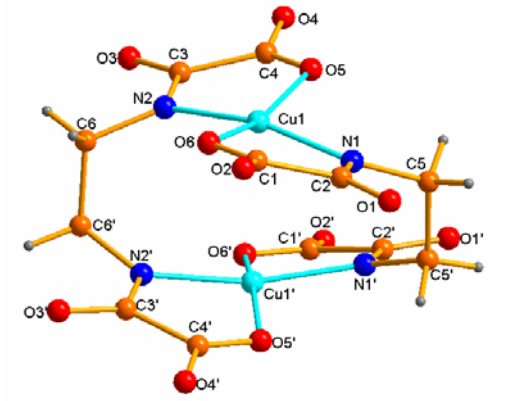

Figure 4. 20 View of the dimeric anion displaying atoms isotropically and showing the atom labelling. Prime denotes symmetry operation 1-x, y, 1½-z.

As in Compound **12**, the crystal has a layered structure where anionic sheets containing $[Cu(oeo)]_2^{4-}$ are alternating with cationic sheets of lithiums and water molecules. In the cationic layer, there are also hydrophobic pockets between rods of dimers. However, the alternating layers run along the *a*-axis direction (Figure 4.21). Moreover, looking down the *c*-axis, it can be observed the face centred lattice where, in this case, the hydrophobic pockets are placed in the centre of the lattice face and in the vertices of the cell. The stack of dimers occupied the centre of the edges.

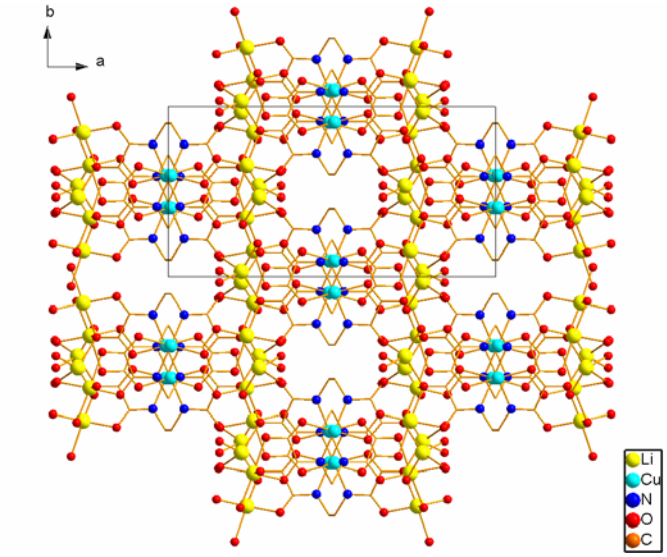

Figure 4. 21 Perspective view of the crystal packing along the *ab*-plane showing the stack of dimers placed in the centre and in the vertices of the cell. Hydrogen atoms are omitted for clarity.

Moreover, like in structure **12**, due to the long distance between dimeric units within the stack, there is no direct linkage between neighbouring dimers and therefore the copper(II) has a distorted square-planar environment. However, the metal has a weak interaction with the nitrogen atom of the nearest dimeric unit (N2) within the stack (3.597(14) Å) (Figure 4.22). The inversion centre standing in the middle point of the quadrangle built by Cu1-N2 and Cu1'-N2' gives rise to a one dimensional pseudo-chain of copper dimers running parallel to the *c*-axis direction. The intermolecular distance between metal ions 3.858(3) Å and the intramolecular distance within the dimer is 2.945(5) Å.

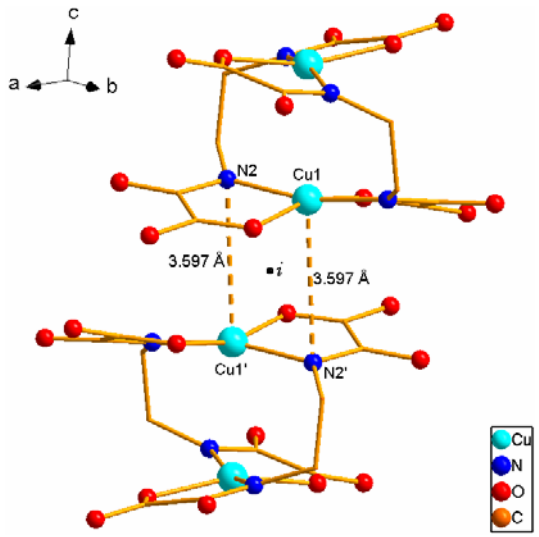

Figure 4. 22 Perspective view of the connection between dimers within the stack. Prime denotes symmetry operation 1-x, -y, 1-z.

On the other hand, the alternation of layers of Δ and Λ enatiomers along the *c*-axis direction is also displayed in the crystal structure, the same as in structure **12** (Figure 4.23).

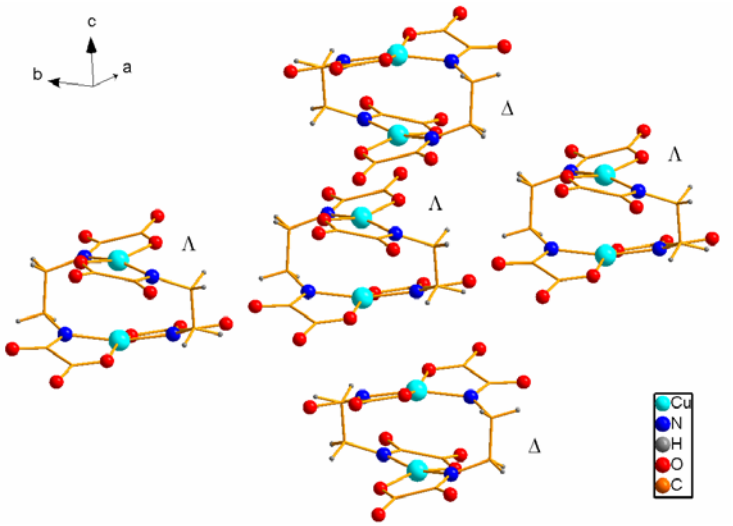

Figure 4. 23 Perspective view showing the chirality of the dimers in the crystal.

Each dimer is connected to four neighbouring copper(II) complexes in the *ab*-plane through lithium atoms (Li1), which are chelated by two oxamato groups of two neighbouring dimers connecting them in a two-dimensional network. Li1 has a square-pyramid environment and the remaining site is filled by a carbonyl oxygen atom of a close dimer. Li2 has a tetrahedral coordination with three oxygens arising from water molecules and another one arising from a carbonyl oxygen of the ligand.

4. 3 Experimental Section

4. 3. 1 *α*-$Li_4[Cu_{0.90}H_{0.20}(oeo)]_2 \cdot 6H_2O$ (10a)

Synthesis

A solution of Bu_4NOH (30.2 ml; 40% w/w water, 46.1 mmols) was added dropwise to a stirring suspension of $Et_2H_2(oeo)$ (3.00 g, 11.53 mmols) in H_2O (10 ml). The resulting mixture which was at pH=10, was stirred at room temperature until complete dissolution, aprox. 1 hr. An aqueous solution (3ml) of $CuCl_2 \cdot 2H_2O$ (1.96 g, 11.53 mmols) was then added slowly and the solution was left stirring overnight. The resulting deep blue solution was filtered off to eliminate the dark brown solid formed

due to the basic conditions. The solid is an impurity which had been previously characterised from other synthesis by PXRD as $CuO_x(OH)_yCl_z$.

A concentrated solution of LiBr in water (10 ml) was added to 10 ml of the final $(Bu_4N)_x[Cu_y(oeo)_2]$ solution and the mixture was allowed to stand at room temperature. Well shaped single crystals of **10a** and **11**, which were filtered off, dried in air and separated by hand, were formed within few days. IR (CsI, cm^{-1}): ν 3556(w), 3474(w), 3361 (w), 3215 (w), 2998-2861 (s), 1657 (w), 1616 (w), 1443 (s), 1353 (s), 1326(s) (See Appendix A1). *Anal*. Calc. for $C_6H_{10.20}Cu_{0.90}N_2Li_2O_9$ (Mw: 325.27): C, 22.15; H, 3.16; N, 8.61. Found: C, 21.54; H, 3.18; N, 8.19%. ^{1}H-NMR (400 MHz, D_2O, δ in ppm): 3.32 (s, CH_2NH). ^{1}H-NMR was run on the mixture of **10a** and **11**crystals. λ_{max}, 637nm.

Crystallographic Data Collection and Structure Determination

Copper site has partial occupancy and initially, it was refined free with the thermal parameters isotropic. Then, it was refined with anisotropic thermal parameters leading to a 89.7(2)% of copper occupancy.

All non-hydrogen atoms were refined anisotropically. The hydrogen atom positions of the organic molecule (also the amide hydrogen atoms for when the copper site is vacant) were assigned to calculated positions and refined with fixed individual displacement parameters [$U_{iso}(H) = 1.2U_{eq}(C_{ethyl})$ or $1.2U_{eq}(N_{amide})$] using a riding mode. Hydrogen atom positions from water molecules where located in difference-Fourier maps, refined with two restraints (O-H distances) and given isotropic thermal parameters [$U_{iso}(H) = 1.2U_{eq}(Ow)$].

Crystal data and selected details of the refinement are listed in Table 4.1.

Table 4. 1 Crystallographic data for **10a**

Empirical formula	$C_6H_{10.20}Cu_{0.90}N_2Li_2O_9$
Formula weight	325.27
Crystal system	monoclinic
Space group	*C*2/*c*
a (Å)	22.5329(8)
b (Å)	9.6996(4)
c (Å)	12.2791(6)
α (°)	90.00
β (°)	122.578(2)
γ (°)	90.00
V (Å^3)	2261.46(17)
T(K)	100(2)
ρ_{calc} (g/cm^3)	1.911
Z	8
F (000)	1314
Reflections collected	14676
Unique reflections	2584
Reflections observed [I>2σ(I)]	2164
R_{int}	0.0602
Parameters refined	200
Number of restraints	6
λ (Å); Mo Kα	0.71073
μ (mm^{-1})	1.790
θ Range (°)	2.15-27.50
Goodness-of-fit (GOF) on F^2	1.033
R [I>2σ(I)]	0.0277
wR_2 (all data)	0.0596
Largest difference in peak and hole (e Å^{-3})	0.31 and -0.35
Crystal size (mm)	0.1×0.1×0.1
Crystal morphology	blue prism

[a] $R_1 = \Sigma(|F_o| - |F_c|)/ \Sigma|F_o|$

[b] $wR_2 = [\Sigma w(F_o^2 - F_c^2)^2]/\Sigma w(F_o^2)^2]^{1/2}$ where $w = 1/[\sigma^2(F_o^2) + (0.2P)^2$ and $P = [F_o^2 + 2F_c^2]/3$

Selected bond lengths (Å) and angles (°) for compound **10a** are given in Table 4.2.[a,b] Also the dihedral angle formed by the chelating oxamato groups (°) and the distance of the atom from the mean plane (Å).

Table 4. 2 Selected bonds (Å) and angles (°) for **10a**

	Cu1-O1	1.9829(13)
	Cu1-O4	1.9925(13)
	Cu1-N1	1.9514(16)
	Cu1-N2	1.9391(16)
	O1-Cu1-N1	84.33(6)
	O1-Cu1-N2	94.73(6)
	N1-Cu1-O4	100.66(6)
	N2-Cu1-O4	83.11(6)
	Dihedral angle	20.39(7)
Atom displacement	Cu1	-0.022(0)
	O1	-0.204(2)
	N2	0.271(2)
	O4	0.171(2)
	N1	0.253(2)

[a]Estimated standard deviations in the last significant digits are given in parenthesis. The dihedral angle for Cu1 was calculated measuring the angle between the plane formed by O1-Cu1-N1 and O4-Cu1-N2.

4. 3. 2 $Li_4[Cu_{0.93}H_{0.14}(oeo)]_2 \cdot 10½\ H_2O$ (11)

Synthesis

The synthesis of **11** was previously described in the synthesis of **10a** (See Section 4.3.1). IR (CsI, cm^{-1}): ν 3557(w), 3470(w), 3355 (w), 3221 (w), 2998-2863 (s), 1657 (w), 1616 (w), 1443 (s), 1353 (s), 1325(s).

Crystallographic Data Collection and Structure Determination

Due to the large cell parameters and the low symmetry of the space group, a lot of data was collected. However, lots of reflections were weak at higher angles, and to avoid over parameterisation, the number of parameters was kept as low as possible. Therefore, the thermal parameters of the lithium atoms were constrained to be equal, and together with carbon atoms, were refined isotropically.

Each copper atom has a different occupancy. Firstly, they were constrained to be equal but significantly better results were obtained when they were freely refined each site. The copper occupancies are Cu1 93.0(2)%, Cu2 94.8(2)%, Cu3 93.8(2)%, Cu4 84.5(2)%.

All non-hydrogen, non-lithium and non-carbon atoms were refined anisotropically. The hydrogen atom positions of the organic molecule (also the amide hydrogens for when the copper site is vacant) were assigned to calculated positions and refined with fixed individual displacement parameters [$U_{iso}(H) = 1.2U_{eq}(C_{ethyl})$ or $1.2U_{eq}(N_{amide})$] using a riding mode. All hydrogen atom positions from water molecules where located in difference-Fourier maps, refined with two restraints (O-H distances) and given isotropic thermal parameters [$U_{iso}(H) = 1.2U_{eq}(OW)$].

Crystal data and selected details of the refinement are listed in Table 4.3.

Table 4. 3 Crystallographic data for **11**

Empirical formula	$C_{24}H_{58.55}Cu_{3.73}Li_8N_8O_{45}$
Formula weight	1471.54
Crystal system	triclinic
Space group	$P\bar{1}$
a (Å)	12.6919(4)
b (Å)	14.5581(4)
c (Å)	16.1371(5)
α (°)	84.505(2)
β (°)	75.740(2)
γ (°)	68.464(2)
V (Å^3)	2687.99(14)
T(K)	100(2)
ρ_{calc} (g/cm^3)	1.818
Z	2
F (000)	1501
Reflections collected	37857
Unique reflections	12262
Reflections observed [I>2σ(I)]	8204
R_{int}	0.0677
Parameters refined	765
Number of restraints	42
λ (Å); Mo Kα	0.71073
μ (mm^{-1})	1.581
θ Range (°)	1.30-27.51
Goodness-of-fit (GOF) on F^2	1.012
[a]R_1 [I>2σ(I)]	0.0458
[b]wR_2 (all data)	0.0989
Largest difference in peak and hole (e Å^{-3})	0.55 and -0.60
Crystal size (mm)	0.1×0.1×0.1
Crystal morphology	Blue prism

[a]$R_1 = \Sigma(|F_o| - |F_c|)/ \Sigma|F_o|$
[b]$wR_2 = [\Sigma w(F_o^2 - F_c^2)^2]/\Sigma w(F_o^2)^2]^{1/2}$ where $w = 1/[\sigma^2(F_o^2) + (0.2P)^2$ and $P = [F_o^2 + 2F_c^2]/3$

Selected bond lengths (Å) and angles (°) for Compound **11** are given in Table 4.4.[a,b,c] Also the dihedral angle formed by the chelating oxamato groups (°) and the distance of the atom from the mean plane (Å).

Table 4. 4 Selected bonds (Å) and angles (°) for **11**

Cu1-O1	1.956(2)	Cu2-O11	1.995(2)
Cu1-O7	1.952(2)	Cu2-O5	1.976(2)
Cu1-N1	1.961(3)	Cu2-N2	1.957(3)
Cu1-N3	1.957(3)	Cu2-N4	1.971(3)
Cu3-O13	1.982(2)	Cu4-O17	1.983(2)
Cu3-O19	1.968(2)	Cu4-O23	1.982(2)
Cu3-N5	1.958(2)	Cu4-N6	1.958(3)
Cu3-N7	1.960(2)	Cu4-N8	1.944(3)
Cu1-Cu2	2.993(2)	Cu1-Cu1’	3.633(2)
Cu2-Cu3	3.498(2)	Cu4-Cu4’’	3.512(2)
Cu3-Cu4	3.084(2)		
O1-Cu1-N1	84.70(10)	O5-Cu2-N2	83.33(9)
O1-Cu1-N3	96.98(10)	O5-Cu2-N4	97.16(9)
N1-Cu1-O7	97.44(10)	N2-Cu2-O11	98.36(9)
N3-Cu1-O7	83.82(9)	N4-Cu2-O11	82.96(9)
O13-Cu3-N5	83.82(10)	O17-Cu4-N6	84.47(10)
O13-Cu3-N7	98.83(10)	O17-Cu4-N8	95.64(10)
N5-Cu3-O19	97.29(10)	N6-Cu4-O23	99.46(10)
N7-Cu3-O19	84.02(10)	N8-Cu4-O23	85.47(10)
Dihedral angle Cu1	20.01(10)	Dihedral angle Cu2	16.24(10)
Dihedral angle Cu3	22.97(10)	Dihedral angle Cu4	23.33(10)
Atom displacement Cu1	0.009(0)	Atom displacement Cu2	-0.011(0)
O1	0.195(2)	O5	-0.148(2)
O7	0.188(2)	O11	-0.147(2)
N1	-0.256(3)	N2	0.213(3)
N3	-0.260(3)	N4	0.214(3)
Atom displacement Cu3	-0.008(0)	Atom displacement Cu(4)	-0.050(4)
O13	0.215(2)	O(17)	-0.227(2)
O19	0.219(2)	O(23)	-0.221(2)
(5	-0.305(3)	N(6)	0.305(3)
N7	-0.300(3)	N(8)	0.301(3)

[a] Estimated standard deviations in the last significant digits are given in parenthesis. [b] The symmetry code denoted by prime is 1-x, 1-y,1-z and by double prime is 2-x, -y, 2-z. [c] The dihedral angle for Cu1 was calculated measuring the angle between the plane formed by O1A-Cu1-N1 and O7-Cu1-N3, for Cu2 it was calculated measuring the angle between the plane formed by O11-Cu2-N4 and O5-Cu2-N2; for Cu3 it was calculated measuring the angle between the plane formed by O19-Cu3-N7 and O13-Cu3-N5 and finally, for Cu4 it was calculated measuring the angle between the plane formed by O23-Cu4-N8 and O17-Cu4-N6.

4. 3. 3 *β*-$Li_4[Cu_{0.94}H_{0.12}(oeo)]_2 \cdot 6H_2O$ (10b)

Synthesis

To a stirred suspension of $(ebo)H_4$ **(31)** (0.16 g, 0.79 mmols) in water (10 ml) was added an aqueous solution (1 ml) of $CuCl_2 \cdot H_2O$ (0.9 eq, 0.12 g, 0.69 mmols) at room temperature.[3] Then a solution of LiOH (0.07 g, 3.07 mmols) in water (3 ml) was added dropwise. The resulting purple solution was charged with 10ml of water to dissolve the white solid that was in suspension and afterwards, the solvent volume was reduced on a water bath. Due to the excess of heat and the basic conditions (pH=12) the copper complex obtained started to decompose and the mixture was filtered to remove the dark green solid formed. Slow addition of ethanol into the mother liquor gave hexagonal shaped crystals of **10b**, as well as **10c** and **12**, which were suitable for X-ray analysis.

Crystallographic Data Collection and Structure Determination

The crystal, as common in chiral space groups, has a merohedral twinning having 88(1)% of inverted structure. Copper atoms are not fully occupied and the anisotropic thermal parameters were constrained to be equal leading to a value of 94.5(2)%. Initially, the occupancy in each copper site was refined freely leading to the same occupancy value and thus they were finally constrained to be equal.

All non-hydrogen atoms were refined anisotropically. The hydrogen atom positions of the organic molecule (also the amide hydrogens for when the copper site is vacant) were assigned to calculated positions and refined with fixed individual displacement parameters [$U_{iso}(H) = 1.2U_{eq}(C_{ethyl})$ or $1.2U_{eq}(N_{amide})$] using the SHELXL riding mode. The hydrogen atoms of the water molecules were located on a ΔF map and refined with three restraints for each molecule (O-H distances and H···H distances) with thermal factors fixed [$U_{iso}(H) = 1.2U_{eq}(Ow)$].

Crystal data and selected details of the refinement are listed in Table 4.5.

Table 4. 5 Crystallographic data for **10b**

Empirical formula	$C_{12}H_{20.22}Cu_{1.88}Li_4N_4O_{18}$
Formula weight	655.97
Crystal system	hexagonal
Space group	$P6_5$
a (Å)	10.4292(2)
b (Å)	10.4292(2)
c (Å)	36.5610(17)
α (°)	90
β (°)	90
γ (°)	120
V (Å^3)	3443.90(19)
T(K)	100(2)
ρ_{calc} (g/cm^3)	1.898
Z	6
F (000)	1985
Reflections collected	54033
Unique reflections	5524
Reflections observed [I>2σ(I)]	5093
R_{int}	0.0664
Parameters refined	399
Number of restraints	18
λ (Å); Mo Kα	0.71073
μ (mm^{-1})	1.843
θ Range (°)	2.25-28.16
Goodness-of-fit (GOF) on F^2	1.031
[a]R_1 [I>2σ(I)]	0.0317
[b]wR_2 (all data)	0.0717
Largest difference in peak and hole (e Å^{-3})	0.59 and -0.43
Crystal size (mm)	0.05×0.05×0.05
Crystal morphology	Hexagonal blue prism

[a]$R_1 = \Sigma(|F_o| - |F_c|)/ \Sigma|F_o|$
[b]$wR_2 = [\Sigma w(F_o^2 - F_c^2)^2]/\Sigma w(F_o^2)^2]^{1/2}$ where $w = 1/[\sigma^2(F_o^2) + (0.2P)^2$ and $P = [F_o^2 + 2F_c^2]/3$

Selected bond lengths (Å) and angles (°) for compound **10b** are given in Table 4.6.[a,b] Also the dihedral angle formed by the chelating oxamato groups (°) and the distance of the atom from the mean plane (Å).

Table 4. 6 Selected bonds (Å) and angles (°) for **10b**

Cu1-O10	1.981(2)		Cu2-O7	1.991(2)	
Cu1-O11	1.992(2)		Cu2-O2	1.975(2)	
Cu1-N1	1.940(2)		Cu2-N3	1.945(3)	
Cu1-N2	1.931(2)		Cu2-N4	1.942(3)	
O10-Cu1-N1	83.96(10)		O7-Cu2-N3	97.72(10)	
O10-Cu1-N2	98.04(10)		O7-Cu2-N4	83.65(10)	
N1-Cu1-O11	97.38(10)		N3-Cu2-O12	83.54(10)	
N2-Cu1-O11	84.17(10)		N4-Cu2-O12	99.02(10)	
Dihedral angle Cu1	21.43(10)		Dihedral angle Cu2	22.88(10)	
Atom displacement	Cu1	-0.052(3)	Atom displacement	Cu2	0.004(0)
	O10	0.179(3)		O7	-0.255(3)
	O11	0.240(3)		O12	-0.255(3)
	N1	-0.241(3)		N3	0.258(3)
	N2	-0.316(3)		N4	0.255(3)

[a] Estimated standard deviations in the last significant digits are given in parenthesis. [b] The dihedral angle for Cu1 was calculated measuring the angle between the plane formed by O10-Cu1-N1 and O11-Cu1-N2 and for Cu2 it was calculated measuring the angle between the plane formed by O7-Cu2-N4 and O12-Cu2-N3.

4. 3. 4 $Li_4[Cu_{0.96}H_{0.08}(oeo)]_2 \cdot 5H_2O$ (12)

Synthesis

Synthesis of **12** has been previously described in the synthesis of **10b** (See Section 4.3.3). Slow addition of ethanol into the mother liquor gave diamond shaped crystals of **12** which were suitable for X-ray analysis.

Crystallographic Data Collection and Structure Determination

The twinning in the structure was studied and it was concluded to have a very small twinned component that was ignored. Copper atom is not fully occupied and the anisotropic thermal parameters were refined leading to a 96.0(5)% of copper occupancy.

All non-hydrogen atoms were refined anisotropically. The hydrogen atom positions of the organic molecule (also the amide hydrogens for when the copper site is vacant) were assigned to calculated positions and refined with fixed individual displacement parameters [$U_{iso}(H) = 1.2U_{eq}(C_{ethyl})$ or $1.2U_{eq}(N_{amide})$] using the SHELXL riding mode.

Only one hydrogen atom of the crystallisation water molecules Ow2 and Ow3 were located from a difference-Fourier maps which were refined with fixed individual displacement parameters [$U_{iso}(H) = 1.2U_{eq}(Ow)$] and with one restraint (O-H distance). Ow3 is placed in a special position and the hydrogen atom was located, refined with isotropic thermal parameter [$U_{iso}(H) = 1.2U_{eq}(Ow)$] and with two restraints (O-H distance and H···H distance). The second hydrogen atom was defined by symmetry operation.

Crystal data and selected details of the refinement are listed in Table 4.7.

Table 4. 7 Crystallographic data for **12**

Empirical formula	$C_6H_{7.08}Cu_{0.96}Li_2N_2O_{8.50}$
Formula weight	318.10
Crystal system	Monoclinic
Space group	*C*2/*c*
a (Å)	9.622(5)
b (Å)	18.676(8)
c (Å)	12.587(7)
α (°)	90
β (°)	105.251(12)
γ (°)	90
V (Å^3)	2182.2(19)
T(K)	100(2)
ρ_{calc} (g/cm^3)	1.936
Z	8
F (000)	1271
Reflections collected	8302
Unique reflections	3192
Reflections observed [I>2σ(I)]	2071
R_{int}	0.0721
Parameters refined	187
Number of restraints	4
λ (Å); Mo Kα	0.71073
μ (mm^{-1})	1.967
θ Range (°)	2.18-30.40
Goodness-of-fit (GOF) on F^2	1.017
[a]R_1 [I>2σ(I)]	0.0687
[b]wR_2 (all data)	0.1829
Largest difference in peak and hole (e Å^{-3})	1.51 and -0.74
Crystal size (mm)	0.1×0.05×0.05
Crystal morphology	Blue prism

[a]$R_1 = \Sigma(|F_o| - |F_c|)/ \Sigma|F_o|$

[b]$wR_2 = [\Sigma w(F_o^2 - F_c^2)^2]/\Sigma w(F_o^2)^2]^{1/2}$ where $w = 1/[\sigma^2(F_o^2) + (0.2P)^2$ and $P = [F_o^2 + 2F_c^2]/3$

Selected bond lengths (Å) and angles (°) for Compound **12** are given in Table 4.8.[a,b] Also the dihedral angle formed by the chelating oxamato groups (°) and the distance of the atom from the mean plane (Å)

Table 4. 8 Selected bonds (Å) and angles (°) for **12**

Cu1-O4		1.976(4)
Cu1-O3		1.971(4)
Cu1-N1		1.928(4)
Cu1-N2		1.934(4)
O3-Cu1-N1		84.58(15)
O3-Cu1-N2		97.89(16)
N1-Cu1-O4		97.09(16)
N2-Cu1-O4		83.66(16)
Dihedral angle		20.36(14)
Atom displacement	Cu1	-0.018(0)
	O3	0.229(4)
	O4	0.233(4)
	N1	-0.231(4)
	N2	-0.231(4)

[a] Estimated standard deviations in the last significant digits are given in parenthesis. [b] The dihedral angle for Cu1 was calculated measuring the angle between the plane formed by O10-Cu1-N1 and O11-Cu1-N2.

4. 3. 5 *γ*-$Li_4[Cu(oeo)]_2 \cdot 6H_2O$ (10c)

Synthesis

Synthesis of **10c** has been previously described in the synthesis of **10b** (See Section 4.3.3). Slow addition of ethanol into the mother liquor gave diamond shaped crystals of **10c** which were suitable for X-ray analysis.

Crystallographic Data Collection and Structure Determination

Because of the large number of weak unique reflections at higher angle and the poor quality of the crystal, the number of parameters was kept as low as possible. As a result, the occupancy of all atoms in the organic molecule was refined with the isotropic thermal parameters constrained to be equal. The same was done with the lithium atoms.

The copper atom and the water molecules were refined with anisotropic thermal parameters. The occupancy of the copper site was initially refined freely with anisotropic thermal displacements leading to an occupancy of 98%. Due to the high percentage of copper, the occupancy was finally fixed at 100% and the copper was refined anisotropically. The hydrogen atom positions of the organic molecule were assigned to calculated positions and refined with fixed individual displacement

parameters [$U_{iso}(H) = 1.2U_{eq}(C_{ethyl})$] using the SHELXL riding mode. The hydrogen atoms of the water molecules were neither founded nor calculated

Crystal data and selected details of the refinement are listed in Table 4.9.

Table 4. 9 Crystallographic data for **10c**

Empirical formula	$C_6H_4CuLi_2N_2O_9$
Formula weight	325.53
Crystal system	Monoclinic
Space group	*C*2/*c*
a (Å)	18.784(7)
b (Å)	9.762(3)
c (Å)	12.642(5)
α (°)	90
β (°)	94.999(19)
γ (°)	90
V (Å^3)	2309.34(14)
T(K)	100(2)
ρ_{calc} (g/cm^3)	1.884
Z	8
F (000)	1288
Reflections collected	11190
Unique reflections	2356
Reflections observed [I>2σ(I)]	1176
R_{int}	0.1933
Parameters refined	87
Number of restraints	0
λ (Å); Mo Kα	0.71073
μ (mm^{-1})	1.936
θ Range (°)	2.18-26.42
Goodness-of-fit (GOF) on F^2	1.056
[a]R_1 [I>2σ(I)]	0.1212
[b]wR_2 (all data)	0.3726
Largest difference in peak and hole (e Å^{-3})	1.53 and -1.42
Crystal size (mm)	0.05×0.05×0.05
Crystal morphology	Blue prism

[a]$R_1 = \Sigma(|F_o| - |F_c|)/ \Sigma|F_o|$
[b]$wR_2 = [\Sigma w(F_o^2 - F_c^2)^2]/\Sigma w(F_o^2)^2]^{1/2}$ where $w = 1/[\sigma^2(F_o^2) + (0.2P)^2$ and $P = [F_o^2 + 2F_c^2]/3$

Selected bond lengths (Å) and angles (°) for compound **10c** are given in Table 4.10.[a,b] Also the dihedral angle formed by the chelating oxamato groups (°) and the distance of the atom from the mean plane (Å)

Table 4. 10 Selected bonds (Å) and angles (°) for **10c**

	Cu1-O5	1.973(11)
	Cu1-O6	1.986(10)
	Cu1-N1	1.951(13)
	Cu1-N2	1.950(14)
	O5-Cu1-N1	98.5(5)
	O5-Cu1-N2	82.8(5)
	N1-Cu1-O6	82.3(5)
	N2-Cu1-O6	100.4(5)
	Dihedral angle	23.24(5)
Atom displacement	Cu1	-0.082(2)
	O5	0.210(11)
	O6	0.207(11)
	N1	-0.314(14)
	N2	-0.308(14)

[a] Estimated standard deviations in the last significant digits are given in parenthesis.[b] The dihedral angle for Cu1 was calculated measuring the angle between the plane formed by O5-Cu1-N2 and O6-Cu1-N1.

4. 3. 6 $Li_4[Cu(oeo)]_2 \cdot 6H_2O$ (13)

Synthesis

To a stirred suspension of Et_2H_2(oeo) (2.00 g, 7.68 mmols) in water (10 ml) was added an aqueous solution (5 ml) of LiOH (2.45equiv, 0.46 g, 18.8 mmols). The mixture was heated in a water bath until the white solid was dissolved and then heated for another 30 min. Then a solution of $CuCl_2 \cdot H_2O$ (0.9 equiv, 1.21 g, 6.91 mmols) in water (4 ml) was added dropwise to lead to the formation of the expected turquoise solid ($CuH_2(oeo) \cdot nH_2O$, **7**). Finally, another solution of LiOH (2.45 equiv, 0.46 g, 18.8 mmols) in water (5 ml) was added. The resulting deep blue solution was then filtered and charged with 25 ml of methanol. After 24 hrs, the microcrystalline deep blue solid that formed was filtered and dried in air (Yield 1.35g; 53%). $CuC_6H_8O_9N_2Li_2$ requires: C, 21.60; H, 3.02; N, 8.40. Found: C, 21.84; H, 3.06; N, 8.40 %. IR (ATR, cm^{-1}): ν 3547(w), 3461(w), 3341 (w), 3272 (w), 3202 (w), 2930-2864 (w), 1654 (s), 1635 (w), 1590 (w), 1441 (s), 1349(s), 1322(s).

[1] K. Nonoyama, H. Ojima and M. Nonoyama, *Inorg. Chim. Acta*, **1976**, *20*, 127
[2] M.-M. Miao, D.-Z. Liao, Z.-H. Jiang, S.-P. Yan, G.-N. Wang, *Polyhedron,* **1995**, *14*, 1577
[3] See Appendix A2 for details on the synthesis of $(ebo)H_4$ **(31)**

Chapter 5: Sodium Compounds

5. 1 Introduction

Two hydrates of the copper(II) dimer complex using sodium as the counter ion, $Na_4[Cu_{0.05}H_{1.90}(oeo)]_2 \cdot 4H_2O$ **(14)** and $Na_4[Cu_{0.18}H_{1.64}(oeo)]_2 \cdot 8H_2O$ **(16)**, have been obtained. They both have a layered structure perpendicular to the *c*-axis in which homochiral anionic layers of the copper(II) dimer, $[Cu(oeo)]^{4-}$, alternate with cationic layers of sodium and water molecules. However, they were obtained in different conditions. **14** was obtained as a co-product of the hydrothermal attempt of synthesis of bimetallic compounds using $[Cu(oeo)]_2^{4-}$ as building block. **16** was obtained from the slow solvent diffusion of polar organic solvents into the final reaction mixture of the synthesis of $Na_4[Cu(oeo)]_2 \cdot nH_2O$ in aqueous solution. The reaction mixture was prepared by the addition of aqueous solutions of $CuCl_2 \cdot 2H_2O$ (0.5 equiv) and NaOH (2 equiv) into a solution of **3** in water. The deep blue solution that resulted was left stirring overnight giving rise to the formation of a purple solid. The precipitate was filtered and dried in air. It was assigned to $Na_4[Cu_xH_{(2-2x)}(oeo)_2] \cdot nH_2O$ solid **(15)**. Crystallographic data of crystals achieved by slow solvent diffusion of ethanol **(16a)** and acetone **(16b)** into the reaction mixture was collected. Both crystals show essentially the same structure and the same occupancy in the copper(II) sites. Thus here we only report the crystallographic data for **16a** since the crystal quality was better leading to better refinement parameters (R_1, wR_2, S). Nonetheless, crystallographic data of **16b** will be reported somewhere else (See Appendix A3).

Surprisingly, slow solvent diffusion of two different solvents into the same reaction mixture afforded two different crystals with the same amount of copper(II). Taking into account the wide variety of copper occupancies that have been observed in the $[Cu(oeo)]_2^{4-}$ dimer, we could expect a wide variety in occupancies depending on the crystallisation techniques and even the solvent that had been used. Moreover, the composition in the solution may change while the crystals are formed and we could also expect some diversity in the amount of copper depending on where in the beaker the crystal was picked up. We will see Chapter 7 that different copper occupancies have been obtained in three different crystals with the same structure that were afforded from the same reaction mixture but using different crystallisation techniques and different

time scales. However, in sodium species, two different crystals which have the same structure and the same copper(II) occupancy have been obtained from the same reaction mixture and the same timescale using two different solvents. Therefore, this suggests that both solvents afford crystals containing all the same amount of copper and also that all the crystals in the beakers might have the same quantities of the transition metal ion.

Furthermore, the appropriate conditions to prepare a solution of $Na_4[Cu(oeo)_2]\cdot nH_2O$ from which a microcrystalline solid of the copper(II) complex could be obtained were found. This solid could be dissolved in water for enough time to run NMR measurements although the solution decomposed fast due to the neutral pH. Characterisation of **15** is consistent with the formation of $Na_4[Cu_x(H_{(2-2x)}oeo)_2]\cdot nH_2O$ solid where x = Cu^{2+} occupancy. The copper site cannot be fully filled as the amount of transition metal that was added was 0.5eq and we know that for the dimer to be form it is not needed stoichiometric quantities of reagents. Thus, the copper site will be partially filled. However, since the solid was formed before the crystals it is reasonable to assume that the amount of copper in the solid will probably be larger than the one present in the crystals as more metal was present in solution.

^{1}H-NMR and ^{13}C-NMR measurements revealed the presence of the copper(II) complex containing the $(oeo)^{4-}$ ligand. IR spectrum is consistent with the formation of the compound since they compare well with the measurements obtained in $Li_4[Cu(oeo)_2]\cdot nH_2O$ crystals. The PXRD of **15** was also measured and it suggested that **15** is a mixture of **16** and another phase. Simulation of the powder diffractogram from the single crystal data of **16** showed that the reflections positions matched well with the powder pattern. Nonetheless, some reflections could not be assigned, probably due to the presence of another hydrate or polymorph. **14** did not compare well with those peaks. However, NMR and IR measurements assure the formation of $Na_4[Cu_x(H_{(2-2x)}(oeo)_2]\cdot nH_2O$ as the only compound formed. As a result, the exact composition of the sample remains unknown.

Alternatively, the addition of a concentrated solution of NaCl to a reaction mixture of $(Bu_4N)_x[Cu_y(oeo)_2]$ (same mixture that afforded **10a** and **11**) gave rise to the formation of a purple solid with the same PXRD pattern that was obtained for **15**. This would

suggest that **15** could be obtained using different synthesis routes and that the compound may be the sodium species with the lower energy to be formed.

On the other hand, **14** was obtained as a co-product of the hydrothermal attempt of synthesis of bimetallic compounds using $[Cu(oeo)]_2^{4-}$ as building block where **7a**, NaOH and $CoCl_2 \cdot 6H_2O$ were placed in a *Teflon lined autoclave* and then heated to 100°C. Slow solvent diffusion of ethanol into the filtered reaction mixture afforded blue prismatic crystals of **14.** The formation of this compound was unexpected since the reaction mixture was at high temperatures, conditions in which the decomposition of the ligand is feasible, leading to a solution with quite low pH (pH = 9) for the dimer be stable. However, few crystals of **14** were obtained. The amount of copper(II) present in the crystal was very low (~ 10%) as a result of the precipitation of decomposition solids in the reaction vessel. The light blue colour of the crystals is consistent with the low occupancy of the metal in the structure. Even more, it is also surprising that even with this low amount of copper present a dimeric structure still can be formed

5. 1. 1 The dimer

As previously mentioned in Chapter 3, in analogy to related copper(II) bis(oxamato) complexes, Cu-N (amide) bond lengths are expected to be significantly shorter compared to Cu-O (carboxylate) bond lengths due to the higher basicity of the amido nitrogens.[1] However, in the two crystal structures reported in this chapter, the expected trend is not observed as the average Cu-N and Cu-O bond distance in **14** is 2.119 Å and 1.779 Å, respectively; whereas in **16,** are 2.060 Å and 1.850 Å, respectively. Some comparable structures have been reported showing this pattern,[2] although they are mononuclear bis(oxamato) complexes in which the difference between bond length was not as significant (*d*(Cu-N) = 1.921(19) Å versus *d*(Cu-O) = 1.869(17) Å) as they are in **14** and **16**.

On the other hand, the amount copper(II) present in the dimer in both crystal structures is very low, specially in **14** where the copper occupancy in the Cu1 and Cu2 sites are 5.5(3)% and 4.2(3)%, respectively. In **16** the occupancies are slightly higher, 14.5(1)% and 22.2(1)%, respectively. Looking at the copper(II) occupancy graph that was drawn in Scheme 3.5, the occupancy value is located on the right side for both compounds, leading to a composition in the solid solution $Na_4\{[Cu(Hoeo)_2]_x\ [(H_2oeo)_2]_{(1-x)}\}$ for **(14)**

and **(16)** where x = 0.10 and 0.37, respectively (Scheme 5.1). Therefore, the main species that is present in both solid solutions is the protonated dimer, $[(H_2oeo)_2]^{4-}$. The apparent atom sites around the metal site are dominated by the hydrogen bonded geometry (Figure 5.1).

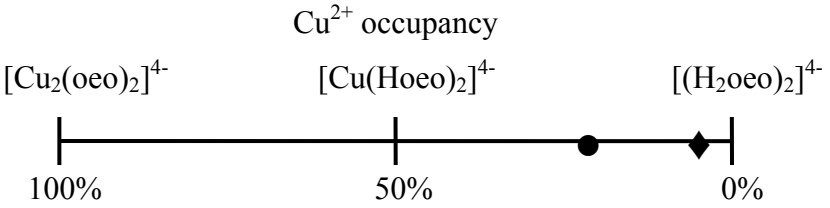

Scheme 5. 1 Representation of the different species present in the crystal structure depending on the amount of copper(II) present in the crystals ● for **(16)** and ♦ for **(14)**.

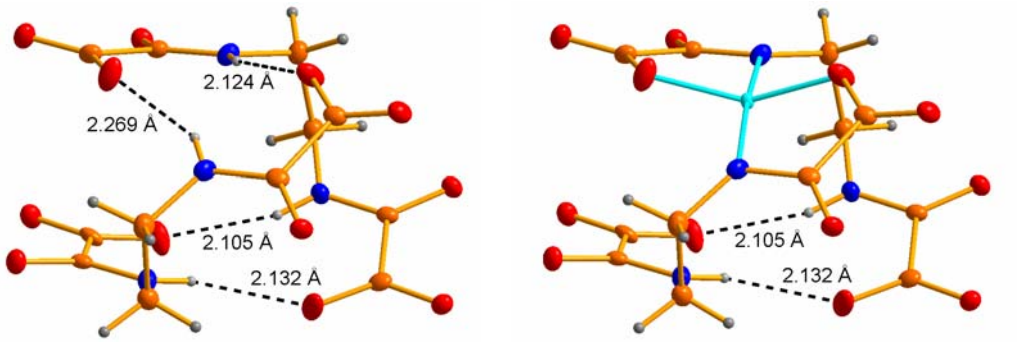

$[(H_2oeo)_2]^{4-}$ $[Cu(Hoeo)_2]^{4-}$

Figure 5. 1 Perspective view of the two species, $[(Hoeo)_2]^{4-}$ and $[Cu(Hoeo)_2]^{4-}$ present in solid solution in **16** showing the hydrogen-bonding between organic molecules.

This dominance of the $[(H_2oeo)_2]^{4-}$ geometry resulted in more deviations in the geometry around the copper site. The dihedral angle, calculated by measuring the angle between the copper atom and the donor atoms of each oxamato group, are among the largest compared with the rest of the dimeric structures obtained. The atoms displacements from the mean plane built by the two donor atoms of each oxamato groups, are also among the highest. Some comparable deviations have been observed in $Rb_4\{[Cu(Hoeo)_2]_x[(H_2oeo)_2]_{(1-x)}\}$compounds (**22b** and **22c**) as well as in the potassium compounds (See Chapter 7 and 6, respectively). In addition, the intramolecular distance between copper sites in compound **14** is the shortest one within all crystal structures found (2.651(16) Å), as well as they are the sites with the lower copper(II) occupancy. Probably, both facts are correlated due to the large dominance of the hydrogen bonded structure.

On the other hand, the lack of apical interactions between dimers in the crystal lattice might be a consequence of the low copper(II) occupancy. It was noted in Chapter 4 and in Chapter 8, that it is needed a high amount of metal to obtain crystals in which there are interactions between dimers.

Consequently, it seems feasible that the copper occupancy may affect the geometry around the copper site since the occupancies in the copper site are pretty low in these structures. The expected trend of the (Cu-N (amide) bond lengths shorter compared to Cu-O (carboxylate) bond lengths) is not observed. As well as deviations in the dihedral angle and the atom displacements are observed. We will see in Chapter 7 that the lower the amount of copper, the more significant is the difference between bond lengths. In addition, the copper occupancy may also affect the packing of the dimer in the crystal structure since it has not been found a crystal with low copper(II) occupancy and with interaction between dimers.

5. 2 Results

5. 2. 1 Description of structure $Na_4[Cu_{0.05}H_{1.90}(oeo)]_2 \cdot 4H_2O$ (14)

Compound **14** consists of discrete dimeric copper complex anions, $[Cu(oeo)]_2^{4-}$, sodium cations and water molecules of crystallisation. It crystallises in the monoclinic space group *C*2/*c*, containing in the asymmetric unit one ligand molecule, two copper atoms and two water molecules of crystallisation. Both copper atoms are placed in special position sites containing one C_2-axis, thus half of each atom is present in the asymmetric unit. Along the crystallographically imposed C_2 symmetry (C_{2y}), which intersects Cu1 and Cu2 sites, the other half of the dimer is generated (Figure 5.2). The occupancy in the Cu1 and Cu2 sites are 5.5(3)% and 4.2(3)%, respectively.

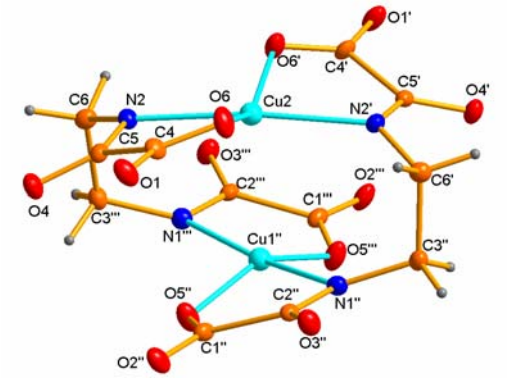

Figure 5. 2 Perspective view of the dinuclear copper (II) complex, $[Cu(oeo)]_2^{4-}$, showing the atom numbering scheme. Thermal ellipsoids, except those for copper atoms, are drawn at the 50% of probability level. The representation of the dimer having the two copper sites filled is not the real scenario present in the crystal structure as both copper sites are never filled at the same time. Here we only show the sites where the copper lies. Prime denotes symmetry operation -x, y,0.5-z ; double prime denotes -x, 2-y, -z; and triple prime denotes x, 2-y, 0.5+z.

The copper(II) is coordinated by two oxamato groups of two different $(oeo)^{4-}$ ligands providing a distorted square-planar coordination. The intramolecular distance between copper sites within the dimer is equal to 2.651(16) Å, being the shortest intramolecular distance between metals within all dimeric structures found. On the other hand, there is no direct interaction between dimers within the crystal structure and they are only interconnected through sodium ions. As a consequence, the whole structure has a definite two-dimensional character which can be viewed as an alternating sequence along the *c*-axis direction of copper(II) dimers layers and cations layers interconnected by oxygen atoms arising from water molecules and carbonyl groups of the ligand (Figure 5.3).

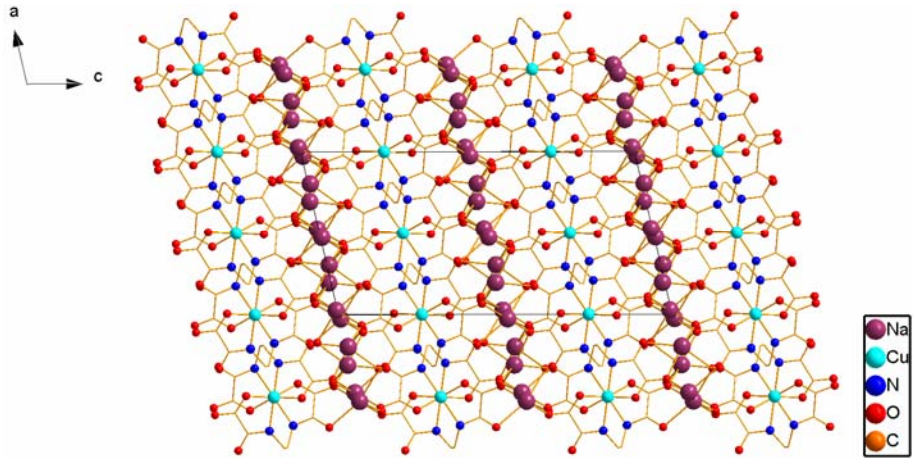

Figure 5. 3 Crystal packing of **14** Viewed along the *a*-axis.

The chirality of the dimers in the crystal packing is displayed in alternated homochiral layers of copper(II) complexes along the *c*-axis direction (Figure 5.4).

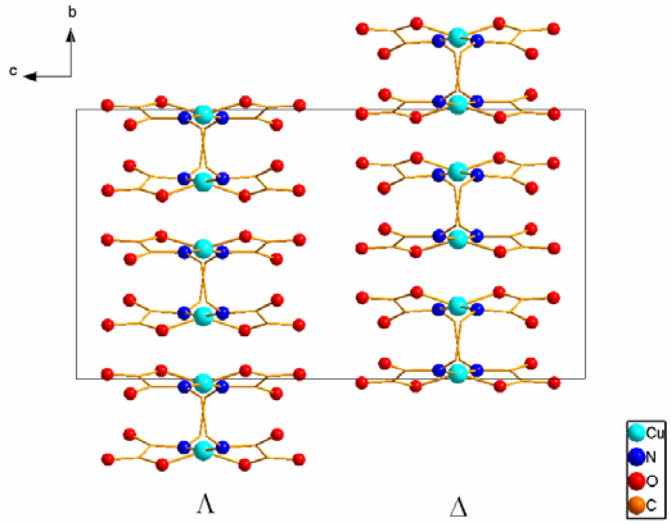

Figure 5. 4 Perspective view of the packing of the copper(II) dimers showing the distribution of the enantiomers along the *c*-axis.

Na1 has a square-pyramidal environment and Na2 has an octahedral coordination with one of the bonds especially long (2.937(3) Å). All the other bonds have normal bond lengths. Both sodium ions are bonded to oxygen atoms arising from two crystallisation water molecules, and two different oxamato groups from different dimeric units, one providing a monodentate coordination and the other one providing a chelating coordination. The last site of the octahedral coordination is filled by a carbonyl oxygen atom of the same dimer that is chelating the cation. In addition, the hydrogen bonding network provided with the water molecules and oxygen atoms of the organic molecule links the cationic and anionic layers into a three dimensional arrangement.

5. 2. 2 Description of structure $Na_4[Cu_{0.18}H_{1.64}(oeo)]_2 \cdot 8H_2O$

The asymmetric unit of **16** consists of one discrete $[Cu(oeo)]_2^{4-}$anion, four sodium cations and eight water molecules. It crystallises in the $P2_1/n$ space group thus the dimer has no higher molecular point symmetry than a C_1 (Figure 5.5). The intramolecular distance between copper atoms sites within the dimer is equal to 2.878(2) Å. The occupancies in the Cu1 and Cu2 sites are 14.5(1)% and 22.2(1)%, respectively.

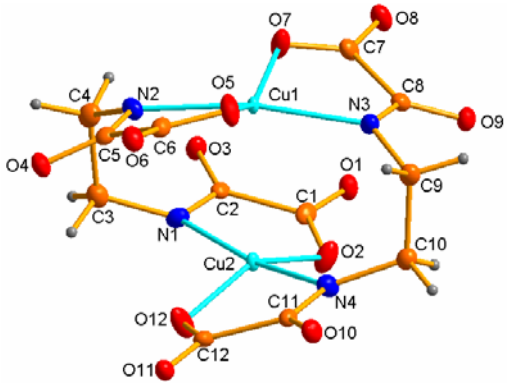

Figure 5. 5 Perspective view of the dinuclear copper (II) complex, $[Cu(oeo)]_2^{4-}$, showing the atom numbering scheme. Thermal ellipsoids are drawn at the 50% of probability level. The representation of the dimer having the two copper sites filled is not the real scenario present in the crystal structure since the copper sites are never filled at the same time. Here we only show the sites where the copper lies.

As seen in the previous sodium copper(II) complex, the crystal has a layered structure along the *c*-axis direction, where anionic sheets containing $[Cu(oeo)]_2^{4-}$ complex are separated by layers containing sodium cations and interconnected by water molecules oxygens and carbonyl oxygens of the ligand (Figure 5.6).

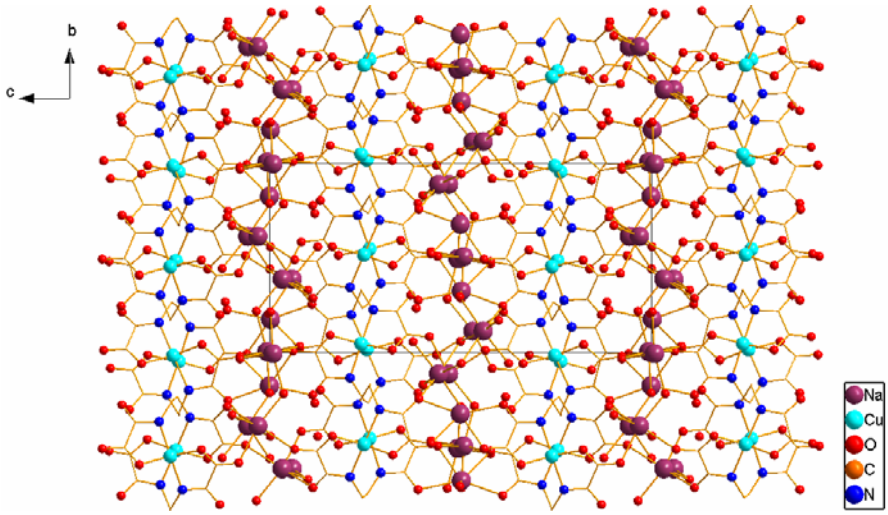

Figure 5. 6 Crystal packing of **16** viewed along the *b*-axis direction.

In the anionic layers, the $[Cu(oeo)]_2^{4-}$ dimers do not pack in rods like in the lithium compounds. In this case, the dimers are displayed in the crystal lattice in an approximate face-centred pattern in the *ab*-plane in which channels of dimers run along the [0 0 1] direction. Sodium cations and water molecules fill the space between dimers along the *c*-axis direction (Figure 5.7). The distance between the centre of the channels along the diagonal of the unit cell is 7.626(5) Å.

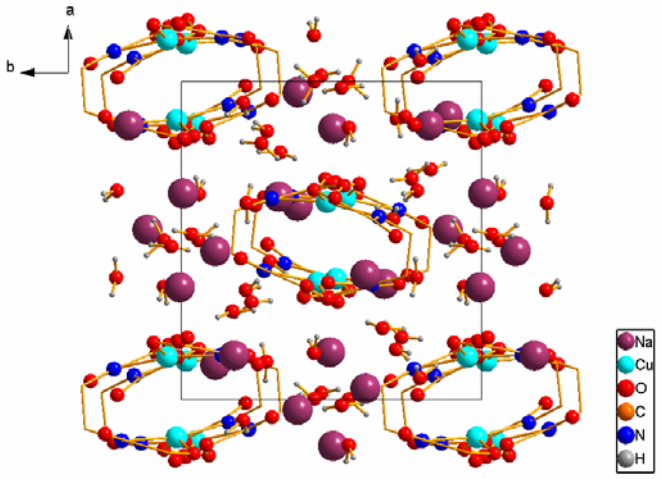

Figure 5. 7 Perspective view of the packing of the copper(II) dimers along the *c*-direction showing the sodium atoms and water molecules in the unit cell. Hydrogen atoms of the methylene groups and Na-O bonds are omitted for clarity.

Similarly to the previous crystal structure, the chirality of the dimers in the crystal packing is also displayed in alternated homochiral anionic layers in the *ac*-plane (Figure 5.8).

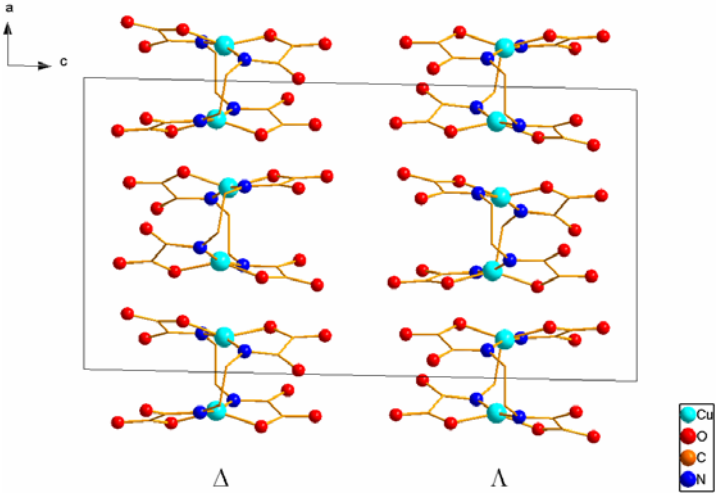

Figure 5. 8 Perspective view of the packing of the copper(II) dimers showing the distribution of the chirality along the *c*-axis direction.

All sodium cations have somewhat distorted octahedral coordination, except Na2 which has pentagonal bipyramid coordination with a quite long bond length (2.820(2) Å). Also, Na3 has a very long bond (3.014(2) Å). All sodium ions are coordinated to crystallisation water molecules and two carbonyl oxygen atoms of two oxamato groups providing a monodentate or a chelating coordination. In addition, the hydrogen bonding network provided with the water molecules and the organic molecule of the copper(II) dimer complex, links the cationic and anionic layers into a three dimensional arrangement.

5. 3 Experimental Section

5. 3. 1 $Na_4[Cu_{0.05}H_{1.90}(oeo)]_2 \cdot 4H_2O$ (14)

Synthesis

A mixture of $CuH_2(oeo) \cdot 3H_2O$ **(7a)** (0.10 g, 0.31 mmols), $CoCl_2 \cdot 6H_2O$ (0.034 g, 0.140 mmols), NaOH (0.03 g, 0.84 mmols) in water (5 ml) were mixed in a 23 ml *Teflon lined autoclave.* The autoclave was sealed and placed inside an oven pre-heated to 100^{o}C for 2 hrs and then heated at 100^{o}C for 1hr. After slow cooling to room temperature during 10 hrs, the mixture was filtered to remove the dark-green and blue precipitates. Slow solvent diffusion of ethanol into the remaining solution afforded blue prismatic crystals of $Na_4[Cu_{0.05}H_{1.90}(oeo)]_2 \cdot 4H_2O$ **(14)** suitable for X-ray analysis.

Crystallographic Data Collection and Structure Determination

The crystal was identified as a non-merohedral twin using CELL_NOW.[3] Two orientation matrices were assigned to the two different components and data reduction was performed with SAINT taking into account the twining.[4] Corrections for absorption, decay and inhomogeneity of the X-ray beam were applied using TWINABS.[5] The twin law is a 180° rotation and the ratio of the two twin components were refined to 0.435(3):0.565 (3).

Cu1 and Cu2 were initially refined free in occupancies with the thermal parameters anisotropic leading to values of occupancy of 5.5(3)% and 4.2(3)%, respectively. In fact, these percentage values only represent 1.6 and 1.2 of an electron, respectively, and therefore the copper atoms were finally refined using isotropic thermal parameters.

The highest residual peaks in the difference electron density map are located close to the sodium sites suggesting some disorder in the sodium sites. However, it was not fixed since the percentage of occupation sites was very low (4%) and the refinement of the disorder did not improve the fit of the model.

All non-hydrogen atoms were refined anisotropically. The hydrogen atom positions of the ethylenediamine fragment were placed to calculated positions and refined with fixed individual displacement parameters [$U_{iso}(H) = 1.2U_{eq}(C_{ethyl})$] using a riding mode. Amide hydrogen atoms for when the copper site is not filled were also refined with fixed individual displacement parameters [$U_{iso}(H) = 1.2U_{eq}(N_{amide})$] using a riding mode, although they could be located in difference-Fourier map. Finally, hydrogen atom positions from water molecules where located in difference-Fourier maps, refined with three restraints (O-H and H···H distances) and given isotropic thermal parameters [$U_{iso}(H) = 1.2U_{eq}(Ow)$].

Crystal data and selected details of the refinement are listed in Table 5.1.

Table 5. 1 Crystallographic data for **14**

Empirical formula	$C_{12}H_{19.80}Cu_{0.10}N_4Na_4O_{16}$
Formula weight	574.28
Crystal system	Monoclinic
Space group	*C*2/c
a (Å)	10.3286(7)
b (Å)	10.5757(8)
c (Å)	20.4963(14)
α (°)	90.00
β (°)	102.913(4)
γ (°)	90.00
V (Å^3)	2182.2(3)
T(K)	100(2)
ρ_{calc} (g/cm^3)	1.748
Z	4
F (000)	1179
Reflections collected	5599
Unique reflections	5489
Reflections observed [I>2σ(I)]	3654
R_{int}	0.0751
Parameters refined	182
Number of restraints	6
λ (Å); Mo Kα	0.71073
μ (mm^{-1})	0.315
θ Range (°)	2.04-36.24
Goodness-of-fit (GOF) on F^2	1.072
[a]R_1 [I>2σ(I)]	0.0754
[b]wR_2 (all data)	0.2441
Largest difference in peak and hole (e Å^{-3})	0.77 and -0.62
Crystal size (mm)	0.05×0.05×0.05
Crystal morphology	cubic blue prism

[a]$R_1 = \Sigma(|F_o| - |F_c|)/ \Sigma|F_o|$
[b]$wR_2 = [\Sigma w(F_o^2 - F_c^2)^2]/\Sigma w(F_o^2)^2]^{1/2}$ where $w = 1/[\sigma^2(F_o^2) + (0.2P)^2$ and $P = [F_o^2 + 2F_c^2]/3$

Selected bond lengths (Å) and angles (°) for compound **14** are given in Table 5.2.[a,b,c] Also the dihedral angle formed by the chelating oxamato groups (°) and the distance of the atom from the mean plane (Å).

Table 5. 2 Selected bonds (Å) and angles (°) for **14**

	Cu1-O5	1.786(4)		Cu2-O6	1.772(4)
	Cu1-N1	2.113(3)		Cu2-N2	2.125(3)
	O5-Cu1-N1	85.92(12)		O6-Cu2-N2	86.74(12)
	O5-Cu1-N1'	96.04(11)		O6-Cu2-N2'	95.46(13)
Dihedral angle	Cu1	33.84(42)	Dihedral angle	Cu2	37.10(46)
Atom displacement	Cu1	0.185(11)	Atom displacement	Cu2	0.207(12)
	O5	-0.314(2)		O6	-0.339(2)
	O5'	-0.314(2)		O6'	-0.339(2)
	N1	0.314(2)		N2	0.339(2)
	N1'	0.314(2)		N2'	0.339(2)

[a] Estimated standard deviations in the last significant digits are given in parenthesis. [b] The symmetry code denoted by prime is -x, y, -0.5-z. [c] The dihedral angle for Cu1 and Cu2 was calculated measuring the angle between the plane formed by O5-Cu1-N1 and O5'-Cu1-N1'; and by O6-Cu2-N2 and O6'-Cu2-N2', respectively.

5. 3. 2 $Na_4[Cu_xH_{(2-2x)}(oeo)_2]\cdot nH_2O$ (15) and $Na_4[Cu_{0.18}H_{1.64}(oeo)]_2\cdot 8H_2O$ (16)

Synthesis

One millilitre of an aqueous solution of $CuCl_2\cdot 2H_2O$ (0.5 equiv, 0.53 g, 3.01 mmols) was added under stirring to a solution of Na_2H_2(oeo) **(3)** (1.50 g, 6.0 4mmols) in water (20 ml). The expected turquoise solid, which had been previously assigned to $CuH_2(oeo)\cdot nH_2O$, was formed. After stirring for 30 min, a solution of NaOH (0.53 g, 12.9 mmols) in water (5 ml) was added slowly to the mixture. The resulting deep blue solution was left stirring overnight. The purple powdered precipitate that was formed was collected by filtration and air-dried **(15)** (See Appendix A6 for PXRD pattern). ^{1}H-NMR (400 MHz, D_2O, δ in ppm): 3.35 (s, CH_2NH). ^{13}C-NMR (400 MHz, D_2O, δ in ppm): 166.0 (O*C*=O), 165.5 (N*C*=O), 38.58 (*C*H_2NH). IR (ATR, cm^{-1}): ν 3412 (w), 3312 (w), 3218 (w), 2974-2851 (s), 1664 (s), 1619 (s), 1595 (vs), 1436 (vs), 1347 (vs), 1316 (vs) (See Appendix A1). λ_{max}, 590 nm. Suitable crystals of $Na_4[Cu_{0.18}H_{1.64}(oeo)]_2\cdot 8H_2O$ **(16)** for X-ray analysis were obtained *via* slow solvent diffusion of ethanol **(16a)** and acetone **(16b)** into the remaining final solution.

Crystallographic Data Collection and Structure Determination

Cu1 and Cu2 were refined free in occupancies with the thermal parameters anisotropic leading to the values of occupancy of 14.5(1)% and 22.2(1)%, respectively.

All non-hydrogen atoms were refined anisotropically. The hydrogen atom positions of the ethylenediamine fragment were assigned to calculated positions and refined with fixed individual displacement parameters [$U_{iso}(H) = 1.2U_{eq}(C_{ethyl})$] using a riding mode. Amide hydrogen atoms for when the copper site is not filled were located from a difference synthesis and refined with fixed individual displacement parameters [$U_{iso}(H) = 1.2U_{eq}(N_{amide})$] and one restraint (N-H distance). Finally, hydrogen atom positions from water molecules where located in difference-Fourier maps, refined with two restraints (O-H distances) and given isotropic thermal parameters [$U_{iso}(H) = 1.2U_{eq}(Ow)$].

Crystal data and selected details of the refinement for **16a** are listed in Table 5.3. Crystal data and selected details of the refinement for **16b** are listed in Appendix A3.

Table 5. 3 Crystallographic data for **16a**

Empirical formula	$C_{12}H_{27.26}Cu_{0.37}N_4Na_4O_{20}$
Formula weight	662.95
Crystal system	Monoclinic
Space group	$P2_1/n$
a (Å)	11.2459(10)
b (Å)	10.5859(9)
c (Å)	21.251(2)
α (°)	90.00
β (°)	91.216(3)
γ (°)	90.00
V (Å^3)	2529.3(4)
T (K)	100(2)
ρ_{calc} (g/cm^3)	1.714
Z	4
F (000)	1368
Reflections collected	16991
Unique reflections	5145
Reflections observed [I>2σ(I)]	4081
R_{int}	0.0422
Parameters refined	441
Number of restraints	20
λ (Å); Mo Kα	0.71073
μ (mm^{-1})	0.514
θ Range (°)	1.92-26.36
Goodness-of-fit (GOF) on F^2	1.088
[a]R_1 [I>2σ(I)]	0.0408
[b]wR_2 (all data)	0.0886
Largest difference in peak and hole (e Å^{-3})	0.32 and -0.27
Crystal size (mm)	0.1×0.1×0.1
Crystal morphology	blue prism

[a]$R_1 = \Sigma(||F_o| - |F_c||)/ \Sigma|F_o|$

[b]$wR_2 = [\Sigma w(F_o^2 - F_c^2)^2]/\Sigma w(F_o^2)^2]^{1/2}$ where $w = 1/[\sigma^2(F_o^2) + (0.2P)^2$ and $P = [F_o^2 + 2F_c^2]/3$

Selected bond lengths (Å) and angles (°) for Compound **16a** are given in Table 5.4.[a,b,c] Also the dihedral angle formed by the chelating oxamato groups (°) and the distance of the atom from the mean plane (Å).

Table 5. 4 Selected bonds (Å) and angles (°) for **16a**

	Cu1-O5	1.816(2)		Cu2-O2	1.865(2)
	Cu1-O7	1.864(2)		Cu2-O12	1.855(2)
	Cu1-N2	2.124(3)		Cu2-N1	2.040(2)
	Cu1-N3	2.061(3)		Cu2-N4	2.015(2)
	O5-Cu1-N2	85.48(10)		O2-Cu2-N1	86.30(9)
	O5-Cu1-N3	97.14(11)		O2-Cu2-N4	95.56(9)
	N2-Cu1-O7	98.69(11)		N1-Cu2-O12	96.63(9)
	N3-Cu1-O7	85.03(10)		N4-Cu2-O12	87.36(9)
	Dihedral angle Cu1	35.35(11)		Dihedral angle Cu2	35.88(11)
Atom displacement	Cu1’	-0.257(2)	Atom displacement	Cu2	-0.203(1)
	O5’	0.291(2)		O2’’	0.318(2)
	O7	0.206(2)		O12	0.355(2)
	N2’	-0.402(2)		N1’’	-0.355(2)
	N3	-0.422(2)		N4	-0.406(2)

[a] Estimated standard deviations in the last significant digits are given in parenthesis. [b] The symmetry code denoted by prime is 3.5-x, -0.5+y, 2.5-z and by double prime is 3.5-x, -0.5+y, 2.5-z. [c] The dihedral angle for Cu1 was calculated measuring the angle between the plane formed by O5-Cu1-N2 and O7-Cu1-N3 and for Cu2 it was calculated measuring the angle between the plane formed by O2-Cu2-N1 and O12-Cu2-N4.

[1] (a) B. Cervera, J.L. Sanz, M.J. Ibañez, G. Vila, F. Lloret, M. Julve, R. Ruiz, X. Ottenwaelder, A. Aukauloo, S. Poussereau, Y. Journaux, M.C. Muñoz, *J. Chem. Soc*., *Dalton Trans.*, **1998**, 781. (b) K. E. Berg, Y. Pellegrin, G. Blondin, X. Ottenwaelder, Y. Journaux, M. Moragues Canovas, T. Mallah, S. Parsons, A. Aukauloo, *Eur. J. Inorg. Chem.,* **2002**, *323-325*, 1434. (c) M. Fettouhi, L. Ouahab, A. Boukhari, O. Cador, C. Mathonière, O. Kahn, *Inorg. Chem.,* **1996***, 35,* 4932. (d) J. Ribas, A. Garcia, R. Costa, M. Monfort, S. Alvarez, Z. Zanchini, X. Solans, M.V. Domenech, *Inorg. Chem*., **1991**, *30*, 841

[2] T. Rüffer, B. Bräuer, F.E. Meva, B. Walfort, G. Salvan, A.K. Powell, I.J. Hewitt, L. Sorace, A. Caneschi, Inorg. Chim. Acta, **2007**, *360*, 3777

[3] Sheldrick, G. M., *CELL_NOW*, **2005**, University of Göttingen, Germany

[4] Bruker *SAINT.* Bruker-AXS Inc., **2005**, Madison, Wisconsin, USA

[5] Sheldrick, G. M., *TWINABS,* **2002**, University of Göttingen, Germany

Chapter 6: Potassium Compounds

6. 1 Introduction

Four different hydrates of the copper(II) complex $[Cu(oeo)]_2^{4-}$ have been obtained when using potassium as the counter ion. The hydrates were obtained from three different syntheses in which the same method was performed but different proportions of reagents were added. Also, differences in the crystal growing techniques were used.

6. 1. 1 $K_4[Cu_x(H_{(2-2x)}oeo)]_2 \cdot nH_2O$ solid (17) and $K_4[Cu_{0.33}H_{1.34}(oeo)]_2 \cdot 5H_2O$ (18)

The first potassium hydrate, $K_4[Cu_{0.33}H_{1.34}(oeo)]_2 \cdot 5H_2O$ **(18)**, was obtained as a co-product of the preparation of the potassium salts of the copper(II) complex as a microcrystalline solid, $K_4[Cu_x(H_{(2-2x)}oeo)]_2 \cdot nH_2O$ **(17)**. The synthesis was carried out adding aqueous solutions of $CuCl_2 \cdot 2H_2O$ and KOH to a solution of **4** in water. As a consequence of the excess of copper(II) and base added, a dark green solid was formed. The solid, which was insoluble in common organic solvents, was probably a coordination polymer of the copper complex. Then, the filtrated reaction mixture was left in the fridge overnight and a dark blue microcrystalline solid, **17**, was precipitated. Using optical microscopy, we noticed that two different morphologies of solids were formed, needle shaped crystals and a powdery solid, suggesting the formation of two different hydrates. Characterisation of **17** was consistent with the formation of $K_4[Cu_x(H_{(2-2x)}oeo)]_2 \cdot nH_2O$ where x = Cu^{2+} occupancy. ^{1}H-NMR and ^{13}C-NMR measurements of **17** revealed the presence of the $(oeo)^{4-}$ ligand and the IR spectrum was consistent with the formation of the compound since it compares well with the spectra obtained for similar compounds when using other counterions. The same as the solid sodium salt **15**,[1] the amount of copper present in the copper(II) complex is indefinite. However, the microcrystalline solid was formed when the reaction mixture had a higher concentration of copper in solution compared with the concentration of the solution when the crystals where grown. Therefore, we expect that the quantity of copper present in the solid will be greater than in the crystals. PXRD of **17** was measured and it was compared with the simulated powder diffractograms of all obtained potassium hydrates. Not all reflections positions matched well with the data of only one of the hydrates suggesting that more than one hydrate was obtained. However, **18** or

$K_4[Cu_{0.78}H_{0.44}(oeo)]_2 \cdot 4.5H_2O$ **(20)** could be one of the hydrates that were formed since some reflection positions of the powder pattern of **17** matched well with the simulation of the diffractograms of the two hydrates.

The conditions in which a microcrystalline solid could be obtained as the only product formed in the synthesis are very narrow. The crystallisation is very susceptible to the exact conditions, as a repeat synthesis carried out the day after did not give the same results. The synthesis gave an impure product as a green solid was formed as well as the expected blue microcrystalline solid.

Crystallographic data of the crystal obtained by slow solvent evaporation from the reactant solution, **18**, was collected. Similarly to the sodium salts, the amount of copper(II) present in the crystal is lower than 50% giving rise to the prevalence of the hydrogen-bonded geometry in the dimer. Thus the solid solution present in the crystal structure is $K_4\{[Cu(Hoeo)_2]_x[H_2(oeo)_2]_{(1-x)}\}$ where x = 0.66. As a consequence, the expected deviations in the geometry around the copper site are observed. The average apparent Cu-N bond distance is 2.033Å whereas the average apparent Cu-O bond distance is 1.873Å. Both bond lengths are similar to the analogous bond lengths of the sodium copper complex salts. Moreover, the dihedral angle between the donor atoms of each oxamato group with the copper, it is comparable with the angles obtained in the sodium salts, the same as the deviations from the mean plane built by the donor atoms. In addition, in this structure, the carboxylate oxygen atoms display a significantly elongated thermal ellipsoid due to the superposition of the two species present in the crystal structure.

6. 1. 2 $K_4[Cu_{0.89}H_{0.22}(oeo)]_2 \cdot 3H_2O$ (19) and $K_4[Cu_{0.78}H_{0.44}(oeo)]_2 \cdot 4.5H_2O$ (20)

On the other hand, three other hydrates were obtained from two different potassium copper(II) complex syntheses that were prepared using very similar conditions (*a* and *b*). The total volume that was used in both syntheses was the same although less amount of solvent was initially added in the first synthesis, *a*. However, the reaction mixture was eventually charged with water until the mixture had the same volume of water that was used in the second synthesis, *b*. Moreover, each reaction was prepared in two

consecutive days and thus the ambient conditions, like the room temperature, are assumed to be pretty similar.

The difference between both syntheses is the amount of copper(II) that was added. One equivalent of copper was added in synthesis *a*, whereas in *b*, 0.8 equivalents were added. Having the reagent proportions in mind, we would expect a higher amount of copper present in the crystals obtained from *a*. However, the higher occupancy was obtained in the crystal grown from *b*.

Two different crystal habits were obtained when methanol was slow diffused into the reaction mixture *a* leading to the formation of prismatic crystals and a needle shaped crystals, $K_4[Cu_{0.89}H_{0.22}(oeo)]_2 \cdot 3H_2O$ **(19)** and $K_4[Cu_{0.78}H_{0.44}(oeo)]_2 \cdot 4.5H_2O$ **(20)**, respectively (Figure 6.1). **19** and **20** have different copper occupancies but both are over 50%. Thus, in these cases, the copper-bonded geometry is dominant in the crystal structure and the composition of the solid solution is $K_4\{[Cu(oeo)_2]_x[Cu(Hoeo)_2]_{(1-x)}\}$ where x = 0.88 and 0.57, respectively. Moreover, the expected trend in the geometry around the copper site, bonds length, dihedral angles and atoms displacement from the mean plane; is observed in both compounds.

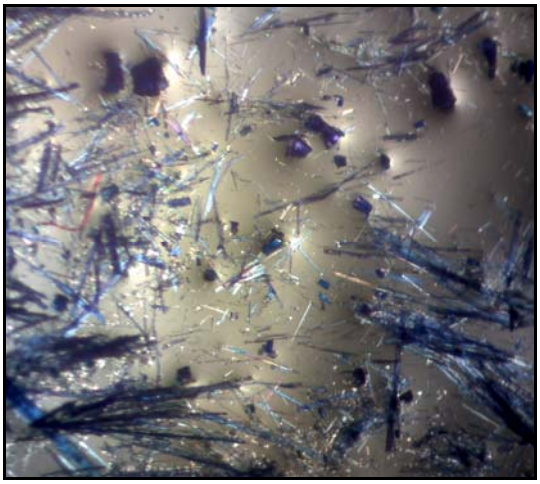

Figure 6. 1 View under the microscope in reflected unpolarized light of the two different crystal habits of **19** and **20**. Approximate scale: width of the image 1cm.

Compounds **18**, **19** and **20** have similar crystal lattices in which cationic layers of potassium atoms and water molecules alternate with copper(II) dimer $[Cu(oeo)]^{4-}$ anionic layers. However, the crystal structures show different packing of the dimer in the anionic layer. In compounds **19** and **18**, the packing can be described as stacks of

dimers running along the diagonal of the *ab*-plane whereas in **20** the dimer packs in a zigzag pattern where stacks of dimers run along the *b*-axis and where each stack has the dimers facing in the opposite direction to the neighbouring ones. Moreover, the distribution of the chirality in the structure is also different. Homochiral anionic layers alternate along the *c*-axis direction in **18** and **19** while in **20**, the chirality alternates within the anionic layer where homochiral stacks of dimers alternate in the *c*-axis direction.

6. 1. 3 $K_4[Cu(oeo)]_2 \cdot 6H_2O$ (21)

From synthesis *b*, slow solvent diffusion of ethanol into the reaction mixture afforded needle shaped crystals of $K_4[Cu(oeo)]_2 \cdot 6H_2O$ **(21)**. Surprisingly, the copper(II) sites in this compound are fully occupied leading to the $[Cu(oeo)]_2^{4-}$ as the only species present in the crystal structure. Furthermore, like in the other crystal structures of the potassium salts, the dimer packs in stacks, but in this case, the stacks are surrounded by counterions instead of forming layers. Each stack is linked to two neighbouring stacks by potassium cations in the *a*-axis direction. Moreover, there is a weak interaction between dimers though Cu-N atoms of neighbouring dimers. This type of crystal packing pattern is the same that was seen in the lithium salts of the copper(II) complex in which stacks of dimers were connected to neighbouring stacks through surrounding lithium ions. We note that a very high copper occupancy (almost 100%) is needed in the dimer for them to pack in such a way that a weak interaction is present between dimers. We will see in Chapter 8 that the crystal obtained for the caesium salt of the copper(II) dimer has the same kind of crystal packing.

It is also worth mentioning the high disorder present in the potassium and water molecules sites in all potassium crystal structures, except in **20**. We will see that when the counter ion is bigger than sodium that this is a common feature.

Lastly, four different hydrates with similar amount of water molecules, have been obtained from different reaction mixtures. Even in the microcrystalline solid, different morphologies of the particles could be observed when looking in detail. Initially, when the crystallographic data was collected from the samples, it was expected that the collection of the data of only one crystal would be representative of the whole sample.

However, due to the wide variety of different hydrates that have been obtained, this statement was probably not right since it is feasible that the careful study of the sample would lead to more than one hydrate present in the sample. Moreover, some crystals having very similar morphologies but obtained from different batches were analysed expecting to be same, like the pair **18** and **19,** and the pair **20** and **21,** which had similar morphologies. Surprisingly, they were four different crystal structures. This emphasizes how difficult is to obtain a sample formed by only one hydrate. It also highlights that the exact composition of a sample cannot be found since cannot know which of the hydrates is present in a microcrystalline solid and neither the amount of copper present in the crystals.

6. 2 Results

6. 2. 1 Description of structure $K_4[Cu_{0.33}H_{1.34}(oeo)]_2 \cdot 5H_2O$ (18)

Compound **18** consists of discrete dimeric copper complex anions, $[Cu(oeo)]_2^{4-}$, potassium cations and water molecules. It crystallises in the monoclinic space group *C*2/c, containing in the asymmetric unit half of the dimer, thus one ligand molecule and one copper(II) atom; and two potassium atoms and 2½ water molecules. Due to the disorder in the structure, the cations are distributed over four sites of which one lies on a 4*a* Wyckoff position being fully occupied. The other three are half occupied. In addition, there are four water molecules sites of which three are half occupied and one is fully occupied. The other half of the molecule is generated through the C_2 symmetry axis that crosses in the mid-point of the two ethylenediamine C-C bond (Figure 6.2). The copper(II) occupancy is 32.87(29)% and the distance between copper sites within the dimer is 2.827(2) Å.

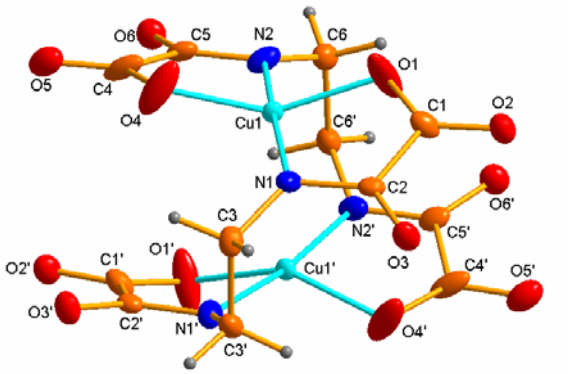

Figure 6. 2 Perspective view of the dinuclear copper (II) complex, $[Cu(oeo)]_2^{4-}$, showing the atom numbering scheme. Anisotropic thermal ellipsoids for non-hydrogen atoms are drawn at the 50% of probability level. This view only shows the atoms sites with their thermal ellipsoids but it is not real as both copper sites are never filled at the same time due to the low occupancy of the site. Prime denotes symmetry operation –x, y, 0.5+z.

As previously stated, the carboxylate oxygen atoms show a significantly elongated thermal ellipsoid as a consequence of the prevalence of the hydrogen-bonded geometry due to the low occupancy if the copper(II) site. Furthermore, the averaged Cu-N bond distance is longer than the averaged Cu-O also as a result of the prevalence of this specie. These distances are similar with the bond lengths of the copper complex sodium salts as well as the dihedral angle between donor atoms of each oxamato group with the copper and the deviations from the mean plane built by the donor atoms.

Like in the sodium salts of the copper(II) complex, the crystal lattice has a layered structure along the *c*-axis direction, in which anionic layers of copper(II) dimeric units alternate with cationic layers of potassium and water molecules (Figure 6.3). The bis(oxamato) copper(II) entities are coordinated towards potassium atoms through the carbonyl oxygen providing a monodentate or chelating coordination to form the 2-D network structure. Additional water molecules complete the coordination sphere of the potassium ions. This leads to interlayer hydrogen-bonding interactions involving the coordinated water molecules and the carbonyl oxygen atoms of the ligands.

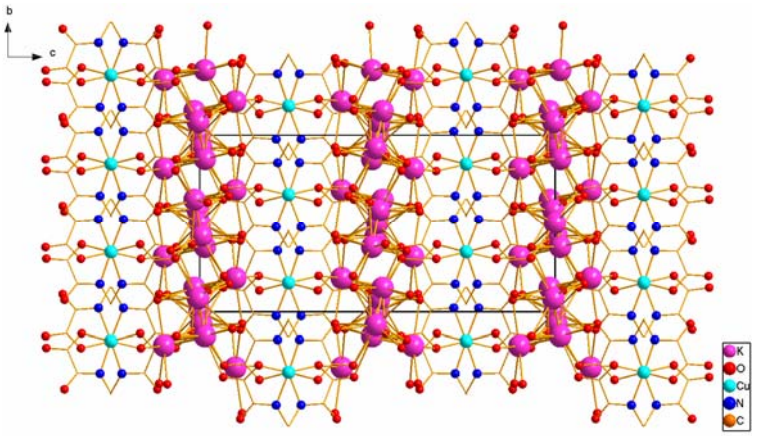

Figure 6. 3 View of the crystal packing of **18** along the *a*-axis. Hydrogen atoms are omitted for clarity. The diagram shows the superposition of the disordered potassium and water molecules sites.

The anionic layer, the $[Cu(oeo)]_2^{4-}$ dimers pack into stacks along the the diagonal of the *ab*-plane. Moreover, the chirality also alternates between layers in which homochiral layers of the enatiomers alternate in the *c*-axis direction (Figure 6.4a). The intermolecular distance between neighbouring dimers within the layer are 10.418(1) Å along the *b*-axis direction and 7.628(1) Å along the diagonal of unit cell (Figure 6.4b).

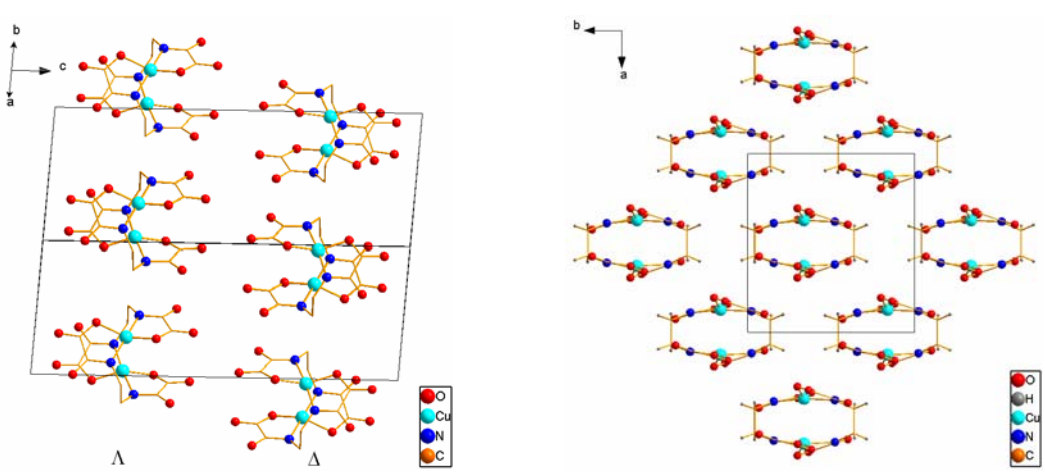

a **b**

Figure 6. 4 a. Perspective view of the packing of the copper(II) dimers along the diagonal of the unit cell showing the distribution of the chirality along the *c*-axis direction. Hydrogen atoms are omitted for clarity. **b.** View of the cationic layer in *ab*-plane.

In the cationic sheet, there is extensive potassium site disorder and consequently, extensive water molecule site disorder. Looking at a section of the layer along the *c*-axis we observe four potassium sites (Figure 6.5).

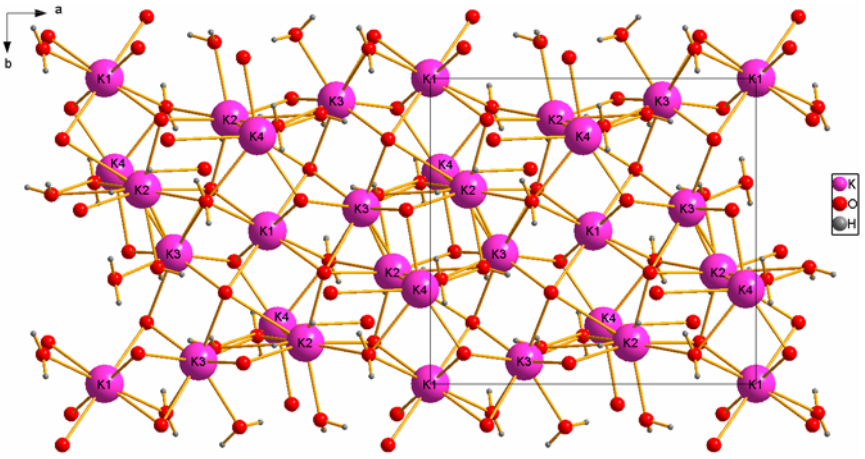

Figure 6. 5 Perspective view in the a*b*-plane of a section of the anionic layer showing a superposition of the potassium and water molecules disordered sites.

The preferred potassium site, K1, lies on a *4*a Wyckoff site and is fully occupied. The rest of the positive charge is distributed over three sites, K2, K3 and K4. They are placed close to the *b*-axis and together with the symmetry related potassium sites of the following unit cell along the *a*-axis, form a "cube" of potassium and oxygen atoms (Figure 6.6).

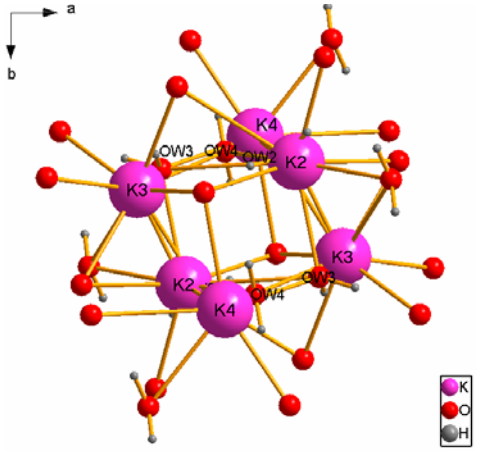

Figure 6. 6 Close view of the potassium-oxygen cube.

K2, K3 and K4 potassium sites are mutually excluded due to the proximity of the sites and thus only one potassium site can be filled at the time. However, when the potassium is not present, the site is filled by a water molecule. This leads to three different scenarios of the potassium disorder in the crystal structure (Figure 6.7). The range of the K-O distances for all potassium sites are 2.635(18)-3.317(6) Å.

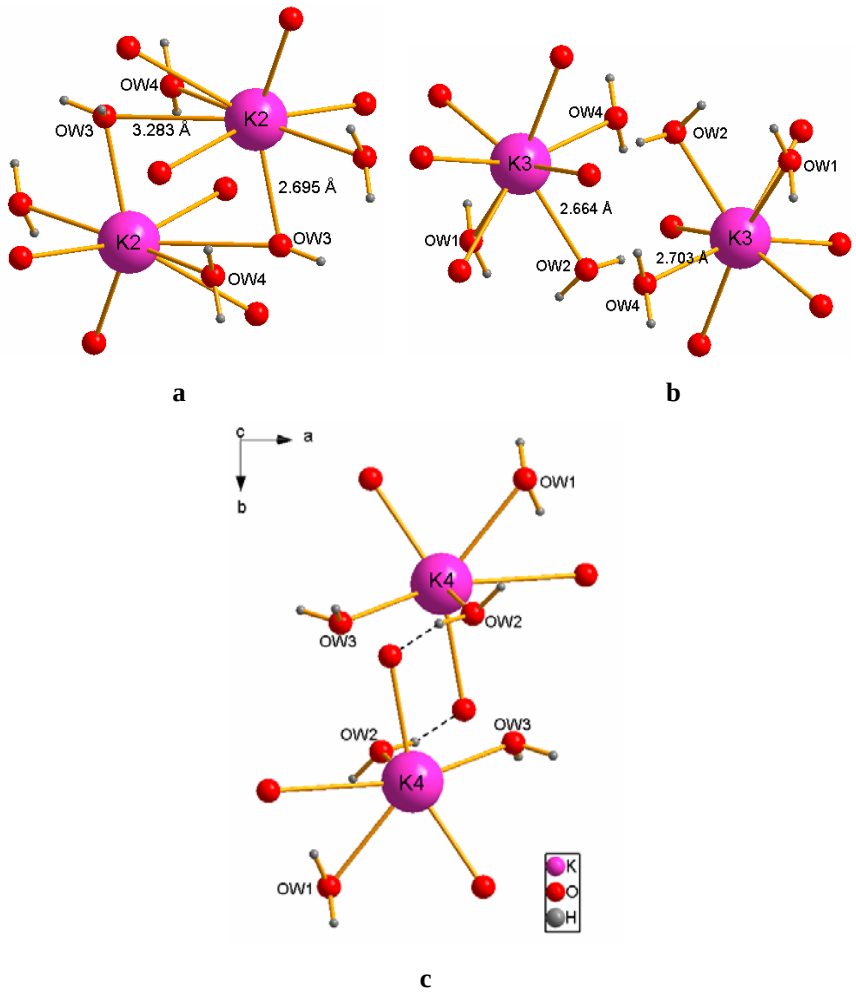

Figure 6. 7 View of the three possible potassium scenarios present in the crystal structure.

6. 2. 2 Description of structure $K_4[Cu_{0.89}H_{0.22}(oeo)]_2 \cdot 3H_2O$ (19)

Compound **19** consists in discrete dimeric copper complex anions, $[Cu(oeo)]_2^{4-}$, potassium cations and water molecules. It crystallises in the monoclinic space group *C*2/c containing in the asymmetric unit half of the copper(II) dimer: one ligand molecule and two copper atom which both lie on a 4*e* Wickoff site (Figure 6.8). It also contains two potassium ions distributed over three sites, one of them fully occupied and the other two are half occupied. Finally, it contains one and a half water molecules shared also over three sites, each one half occupied.

As previously stated, the copper atoms are placed in special position sites in which a C_2-axis passed through, thus only half atom is present in the asymmetric unit. Along a crystallographically imposed C_2 symmetry, which intersects Cu1 and Cu2, the other half

of the dimer is generated. The copper(II) occupancy of Cu1 and Cu2 sites are 85.3(4)% and 91.9(4)%, respectively. The distance between copper atoms is 2.995(1) Å.

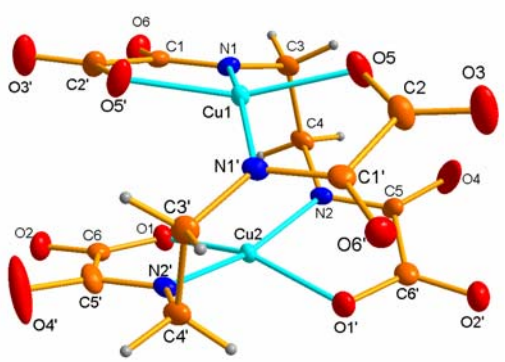

Figure 6. 8 Perspective view of the dinuclear copper (II) complex, $[Cu(oeo)]_2^{4-}$, showing the atom numbering scheme. Anisotropic thermal ellipsoids for non-hydrogen atoms are drawn at the 50% of probability level. Prime denotes symmetry operation -x, y, 0.5-z.

The crystal has a layered structure perpendicular to the *a*-axis direction in which layers of dimeric units containing $[Cu(oeo)]_2^{4-}$ are alternated with layers of potassium cations and interconnected by oxygen atoms provided by water molecules and oxamato carbonyls groups (Figure 6.9).

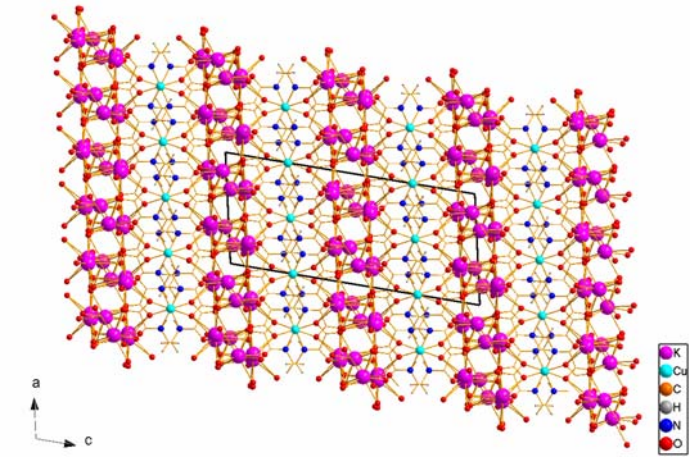

Figure 6. 9 Crystal packing view of **19** of the *ac*-plane. Hydrogen atoms are omitted for clarity. The diagram it is a superposition of the disorder in the potassium and water molecules sites.

As in **18**, the packing of the dimers in the cationic $[Cu(oeo)]_2^{4-}$ layer can be described as stacks of dimers growing though the diagonal of the *ab*-plane (Figure 6.10a). Like in all the sodium salts of the copper(II) complex, chirality alternates within layers in which homochiral layers of the two enatiomers alternate in the *c*-axis direction. The distance between neighbouring dimers within the cationic layer (measuring it between the

centres of the dimers) along the *a*-axis direction is 7.274(2) Å, whereas the distance along the diagonal of the unit cell is 9.656(3) Å (Figure 6.10b).

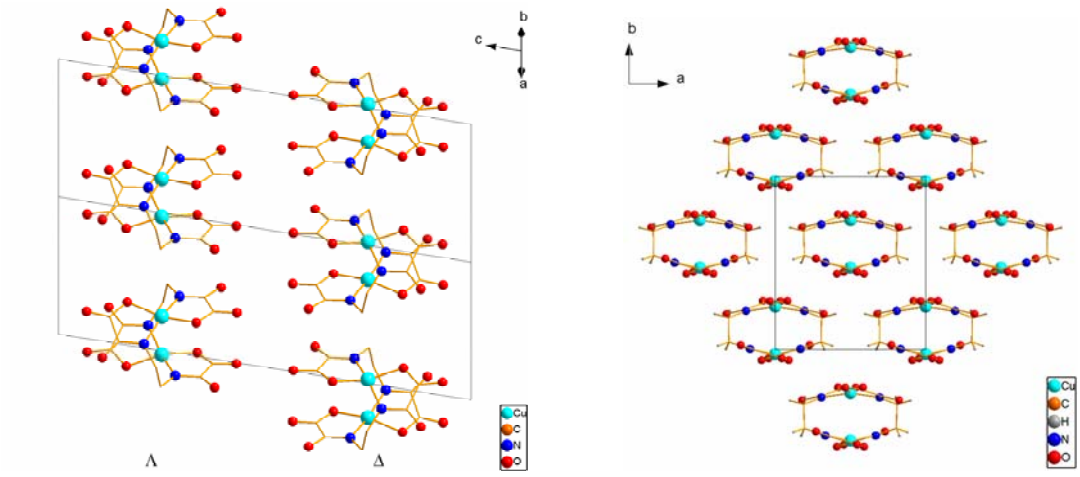

a **b**

Figure 6. 10 a. Perspective view of the packing of the copper(II) dimers along the diagonal of the unit cell showing the distribution of the chirality along the *c*-axis direction. Hydrogen atoms are omitted for clarity. **b.**View of the cationic layer in *ab*-plane.

In the cationic layer, there is some potassium site disorder and as a result also some water molecule site disorder. Looking to a portion of the anionic layer along the *bc*-plane we observe three potassium sites of which K2A and K2B are mutually exclusive, as well as OwA2 and OwB, due to proximity reasons (Figure 6.11).

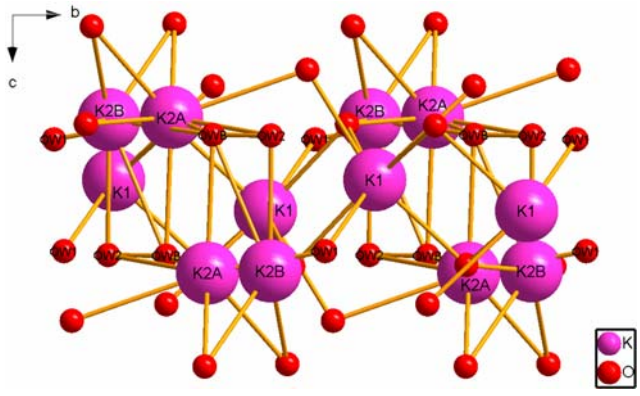

Figure 6. 11 Perspective view in the *bc*-plane of a section of the anionic layer showing a superposition of the potassium and water molecules disordered sites.

K1 is the preferred potassium site since it is always filled. K2A and K2B sites are too close to each other and must occupied 50% of the time. This disorder influenced the water molecules since due to proximity reasons their sites cannot always be filled. Therefore, OwA1 and OwA2 sites are filled when K2A is present while OwB and K2B are vacant; and vice versa (Figure 12a). This causes two situations, one when K2A site

is filled and another when K2B is filled (Figure 12b and 12c). The range of the K-O distances for K2A and K2B are 2.662(1)-3.242(1) Å and 2.730(1)-3.351(1) Å, respectively.

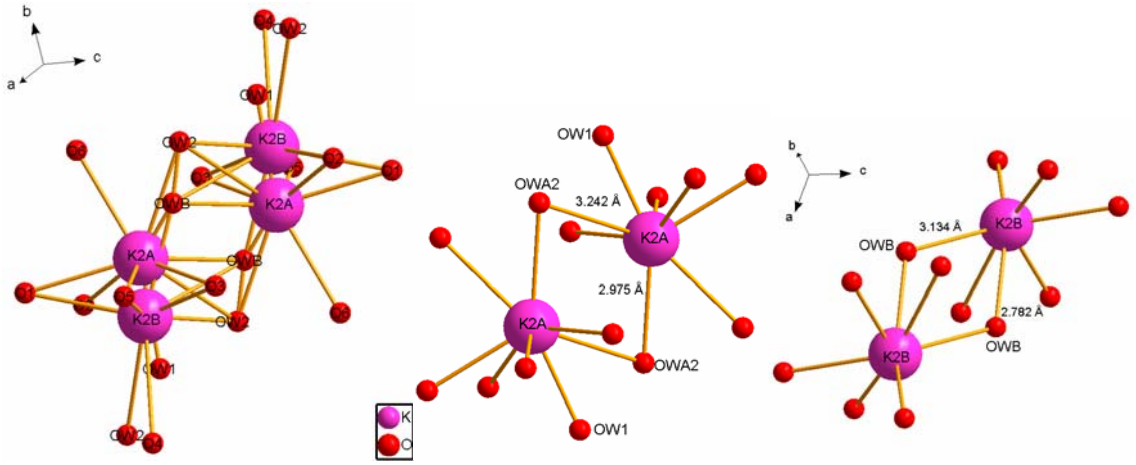

a **b** **c**

Figure 6. 12 Simplified view of the two possible potassium scenarios present in the crystal structure, where **a** represents the superposition if the disorder and **b** and **c** the two possible situation that can be found in the structure.

6. 2. 3 Description of structure $K_4[Cu_{0.78}H_{0.44}(oeo)]_2 \cdot 4.5H_2O$ (20)

Compound **20** crystallises in the space group *P*2/*c* containing one dimeric unit $[Cu(oeo)]_2^{4-}$, four potassium cations and 4 ½ water molecules in the asymmetric unit. The dimer has no higher symmetry implied than the identity (Figure 6.13). The copper(II) occupancy in both sites is 78.4(3)%, and the distance between Cu1 and Cu2 is 2.927(1) Å.

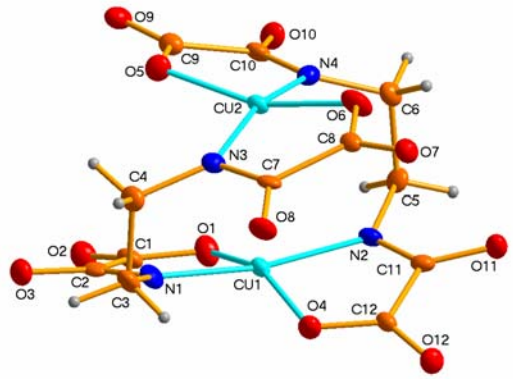

Figure 6. 13 Perspective view of the dinuclear copper (II) complex, $[Cu(oeo)]_2^{4-}$, showing the atom numbering scheme. Anisotropic thermal ellipsoids for non-hydrogen atoms are drawn at the 50% of probability level.

As in the previous potassium copper(II) complex, the crystal has a layered structure along the *a*-axis direction, where anionic layers containing $[Cu(oeo)]_2^{4-}$anion are separated by layers having potassium cations and coordinated water molecules. The two layers are interconnected by the coordination of carbonyl oxygen atoms towards potassium ions providing either a monodentate or a chelating coordination to the metal. Potassium atoms have coordination seven or eight, and the rest of the coordination sites are filled by water molecules which provide a hydrogen bonding system that also interconnects the anionic and the cationic layers (Figure 6.14).

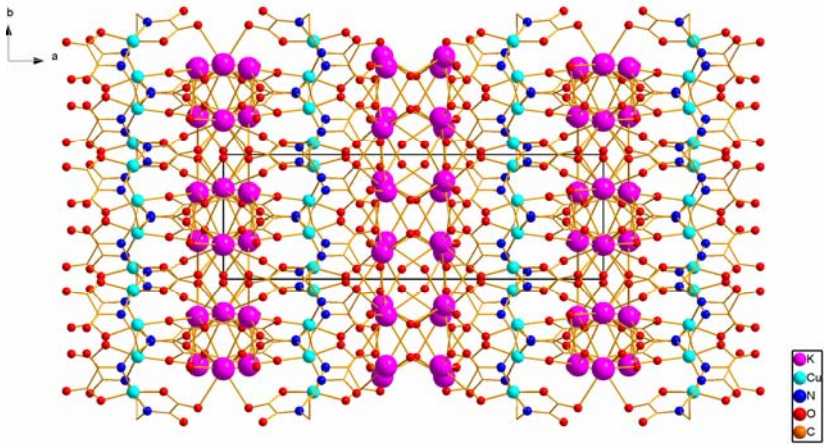

Figure 6. 14 View of the layered structure of **20** along the *ab*-plane. Hydrogen atoms are omitted for clarity**.**

The distribution of the chirality of the dimers in structure in this case, is alternated within the anionic layer in which homochiral stacks of dimers grow along the *b*-axis direction. These homochiral stacks alternate within the layer in the *c*-axis direction (Figure 6.15).

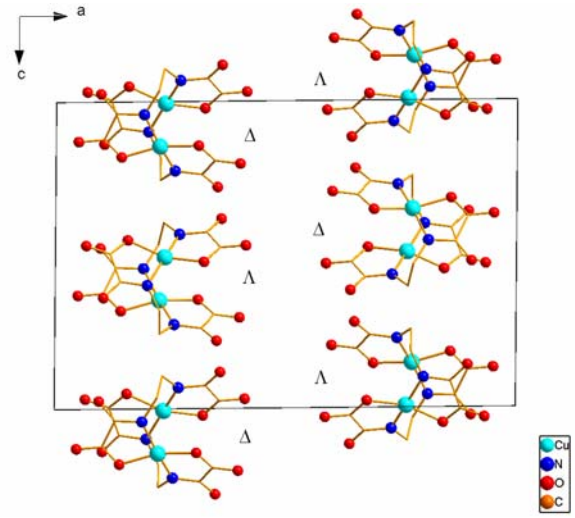

Figure 6. 15 Perspective view of the packing of the copper(II) dimers along the *ac*-plane showing the distribution of the chirality along the *c*-axis direction. Hydrogen atoms are omitted for clarity.

Moreover, the packing of the dimer in the anionic sheet has a zigzag pattern in which the direction of the dimer is the opposite in alternated stacks of dimers. The intermolecular distance between dimers along the *b*-axis and the *c*-axis are equal to 8.179(1) Å and 7.283(1) Å, respectively, being the latter being the shortest distance between dimers within the crystal structure (Figure 6.16).

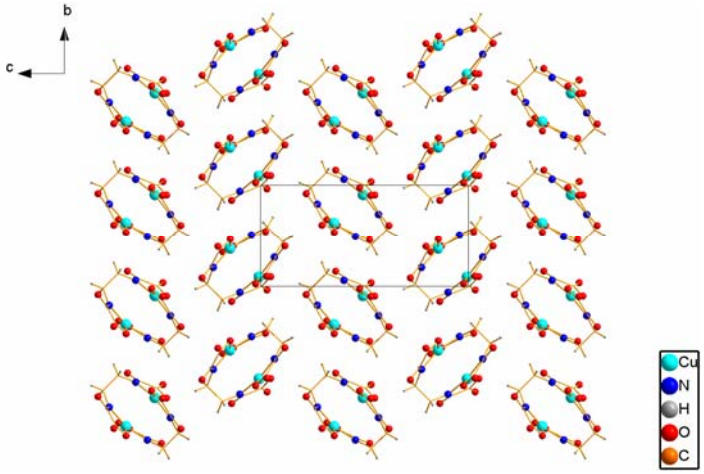

Figure 6. 16 Perspective view in the *bc*-plane of the packing of the dimers in the cationic layer.

6. 2. 4 Description of structure $K_4[Cu(oeo)]_2 \cdot 6H_2O$ (21)

Structure **21** crystallises in the triclinic space group $P\bar{1}$ containing one copper(II) complex, four potassium cations, which are disordered over seven sites; and six water molecules, which due to the disorder in the potassium sites, are also disordered. As the

whole dimer is present in the asymmetric unit, it has no higher symmetry than the point group C_1 (Figure 6.17). The copper sites are both fully occupied and the distance between sites is 2.941(2) Å.

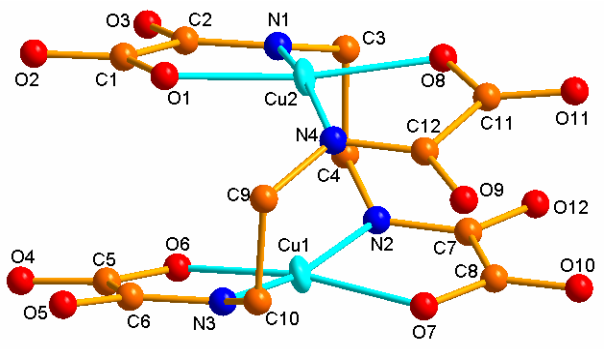

Figure 6. 17 Perspective view of the dinuclear copper (II) complex, $[Cu(oeo)]_2^{4-}$, showing the atom numbering scheme. Anisotropic thermal ellipsoids for copper atoms are drawn at the 50% of probability level.

The crystal has a layered structure perpendicular to the *a*-axis direction in which anionic layers of copper(II) complex alternate with cationic layers of potassium and water molecules (Figure 6.18). In the anionic layer, the dimers pack into stacks running along the [010] direction. Each stack is connected to two neighbouring stacks in the *a*-axis direction by the potassium sites K1, K2 and K3; and through the carbonyl oxygen atoms of the ligand providing a monodentate or chelating coordination to the cation. The rest of the potassium sites, K4, K5, K6A and K6B; are placed along the cationic layer where the disorder in mostly observed and where water molecules are also present. However, the layers in this crystal lattice are not as well defined as in the other crystal structures due to the high disorder in the structure as the K4 and K5 are placed in the space between stacks along the *c*-axis direction.

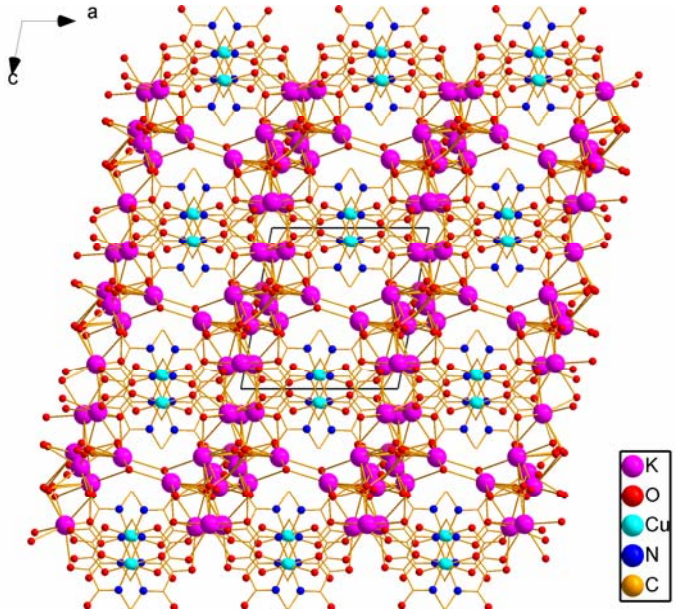

Figure 6. 18 Crystal packing view of **21** along the *b*-axis. The diagram shows the superposition of the disordered sites of the potassium and water molecules.

The chirality of dimers in the crystal alternates within the stacks due to the inversion centre present in the middle point between dimers (Figure 6.19). The distance between copper atoms of the dimers related by the inversion centre is 3.463(3) Å whereas the distance between copper atoms of neighbouring unit cells is 3.538(11) Å. Moreover, there is a weak interaction between the dimers related by the inversion centre though the nitrogen atoms and the copper atoms of the neighbouring dimer (Cu2-N4 3.094(13) Å) and even a weaker interaction between dimers of neighbouring unit cell (Cu1-N3 3.225(10) Å).

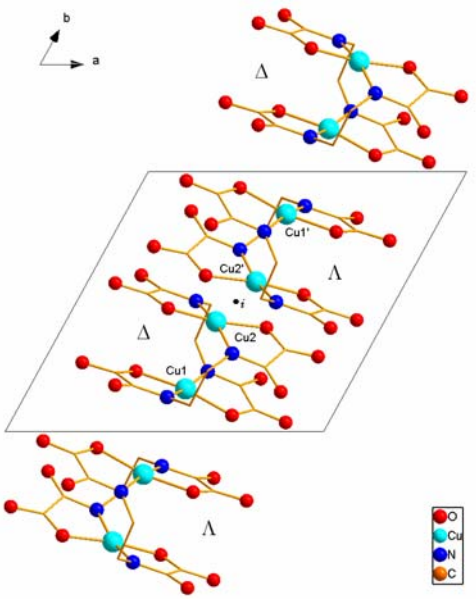

Figure 6. 19 Perspective view of the packing of the copper(II) dimers along the *ab*- plane showing the distribution of the chirality. Prime denotes symmetry operation 1-x, 1-y, 2-z.

In the cationic layer perpendicular to the *c*-axis is where most of the potassium and water molecules are disordered (Figure 6.20). Looking at the cationic layer, we see seven potassium sites, of which the preferred sites are K1 and K2, and are fully occupied. The next favoured position is K3 as its occupancy is 86.3(2)%. When this site is filled, all the K6 sites are vacant and these vacancies are filled by one of the mutually exclusive Ow7. K6 is distributed over two sites, K6A and K6B, which both have a nearby symmetry equivalent and they all add up to one. When K3 is vacant, only one of the four K6 sites is filled, since all four sites are mutually exclusive. This condition preserves the electroneutrality in the crystal structure.

On the other hand, K4 and K5 sites are so close to each other that each one must occupied 50% of the time. The occupancy of K4 and K5 are not related to the occupancy of the rest of the potassium sites.

As a result, we have two disordered groups of potassium: K4 and K5, and K3 and K6. Therefore, several different arrangements of potassium ions can be present in the crystal structure: K3 is filled and then, K4 or K5 is filled; or one of the four K6 sites is filled and then either K4 or K5 is filled. Moreover, K6 can be placed in four different sites giving rise to even more scenarios of the disorder in the structure. The occupancy of the different water molecules sites depends on the filling or the vacancy of the potassium sites of which they are coordinated to. Pictures of all the possible scenarios of the disorder in the potassium and water molecules sites can be found in (Appendix A4).

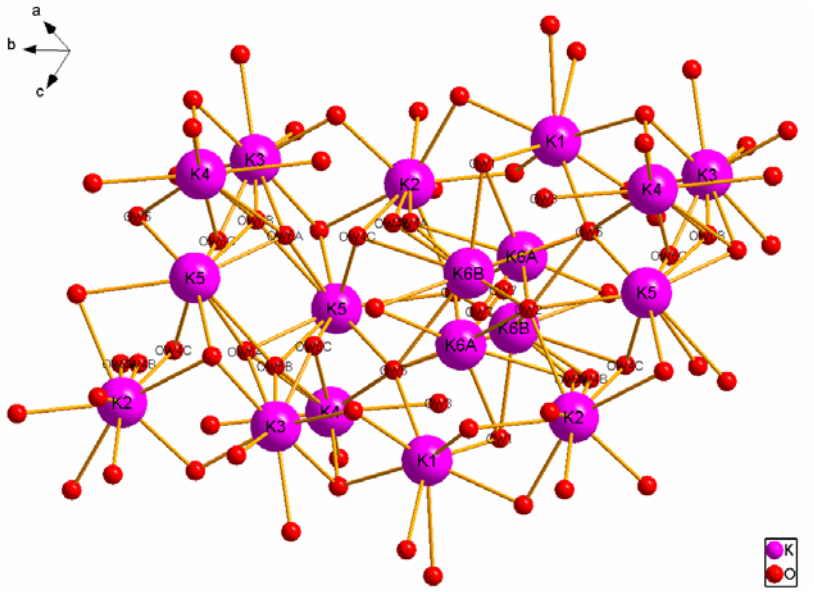

Figure 6. 20 Perspective view along the diagonal of the *ac*-plane of a section of the anionic layer showing a superposition of the potassium and water molecules disordered sites.

6. 3 Experimental Section

6. 3. 1 $K_4[Cu_x(H_{(2-2x)}oeo)]_2 \cdot nH_2O$ (17) and $K_4[Cu_{0.33}H_{1.34}(oeo)]_2 \cdot 5H_2O$ (18)

Synthesis

To an aqueous solution (3.5 ml) of **4a** (1.00 g, 3.35 mmols) a solution of $CuCl_2 \cdot 2H_2O$ (0.84 g, 4.78 mmols) dissolved in water (3 ml) was added drop-wise at room temperature giving rise to the formation of the expected $CuH_2(oeo) \cdot 3H_2O$ solid. Then 4.5 ml of an aqueous solution (5 ml) of KOH (0.70 g, 10.7mmols) were added dropwise to reaction mixture. The resulting deep blue solution was left stirring overnight and then filtered to eliminate the dark green solid that formed. The mixture was left in the fridge for three days which leaded to the formation a dark blue precipitate. The precipitate was solid filtered off and dried in air **(17)**. ^{1}H-NMR (400 MHz, D_2O, δ in ppm): 3.33(s, C*H*$_2$NH). ^{13}C-NMR (400 MHz, D_2O, δ in ppm): 166.0 (O*C*=O), 165.5 (N*C*=O), 38.54 (*C*H$_2$NH). IR (ATR, cm^{-1}): ν 3349 (w), 2909 (w), 2846 (w), 1659 (w), 1591 (s), 1430 (w), 1312 (s) (See Appendix A1). λ_{max}, 631 nm. Slow solvent evaporation of final reaction mixture afforded deep blue crystals of $K_4[Cu_{0.33}H_{1.34}(oeo)]_2 \cdot 5H_2O$ **(18).** IR (ATR, cm^{-1}): ν 3513 (w), 3407 (w), 3292 (w), 2988-2850 (w), 1660 (s), 1606 (w), 1524 (s), 1429 (w), 1386 (s) (See Appendix A1).

Crystallographic Data Collection and Structure Determination

The occupancy of the copper site was refined freely with anisotropic thermal parameters leading to a copper(II) occupancy of 32.8(2)%.

Extensive disorder was observed in the potassium sites of the crystal structure. Since half of the dimer $[Cu(oeo)]_2^{4-}$ is present in the asymmetric unit, two potassium are needed to balance the charges. The preferred site for the potassium is K1, which lies on a 4*a* Wyckoff position and is fully occupied. Therefore it contributes to the asymmetric unit with half of a positive charge. The charges that are left are balanced by three potassium sites, K2, K3 and K4. Due to proximity reasons only one potassium site can be filled at a time and thus they were refined with fixed 0.5 occupancies. Initially, the K4 occupancy was refined with a fix parameter of 0.5 and the occupancies of K2 and K3 were refined freely with combined occupancies that sum to 100%. Because this model leaded to an occupancy of 50.14(48)%, the occupancies for K2 and K3 were finally fixed to be half occupied. When the potassium sites are vacant, the sites are filled by a water molecule. So there are three water molecules sites (Ow2, Ow3 and Ow4) which were refined with fixed half occupancies. Ow1 site is fully occupied and does not affect the disorder in the structure.

All non-hydrogen atoms were refined anisotropically. The hydrogen atom positions of the organic molecule (also the amide hydrogens for when the copper site is vacant) were assigned to calculated positions and refined with fixed individual displacement parameters [$U_{iso}(H) = 1.2U_{eq}(C_{ethyl})$ or $1.2U_{eq}(N_{amide})$] using the SHELXL riding mode. All hydrogen atoms positions from water molecules where located on a ΔF map and refined with three restraints for each molecule (O-H and H···H distances) with thermal factors fixed [$U_{iso}(H) = 1.2U_{eq}(Ow)$].

Crystal data and selected details of the refinement are listed in Table 6.1.

Table 6. 1 Crystallographic data for **18**

	18
Empirical formula	$C_6H_{10.34}Cu_{0.33}K_2N_2O_{8.50}$
Formula weight	345.67
Crystal system	Monoclinic
Space group	*C*2/*c*
a (Å)	11.1447(4)
b (Å)	10.4182(4)
c (Å)	20.9438(7)
α (°)	90.00
β (°)	96.202(2)
γ (°)	90.00
V (Å^3)	2417.50(15)
T(K)	100(2)
ρ_{calc} (g/cm^3)	1.899
Z	8
F (000)	1407
Reflections collected	22680
Unique reflections	2472
Reflections observed [I>2σ(I)]	2253
R_{int}	0.0431
Parameters refined	230
Number of restraints	12
λ (Å); Mo Kα	0.71073
μ (mm^{-1})	1.390
θ Range (°)	1.96-26.37
Goodness-of-fit (GOF) on F^2	1.227
[a]R_1 [I>2σ(I)]	0.0493
[b]wR_2 (all data)	0.1124
Largest difference in peak and hole (e Å^{-3})	0.47 and -0.68
Crystal size (mm)	0.1×0.1×0.1
Crystal morphology	deep blue prism

[a]$R_1 = \Sigma(|F_o| - |F_c|)/ \Sigma|F_o|$

[b]$wR_2 = [\Sigma w(F_o^2 - F_c^2)^2]/\Sigma w(F_o^2)^2]^{1/2}$ where $w = 1/[\sigma^2(F_o^2) + (0.2P)^2$ and $P = [F_o^2 + 2F_c^2]/3$

Selected bond lengths (Å) and angles (°) for compound **18** are given in Table 6.2.[a,b] Also the dihedral angle formed by the chelating oxamato groups (°) and the distance of the atom from the mean plane (Å).

Table 6. 2 Selected bonds (Å) and angles (°) for **18**

	Cu1-O1	1.895(3)
	Cu1-N1	2.068(3)
	Cu1-O4	1.851(3)
	Cu1-N2	1.999(3)
	O4-Cu1-N1	97.52(12)
	N2-Cu1-O4	87.27(12)
	O1-Cu1-N1	83.85(12)
	N2-Cu1-O1	96.24(13)
Dihedral angle	Cu1	36.20(13)
Atom displacement	Cu1	0.151(1)
	O1	0.407(3)
	O4	0.399(3)
	N1	-0.177(2)
	N2	-0.414(3)

[a] Estimated standard deviations in the last significant digits are given in parenthesis. [b] The dihedral angle for Cu1 was calculated measuring the angle between the plane formed by O4-Cu1-N2 and O1-Cu1-N1.

6. 3. 2 $K_4[Cu_{0.89}H_{0.22}(oeo)]_2 \cdot 3H_2O$ (19)

Synthesis

To a stirred solution of **4a** (0.50 g, 1.66 mmols) in water (2 ml) an aqueous solution (1 ml) of $CuCl_2 \cdot 2H_2O$ (0.29 g, 1 equiv, 1.66 mmols) was added slowly at room temperature and the expected turquoise $CuH_2(oeo) \cdot 3H_2O$ solid was formed. The resulting mixture was stirred for few minutes and an aqueous solution (1 ml) of KOH (0.22 g, 2 equiv, 3.30 mmols) was then added. The resulting deep blue solution was charged with 3ml of water due to the high concentration and left stirring overnight at room temperature. Then, the solution was filtered to eliminate the dark green solid that formed. Slow solvent diffusion of methanol into the reaction mixture afforded prismatic deep blue crystals of $K_4[Cu_{0.89}H_{0.22}(oeo)]_2 \cdot 3H_2O$ **(19)** and long flat needle shaped of $K_4[Cu_{0.78}H_{0.44}(oeo)]_2 \cdot 4.5H_2O$ **(20)**.

Crystallographic Data Collection and Structure Determination

Cu1 and Cu2 lie on a 2*e* Wyckoff site and thus they sump one copper atom in the asymmetric unit. Both atoms were refined free in occupancies with the thermal

parameters anisotropic leading to the values of occupancy 85.3(4)% and 91.9(4)%, respectively.

Some disorder was noted in the potassium sites, and consequently, in the water molecules sites. Only half of the copper(II) dimer $[Cu(oeo)]_2^{4-}$ is present in the asymmetric unit. Therefore two positive charges are needed to maintain the electroneutrality. However there are three potassium sites. K1 site was fully occupied and the occupancy of the other two sites (K2A and K2B) was initially refined free with occupancies mutually excluded. The disorder in the potassium sites affected the water molecules sites since due to proximity reasons, some water molecules sites had to be excluded when the one potassium site was filled. OwA1 and OwA2 sites were filled when K2A site was filled and thus, OwB and K2B were vacant, and vice versa. This model leaded to an occupancy of 52.0(3)% and 12.17 water molecules per unit cell. Finally, a better model was obtained when the occupancies of K2A and K2B sites were fixed to 50% and water molecules were also fixed to 50% each site. Finally, water molecule OwA1 was restrained to have an approximate isotropic behaviour.

All non-hydrogen atoms were refined anisotropically. The hydrogen atom positions of the ethylenediamine fragment were assigned to calculated positions and refined with fixed individual displacement parameters [$U_{iso}(H) = 1.2U_{eq}(C_{ethyl})$] using a riding mode. Amide hydrogen atoms for when the copper site is vacant were also refined with fixed individual displacement parameters [$U_{iso}(H) = 1.2U_{eq}(N_{amide})$] using a riding mode. Finally, hydrogen atom positions of all water molecules were neither located nor calculated.

Crystal data and selected details of the refinement are listed in Table 6.3.

Table 6. 3 Crystallographic data for **19**

Empirical formula	$C_6H_{4.23}Cu_{0.89}K_2N_2O_{7.50}$
Formula weight	358.85
Crystal system	Monoclinic
Space group	*C*2/*c*
a (Å)	9.656(3)
b (Å)	10.881(3)
c (Å)	21.978(7)
α (°)	90.00
β (°)	102.048(12)
γ (°)	90.00
V (Å^3)	2258.3(11)
T(K)	100(2)
ρ_{calc} (g/cm^3)	2.111
Z	8
F (000)	1425
Reflections collected	10410
Unique reflections	2635
Reflections observed [I>2σ(I)]	1992
R_{int}	0.0599
Parameters refined	193
Number of restraints	6
λ (Å); Mo Kα	0.71073
μ (mm^{-1})	2.496
θ Range (°)	1.89-27.68
Goodness-of-fit (GOF) on F^2	1.097
[a]R_1 [I>2σ(I)]	0.0487
[b]wR_2 (all data)	0.1160
Largest difference in peak and hole (e Å^{-3})	0.81 and -0.77
Crystal size (mm)	0.05×0.05×0.05
Crystal morphology	blue prism

[a]$R_1 = \Sigma(|F_o| - |F_c|)/ \Sigma|F_o|$
[b]$wR_2 = [\Sigma w(F_o^2 - F_c^2)^2]/\Sigma w(F_o^2)^2]^{1/2}$ where $w = 1/[\sigma^2(F_o^2) + (0.2P)^2$ and $P = [F_o^2 + 2F_c^2]/3$

Selected bond lengths (Å) and angles (°) for compound **19** are given in Table 6.4.[a,b] Also the dihedral angle formed by the chelating oxamato groups (°) and the distance of the atom from the mean plane (Å).

Table 6. 4 Selected bonds (Å) and angles (°) for **19**.

	Cu1-O5	1.946(3)		Cu2-O1	1.965(3)
	Cu1-N1	1.929(3)		Cu2-N2	1.934(3)
	O5-Cu1-N1	98.98(14)		O1-Cu2-N2	98.41(13)
	N1-Cu1-O5’	84.79(13)		N2-Cu2-O1’	84.49(13)
Dihedral angle	Cu1	31.30(12)	Dihedral angle	Cu2	27.457
Atom displacement	Cu1	0.031(3)	Atom displacement	Cu2	-0.0295
	O5	-0.351(3)		O1	0.3103
	O5’	-0.351(3)		O1’	0.3103
	N1	0.351(3)		N2	-0.3103
	N1’	0.351(3)		N2’	-0.3103

[a]Estimated standard deviations in the last significant digits are given in parenthesis. [b]The dihedral angle for Cu1 and Cu2 was calculated measuring the angle between the plane formed by O5’-Cu1-N1 and O5-Cu1-N1’, and by O1-Cu2-N2’ and O1’-Cu2-N2, respectively.

6. 3. 3 $K_4[Cu_{0.78}H_{0.44}(oeo)]_2 \cdot 4.5H_2O$ (20)

Synthesis

Synthesis of compound **19** has been described in the synthesis of **20**.

Crystallographic Data Collection and Structure Determination

Cu1 and Cu2 were initially refined free in occupancies with the thermal parameters anisotropic leading to the values of occupancy 78.1(4)% and 78.6(4)%, respectively. Since both values are indistinguishable within their error, the two copper(II) occupancies were tied together. Thus both occupancies were refined free with anisotropic thermal parameters and constrained to have equal occupancies leading to an occupancy of 78.4(3)%.

Some disorder was observed in the potassium sites. However, it was not modelled since the percentage of occupation sites was very low (3%) and the refinement of the disorder did not improve the fit of the model. The water molecule Ow5 was restrained to have an approximate isotropic behaviour.

All non-hydrogen atoms were refined anisotropically. The hydrogen atom positions of the ethylenediamine fragment were assigned to calculated positions and refined with fixed individual displacement parameters [$U_{iso}(H) = 1.2U_{eq}(C_{ethyl})$] using a riding mode. Amide hydrogen atoms for when the copper site is vacant were also refined with fixed individual displacement parameters [$U_{iso}(H) = 1.2U_{eq}(N_{amide})$] using a riding mode, although they could be located in difference-Fourier map.

Moreover, hydrogen atom positions of water molecules Ow2, Ow3 and Ow4, where located in difference-Fourier maps, refined with three restraints (O-H and H···H distances) and given isotropic thermal parameters [$U_{iso}(H) = 1.2U_{eq}(Ow)$]. Ow5 is placed in a special position and the hydrogen atom was located, refined with isotropic thermal parameter [$U_{iso}(H) = 1.2U_{eq}(Ow)$] and using two restraints (O-H distance and H···H distance). The symmetry equivalent hydrogen atom was defined by symmetry operation. Finally, only one hydrogen atom of the Ow1 was located in difference-

Fourier maps which was refined with fixed individual displacement parameters [U_{iso}(H) = 1.2U_{eq}(Ow)] and with one restraint (O-H distance).

Crystal data and selected details of the refinement are listed in Table 6.5.

Table 6. 5 Crystallographic data for **20**

Empirical formula	$C_{12}H_{16.86}Cu_{1.57}K_4N_4O_{16.50}$
Formula weight	737.16
Crystal system	Monoclinic
Space group	*P*2/*c*
a (Å)	22.211(4)
b (Å)	7.2830(12)
c (Å)	14.879(2)
α (°)	90.00
β (°)	91.020(10)
γ (°)	90.00
V (Å^3)	2406.5(7)
T(K)	100(2)
ρ_{calc} (g/cm^3)	2.035
Z	4
F (000)	1481
Reflections collected	20337
Unique reflections	5832
Reflections observed [I>2σ(I)]	3484
R_{int}	0.1045
Parameters refined	374
Number of restraints	18
λ (Å); Mo Kα	0.71073
μ (mm^{-1})	2.175
θ Range (°)	0.92-28.36
Goodness-of-fit (GOF) on F^2	1.009
[a]R_1 [I>2σ(I)]	0.0675
[b]wR_2 (all data)	0.1698
Largest difference in peak and hole (e Å^{-3})	0.91 and -0.98
Crystal size (mm)	0.05×0.01×1.00
Crystal morphology	flat light blue needle

[a]$R_1 = \Sigma(|F_o| - |F_c|)/ \Sigma|F_o|$

[b]$wR_2 = [\Sigma w(F_o^2 - F_c^2)^2]/\Sigma w(F_o^2)^2]^{1/2}$ where $w = 1/[\sigma^2(F_o^2) + (0.2P)^2$ and $P = [F_o^2 + 2F_c^2]/3$

Selected bond lengths (Å) and angles (°) for compound **20** are given in Table 6.6.[a,b] Also the dihedral angle formed by the chelating oxamato groups (°) and the distance of the atom from the mean plane (Å).

Table 6. 6 Selected bonds (Å) and angles (°) for **20**

Cu1-O1	1.965(5)		Cu2-O5	1.979(5)
Cu1-O4	1.955(4)		Cu2-O6	1.948(5)
Cu1-N1	1.942(6)		Cu2-N3	1.965(5)
Cu1-N2	1.958(5)		Cu2-N4	1.940(5)
O1-Cu1-N1	84.9(2)		O5-Cu2-N3	100.4(2)
O1-Cu1-N2	100.7(2)		O5-Cu2-N4	84.4(2)
N1-Cu1-O4	95.1(2)		N3-Cu2-O6	84.6(2)
N2-Cu1-O4	84.9(2)		N4-Cu2-O6	95.6(2)
Dihedral angle Cu1	27.0(2)		Dihedral angle Cu2	25.7(2)
Atom displacement Cu1	-0.104(1)		Atom displacement Cu2	0.056(1)
O1	0.275(5)		O5	-0.237(4)
O4	0.287(5)		O6	-0.299(5)
N1	-0.346(5)		N3	0.334(5)
N2	-0.271(5)		N4	0.297(5)

[a]Estimated standard deviations in the last significant digits are given in parenthesis. [b]The dihedral angle for Cu1 and Cu2 was calculated measuring the angle between the plane formed by O4-Cu1-N2 and O1-Cu1-N1, and by O6-Cu2-N3 and O5-Cu2-N4, respectively.

6. 3. 4 $K_4[Cu(oeo)]_2 \cdot 6H_2O$ (21)

Synthesis

To a stirred solution of **4a** (0.25 g, 0.83 mmols) in water (5 ml) an aqueous solution (1 ml) of $CuCl_2 \cdot 2H_2O$ (0.12 g, 0.8 equiv, 0.67 mmols) was added slowly at room temperature and the expected turquoise $CuH_2(oeo) \cdot 3H_2O$ solid was formed. The resulting mixture was stirred for few minutes and an aqueous solution (1ml) of KOH (0.11 g, 2 equiv, 1.65 mmols) was then added. The resulting deep blue solution was left stirring for 2 hrs at room temperature and then filtered to eliminate the dark green solid that formed. Slow solvent diffusion of ethanol into the reaction mixture afforded needle shaped blue crystals of $K_4[Cu(oeo)]_2 \cdot 6H_2O$ **(21)**

Crystallographic Data Collection and Structure Determination

Cu1 and Cu2 sites are fully occupied. The occupancy of both sites was checked by refining them freely leading to an occupancy of 100%. Both atoms were refined using anisotropic thermal parameters.

Due to the lack of data, as high angle data was weak, the amount of parameters for a low symmetry space group such as a triclinic space group, was kept as low as possible to obtain a sensible model for the crystal structure. Therefore, all ligand atoms (carbon, oxygen and nitrogen) were constrained to have the same isotropic thermal parameter. This leads to a sensible displacement parameter for the ligand atoms with a low standard deviation (0.0269(6)). Moreover, the thermal parameter for all water molecules were also constrained to be equal and refined with a isotropic thermal parameter (0.482(1)). The two ligand molecules present in the asymmetric unit were restrained to have similar distances to equivalent atoms (carbon, oxygen and nitrogen) of the two molecules.

A lot of disorder was observed in the potassium and water molecules sites. Potassium ions are disordered over seven sites. K1 and K2 sites are fully occupied, which in total contribute to two of the four positive charges that are needed to preserve electroneutrality in the asymmetric unit. K4 and K5 occupancies were initially refined free leading to values very close to 50%. Due to proximity reasons they are mutually exclusive sites (d(K4-K5) = 2.7029(7) Å) and therefore, they both were modelled with fixed 0.5 occupancies.

Finally, the last positive charge needed in the asymmetric unit was distributed over three sites, K3, K6A and K6B. K3 site was refined with a free occupancy leading to 86.3(2)%. K6A and K6B sites, which are mutually exclusive since they are too close to be present at the same time (d(K6A-K6B) = 1.8568(5) Å), and each site is nearby to a symmetry equivalent position (d(K6A-K6A') = 2.8204(8) Å and d(K6B-K6B') 2.0001(4) Å); were refined with free occupancies leading to the values of 7.4(6)% and 6.3(6)%, respectively. In order to preserve electroneutrality, K3, K6A and K6B were refined subject to a linear constraint which must contribute to two positive charges per unit cell.

All potassium atoms were refined anisotropically, except K6A and K6B, which due to the low occupancy of the sites, were constrained to have the same isotropic thermal parameter as the water molecules.

Furthermore, due to the disorder in the potassium sites, extensive disorder in the water molecules sites was also observed. Ow1, Ow2 and Ow3 sites are fully occupied. Ow4 is disordered over three sites, Ow4A, Ow4B and Ow4C. At the beginning, the occupancy of each position was refined freely. But due to proximity of some of these oxygen sites to disordered potassium positions (K3, K4, K5, K6A and K6B) and also due to the proximity among themselves, the occupancies of these disordered oxygen sites were finally fixed to 0.50, 0.25 and 0.25, respectively.

Nearby disordered Ow4 group there is the disordered Ow6 group, which is also disordered over three sites, Ow6A, Ow6B and Ow6C. The disorder of these sites is affected by the disorder of the Ow4 group but also by the proximity of potassium sites (K3, K4, K5, K6A and K6B). The occupancy of each was initially freely refined and then they were refined with fixed to 0.50, 0.25 and 0.25, respectively.

The site Ow7 is placed within the K6A and K6B sites so when the potassium sites are vacant, the site is filled by the water molecule. In addition, it is nearby to a symmetry equivalent position (d(Ow7-Ow7') = 0.8437(2) Å). Because of this, the oxygen site in this case, was fixed to be half occupied and refined with a free occupancy leading to 69.2(4)%.

Finally, the occupancy of Ow5 was freely refined leading to 65.4(2) %. The occupancy of Ow5 and Ow7 were refined subject to a linear constraint that must be two water molecules per unit cell. Hydrogen atoms were neither located nor calculated.

Crystal data and selected details of the refinement are listed in Table 6.7.

Table 6. 7 Crystallographic data for **21**

Empirical formula	$C_{12}Cu_2K_4N_4O_{18}$
Formula weight	771.64
Crystal system	Triclinic
Space group	$P\bar{1}$
a (Å)	11.652(3)
b (Å)	11.798(3)
c (Å)	11.810(4)
α (°)	67.542(17)
β (°)	89.053(16)
γ (°)	63.253(14)
V (Å^3)	1315.8(7)
T(K)	100(2)
ρ_{calc} (g/cm^3)	1.948
Z	2
F (000)	756
Reflections collected	10124
Unique reflections	2859
Reflections observed [I>2σ(I)]	1834
R_{int}	0.0700
Parameters refined	194
Number of restraints	35
λ (Å); Mo Kα	0.71073
μ (mm^{-1})	2.335
θ Range (°)	1.90-21.29
Goodness-of-fit (GOF) on F^2	1.046
[a]R_1 [I>2σ(I)]	0.0708
[b]wR_2 (all data)	0.1948
Largest difference in peak and hole (e Å^{-3})	1.0 and -1.6
Crystal size (mm)	0.05×0.05×0.8
Crystal morphology	deep blue needles

[a]$R_1 = \Sigma(|F_o| - |F_c|)/ \Sigma|F_o|$

[b]$wR_2 = [\Sigma w(F_o^2 - F_c^2)^2]/\Sigma w(F_o^2)^2]^{1/2}$ where $w = 1/[\sigma^2(F_o^2) + (0.2P)^2$ and $P = [F_o^2 + 2F_c^2]/3$

Selected bond lengths (Å) and angles (°) for compound **21** are given in Table 6.8.[a,b] Also the dihedral angle formed by the chelating oxamato groups (°) and the distance of the atom from the mean plane (Å).

Table 6. 8 Selected bonds (Å) and angles (°) for **21**

Cu1-O6	1.966(8)		Cu2-O1	1.971(8)
Cu1-O7	1.979(8)		Cu2-O8	1.967(8)
Cu1-N2	1.919(10)		Cu2-N1	1.927(10)
Cu1-N3	1.930(10)		Cu2-N4	1.940(10)
O6-Cu1-N2	97.2(4)		O1-Cu2-N1	84.1(4)
O6-Cu1-N3	84.3(4)		O1-Cu2-N4	97.5(4)
N2-Cu1-O7	84.2(4)		N1-Cu2-O8	97.3(4)
N3-Cu1-O7	96.7(4)		N4-Cu2-O8	83.4(4)
Dihedral angle Cu1	17.1(5)		Dihedral angle Cu2	17.8(5)
Atom displacement Cu1	0.023(2)		Atom displacement Cu2	0.014(2)
O6	-0.162(10)		O1	0.163(10)
O7	-0.163(10)		O8	0.165(10)
N2	0.208(11)		N1	-0.244(12)
N3	0.242(12)		N4	-0.214(12)

[a]Estimated standard deviations in the last significant digits are given in parenthesis. [b]The dihedral angle for Cu1 and Cu2 was calculated measuring the angle between the plane formed by O6-Cu1-N3 and O7-Cu1-N2, and by O1-Cu2-N1 and O8-Cu2-N4, respectively.

[1] See Chapter 5

Chapter 7: Rubidium Compounds

7. 1 Introduction

X-ray diffraction data was collected on three separate crystals of $Rb_4[Cu_xH_{(2-2x)}(oeo)]_2 \cdot 4H_2O$ **(22),** all showing essentially the same structure but having quite varied occupancy in copper site. They all were obtained from the same reaction mixture but using different crystallisation techniques and different timescales. The model that was used in the refinement for every crystal was the same but the quality of the crystals was different leading to different refinement parameters (R_1, wR_2, S) for each crystal (See Table 7.1).

The reaction mixture was prepared adding aqueous solutions of two equivalents of RbOH and 0.52 equivalents of $CuCl_2 \cdot 2H_2O$ into a stirred solution of $Rb_2H_2(oeo)$ in water giving rise to a deep blue solution that was filtered to eliminate impurities. Two different crystal growing techniques were carried out: slow solvent diffusion of polar organic solvents into the reaction mixture and slow solvent evaporation of the reaction mixture. The first technique afforded deep blue crystals when using a mixture of MeOH/EtOH (1:2). The composition of the crystal of which data was collected is $Rb_4[Cu_{0.80}H_{0.40}(oeo)]_2 \cdot 4H_2O$ **(22a)**.

On the other hand, data was collected of two separate crystals grown using the second technique. These two crystals were grown in different timescales. Slow solvent evaporation of the first crystal was carried out following the preparation of the reaction mixture, affording a crystal structure with the composition $Rb_4[Cu_{0.30}H_{1.40}(oeo)]_2 \cdot 4H_2O$ **(22b)** (Figure 7.1). Slow solvent evaporation procedure of the second crystal was carried out five months after the reaction mixture was prepared leading to the crystal structure with a lower amount of copper(II), $Rb_4[Cu_{0.18}H_{1.64}(oeo)]_2 \cdot 4H_2O$ **(22c).**

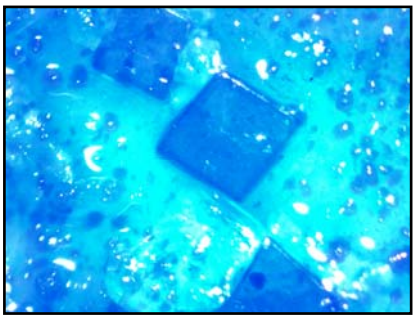

Figure 7. 1 View under a microscope in reflected unpolarized light of the blue crystals of **22b** obtained using slow solvent evaporation of the reaction batch. Approximate scale: width of image 0.5mm.

From both techniques, light turquoise crystals of $Rb_2[Cu(ox)_2].2H_2O$ were obtained as a co-product.[1] Thus, not all the copper(II) that was added to the reaction results in the formation of the cooper(II) dimer complex**.** Some was lost in the formation of co-products, copper oxide or copper hydroxide.

7. 1. 1 The dimer

It is surprising how variable can be the amount of copper(II) present in the crystal structure. Three different crystals obtained from the same reaction mixture have given three different amounts of copper(II), the values of which are not even similar. However, as stated earlier, they were obtained using two different crystallisation techniques and different timescales. **22a** and **22b** were obtained approximately within same periods of time but using different crystallisation techniques. This would suggests that slow solvent diffusion technique affords crystals with larger amount of copper(II) in the crystal. Nonetheless, due to the wide range of copper(II) occupancies that have been observed in the copper dimer species, it is probable that not all the crystals that are grown in the beaker will have the same composition. That is to say that while the solvent diffuses into the reaction mixture, or either the solvent evaporates from the reaction mixture, the composition of the solution changes making the less soluble compounds precipitate first. If the less soluble crystals that grow at the top of the vial are the species containing a larger amount of copper in the structure, less copper will be left in the solution and thus, the crystals that precipitate at the bottom will have less amount of copper, or vice versa. As a result, it is probable that the composition of the crystal probably varies depending on where in the beaker the crystal is picked up. This is a consequence that not all the copper that was added goes to the formation of the copper(II) dimer. Some amount of copper is lost by the precipitation of some

coordination polymers, copper oxide or copper hydroxide; and the formation of some co-products, like $Rb_2[Cu(ox)_2].2H_2O$.

On the other hand, we have observed that when using the same crystallisation technique but different timescales, the longer the period between the preparation of the copper(II) complex solution and the formation of the crystal, the lower the amount of copper(II) present in the crystal. We imagine that a number of irreversible reactions may exist, particularly reactions that remove the copper from the reaction. We emphasise again that the composition of the crystal probably varies depending on where in the beaker the crystal is picked up.

It is noteworthy to mention the different species that are present in the solid solution of the crystal structures. **22a** has a copper site occupancy of 79.8(2)%, being the crystal with the largest amount of copper in the structure, and **22b** has 29.1(2)% and **22c** 17.1(3)%. Looking at the occupancy graph that we drew in Scheme 3.5, we can see that **22a** is located on the left side of the graph where the occupancy is over 50%, whereas **22b** and **22c** are located on the right side (Scheme 7.1).

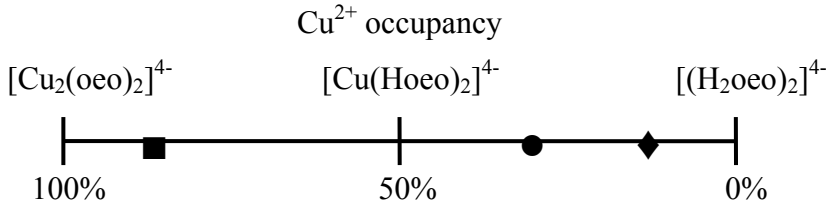

Scheme 7. 1 Representation of the different species present in the crystal structure depending on the amount of copper(II) present in the crystals. ■ stands for (**22a**), ● for (**22b**) and ♦ for (**22c**).

Thus, the composition of three solid solutions are $Rb_4\{[Cu(oeo)_2]_x[Cu(Hoeo)_2]_{(1-x)}\}$ for **22a** where x = 0.60**,** and $Rb_4\{[Cu(Hoeo)_2]_x[(H_2oeo)_2]_{(1-x)}\}$ for **22b** and **22c** where x = 0.60 and 0.36, respectively. That is to say that, technically, in **22b** and **22c** there is no copper(II) dimer $[Cu_2(oeo)_2]^{4-}$.

In addition, as discussed in Chapter 5, when the occupancies in the copper(II) site are quite low, the expected trend where Cu-N (amide) bond lengths are shorter compared to Cu-O (carboxylate) bond lengths is not observed.[2] This tendency is neither seen in these structures. Furthermore, they are a good example to show that the lower the amount of copper, the more significant is the difference between bond lengths.

In Table 7.2 it can be observed that three crystals which have the same structure but different amounts of copper (**22a**, **22b** and **22c**), the bond lengths around the metal ion change depending on the amount of copper present in the site. Thus, the apparent Cu-N increases in length while Cu-O decreases when the amount of copper(II) present in the dimer decreases. Similarly, the N-O distance of the atoms implied in the hydrogen bond increases with the amount of copper(II). This is consistent with the dominance of the hydrogen-bonded dimer geometry in the crystal structure. Moreover, the dihedral angle between the planes built with the donor atoms of each oxamato group and the copper, increase with the decrease of the copper present in the dimer. These compare well with other copper(II) complexes with similar quantities of copper(II), **14, 16** and **18.** However, deviations from the mean plane built by the donor atoms are only comparable with **14, 16** and **18** when the copper left in the dimer is the lowest**, 22c.**

We have shown that the variation in the amount of copper affects the geometry around the metal ion in the dimers. The lower the amount of copper, the more significant is the difference between bond lengths as well as the angle between oxamato donor atoms planes.

7. 2 Results

Description of structure $Rb_4[Cu_xH_{(2-x)}(oeo)]_2 \cdot 4H_2O$ (22)

Compound **(22)** consists of dinuclear dianionic copper(II) units, $[Cu(oeo)]_2^{4-}$, coordinated rubidium cations and coordinated water molecules. It crystallises in the orthorhombic space group *Cccm* containing a quarter of the dimer in the asymmetric unit: half of a organic molecule and half of a copper(II) atom, since the copper site lies in a *8h* Wyckoff position. In addition, it contains one rubidium atom which is distributed over three sites and one water molecule distributed over two sites, each of them half occupied.

The dimer has a D_2 symmetry as the centre of it lies on the Wyckoff position (either 4*a* or 4*b*) which has implicit three perpendicular C_2-axis. One axis passes through the two copper atom sites, the second one through the mid-point of the C-C bond of the two ethylenediamines fragments and finally, the third one goes through the middle point of

the dimer (See Figure 3.2 for details). As a consequence, these three two fold axis present in the dimer generate the rest of the molecule in three dimensions (Figure 7.2). In this space group, the maximal point group symmetry of the molecule is realised. The intramolecular distance between copper atoms sites within the dimer is 2.984(2) Å.

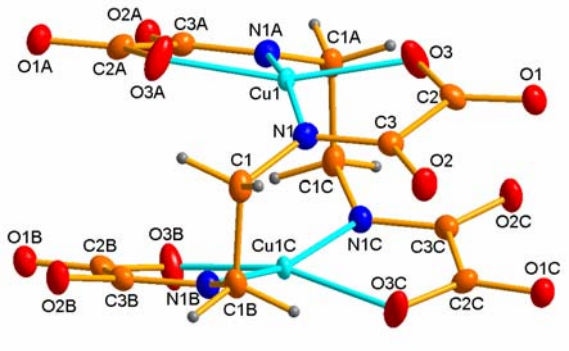

Figure 7. 2 Perspective view of the copper(II) complex, $[Cu(oeo)]_2^{4-}$, showing the atom numbering scheme. Anisotropic thermal ellipsoids for non-hydrogen atoms are drawn at the 50% probability level. Symmetry codes: A = 1-x, y, 0.5-z; B = x, -y, 0.5-z; C = 1-x, -y, z. As previously mentioned, depending on the copper(II) occupancy different solid solutions are founded in the crystals. Therefore, the picture only shows the case where both copper sites are filled though they might not be filled at the same time.

The crystal has a layered structure perpendicular to the *c*-axis direction, in which anionic layers of copper(II) dimeric units alternate with cationic layers of rubidium and water molecules (Figure 7.3). The bis(oxamato) copper(II) entities are coordinated to the rubidium atoms through the carbonyl oxygen atoms providing a monodentate or chelating coordination to form the 2-D network. Additional water molecules complete the coordination sphere of the rubidium atoms. This leads to interlayer hydrogen-bonding interactions involving the coordinated water molecules and the carbonyl oxygen atoms of the oxamate ligands.

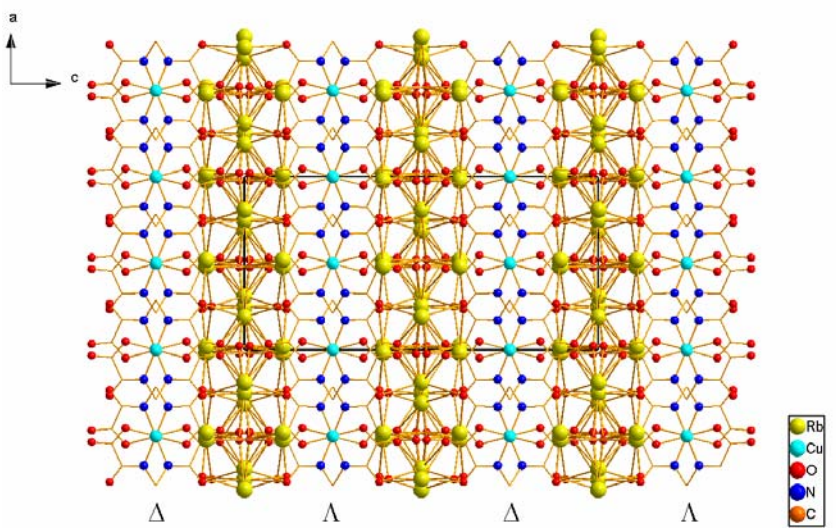

Figure 7. 3 Crystal packing of **22** view of the *ac*-plane with the superposition of the disorder in the rubidium sites. The diagram shows the extensive site disorder in the rubidium and water molecules sites.

In the cationic layer, rubidium shows extensive site disorder and consequently, also water molecule site disorder. The preferred rubidium sites are Rb1 and Rb2 since they are both almost fully occupied (~95%). The rest of the rubidium needed to balance the charges is placed in Rb3. Looking in detail at the cationic layer in the *bc*-plane (Figure 7.4), it can be noticed that rubidium Rb3 sites have a nearby symmetry equivalent site that it is too close for them to be both occupied at the same time. Also, some water molecules are also related and excluded by symmetry (Ow2). The occupancies of the rubidium sites were tied together to preserve electroneutrality leading to a value lower than 50% for Rb3 (28.4(1) %).

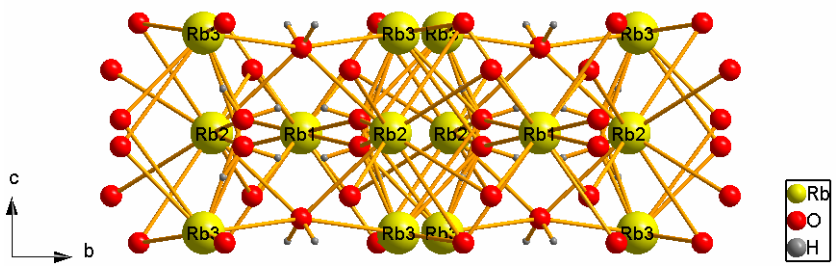

Figure 7. 4 Perspective view in the *bc*-plane of a section of the anionic layer showing a superposition of all rubidium and water molecules sites. From this perspective, Rb2 sites seem to be very close to be present at the same time but distance between atoms is 6.675(2) Å.

Therefore, there are two situations of rubidium sites that we can be found in the crystal structure (Figure 7.5). Depending on the rubidium site that is filled, one of the Ow2 sites will be filled and the symmetry equivalent site will remain empty.

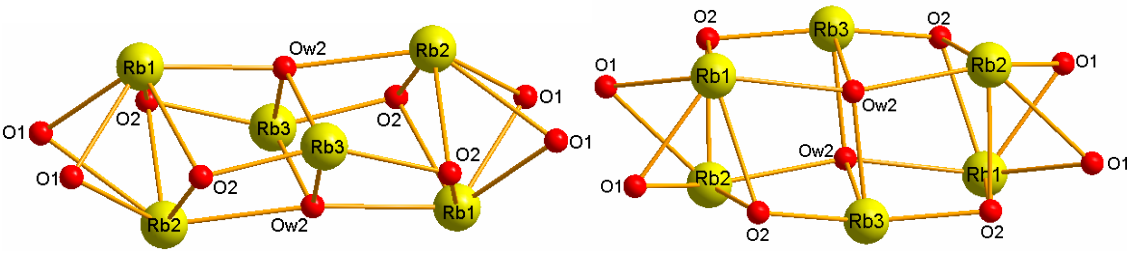

Figure 7. 5 Simplified view of the *bc*-plane (Figure 7.4) of the two possible rubidium sites scenarios present in the crystal structure showing the environment between rubidium sites.

On the other hand, in the anionic layer, the $[Cu(oeo)]_2^{4-}$ units are distributed in a rhombic pattern in which the dimeric units are placed in the middle of the edge of the unit cell in the *ab*-plane (Figure 7.6). The intermolecular distance between the centre of the dimers along the [1 0 0] direction is 10.5033(6) Å and along [½ ½ 0] direction is 7.6449(3) Å. The latter distance would be the lengths of the edges of the imaginary rhombus in the packing pattern of the dimer.

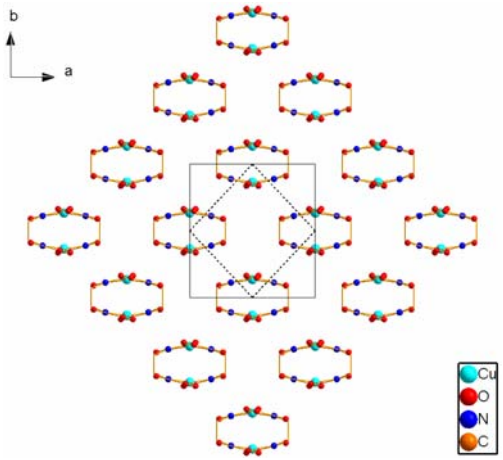

Figure 7. 6 Perspective view in the *ab*-plane of the packing of the copper(II) dimers in the anionic layer. Dashed lines show the imaginary rhombic pattern. Hydrogen atoms omitted for clarity.

The distribution of the two enatiomers in the crystal lattice is displayed within the layers in which homochiral layers of the two enantiomers alternate in the *c*-axis direction (Figure 7.7).

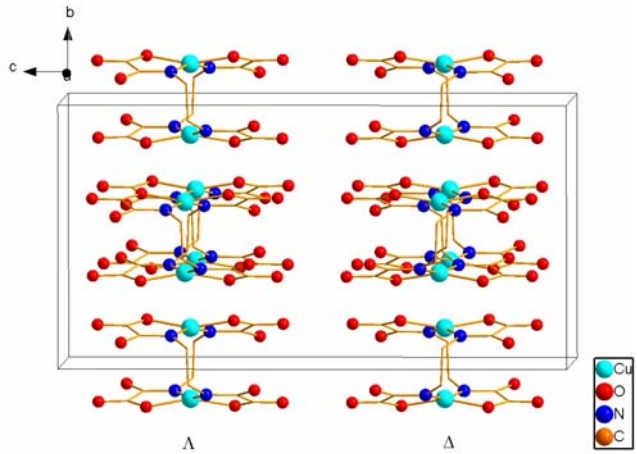

Figure 7. 7 Perspective view of the packing of the copper(II) dimers along the *bc*-plane showing the distribution of the chirality along the *c*-axis direction. Hydrogen atoms omitted for clarity.

7. 3 Experimental Section

$Rb_4[Cu_xH_{(2-2x)}(oeo)]_2{\cdot}4H_2O$ (22)

Synthesis

To a stirred solution of **5a**·H_2O (0.60 g, 1.53 mmols) in water (8 ml) was added slowly an aqueous solution (1 ml) of $CuCl_2{\cdot}2H_2O$ (0.14 g, 0.52 equiv, 0.80 mmols) at room temperature and the expected turquoise $CuH_2(oeo){\cdot}3H_2O$ solid was formed. The resulting mixture was stirred for few minutes and an aqueous solution of RbOH (0.38 ml, 50 wt.%, 4.26 mmols) was then added. The resulting deep blue solution was covered and left stirring for two days at room temperature. Then, the solution was filtered to eliminate the dark brown solid that formed. λ_{max} = 574 nm. Slow evaporation of the reaction mixture afforded deep blue crystals of $Rb_4[Cu_{0.30}H_{1.40}(oeo)]_2{\cdot}4H_2O$ **(22b)** and five months later, $Rb_4[Cu_{0.18}H_{1.64}(oeo)]_2{\cdot}4H_2O$ **(22c).** In addition, deep blue crystals of $Rb_4[Cu_{0.80}H_{0.40}(oeo)]_2{\cdot}4H_2O$ **(22a)** were afforded by from the slow solvent diffusion of a mixture of MeOH/EtOH (1:2) into the final solution.

Crystallographic Data Collection and Structure Determination

The copper site is not fully occupied and the anisotropic thermal parameters were refined free leading to 79.8(2)% of occupancy for **22a**, 29.1(2)% for **22b** and 17.1(3)% for **22c**.

A lot of disorder was observed in the rubidium and water molecules positions. The rubidium cations are disordered over three sites: Rb1, Rb2 and Rb3 which lie on a 4*f*, 8*l* and 16*m* Wykoff sites. First, preliminary refinements suggested that the Rb1 and Rb2 sites were fully occupied, and Rb3 was ¼ occupied. In fact the Rb3 site is nearby to a symmetry equivalent position (1.0995(1) Å) and therefore it must have an occupancy of <50 %. Then, a better model was achieved when the occupancies of the three Rb sites were refined freely, subject to the linear constraint that there must be 16 Rb atoms per unit cell to preserve electroneutrality. This led to occupancies of Rb1 95.5(2)%, Rb2 95.4(2)% and Rb3 28.4(1)%.

Moreover, some disorder was also observed in the position of water molecules Ow2 since its the position is correlated with the occupancy of the Rb3 cation. Initially, free refinement of the occupancy gave a value just over 50%. However, the presence of a nearby symmetry equivalent site (0.6309(0) Å) required that the occupancy must be ≤50%. Because of that, the occupancy was fixed to 50 %. The highest residual peaks in the difference electron density map are located close to the rubidium sites.

All non-hydrogen atoms were refined anisotropically. The hydrogen atom positions of the ethylenediamine fragment were assigned to calculated positions and refined with fixed individual displacement parameters [$U_{iso}(H) = 1.2U_{eq}(C_{ethyl})$] using a riding mode. Amide hydrogen atoms for when the copper site is vacant were also refined with fixed individual displacement parameters [$U_{iso}(H) = 1.2U_{eq}(N_{amide})$] using a riding mode.

Finally, hydrogen atom positions of water molecule Ow2 for each crystal were located in difference-Fourier maps, refined with three restraints (O-H and H···H distances) and given isotropic thermal parameters [$U_{iso}(H) = 1.2U_{eq}(Ow)$]. Ow1 is placed in a special position and the hydrogen atom was located, refined with isotropic thermal parameter [$U_{iso}(H) = 1.2U_{eq}(Ow)$] and with two restraints (O-H distance and H···H distance). The symmetry equivalent hydrogen atom was defined by symmetry operation.

Crystal data and selected details of the refinement are listed in Table 7.1.

Table 7. 1 Crystallographic data for **22.**

	22a	**22b**	**22c**
Empirical formula	$C_3H_{4.20}Cu_{0.40}NO_4Rb$	$C_3H_{4.71}Cu_{0.15}NO_4Rb$	$C_3H_{4.83}Cu_{0.09}NO_4Rb$
Formula weight	229.12	213.51	209.86
Crystal system	Orthorombic	Orthorombic	Orthorombic
Space group	*Cccm*	*Cccm*	*Cccm*
a (Å)	10.5033(6)	10.556(3)	10.5566(7)
b (Å)	11.1113(6)	11.073(2)	11.0183(7)
c (Å)	21.4450(11)	21.309(5)	21.1077(16)
α (°)	90.00	90.00	90.00
β (°)	90.00	90.00	90.00
γ (°)	90.00	90.00	90.00
V (Å^3)	2502.7(2)	2490.9(9)	2455.2(3)
T(K)	100(2)	100(2)	100(2)
ρ_{calc} (g/cm^3)	2.432	2.277	2.271
Z	16	16	16
F (000)	1757	1647	1621
Reflections collected	23973	12474	11371
Unique reflections	2159	1948	1395
Reflections observed [I>2σ(I)]	1829	1544	1200
R_{int}	0.0541	0.0594	0.0657
Parameters refined	115	114	115
Number of restraints	6	6	6
λ (Å); Mo Kα	0.71073	0.71073	0.71073
μ (mm^{-1})	9.177	8.377	8.299
θ Range (°)	1.90-31.59	1.91-30.53	1.93-27.03
Goodness-of-fit (GOF) on F^2	1.040	1.035	1.125
[a]R_1 [I>2σ(I)]	0.0295	0.0410	0.0397
[b]wR_2 (all data)	0.0698	0.1105	0.1087
Largest difference in peak and hole (e Å^{-3})	0.79 and -0.61	1.47 and -1.17	1.04 and -0.81
Crystal size (mm)	0.05×0.2×0.2	0.1×0.1×0.1	0.1×0.1×0.1
Crystal morphology	blue cubic prism	blue cubic prism	blue cubic prism

[a]$R_1 = \Sigma(|F_o| - |F_c|)/ \Sigma|F_o|$

[b]$wR_2 = [\Sigma w(F_o^2 - F_c^2)^2]/\Sigma w(F_o^2)^2]^{1/2}$ where $w = 1/[\sigma^2(F_o^2) + (0.2P)^2$ and $P = [F_o^2 + 2F_c^2]/3$

Selected bond lengths (Å) and angles (°) for compound **22** are given in Table 7.2. [a,b,c] Also the dihedral angle formed by the chelating oxamato groups (°) and the distance of the atom from the mean plane (Å).

Table 7. 2 Selected bonds (Å) and angles (°) for **22a, 22a** and **22a**.

		22a	**22b**	**22c**
	Cu1-O3	1.944(2)	1.869(3)	1.845(4)
	Cu1-N1	1.955(2)	2.042(3)	2.065(4)
	O3-N1'	2.947(3)	2.938(4)	2.935(5)
	O3-Cu1-N1	84.28(8)	85.25(10)	85.57(15)
	O3-Cu1-N1'	98.17(9)	97.33(9)	97.13(15)
Dihedral angle	Cu1	25.48(9)	37.14(13)	40.40(23)
Atom displacement	Cu1	-0.037(0)	0.069(2)	0.232(4)
	O3	0.286(2)	-0.496(3)	-0.378(4)
	O3'	0.286(2)	-0.496(3)	-0.378(4)
	N1	-0.286(2)	0.220(2)	0.378(4)
	N1'	-0.286(2)	0.220(2)	0.378(4)

[a]Estimated standard deviations in the last significant digits are given in parenthesis. [b]The symmetry code denoted by prime is 1-x, y, 0.5-z. [c]The dihedral angle for Cu1 was calculated measuring the angle between the plane formed by O5-Cu1-N1 and O5'-Cu1-N1'.

[1] U. Kolitsch, *Acta Crystallogr.,* **2004**, *C60*, m129.
[2] (a) B. Cervera, J.L. Sanz, M.J. Ibañez, G. Vila, F. Lloret, M. Julve, R. Ruiz, X. Ottenwaelder, A. Aukauloo, S. Poussereau, Y. Journaux, M.C. Muñoz, *J. Chem. Soc*., *Dalton Trans.*, **1998**, 781. (b) K. E. Berg, Y. Pellegrin, G. Blondin, X. Ottenwaelder, Y. Journaux, M. Moragues Canovas, T. Mallah, S. Parsons, A. Aukauloo, *Eur. J. Inorg. Chem.,* **2002**, *323-325*, 1434. (c) M. Fettouhi, L. Ouahab, A. Boukhari, O. Cador, C. Mathonière, O. Kahn, *Inorg. Chem.,* **1996***, 35,* 4932. (d) J. Ribas, A. Garcia, R. Costa, M. Monfort, S. Alvarez, Z. Zanchini, X. Solans, M.V. Domenech, *Inorg. Chem*., **1991**, *30*, 841.
[2] T. Rüffer, B. Bräuer, F.E. Meva, B. Walfort, G. Salvan, A.K. Powell, I.J. Hewitt, L. Sorace, A. Caneschi, Inorg. Chim. Acta, **2007**, *360*, 3777

Chapter 8: Caesium Compounds

8. 1 Introduction

For compound $Cs_4[Cu(oeo)]_2$ only one crystal structure has been obtained containing 5½ coordination water molecules, $Cs_4[Cu(oeo)]_2 \cdot 5½H_2O$ **(23)**. However, the crystallisation chemistry of $Cs_4[Cu(oeo)]_2$ has not been thoroughly explored. The X-ray diffraction data was collected by Dr. Louis Farrugia.

Single crystals of **23** suitable for X-ray analysis were obtained from slow diffusion of a mixture of organic solvents, EtOH/MeOH (2:1), into the reaction mixture of $Cs_4[Cu(oeo)]_2$. The $Cs_4[Cu(oeo)]_2$ solution was prepared by adding aqueous solutions of 0.5 equivalents of $CuCl_2 \cdot 2H_2O$ and 2.04 equivalents of $CsOH \cdot H_2O$ into a solution of $Cs_2H_2(oeo)$ in water. All other attempts of obtaining crystals leaded to the formation of crystals of the decomposition product of the ligand, such as $Cs_xCu(ox)_y$ when using MeCN, or a mixture of solids.

$Cs_4[Cu(oeo)]_2 \cdot 5½H_2O$ **(23)** and $Li_4[Cu_{0.93}H_{0.14}(oeo)]_2 \cdot 11½H_2O$ **(11)** are comparable copper(II) dimer structures. They both crystallise in the triclinic space group $P\bar{1}$ containing two dimers in the asymmetric unit and eight counterions. Probably, due to the difference in size of the cations, the former crystallises with eleven water molecules and the later with twenty-one. Moreover, they have very similar crystal packing**.** In both structures the copper(II) dimer packs in infinite stacks surrounded by counterions and water molecules along the *b*-axis in **23**, whereas in **11** the dimer packs along the diagonal of the unit cell.

The interaction between dimers within the stack through the calcium atoms and the carboxylate oxygen atoms of the neighbouring dimer links two dimers within the asymmetric unit and two asymmetric units within the stack. Both structures have also a weak interaction in the asymmetric unit between a copper atom and the nitrogen atom of the neighbouring dimer. Therefore, all copper(II) atoms have a distorted-squared pyramid environment, except those with a weak interaction with the nitrogen of the neighbouring dimer. However, in **23** one of the copper atoms that links two asymmetric

units has no interaction between dimers, being the only copper(II) atom with square-planar geometry.

The distribution of the chirality of the dimers within the crystal lattice is different between structures. In **11** the distributions goes though the stack of dimers and in 23 layers of enantiomorphic stacks are alternated in the *c*-axis direction.

Surprisingly, the amount of copper(II) added in the reaction mixture was 0.5 equivalents and the species crystallises containing 100% of copper present in the structure. This is consistent with concept that raised in Chapter 4, in which due to the interaction between dimers through the copper and the carboxylate oxygen atoms it is needed a very high amount of metal for the crystal to be formed. In $M_4[Cu(oeo)]_2 \cdot nH_2O$ compounds where M = Na, K (except for **21**), Rb; there is no interaction between dimers in the crystal lattice and therefore, it is not needed a high copper occupancy in the structure to be formed since the hydrogen bonds can fill the copper vacancy producing no change in the crystal structure. So, looking at the crystal data of those crystals it can be noted a wide range of copper present in those structures. On the other hand, in **11** and **23,** when copper site is vacant there is no direct interaction between dimers since the site is filled by hydrogen bonds.

8. 2 Results

8. 2. 1 Description of structure $Cs_4[Cu(oeo)]_2 \cdot 5\ ½\ H_2O$ (23)

Structure **23** crystallises in the triclinic space group $P\bar{1}$. It crystallises with a large asymmetric unit containing two dimeric $[Cu(oeo)]_2^{4-}$ units (Figure 8.1), eight caesiums cations, of which two are disordered over two sites; and eleven water molecules, one of them also disordered over two sites. As a result, there are only two asymmetric units present in the unit cell, which are related through the inversion centre present in the middle of the unit cell (Figure 8.3). The dimers have no higher molecular point symmetry than C_1. The distance between copper(II) atoms within dimers is 3.023(9) Å and 3.037(9) Å for Cu1-Cu2 and Cu3-Cu4, respectively.

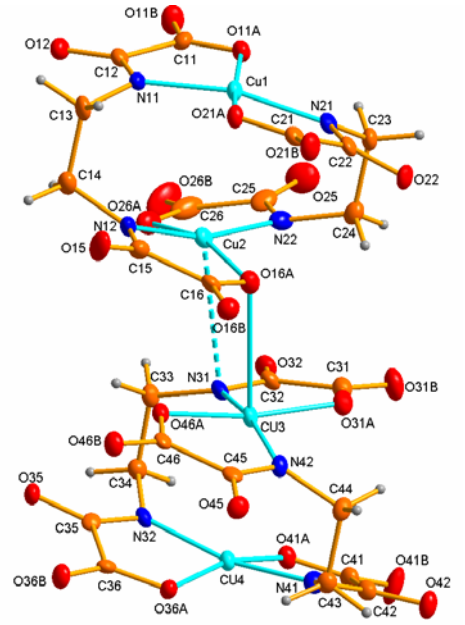

Figure 8. 1 Perspective view of the asymmetric unit showing the atom numbering scheme. Caesium ions and water molecules are omitted for clarity. Anisotropic thermal ellipsoids for non-hydrogen atoms are drawn at the 50% of probability level. The dashed line represents the weak interaction between dimers.

Each copper(II) atom is bonded to two nitrogen and two oxygen atoms arising from two chelating oxamato groups and leading to a distorted square-planar environment. The two dimers in the asymmetric unit are linked though the Cu-O bond between Cu3 and the carboxylate oxygen of the neighbouring dimer, O16A (2.846(4) Å), giving a distorted square-pyramid geometry to the metal. The dimers are also linked though a weak interaction between Cu2 and N31 (3.285(5) Å).

On the other hand, two asymmetric units are linked as well through a Cu-O bond between Cu1 and the carboxylate oxygen atom of the next asymmetric unit within the stack, O36A (2.707(4) Å), also leading to a distorted square-pyramid coordination in the metal. This type of pattern gives rise to a crystal lattice where infinite $[Cu(oeo)]_2^{4-}$ stacks pack along the [010] direction being surrounded by caesium atoms and water molecules. Dimer stacks are connected through the cations and water molecules (Figure 8.2). Lastly, due to the long distance between dimers, Cu4 has no interaction with the neighbouring dimer and it has a distorted square-planar environment.

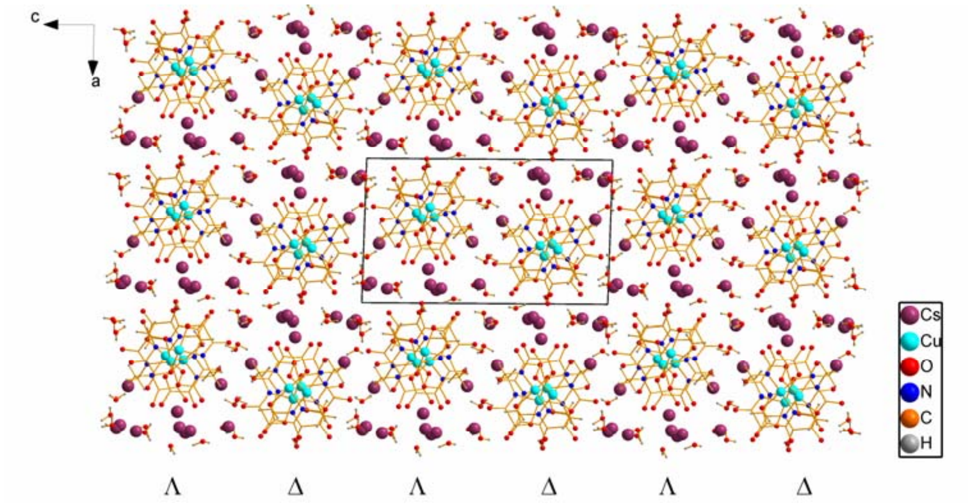

Figure 8. 2 View of crystal packing of **23** in the *ac*-plane showing the distribution of the chirality along the crystals lattice. Cs-O bonds are omitted for clarity. The diagram shows the superposition of the disorder of the caesium ions and water molecules present in the crystal structure.

The chirality of the two asymmetric units present in the unit cell is related thought the inversion centre in the middle point (½ ½ ½) of the unit cell (Figure 8.3). Because of this, the chirality of the dimers in the crystal lattice is displayed with the alternation of monochiral layers of stacks along the *c*-axis.

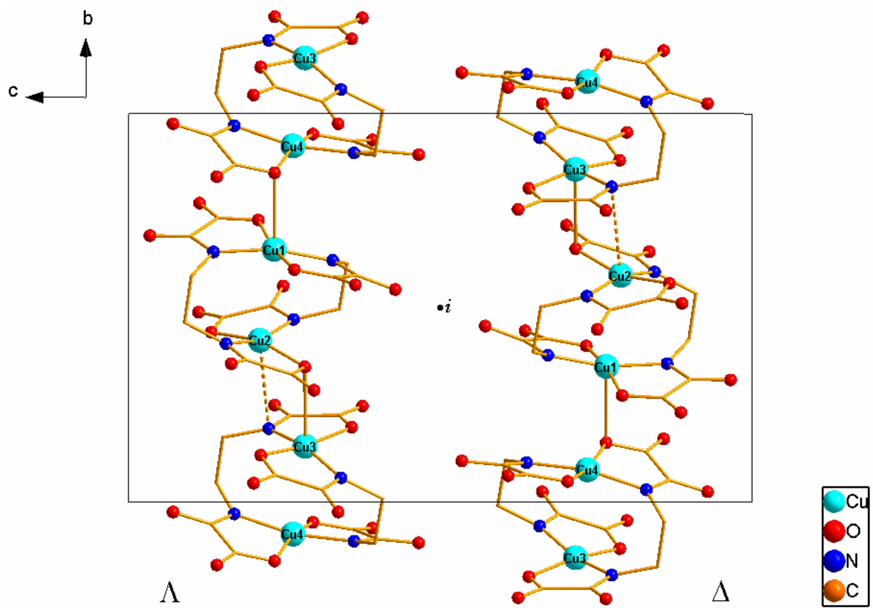

Figure 8. 3 Perspective view of the packing of the copper(II) dimers along *a*-axis direction showing the relation of the chirality within thedimers. Hydrogen atoms are omitted for clarity.

Caesium atoms are coordinated to waters molecules and carbonyl and carboxylate oxygen atoms of the ligand, having 8, 9 or 10 coordination number. In addition, the network of hydrogen bonds that involves the carbonyl and carboxylate oxygens with the

water molecules, links the stacks of $[Cu(oeo)]_2^{4-}$ complexes into a three dimensional network (Figure 8.2).

8. 3 Experimental Section

8. 3. 1 $Cs_4[Cu(oeo)]_2 \cdot 5\frac{1}{2} H_2O$ (23)

Synthesis

To a solution of **6** (0.66 g, 1.41 mmol) in water (6.4 ml), an aqueous solution (1.5 ml) of $CuCl_2 \cdot 2H_2O$ (0.12 g, 0.5 equiv, 7.04 mmol) was added. The expected fine turquoise solid, which was previously assigned to $CuH_2(oeo) \cdot nH_2O$, was formed. Then a solution of $CsOH \cdot H_2O$ (0.51 g, 2.04 equiv, 2.88 mmols) in water (1.5 ml) was added dropwise. The resulting deep blue solution was left stirring overnight at room temperature. λ_{max}, 636 nm. Slow solvent diffusion of a mixture of EtOH/MeOH (2:1) into the final solution afforded deep blue crystals of **23** suitable for X-ray analysis.

Crystallographic Data Collection and Structure Determination

X-ray diffraction data of a deep blue flat shaped single crystal of **23** was collected using a Bruker-Nonius KAPPA-CCD[1] diffractometer. The structure was solved using SIR-92[2] and refined using the SHELXL-97 package. Crystal data was collected, solved and refined by Dr Louis J. Farrugia.

The model presented by Dr Louis J. Farrugia refines all the copper sites fully occupied. Knowing the issue in the occupancies of the copper sites in the previous crystals, the occupancy in this structure was checked refining the anisotropic thermal parameters of these atoms sites freely. The refinement leads to occupancies of Cu1 96.6(3)%, Cu2 98.0(3)%, Cu3 98.4(3)% and Cu4 98.1(3)%. Because of the occupation values, which are very high, and the errors values, it is not clear if the sites are fully occupied or almost fully occupied. As a result, the model was left with all copper sites 100% filled.

The caesium atoms Cs3 and Cs7 were disordered over two sites (7:3 and 8:2 populations respectively). Because of this, the water molecule O11w/O12w was disordered over two sites with a 1:1 population.

All non-hydrogen atoms were refined anisotropically. The methylene C-H atoms were placed in calculated positions, with C-H = 0.99 Å and refined with a riding constraint and with [U_{eq}(H) = 1.2(U_{eq})C]. The initial positions of the water H atoms were determined either from Fourier difference maps, or using the procedure of Nardelli[3]. The water molecules were subsequently refined as rigid groups, with the O atom as the pivot atom of the group, and with O-H = 0.82 Å. The exceptions were the disordered water molecules on O11W/O12W, in which the H atoms were refined with a riding model. A single refined U_{eq} of 0.070(7) Å^2 was used for all the ordered water H atoms, while for the disordered water molecules [U_{eq}(H) = 1.2(U_{eq})O].

Crystal data and selected details of the refinement are listed in Table 8.1.

Table 8. 1 Crystallographic data for **23**

Empirical formula	$C_{24}H_{38}Cs_8Cu_4N_8O_{35}$
Formula weight	2316.06
Crystal system	Triclinic
Space group	$P\bar{1}$
a (Å)	11.5747(3)
b (Å)	12.2946(3)
c (Å)	19.4613(5)
α (°)	89.680(2)
β (°)	88.3720(10)
γ (°)	80.525(2)
V (Å^3)	2730.58(12)
T(K)	100(2)
ρ_{calc} (g/cm^3)	2.817
Z	2
F (000)	2148
Reflections collected	51757
Unique reflections	11932
Reflections observed [I>2σ(I)]	9216
R_{int}	0.049
Parameters refined	760
Number of retraints	0
λ (Å); Mo Kα	0.71073
μ (mm^{-1})	6.896
θ Range (°)	2.04-27.06
Goodness-of-fit (GOF) on F^2	1.057
R [I>2σ(I)]	0.0324
wR_2 (all data)	0.0823
Largest difference in peak and hole (e Å^{-3})	1.785 and -1.068
Crystal size (mm)	0.58×0.2×0.04

[a] $R_1 = \Sigma(|F_o| - |F_c|)/ \Sigma|F_o|$

[b] $wR_2 = [\Sigma w(F_o^2 - F_c^2)^2]/\Sigma w(F_o^2)^2]^{1/2}$ where $w = 1/[\sigma^2(F_o^2) + (0.2P)^2$ and $P = [F_o^2 + 2F_c^2]/3$

Selected bond lengths (Å) and angles (°) for compound **23** are given in Table 8.2 [a,b,c]. Also the dihedral angle formed by the chelating oxamato groups (°) and the distance of the atom from the mean plane (Å).

Table 8. 2 Selected bonds (Å) and angles (°) for **23**

Cu1-O11A	1.969(4)	Cu2-O16A	1.981(4)
Cu1-O21A	1.983(4)	Cu2-O26A	1.973(4)
Cu1-N11	1.915(4)	Cu2-N12	1.932(5)
Cu1-N21	1.929(4)	Cu2-N11	1.939(5)
Cu3-O31A	1.975(4)	Cu4-O36A	1.972(4)
Cu3-O46A	1.972(4)	Cu4-O41A	1.995(4)
Cu3-N31	1.946(5)	Cu4-N32	1.941(4)
Cu3-N42	1.936(5)	Cu4-N41	1.943(4)
Cu1-Cu2	3.023(9)	Cu3-Cu4	3.037(9)
Cu2-Cu3	3.605(9)	Cu1-Cu4’	3.310(8)
O11A-Cu1-N11	84.01(18)	O16A-Cu2-N12	83.74(18)
O11A-Cu1-N21	95.29(18)	O16A-Cu2-N22	101.08(17)
N11-Cu1-O21A	99.69(17)	N12-Cu2-O26A	96.24(19)
N21-Cu1-O21A	83.33(17)	N22-Cu2-O26A	83.90(19)
O31A-Cu3-N31	83.30(17)	O36A-Cu4-N32	83.74(17)
O31A-Cu3-N42	96.34(17)	O36A-Cu4-N41	95.43(18)
N31-Cu3-O46A	99.53(17)	N32-Cu4-O41A	101.52(17)
N42-Cu3-O46A	83.60(17)	N41-Cu4-O41A	82.84(17)
Dihedral angle Cu1	18.29(18)	Dihedral angle Cu2	25.34(18)
Dihedral angle Cu3	19.43(17)	Dihedral angle Cu4	21.41(17)
Atom displacement Cu1	-0.009(1)	Atom displacement Cu2	0.084(1)
O11A	0.148(4)	O16A	-0.200(4)
O21A	0.142(4)	O26A	-0.223(4)
N11	-0.252(5)	N12	0.370(5)
N21	-0.261(5)	N22	0.353(5)
Atom displacement Cu3	-0.019(1)	Atom displacement Cu4	0.070(1)
O31A	0.175(4)	O36A	-0.180(4)
O46A	0.151(4)	O41A	-0.171(4)
N31	-0.267(5)	N32	0.300(5)
N42	-0.275(5)	N41	0.318(5)

[a]Estimated standard deviations in the last significant digits are given in parenthesis. [b]The symmetry code denoted by prime is x, 1+y, z. [c]The dihedral angle for Cu1 was calculated measuring the angle between the plane formed by O21A-Cu1-N21 and O11A-Cu1-N11, for Cu2 it was calculated measuring the angle between the plane formed by O16A-Cu2-N12 and O26A-Cu2-N22; for Cu3 it was calculated measuring the angle between the plane formed by O46A-Cu3-N42 and O31A-Cu3-N31 and finally, for Cu4 it was calculated measuring the angle between the plane formed by O46A-Cu4-N42 and O31A-Cu4-N31.

[1] Nonius. *COLLECT*. Nonius B.V., **2004**, Delft, The Netherlands.
[2] A. Altomare, G. Cascarano, C. Giacovazzo and A. Guagliardi, *J. Appl. Crystallogr*. **1993**, *26*, 343
[3] Nardelli, M., *J. Appl. Cryst.,* **1999**, *32*, 563

Chapter 9: Tetrabutylammonium Compounds

9. 1 Introduction

The initial attempts of the synthesis of the copper(II) complex using ethylenediamine-1,2-dioxamate as the ligand were carried out using tetrabutylammonium hydroxide. The preparation of the complex was achieved by adding aqueous solutions of four equivalents of base and one equivalent of copper(II) salt to an aqueous suspension of **1**. ^{1}H-NMR, ^{13}C-NMR, IR and UV-Vis measurements of the deep blue oil obtained by rotator evaporation of the final solution assured the formation of the copper(II) complex **(24)**. However, due to the similar solubility properties of a copper(II) complex and the corresponding base, no pure copper(II) complex solid could be obtained. As a consequence, the base that was used was changed to alkali metal bases.

Several attempts of crystal growing of the copper(II) complex from the reaction mixture **24** were performed but with no success. The mixture was miscible with all common organic solvents and when the solvent was evaporated only an oil could be afforded. However, when the synthesis was carried out with the minimum amount of water, thus only water provided from the base and from the solution of $CuCl_2 \cdot 2H_2O$, crystals could be finally achieved by slow solvent evaporation of the reaction mixture, $(Bu_4N)_4Cu(oeoH)_2 \cdot 4H_2O$ **(25a)**.

Surprisingly, the copper(II) complex crystallises in a mononuclear entity when using tetrabutylammonium as the counterion. Instead of obtaining the expected dimeric structure like in all previous bis(oxamato) copper(II) complexes obtained, the complex is formed by a copper(II) atom and two $(Hoeo)^{3-}$ molecules. Similarly to the dimeric complexes, each ligand is chelating towards the metal through the deprotonated amide nitrogen and the carboxylate oxygen of the oxamato group in a *trans*-bis(*N,O*) arrangement around the metal ion. As a result, the ligands lay in opposite directions in the crystal packing in such a way that the other two oxamato groups remain *non*-coordinated. Therefore, although four equivalents of base are added, only the hydrolysis of the two esters is achieved as well as the deprotonation of only one of the amides. The other amides remain protonated. Probably, this is a consequence of the bulky of the $[n Bu_4N]^+$, preventing the possible interaction between neighbouring monomeric units in

the crystal lattice and also leaving the protonated amide *non*-associated. Moreover, as a result of the type of coordination where the ligand metal ratio is 1:2, unforeseen large amounts of copper oxides, copper hydroxides and coordination polymers were formed due to the excess of base and copper added to the reaction mixture.

When **25a** was obtained and analysed, to the best of our knowledge, diethyl ethylene-1,2-dioxamate was never used for the synthesis of bis(oxamato) complexes. However, sometime after the crystal was analysed and while other ethylene-1,2-dioxamato copper(II) complexes were being studied, it came published elsewhere a pseudo-polymorph of **25a**, $(Bu_4N)_4Cu(oeoH)_2$ **(25b)**.[1] The notation that was originally used for **25b** was $[n Bu_4N][Cu(endaH)_2]$. However, to be consistent with the notation used over this thesis we will name it $(Bu_4N)_4Cu(oeoH)_2$.

The synthesis methods used in the two pseudo-polymorphs are different, although both methods add four equivalents of base to the reaction mixture. Compound **25a** crystallises with two water molecules whereas **25b** crystallises with no solvent molecules. Nonetheless, the way that the complex and the counterions pack is the same in both crystal structures. This is because the mononuclear units are well isolated in the crystal lattice from the $[n Bu_4N]^+$ cations and as a result, the water molecules that are hydrogen-bonded to the ligand, do not interfere in the type of packing, resulting in a comparable crystal packing in both crystals.

9. 2 Results

Description of structure $(Bu_4N)_4Cu(oeoH)_2 \cdot 4H_2O$ (25a)

Structure of **25a** consists of discrete mononuclear entities of complex anions of the copper salt of diethyl ethylene-1,2-dioxamate and discrete $[n Bu_4N]^+$ cations. It crystallises in the space group $P\bar{1}$ containing half of the mononuclear entity, two $[n Bu_4N]^+$ cations and two water molecules in the asymmetric unit. The other half of the molecule is generated by symmetry through the inversion centre that lies in the metal atom. Mononuclear units are well isolated in the crystal lattice due to the presence of the bulky $[n Bu_4N]^+$ cations (Figure 9.1).

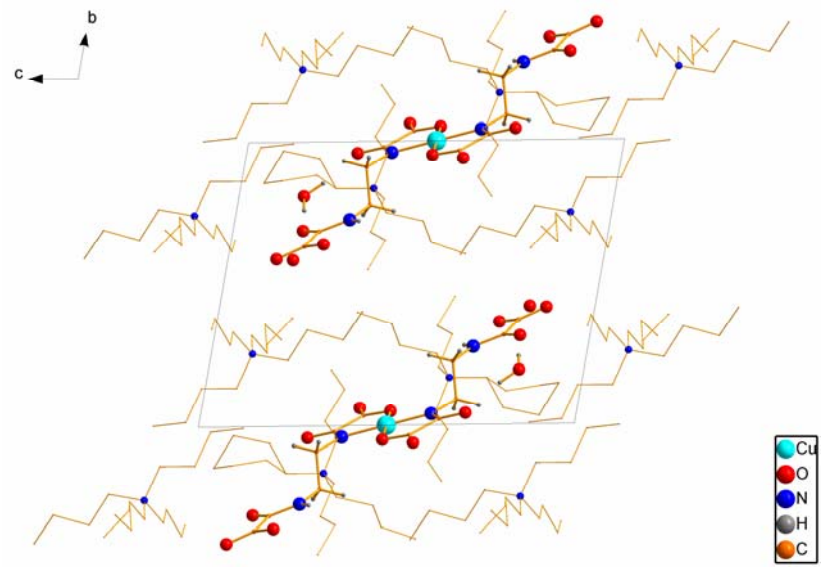

Figure 9. 1 Crystal packing view of **25a** along the *a*-axis. $[n\text{BuN}]^+$ groups are drawn using thin lines for the bonds and nitrogen atoms smaller in size compared with the nitrogen atoms of the ligand. Hydrogen atoms of the $[n\text{Bu}_4\text{N}]^+$ cations are omitted for clarity. The diagram shows the superposition of the disorder in the $[n\text{Bu}_4\text{N}]^+$ cations.

The mononuclear anion is built with one copper atom and two trideprotonated ligand molecules, $(\text{Hoeo})^{3-}$, resulting in a $\eta^2(\kappa N{:}\kappa O)$ coordination. The copper atom, which lies on a 1*f* Wyckoff site, is coordinated to two deprotonated amido nitrogens and two carboxylate oxygens of two oxamato groups from two different $(\text{Hoeo})^{3-}$ molecules leading to a non-distorted square-planar geometry. The copper environment can be considered planar as the standard deviations from the Cu, N1, O1, N1, O1' mean plane are below 0.0041Å (Figure 9.2).

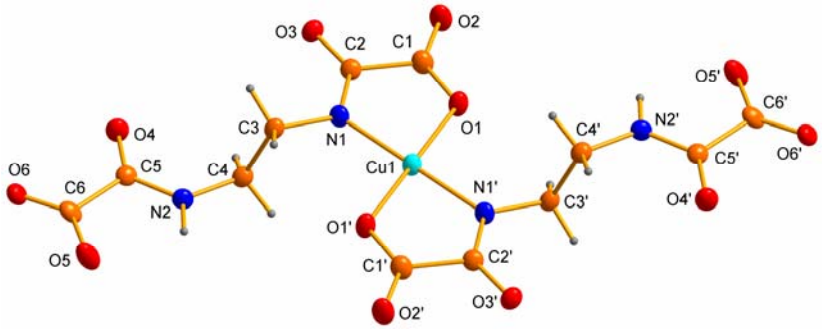

Figure 9. 2 Diamond-plot (50% of probability level) of the molecular structure of **25a** with atom numbering scheme. Prime denotes symmetry operation 1-x, -y, 1-z.

The same as in compound **25b**, the ethylenediamine fragment of the $(\text{Hoeo})^{3-}$ ligand displays an anti conformation. However, the coordinated and the *non*-coordinated oxamato groups in each ligand molecule display different orientations. In **25b** they are close to be perpendicular, while in compound **25a** they are almost parallel (Figure 9.3).

The dihedral angle formed by the planes of the coordinated and *non*-coordinated oxamato groups of the $(Hoeo)^{3-}$ ligand, taking into account all the atoms that form it, is $75.583(84)^{o}$ for the former and $3.739(94)^{o}$ for the later. The anti conformation of the ethylenediamine fragment has been also observed in structures **1**, **2a**, **4a, 7c** and **8a** in which the two oxamato groups of the ligand are also close to be parallel, except in **8a** where, like in **25b**, are close to be parallel.

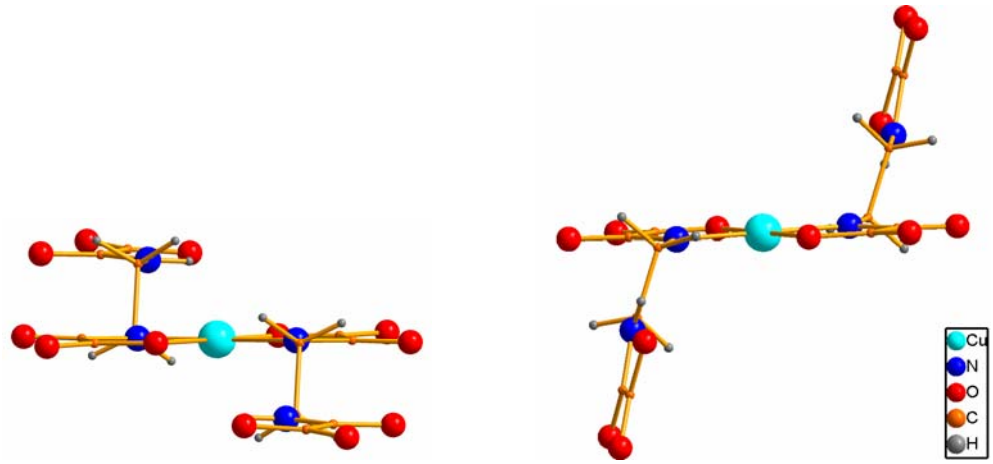

a **b**

Figure 9. 3 Perspective view of the $(Bu_4N)_4Cu(oeoH)_2$complexes showing the parallel **(a)** and perpendicular **(b)** orientation of the two oxamato groups in **25a** and **25b**, respectively.

Furthermore, **25a** crystallises with four water molecules which form hydrogen bonds with $[Cu(oeoH)_2]^{4-}$ anions, whereas **25b** crystallises with no solvent molecules. Water molecule Ow1 has two directional hydrogen bonds to the two amide carbonyl oxygen atoms of the same ligand, leading to a second order $R_2^2(11)$ motif (Figure 9.3).[2] Probably, these hydrogen bonds stabilize the anti conformation of the ethylenediamine fragment with the two oxamato groups parallel between them. This is the only crystal structure containing the diethyl ethylene-1,2-dioxamate ligand that has been observed with this hydrogen bond motif. Hydrogen atoms of Ow2 have not been found although a hydrogen bond between the molecule and the ionic carboxylato oxygen is consistent with the bond distance between atoms.

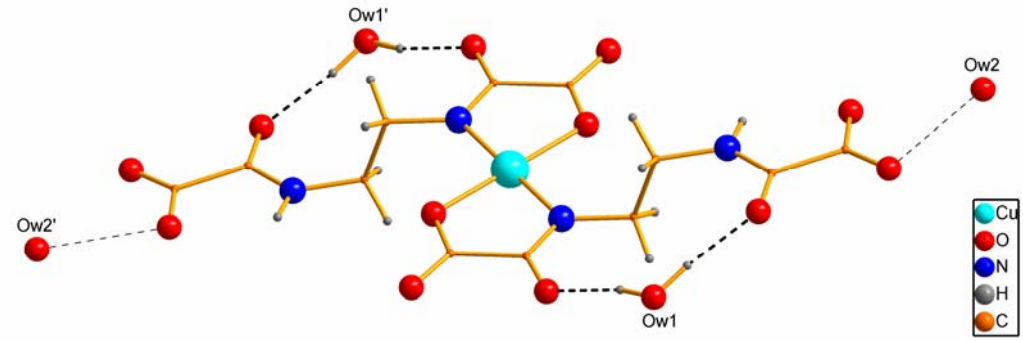

Figure 9. 4 Representation of the hydrogen bonds (dashed lines) between ligand molecule and water molecules. Thin dashed lines represent the probable hydrogen bond between Ow2 and the ligand.

The formation of the classical hydrogen bonds between two oxamato groups of two different ligands, involving the hydrogen of the protonated amide and the carboxylate oxygen, has not been observed. This pattern has been noted in all crystal structures of the salts of ethylene-1,2-diamine, **2a**, **4a, 7c** and **8a**. Probably, this is a consequence of the presence of the bulky $[n\text{Bu}_4\text{N}]^+$ cations in the crystal lattice. Moreover, it has been noted that there is not even hydrogen bond between the protonated amide and a oxygen atom, such as a acarbonyl oxygen from a neighbouring ligands or a water molecule as seen in **7c**. Also, it is probable to be a consequence of the large size of the counterions. This leads to the hydrogen amide atom that is not hydrogen-bonded. This feature can be observed in the IR spectrum of the crystal. In the 3000-3500 cm^{-1} region, there are four differentiated bands at 3487, 3396 and 3383, and 3287 cm^{-1} (See Appendix A1). The first band could be the associated O-H stretching, while the next two might be the two free N-H stretching of the ligand and the last band another O-H stretching.

9. 3 Experimental Section

9. 3. 1 $(n\text{Bu}_4\text{N})_4\text{Cu(oeoH)}_2\cdot n\text{H}_2\text{O}$ (24)

Synthesis

To a stirring mixture of **1** (2.60 g, 1.00 mmols) in water (10 ml) at room temperature, a solution of Bu_4NOH (26.2 ml, 40.0 mmols, 4.0 equiv, 40% w/w in water) was added. The mixture was stirred for two hours and then an aqueous solution (2.5 ml) of $\text{CuCl}_2\cdot 2\text{H}_2\text{O}$ (1.70 g, 1.00 mmols, 1 equiv) was added dropwise. The deep blue solution was left stirring overnight and the dark brown solid that was formed was filtered. Some amount of solution was then taken and rotaevaporated until getting the oil that was

analysed **(24)**. ^{1}H-NMR (400 MHz, $CDCl_3$, δ in ppm): 2.71 (s, $^{+}NCH_2$), 1.77 (s, $CH_2(NH)$), 1.06 ($CH_2CH_2CH_2$), 0.83 (CH_2CH_3), 039 (CH_3). ^{13}C-NMR (400 MHz, $CDCl_3$, δ in ppm): 165.31 (*CO*-O), 163.35 (*CO*-NH), 53.32 (CH_2-NH), 38.34 ($^{+}NCH_2$), 28.71 ($CH_2CH_2CH_2$), 20.17 (CH_2CH_3), 13.57 (CH_3). λ_{max}, 629 nm. The oil also contained a co-product with the $[n\text{Bu}_4\text{N}]^+$ as the counterion. It resulted in broad peaks in the ^{1}H-NMR and some residual peaks in the ^{13}C-NMR which were assigned to a second set of $[\text{Bu4N}]^+$. ^{13}C-NMR (400 MHz, $CDCl_3$, δ in ppm): 58.06 (CH_2-NH), 23.41 ($CH_2CH_2CH_2$), 19.11 (CH_2CH_3), 13.13 (CH_3). IR (ATR, cm^{-1}): ν 3395 (w), 2960-2874(w), 1656 (w), 1637 (w), 1486 (s), 1380 (s).

9. 3. 2 $(n\text{Bu}_4\text{N})_4\text{Cu(oeoH)}_2\cdot 4\text{H}_2\text{O}$ (25a)

Synthesis

A solution of $(n\text{Bu}_4\text{N})\text{OH}$ (11 ml, 16.8 mmols, 4.4 equiv, 40% w/w in water) was added to **1** (1.00 g, 3.84 mmols) at room temperature. The mixture was stirred until the white solid was dissolved and then 1.9 ml of an aqueous solution (2 ml) of $CuCl_2\cdot 2H_2O$ (0.64 g, 3.64 mmols) were added dropwise. The deep blue solution was left stirring overnight and then filtered to eliminate the green solid that formed. Slow solvent evaporation of the reaction mixture gave deep blue crystals suitable for X-ray analysis **(25a)**. IR (ATR, cm^{-1}): ν 3484(w), 3396(w), 3382 (w), 3287 (w), 2959-2872 (s), 1688 (s), 1667 (s), 1644 (s), 1600 (s), 1490(w), 1287 (s) (See Appendix A1) .

Crystallographic Data Collection and Structure Determination

Structure **25a** was solved using SIR-92[3] and refined by full-matrix least-squares on F^2 with SHELXL-97 package.

Some of the carbon atoms of two $[n\text{Bu}_4\text{N}]^+$ cations were disordered. Each of the two $[n\text{Bu}_4\text{N}]^+$ cation of the asymmetric unit has a group of two carbons where each atom is disordered over two sites, C21/C22 and C24/C25. Each group was initially refined with isotropic thermal parameters and mutually exclusive free occupancies for each pair of carbon atoms leading to occupancies of 73.3(1)% for the pair C21/C22 and 60.0(1)% for the pair C24/C25. Finally, they were refined isotropically with the occupancies of

the two disordered parts of each group fixed to 0.73/0.27 for C21/C22 and 0.57/0.43 for C24/C25.

All non-hydrogen atoms were refined anisotropically, except the carbon atoms implied in the disorder which were constrained to be equal for like atoms, including the neighbouring atom, C26. Within the $[n\mathrm{Bu_4N}]^+$ cations, in all non-disordered atoms, corresponding pairs of chemically equivalents bond lengths were restrained to be equal. Also, all bonds for non-disordered atoms were refined subject to a 'rigid bond' restraint for each $[n\mathrm{Bu_4N}]^+$ cation.

Hydrogen atoms of the ligand and the $[n\mathrm{Bu_4N}]^+$ cations were placed in calculated positions and refined with fixed individual displacement parameters [$U_{iso}(H) = 1.2U_{eq}(C)$ and $U_{iso}(H) = 1.2U_{eq}(N_{amide})$]. Hydrogen atoms of the water molecule Ow1 were located on a difference Fourier map and refined with three restraints (O-H and H···H distances) with thermal parameters [$U_{iso}(H) = 1.2U_{eq}(Ow)$]. Hydrogen atoms for Ow2 and the disordered carbon atoms, including C26, were neither found nor calculated.

Crystal data and selected details of the refinement are listed in Table 9.1.

Table 9. 1 Crystallographic data for **25a**

Empirical formula	$C_{38}H_{67}Cu_{0.50}N_4O_8$
Formula weight	739.73
Crystal system	Triclinic
Space group	$P\bar{1}$
a (Å)	12.587(5)
b (Å)	12.716(5)
c (Å)	15.088(5)
α (°)	99.455(5)
β (°)	90.628(5)
γ (°)	114.073(5)
V (Å^3)	2166.8(14)
T(K)	100(2)
ρ_{calc} (g/cm^3)	1.134
Z	2
F (000)	803
Reflections collected	15451
Unique reflections	4690
Reflections observed [I>2σ(I)]	3766
R_{int}	0.0374
Parameters refined	450
Number of retraints	79
λ (Å); Mo Kα	0.71073
μ (mm^{-1})	0.314
θ Range (°)	1.37-21.10
Goodness-of-fit (GOF) on F^2	1.055
R [I>2σ(I)]	0.0683
wR_2 (all data)	0.1989
Largest difference in peak and hole (e Å^{-3})	1.078 and -0.541
Crystal size (mm)	0.1×0.1×0.1
Crystal morphology	blue platty shaped

[a] $R_1 = \Sigma(|F_o| - |F_c|)/ \Sigma|F_o|$

[b] $wR_2 = [\Sigma w(F_o^2 - F_c^2)^2]/\Sigma w(F_o^2)^2]^{1/2}$ where $w = 1/[\sigma^2(F_o^2) + (0.2P)^2$ and $P = [F_o^2 + 2F_c^2]/3$

Selected bond lengths (Å) and angles (°) for Compound **25a** are given in Table 9.2 [a,b]. Also the dihedral angle formed by the chelating oxamato groups (°) and the distance of the atom from the mean plane (Å).

Table 9. 2 Selected bonds (Å) and angles (°) for **25a**

Cu1-O1	1.963(3)	Cu2-N1	1.922(4)
O1-Cu1-N1	84.35(15)	O1-Cu-N1’	95.65(15)

[a] Estimated standard deviations in the last significant digits are given in parenthesis.

[b] The symmetry code denoted by prime is 1-x, -y, 1-z.

[1] T. Rüffer, B. Bräuer, B. Walfort, *Inorg. Chem. Commun.,* **2006**, *9*, 1111

[2] M. C. Etter, J. C. MacDonald. *Acta Cryst*. **1990**, *B46*, 256

[3] A. Altomare, G. Cascarano, C. Giacovazzo and A. Guagliardi, J. Appl. Crystallogr. 1993, 26, 343-350

Chapter 10: Bimetallic and Cobalt Compounds

10. 1 Introduction and results

Preparation of bimetallic compounds have been carried out using either the mononuclear copper(II) complex, $[Cu(H_2oeo)_2]^{4-}$, or the copper(II) dimeric complex, $[Cu(oeo)]_2^{4-}$, as starting materials (Figure 10.1). Both building blocks are flexidentate systems with several potential coordinating chelating units and the addition of $CoCl_2 \cdot 6H_2O$ may give rise to the formation of cobalt/copper bimetallic bis(oxamato) complexes.

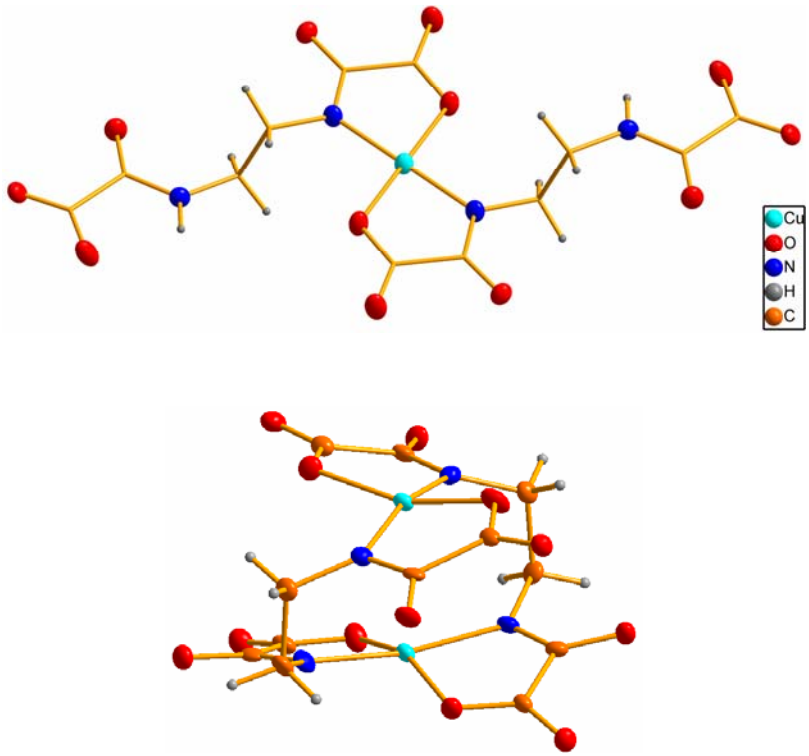

Figure 10. 1 View of $[CuH_2(oeo)_2]^{4-}$ complex (top) and $[Cu(oeo)]_2^{4-}$ complex (bottom).

The procedure was to bring together the copper complex and a second transition metal by adding a solution of a transition metal salt into the copper(II) complex solution or by using slow diffusion of both solutes through a solvent. The transition metal that was chosen was cobalt(II) since it can form interesting magnetic materials with copper(II).

10. 1. 1 $Co_x(Hoeo)_2{\cdot}(H2O)_yCl_z$

Slow addition of a concentrated solution of $CoCl_2{\cdot}6H_2O$ into an aqueous reaction mixture of $[n Bu_4N]_4Cu(H_2oeo)_2$ was performed giving rise to the rapid formation of a fine pink solid **(26)**. Microanalysis and IR measurements of **26** reveal the presence of the ligand. The classical features assigned to the $(oeo)^{4-}$ ligand were observed in the IR spectrum (See Appendix A1), and the elemental analysis reveals a C, 18.48; H, 3.03; N, 6.99; Cl, 4.26% composition of the sample where the C/N ratio is equal to 2.6. The C/N ratio in the $(oeo)^{4-}$ ligand, of which composition is $(C_6H_4O_6N_2)^4$, is equal to 3.0 and thus, the presence of the ligand and its no decomposition is consistent with these results. In addition, the C/Cl and N/Cl ratios are 4.0 and 1.6, respectively, when the ligand/Cl ratio is 1:1. These are comparable with the ratios in the elemental analysis which are 4.3 and 1.6, respectively. In addition, EDX analysis reveals the presence of the ligand, chlorine and cobalt, but no copper. Consequently, the results suggest a $Co_x(H_yoeo)Cl(H_2O)_z$ composition for **26** in which the transmetallation reaction has occurred. However, at the present, the precise composition of **26** cannot be determined. Lastly, the PXRD pattern of **26** shows a crystalline phase (See Appendix A6). Although having a crystalline pattern with well defined peaks, we were unable to index the cell. SEM investigation shows the small size of the particles (≈ 30 μm) formed.

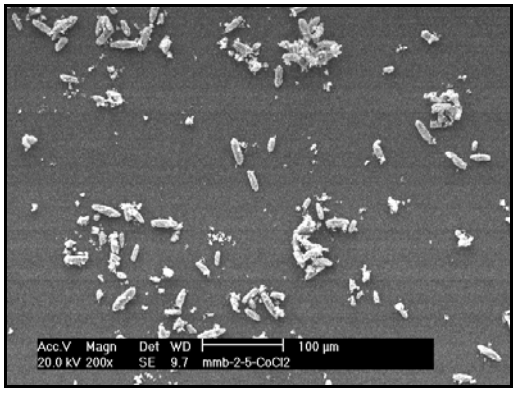

Figure 10. 2 SEM images of **26** showing the size of the particles (≈ 30 μm).

Therefore, the addition of large amounts of cobalt to a $[n Bu_4N]_4Cu(H_2oeo)_2$ solution leads to the precipitation of a crystalline cobalt(II) salt of ethylene-1,2-dioxamate, which contains chlorine with some possible water molecules. However, the solid is very insoluble and it precipitates immediately, leading to the formation of very small particles. Magnetic behaviour of **26** was studied suggesting antiferromagnetic interactions with ferrimagnetic ordering. Field Cooled Magnetisation (FCM) shows a

field dependence of the magnetic susceptibility below 10K. Also, magnetism showed some unusual slow relaxation features. However, since the composition of the solid is unknown, the magnetic data could not be modelled.

Due to the high insolubility of the solid when adding cobalt to a $(Bu_4N)_4CuH_2(oeo)_2$ solution, we tried to grow crystals of **26** using a slow solute diffusion technique with H-shaped tubes. This technique has been proved to be an effective method for growing crystals of insoluble polymetallic complexes, like bis(oxamide) polymetallic complexes. A solution of the metal building block is placed in one arm of the tube and in the other arm a solution of a transition metal salt and afterwards the tube is filled with solvent. Then, by slow diffusion of both solutes through the tube, the two reactant solutions come in contact in the middle of the tube at very low rates and concentrations where the crystals can grow. Our copper(II) complex solution is only stable at basic pH and thus a basic pH is needed in the H-shaped tube. However, although cobalt(II) salts decompose in solution to form cobalt hydroxide, this method was attempted using basic conditions as well as neutral conditions.

A deep blue concentrated solution of copper(II) complex and a concentrated solution of the cobalt salt, $CoCl_2 \cdot 6H_2O$, were placed in each side of the tube filling it carefully with an aqueous solution and allowing the solutes to diffuse for several weeks. The copper(II) complex solution that was used was either a $(Bu_4N)_4CuH_2(oeo)_2$ solution or a $Li_4[Cu(oeo)]_2$ solution and when the reaction was carried out under basic conditions, the copper complex side of the tube was filled with an aqueous solution of the corresponding base while the cobalt side of the tube was filled with water. The mixtures ended up with the decomposition of the solutes although a light pink solid was always formed in the middle arm. Also, some hedgehogs of microcrystals were afforded but they were too small to study them by X-ray diffraction analysis **(27)**. IR spectrum of **27** is consistent with the formation **26**. IR (ATR, cm^{-1}): ν 3546(w), 3447 (w), 3246 (w), 3165 (w), 3088(s) 2895(w), 1669 (w), 1622 (w), 1558(s), 1511 (s), 1471 (s), 1369 (s), 1317(s), 1249 (s), 1219 (s).

10. 1. 2 Bimetallic compounds, $Co[CuH_{1.98}(oeo)]\cdot DMSO$ (28) and $Co_xCu_y(oeo)(DMSO)(H_2O)_3$ (29)

From the same reaction mixture and the same batch of which crystals of **8** where obtained, a crystal with the same morphology and the essentially same crystal structure as **8** was analysed by X-ray diffraction, $Co[CuH_{1.98}(oeo)]\cdot DMSO$ **(28)**. During the last circles of the refinement of the crystal structure, we noted that some electron density between two oxamato groups of two neighbouring dimers was left. This electron density is placed in a *2d* Wyckoff site and lies in middle point of a cyclic $R_2^2(10)$ hydrogen-bonding motif. Due to the presence of copper(II) in the reaction mixture and the environment around the site, this suggested the presence of some copper(II) as a result of the deprotonation of the amide nitrogens. Consequently, a copper(II) atom was placed in the site and refined with a free occupancy leading to 1.9(2)% of copper(II) occupancy and a $Co[CuH_{1.98}(oeo)]\cdot DMSO$ composition (Figure 10.3).

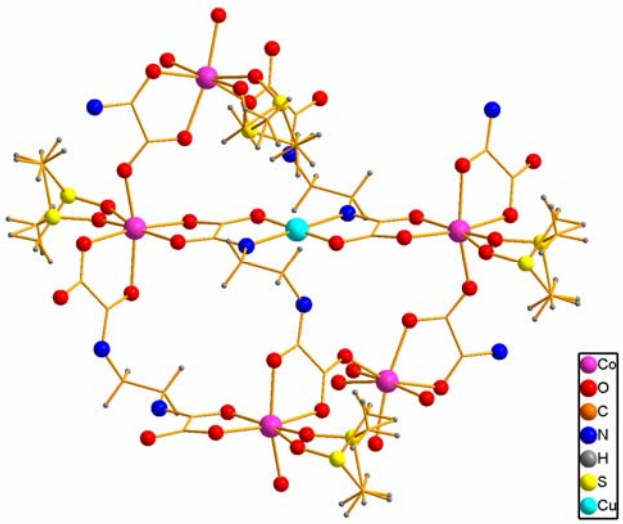

Figure 10. 3 View of the CoH2(oeo) with the superposition of the disorder in the DMSO molecule showing the presence of the copper(II) in the cobalt(II) complex.

This model afforded better refinement parameters (*R, wR_2 and S*) and a better difference Fourier electron density map of the region around the hypothetic copper site (Figure 10.4), suggesting that a polynuclear cobalt(II)-copper(II) bis(oxamato) complex is feasible. However, due to the low amount of copper(II) present in the site and the low quality of the crystallographic data, these results are not conclusive.

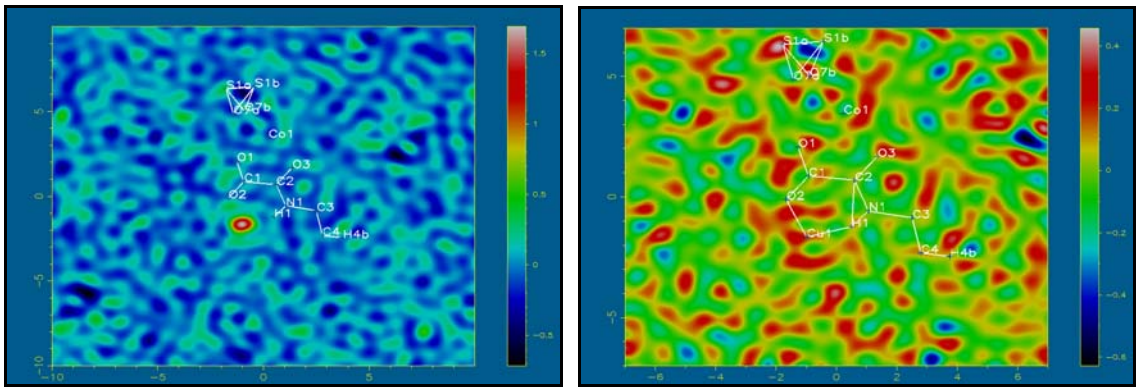

Figure 10. 4 Slant plane difference Fourier electron density contour map of the plane containing N1Cu1O3 atoms in **28** (electron density units in $e^-/Å$). On the map on the right it can be noted some positive density charge present in the hypothetical copper(II) site. On the map on the left, the copper(II) site has been filled with a free occupancy suggesting the presence of the metal in the site.

Moreover, several weeks after the reaction mixture was prepared, a purple solid precipitated from the mixture and it was filtered and dried in air **(29)**. The colour of the solid suggested that a bimetallic compound was formed since the copper(II) complex are blue and the cobalt salts of the ligand are pink. The PXRD pattern shows a crystalline phase (See Appendix A6), and the IR measurements as well as elemental analysis, evidences the presence of the ligand in the sample.

Elemental analysis reveals a C, 23.65; H, 3.86; N, 6.83; S, 7.54% composition with no chlorine in it, showing the presence of the ligand and DMSO molecules. The ligand/DMSO ratio in **29** is 1:1 since the C/S ratio in the ligand and in the elemental analysis are comparable (3.0 and 3.1, respectively). It is also confirmed by the C/N ratio which is equal to 3.4 when ligand/DMSO = 1, and which is equal to 3.5 in the analysis. Based on this, we can guess that the amount of water molecules per DMSO and ligand molecules is three. However, the proportion of cobalt and copper remains unknown leading to a composition of $Co_xCu_y(oeo)(DMSO)(H_2O)_3$ for **29**. On the other hand, neither the simulation of the diffractogram of **8** nor the IR spectrum, are comparable with **29** also suggesting the formation of a new compound. However, we were unable to index the pattern is responsible for not being able to solve the crystallographic data of the compound.

Getting back to the previously mentioned preparation of **26**, the addition of $CoCl_2{\cdot}6H_2O$ into the reaction mixture of $(Bu_4N)_4CuH_2(oeo)_2$ gave rise to the formation of a fine pink solid which probably was the cobalt(II) salt of ethylene-1,2-dioxamate. On the other

hand, we have seen that it seems feasible the preparation of bimetallic compounds of the ligand. As a consequence, the evolution of the synthesis of the cobalt(II) salt was studied by adding a range of different concentrations of aqueous solutions of $CoCl_2 \cdot 6H_2O$ into several portions of a $(Bu_4N)_4CuH_2(oeo)_2$ reaction mixture. An approximation of the concentration of the copper(II) complex solution was calculated by knowing that the limitant reagent is the copper(II) and that the final volume of the solution is 23 ml. Assuming that the yield of the reaction is 100% and no quantity was lost in the filtration process, the approximate concentration copper(II) complex is 0.23 M. Also, we know that $(Bu_4N)_4CuH_2(oeo)_2$ has a maximum number of six potential coordinating sites. So if we take 5 ml of the final reaction mixture we would need 0.28 g of $CoCl_2 \cdot 6H_2O$ to add equimolar amounts to the copper(II) complex. However, since probably the reaction has not a 100% yield and some copper(II) complex is lost in the filtration, we add 90% of the cobalt(II) needed. From here, we will double the amounts of cobalt added to the different reaction mixtures until six equivalents of cobalt(II) are added into the $(Bu_4N)_4CuH_2(oeo)_2$.

In all mixtures a solid precipitated after the addition of $CoCl_2 \cdot 6H_2O$. However, the appearance and the structure of the solids evolved from a blue-grey solid, through purple until light pink. The analysis of the solid formed when adding 1.80 equivalents of $CoCl_2 \cdot 6H_2O$ **(30)** was carried out. EDX analysis showed that it contains both transition metals, cobalt and copper, as well as chlorine and the ligand. It also suggested that the Co:Cu ratio is 2:1. In addition, the electronic spectrum of **30** dispersed in a KBr disk at room temperature evidenced the presence of both transition metals. The band at approximately 530 nm was assigned to a $^4T_1 \rightarrow {}^4T_2$ transition of the cobalt(II) with an octahedral environment. The typical band observed in the copper(II) complexes at around 630nm was also observed. The PXRD pattern shows a crystalline phase of the compound and the IR spectrum is comparable with the spectrum obtained for **29** (See Appendix A1). Magnetic measurements of **30** suggested that it has Spin Glass like behaviour. A spin glass is a disordered and frustrated system in which a set of randomly interacting magnetic moments, which are placed in random positions in a lattice, interact with neighbouring magnetic moments that are separated by a random distance. This type of magnetism is consistent with the type of compounds that we have since different amounts of copper(II) are present in the compounds. Also, if the cobalt(II) is present in **30** it leads to random interacting magnetic moments in the lattice. Again,

since the exact composition of the compounds is unknown, the magnetic behaviour could not be modelled. Finally, the evolution of the addition of $CoCl_2 \cdot 6H_2O$ into the reaction mixture leaded to the formation of a pink solid of which analyses, IR and PXRD measurements, are consistent with the formation of **26**.

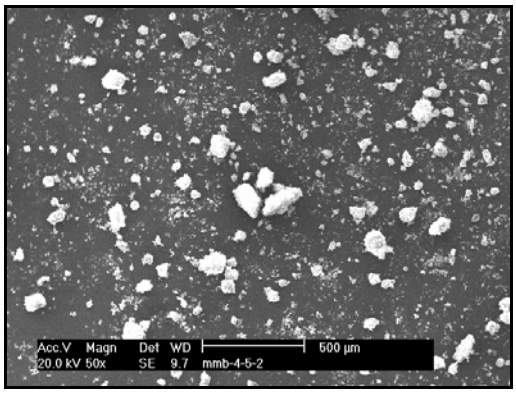

Figure 10. 5 SEM images of **30**.

10. 1. 3 Bimetallic compounds using $[Cu(oeo)]_2^{4-}$ as building blocks

The preparation of bimetallic compounds using the copper(II) dimeric complex, $[Cu(oeo)]_2^{4-}$, as starting material have not been successful. As in the $(Bu_4N)_4CuH_2(oeo)_2$ synthesis, the two methods that have been used are slow solute diffusion using H-shaped tubes, which has been reported previously (See 10.1.1), and the addition of cobalt(II) salts into the $[Cu(oeo)]_2^{4-}$ reaction mixtures. However, all solids that were obtained showed an amorphous phase in the PXDR pattern.

The attempt of crystal growing by slow solvent diffusion in a test tube was performed. $Li_4[Cu(oeo)]_2$ solution was placed at the bottom of the tube which was separated from an aqueous solution of $CoCl_2 \cdot 6H_2O$ through a dichloromethane layer and the two solutions were allowed to diffuse through the organic layer for several weeks. However, only a pink solid and the decomposition of the copper(II) solution was obtained.

In the Chapter 1, we talk about the idea of obtaining bimetallic compounds using $[Cu(oeo)]_2^{4-}$ as the building block to form two-dimensional networks through the coordination of the transition metal in the chelating oxamato sites of the dimer (Figure 10.6). The dimer has four potential chelating sites and four positive charges (Figure 1.1, bottom). The transition metal that is added is Co(II) and thus only two Co(II) atoms will be needed to balance the charges. However, the ion can be placed in four sites.

Therefore, when the cobalt(II) was added, the ions are probably placed at the first oxamato group that is found instead of being placed in the lower energy site. Then, from the first site, the bimetallic compound randomly grew to form the amorphous solids that have been obtained. Consequently, the kinetical form was formed instead of the thermodinamical form.

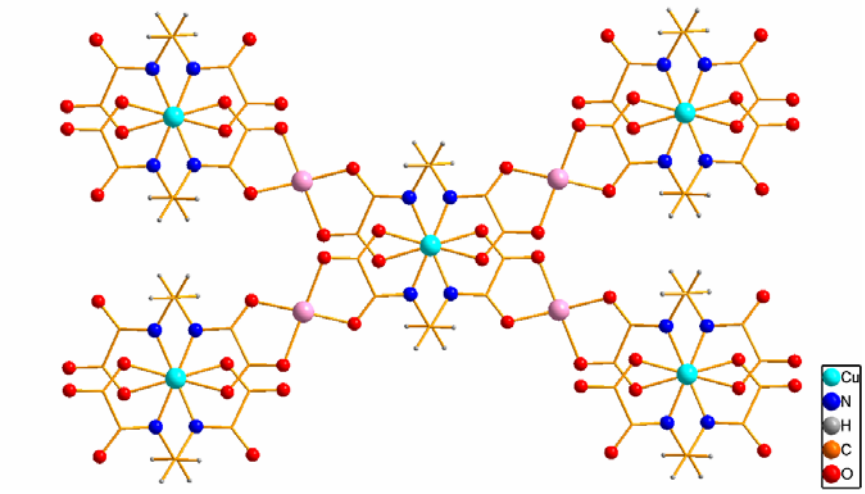

Figure 10. 6 Perspective view of the interaction between $[Cu(oeo)]_2^{4-}$ dimers through the transition metal ions, which are coloured in pink.

Alternatively, when alkali metals, like lithium, were used, the four positive charges that are needed to balance the charges are placed in the four chelating groups of the dimer giving rise to the formation of crystals with a two-dimentional network. However, dimers built using a monovalent metals with the possibility of a square-planar environment could give rise to a bimetallic two-dimentional network with magnetic interesting behaviour. Also, the addition of another ligand to coordinate the cobalt(II) and valance the extra positive charges that are left when four metals are coordinating the dimer, seems also possible.

10. 2 Experimental Section

10. 2. 1 $Co_x(H_yoeo)_2Cl(H_2O)_z$ (26)

Synthesis

To a suspension of $Et_2H_2(oeo)$ (2.61 g, 10.0 mmol) in water (10 ml) was added dropwise a 40% aqueous solution (26.2 ml) of tetrabutylammonium hydroxide (40.0 mmols) and stirred at room temperature for 2 hr. An aqueous solution of $CuCl_2{\cdot}2H_2O$

(1.70 g, 9.6 mmol) dissolved with the minimum amount of water was added and the mixture was stirred for another hour. The resulting deep blue solution was filtered to eliminate the solid precipitated. A very concentrated aqueous solution (15 ml) of $CoCl_2 \cdot 6H_2O$ was added under stirring to 10 ml of the previous final solution. The fine insoluble pink solid that formed was filtered off, washed with water and dried in air **(26)** (See Appendix A6 for PXRD pattern). Elemental analysis: C, 18.48; H, 3.03; N, 6.99%. IR (KBr, cm^{-1}): ν 3546 (w), 3447(w), 3247(w), 3165 (w), 3088 (w) 2979-2850 (m), 1669 (w), 1622 (w), 1558(s), 1510 (s), 1471 (s), 1369(s), 1317(s), 1249 (s), 1219 (s) (See Appendix A1).

10. 2. 2 $Co[CuH_{1.98}(oeo)] \cdot DMSO$ (28) and $Co_xCu_y(oeo)(DMSO)(H_2O)_3$ (29)

Synthesis

To a suspention of $Et_2H_2(oeo)$ (2.60 g, 9.99 mmols) in water (10 ml) was added dropwise a 40% aqueous solution (26.2 ml) of tetrabutylammonium hydroxide (40.0 mmols). The resulting mixture was stirred at room temperature for 1 hr and then an aqueous solution of $CuCl_2 \cdot 2H_2O$ (1.30 g, 7.40 mmols) dissolved with the minimum amount of water was added. The deep blue solution was left stirring overnight and then it was filtered to eliminate the solid that formed. 3ml of the final solution were added dropwise to a stirring solution of $CoCl_2 \cdot 6H_2O$ (1.00 g, 4.11 mmols) in DMSO (4 ml) and the mixture was stirred overnight. Slow solvent diffusion of ethanol into the final solution gave small purple crystals of **28** suitable for X-ray analysis. After several weeks, a purple solid was formed and it was collected by filtration and dried in air **(29)** (See Appendix A6 for PXRD pattern). IR (ATR, cm^{-1}): ν 3319 (w), 3235 (w), 3133 (w), 3080 (w), 2950 (w), 1625 (s), 1995 (s), 1547(s), 1447 (s), 1437 (s), 1357(s), 1335 (s), 1270 (s), 1234(s) (See Appendix A1).

Crystallographic Data Collection and Structure Determination

The same refinement that was as applied to **8** was applied to **28**, except that the copper(II) occupancy was refined free using isotropic thermal parameters.

Crystal data and selected details of the refinement are listed in Table 10.1.

Table 10. 1 Crystallographic data for **28**

Empirical formula	$C_8H_{11.98}CoCu_{0.02}N_2O_7S$
Formula weight	340.44
Crystal system	monoclinic
Space group	$P2_1/n$
a (Å)	7.5752(14)
b (Å)	9.3294(17)
c (Å)	17.9508(31)
α (°)	90.00
β (°)	96.193(10)
γ (°)	90.00
V (Å^3)	1261.2(4)
T(K)	100(2)
ρ_{calc} (g/cm^3)	1.793
Z	4
F (000)	694
Reflections collected	9130
Unique reflections	1593
Reflections observed [I>2σ(I)]	1131
R_{int}	0.0793
Parameters refined	187
Number of restraints	5
λ (Å); Mo Kα	0.71073
μ (mm^{-1})	1.590
θ Range (°)	2.28-22.96
Goodness-of-fit (GOF) on F^2	1.047
[a]R_1 [I>2σ(I)]	0.0445
[b]wR_2 (all data)	0.1082
Largest difference in peak and hole (e Å^{-3})	0.44 and -0.52
Crystal size	0.05×0.05×0.05
Crystal morphology	pink

[a]$R_1 = \Sigma(|F_o| - |F_c|)/ \Sigma|F_o|$
[b]$wR_2 = [\Sigma w(F_o^2 - F_c^2)^2]/\Sigma w(F_o^2)^2]^{1/2}$ where $w = 1/[\sigma^2(F_o^2) + (0.2P)^2$ and $P = [F_o^2 + 2F_c^2]/3$

10. 2. 3 $Co_x(H_yoeo)_2Cl_w(H_2O)_z$ (30)

Synthesis

To a stirring mixture of **1** (2.60 g, 10.0 mmols) in water (10 ml) at room temperature, a solution of Bu_4NOH (26.2 ml, 40.0 mmols, 4.0 equiv, 40% w/w in water) was added. The mixture was stirred for two hours and then an aqueous solution (2.5 ml) of $CuCl_2{\cdot}2H_2O$ (1.30 g, 7.40 mmols, 0.75 equiv) was added dropwise. The deep blue

solution was left stirring overnight and then filtered by gravity. Then, to 5 ml of the reaction mixture, an aqueous solution (2 ml) of $CoCl_2 \cdot 6H_2O$ (0.50 g, 2.06 mmols) was added dropwise. The reaction mixture was left stirring overnight and the purple solid that formed was filtered and dried in air **(30)**. IR (ATR, cm^{-1}): ν 3257 (w), 3086(w), 2941 (w), 2868 (w), 1602 (w), 1557(w), 1442 (s), 1358(s), 1329(s), 1242(s) (See Appendix A1). λ_{max} (dispersed in a KBr disc, nm) ~533, ~ 630.

Chapter 11: Conclusions and Outlook

11. 1 Synthesis of the building block

The standardised synthesis method of the mononuclear bis(oxamato) transition metal complexes is the treatment of the ester of the ligand, diethyl *N*,*N*-bis(oxamates), with four equivalents of base followed with the addition of a transition metal salt to the reaction mixture.[1] The colour change in the reaction solution indicates the formation of the metal complex.

This one-step reaction was the initial synthesis method that was performed to prepare the metal containing building block using diethyl ethylene-1,2-dioxamate, Et_2H_2(oeo), as the ligand precursor and copper(II) as the transition metal ion. Tetrabutylammonium hydroxide was initially chosen as the base. Thus, to an aqueous mixture of diethyl ethylene-1,2-dioxamate four equivalents of base were added. Then, the reaction mixture was heated in a water bath until the total dissolution of the solid and afterwards, an aqueous solution of copper(II) was added when the mixture was cooled to room temperature. A beautifully deep blue coloured solution indicated the formation of the copper(II) complex. NMR measurements of the oil obtained by evaporation of the solvent of the final solution indicated the formation of the complex. The addition of the metal was carried out at room temperature since the synthesis of the compound at high temperatures would result on the decomposition of the copper complex and the formation of insoluble dark precipitates of copper(II) oxides or hydroxides, $CuO_x(OH)_yCl_z$.

All initial attempts of crystal growing of the copper(II) complex using tetrabutylammonium as the counterion were unsuccessful. The similar solubility of the copper(II) complex with the base prevent us from obtaining the complex pure for the subsequent crystallisation . Eventually, the addition of a concentrated aqueous solution of LiBr to the reaction mixture afforded prismatic deep blue crystals within few days. The crystals that were formed were collected and analysed with X-Ray diffraction. Surprisingly, the preparation of bis(oxamato) copper(II) complexes using Et_2H_2(oeo) as the ligand precursor does not result in the formation of the expected mononuclear building block (Scheme 1.11). A dimeric structure of the copper(II) complex was

obtained instead. The dimer is built with two ligand molecules where each molecule is chelating to two different metal ions through the carboxylate oxygen and the amido nitrogen giving a square planar environment. From this initial synthesis, two different hydrates of the dimeric copper(II) complex were obtained, $Li_4[Cu(oeo)]_2 \cdot 6H_2O$ **(10a)** and $Li_4[Cu(oeo)]_2 \cdot 10½H_2O$ **(11)** (See Chapter 4).

11. 2 The dimer

The dimeric structure, $[Cu(oeo)]_2^{4-}$, is made up of two tetraanionic ligands, $(oeo)^{4-}$, and two copper(II) ions, in which each oxamato group is coordinated towards one copper(II) ion (Scheme 11.1). Both copper(II) ions are $\eta^4(\kappa^2N, \kappa^2O)$ coordinated by the $(oeo)^{4-}$ ligands as expected in the monomeric structure of the copper(II) complex (Scheme 1.11), but in this case, displaying a *trans* environment around the metal. As a result of the *trans*-bis(*N,O*) arrangement, the copper(II) dimer exhibits an helicoidal structure having both ethylendiamine fragments in a *gauche* conformation.

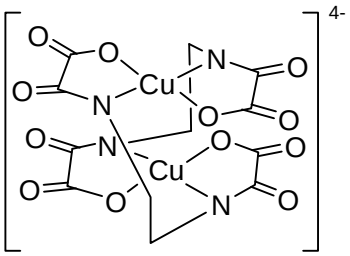

Scheme 11. 1 Dimeric structure of the bis(oxamato) copper(II) complex, $[Cu(oeo)]_2^{4-}$.

Due to the specific morphology of the dimer, it displays a helicoidal chirality adopting Δ and Λ conformations (Figure 11.1). The two crystals obtained have racemic compositions, but the exploration of the chemistry of the copper(II) dimer complex may show a synthesis method for the preparation of homochiral species.

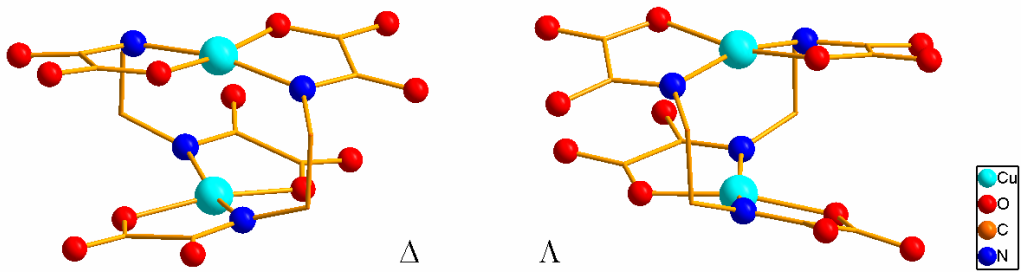

Figure 11. 1 Perspective view of the Δ and Λ enantiomers of the $[Cu(oeo)]_2^{4-}$ complex. Hydrogen atoms are omitted for clarity.

The dimer has several *non*-coordinated units (the carbonyl chelating groups of the omaxate group) which may give rise to the formation of hexametallic transition metal complexes by the addition of further transition metal ions to the complex. Therefore, preparation of polymetallic chiral complexes using ethylene-1,2- dioxamato, $(oeo)^{4-}$, as the ligand in the building block may afford compounds with interesting magnetic properties.

Two other structurally similar dinuclear compounds have been previously reported. These complexes used alkyl *N,N'*-bisethyl(oxamides) as ligands: $[Cu_2(L^1)_2]$ where H_2L^1 = 1,8-diamino-3,6-diazaoctane-4,5-dione,[2] and $[Cu_2(L^2)]$ where L^2 = 7,16-bis(2-aminoethyl)-1,4,7,10,13,16-hexaazacyclooctadecane-2,3,11,12-tetraonate(4-)) (Scheme 11.2).[3]

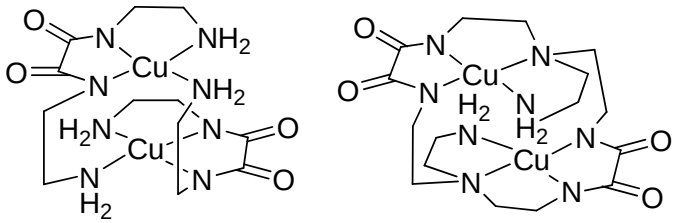

$[Cu_2(L^1)_2]$ $[Cu_2(L^2)]$

Scheme 11. 2

Comba *et al*,[2] studied the thermodynamics implied in the dimerization of an oxamidato mononuclear building block to form its dinuclear system by synthesising both compounds and characterising them. The compounds that were used are $[Cu(L^1)]$ (Scheme 1.10), and its dimer, $[Cu_2(L^1)_2]$ (Scheme 11.2). Dimerization leads to a loss of entropy, and the driving force for the formation of dinuclear compounds may involve relief of steric strains and optimization of electronic effects, electrostatic interactions, hydrogen bonding and van der Waals interactions. Using molecular modelling, they

reported that the dimer is more stable than the monomer since some of the stabilization energy is due to the relaxations of the strain that results from the three fused chelate rings present in the monomer. The rest of the stabilization energy was due to the attractive forces, mainly Van deer Waals. On the other hand, Colin *et al*. studied the variable-temperature magnetic susceptibility of the dinuclear copper(II) complex $[Cu_2(L^2)]$. A thorough analysis of the different possible exchange pathways within the dinuclear species using extended Hückel calculations showed that a through-bond mechanism involving the N-C-C-N sequences was effective exchange pathway.

Consequently, we decided that a thorough study of the chemistry of this system and the dimer was warranted. The next step in our research was the study of the stability of the dimer in solution and the feasibility of achieving the dimer as a solid compared with the monomer. NMR measurements of the solution of ou initial copper(II) complex obtained using tetrabutylammonium hydroxide as the base indicated the formation of the complex but they could not distinguish between the formation of the dimer and the monomer.

In order to obtain more information about the chemistry of the dimer, the synthesis using other counterions (alkali, earth alkaline and transition metals) was attempted. Analogously to the initial preparation of $Li_4[Cu(oeo)]_2 \cdot nH_2O$ crystals, addition of concentrated solutions of the metal salts to the tetrabutylammonium copper(II) complex reaction mixture was carried out. However, they resulted in the formation of solids which are insoluble in all common organic solvents, probably due to the formation of coordination polymers. Nevertheless, the purple solids obtained with the addition of the sodium salts showed a crystalline phase in the PXRD measurements. This gave us some indications that the synthesis using alkali metals was feasible.

11. 3 New synthesis strategy and nature of the intermediate compounds

As a result, a new synthesis route of the copper(II) bis(oxamato) complexes was explored. With the formation of insoluble solids such as coordination polymers as well as copper(II) oxides and hydroxides, it seemed evident that a sequential strategy was needed in which reagents and products could be more controlled. Therefore, bearing in mind that the copper(II) complex was soluble in water but insoluble in common organic

solvents, a new stepwise approach was designed (Scheme 1.11). Firstly, the alkali metal salt of diethyl ethylene-1,2-dioxamate, M_2H_2(oeo) M = Li, Na, K, Rb, Cs; was prepared by saponification of the ester with the addition of two equivalents of base, M(OH). Afterwards, the transmetallation was carried out with the addition of a copper(II) salt solution giving rise to the precipitation of a turquoise solid, CuH_2(oeo) (See Chapter 2). The final copper(II) complex solution, $M_4[Cu(oeo)]_2$, was eventually obtained when two more equivalents of base where added to the reaction mixture affording a deep blue solution (See Chapters 4-8). Using this stepwise approach and adding less than one equivalent of copper, the formation of co-products could be reduced.

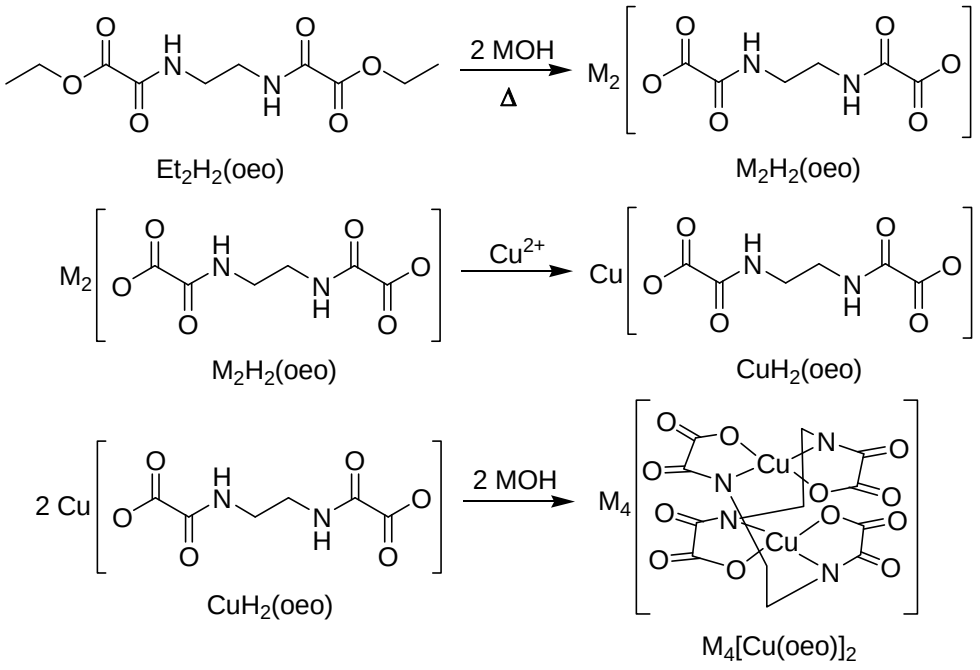

Scheme 11. 3 Stepwise approach for the synthesis of the copper(II) dimeric complex.

Moreover, using this "step-by-step" route, it could be observed the nature of the intermediate compounds in the formation of the bis(oxamato) complex (See Chapter 2). Crystals of the lithium and potassium salts of the ester, Li_2H_2(oeo) **(2a)** and K_2H_2(oeo) **(4a)**, could be afforded. In these compounds, the ligand is coordinating towards the metal through the oxygen atoms providing a monodentate or chelating coordination. Then, by transmetallation of the alkali salt using copper(II), CuH_2(oeo) **(7c)** is formed, crystals of which were grown by gel-tube method. The crystal structure revealed a dimeric unit built by two copper ions and two doubly hydralised ligand molecules. In the octahedral environment of copper two oxamato groups are chelating towards the copper in the basal plane through the carboxylate oxygen and the carbonyl amide

oxygen. Therefore, based upon the mechanism proposed in Scheme 1.15, the intermediate in which the oxamato group coordinates the transition metal ion in neutral conditions (species num. **3**) is observed.

The addition of two more equivalents of base, M(OH), to CuH_2(oeo) achieves the dissociation of the hydrogen bound to the nitrogen followed by the rotation of the C-C bond of the oxamato group and the linkage of the nitrogen atom to the copper ion affording the copper(II) complex $M_4[Cu(oeo)]_2$. As stated in Chapter 1, this is probably achieved thanks to the anchor provided by the oxamato carboxylate oxygen in CuH_2(oeo) as well as the possibility of chelation with the amide group to form a 5-membered chelate ring.

Slow solvent evaporation and slow solvent diffusion of organic solvents into the reaction mixture afforded deep blue crystals of the copper(II) complex with all alkali metals (Figure 11.2). X-ray diffraction analysis of the crystals evidenced the dimer present in all crystal structures. No monomeric structures were observed. The monomer, $[Cu(oeo)]^{2-}$ (Scheme 1.11), is probably subject to the strains produced by the formation of three fused chelate rings around the metal as well as the strains produced by the less flexible character of the shorter alky bridge of the ligand, making the monomer not stable. The repeated observation of the dimeric complex and the absence of any other, such as the planar mononuclear complex, seems good evidence for the stability of the dimeric complex species and its dominance in solution.

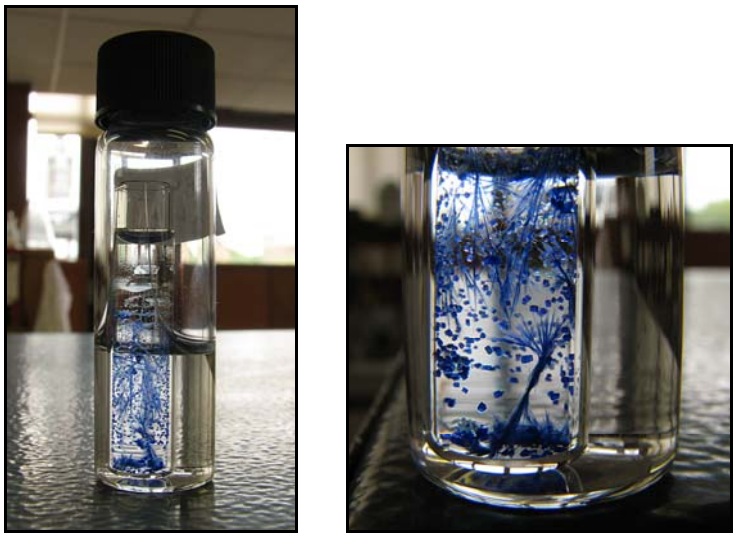

Figure 11. 2 Pictures of the copper(II) complex crystals obtained by slow solvent diffusion of organic solvents. The picture on the right shows the technique in which crystals with two different morphologies can be observed in the close view picture on the left.

As stated earlier, Comba *et al.* reported the synthesis of a structurally similar monomer $[Cu(L^1)]$ (H_2L^1 = 1,8-diamino-3,6-diazaoctane-4,5-dione) using bis(ethylamine)oxamide, H_2(eoe), as the ligand precursor (Scheme 1.3). Due to the morphology of the organic molecule, the $[Cu(L^1)]$ monomer could be formed probably due to the greater flexibility of the ligand since it contains only one rigid group, the oxamidato group. However, our ligand has two rigid oxamato groups which most likely they give too much strains to the monomer to be stable. Because of the relief of strains probably makes more favourable the formation of a dimeric structure, $[Cu(oeo)]_2^{4-}$, when using the ethylene-1,2-dioxamato as the proligand.

11. 4 Solubility of the $[Cu(oeo)]_2^{4-}$ complex

The $[Cu(oeo)]_2^{4-}$ complex is only soluble in water, probably as a result of the large negative charge that the complex has. Once the complex is obtained in the solid form, it is only soluble in concentrated aqueous basic solutions when it is in a crystalline phase and it remains dissolved for relatively short periods of time. When the crystalline solid is dissolved in water, as a consequence of the equilibria in solution, the complex decomposes to form a light blue insoluble solid which is likely to be some type of coordination polymer (Scheme 11.4). Nevertheless, if the solution is under basic conditions, the copper(II) complex is stable for much longer periods of time since the equilibria tends to the formation of the dimeric compound.

$$[Cu_2(oeo)_2]^{4-} \underset{-2H^+ + Cu^{2+}}{\overset{+2H^+ - Cu^{2+}}{\rightleftharpoons}} [Cu(Hoeo)_2]^{4-} \underset{Cu^{2+}}{\overset{2H^+}{\rightleftharpoons}} 2(H_2oeo)^{2-}$$

a

$$[Cu_2(oeo)_2]^{4-} \xrightarrow{2Cu^{2+}} 2[Cu_2(oeo)]_n$$

b

Scheme 11. 4 a. Probable equilibria of $[Cu(oeo)]_2^{4-}$ complex in aqueous solution. The reaction of the ligand and the copper(II) under basic conditions must undergo a step-wise insertion of the copper atom. Moreover, based on the observed structures of the ligand (Chapter 2 and 9), there is clear an equilibrium between the mononuclear, $[Cu(Hoeo)]_2^{4-}$, and the dimeric, $[Cu_2(oeo)_2]^{4-}$, structures as well as between the mononuclear structure and the free ligand, $(H_2oeo)^{2-}$. **b.** Formation of the coordination polymers.

On the other hand, if the volume of the mixture solution is reduced drastically, like in rotatory evaporation, the solid that is formed is insoluble in water. It seems feasible that the rapid generation of the solid leads to the formation of an amorphous coordination polymer due to the lack of time for the apparent polymer to grow in an ordered way. The solid that is formed is light blue coloured and the IR measurements show the common features of the ligand molecule. However, if the solvent is reduced very slowly, like in the open air, crystals of the copper(II) complex can be obtained.

Therefore, a $[Cu(oeo)]_2^{4-}$ microcrystalline solid can be achieved with the careful addition of an organic solvent to the final reaction mixture of the synthesis of the compound. However, the conditions in which the pure crystalline solid of the copper(II) complex can obtained are very narrow since it can be formed together with one of the above mentioned impurities. The separation of mixture of the dinuclear copper complex with the impurities was unfeasible. Once the $[Cu(oeo)]_2^{4-}$ building block could be obtained, a way to obtain a polymetallic compound is starting from a concentrated solution of the pure microcrystalline copper(II) complex followed with the addition of a transition metal solution.

11. 5 Microcrystalline solid

In general, these blue solutions are quite fragile, being destroyed by an excess of base, or too much copper (frequently as one equivalent is approached), or by too high temperature, or upon standing for too long time.

One of the common procedures to obtain or purify a compound that is dissolved in a solution is reducing the volume of the solvent by rotatory evaporation in order to make the compound precipitate. Then, the solid can be purified by recrystallisation under the proper conditions. However, this procedure cannot be followed in this system since as mentioned above; the solution is quite fragile and decomposes with heating to form a copper oxide form. Moreover, the volume needs to be reduced very slowly in order to give enough time to the system to precipitate in an ordered manner. If the volume is reduced drastically, an amorphous phase is formed, probably an insoluble coordination polymer as well as an oil when the counterion is Bu_4N^+ cation. This is most likely to be a result of the many equilibria that exist in solution as well as the many possible sites that the copper and the alkali metal ions can be placed in the $[Cu(oeo)]_2^{4-}$ complex.

Nevertheless, patience and careful control of the conditions can yield to a polycrystalline solid of the form $[Cu(oeo)]_2^{4-}$. Slow cooling down of the temperature of the reaction mixture can lead to the formation of a polycrystalline solid, such as compound **17** (See Chapter 6). Also when a quite concentrated solution is left standing overnight microcrystalline solid, which is soluble in water, can be achieved, like compound **15** (See Chapter 5). However, the best results were afforded when a reaction mixture that was previously charged with a polar organic solvent was left standing during 24 hours like compound **13** (See Chapter 4).

11. 6 Polymorphs and hydrates

Polymorphism is the property of a substance to exist in different crystalline phases resulting from different structural arrangements of the molecules in the solid state.[4] One of the types of polymorphism is pseudo-polymorphism which refers to cases in which a given substance is known to crystallise with different amounts or types of solvent molecules. In inorganic and organic chemistry, when the pseudo-polymorph crystallises with water molecules, it is called hydrate. Even though polymorphic modifications contain exactly the same substance, they have different chemical and physical properties such as density, diffraction pattern, solid state spectroscopy, melting point, stability, solubility, reactivity, mechanical properties.

Several polymorphs and hydrates of the copper(II) dimeric building block $[Cu(oeo)]_2^{4-}$ have been obtained. Crystal structures of the copper(II) dimer complex using all stable

alkali metals (Li, Na, K, Rb, Cs) as the counterion have been prepared. Moreover, for some of them, more than one hydrate were obtained and even a number of polymorphs could be characterised with the lithium cation. This is a result of the characteristic structure of the dimer. The anion has an approximately spherical character with several coordinating sites (carboxylate groups), in which the cations and the solvent molecules (water molecules) can be interacting with the anion through several different sites and in different manners. The list of the different polymorphs and hydrates obtained so far includes (See Appendix A5):

- α-$Li_4[Cu_{0.90}H_{0.20}(oeo)]_2 \cdot 6H_2O$ **(10a)**
- β-$Li_4[Cu_{0.94}H_{0.12}(oeo)]_2 \cdot 6H_2O$ **(10b)**
- γ-$Li_4[Cu(oeo)]_2 \cdot 6H_2O$ **(10c)**
- $Li_4[Cu_{0.93}H_{0.14}(oeo)]_2 \cdot 10½H_2O$ **(11)**
- $Li_4[Cu_{0.96}H_{0.08}(oeo)]_2 \cdot 5H_2O$ **(12)**
- $Na_4[Cu_{0.05}H_{1.90}(oeo)]_2 \cdot 4H_2O$ **(14)**
- $Na_4[Cu_{0.18}H_{1.64}(oeo)_2] \cdot 8H_2O$ **(16)**
- $K_4[Cu_{0.33}H_{1.34}(oeo)]_2 \cdot 5H_2O$ **(18)**
- $K_4[Cu_{0.89}H_{0.22}(oeo)]_2 \cdot 3H_2O$ **(19)**
- $K_4[Cu_{0.78}H_{0.44}(oeo)]_2 \cdot 4.5H_2O$ **(20)**
- $K_4[Cu(oeo)]_2 \cdot 6H_2O$ **(21)**
- $Rb_4[Cu_xH_{(2-2x)}(oeo)]_2 \cdot 4H_2O$, x = 0.80, 0.30, 0.18 **(22a, 22b, 22c)**
- $Cs_4[Cu(oeo)]_2 \cdot$ 5 ½ H_2O **(23)**

As we can see, three $Li_4[Cu(oeo)]_2$ pseudo-polymorphs have been obtained which contain 5, 6, and 10½ water molecules and three polymorphs of $Li_4[Cu(oeo)]_2 \cdot 6H_2O$ have been found, one of which crystallises in the polar chiral space group $P6_5$, being the only chiral crystal structure obtained (See Chapter 4). The most characteristic feature of the packing of these crystals is that the dimers pack in rods where each rod is linked to four neighbouring rods by the lithium cations. The dimers are chelating towards the lithium ions through the four *non*-coordinated units connecting the rods of dimers in two dimensions (Figure 1.4). This type of packing provides a glimpse of which type of bimetallic transition chiral compounds we could be made, in which a transition metal could be placed in the lithium site being chelated by two $[Cu(oeo)]_2^{4-}$ units.

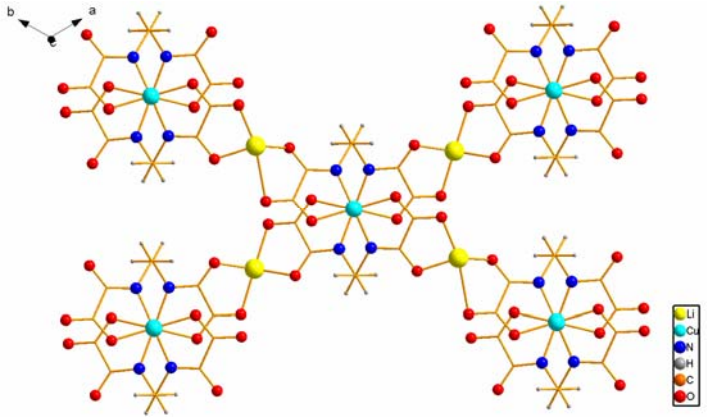

Figure 11. 3 Perspective view along the *c*-axis direction of the interaction between dimers in the crystal packing of *β*- $Li_4[Cu(oeo)]_2 \cdot 6H_2O$. It can be noted that the lithium atoms are chelated by the oxamato groups of the copper(II) complex connecting the dimeric units in 2-D.

Two hydrates of $Na_4[Cu(oeo)]_2$ have been found: one crystallises with four water molecules and the other one with eight (See Chapter 5). $K_4[Cu(oeo)]_2$ can crystallise with 3, 4½ , 5 and 6 water molecules (See Chapter 6). The whole structure in those compounds, except for $K_4[Cu(oeo)]_2 \cdot 6H_2O$ **(21)** which packs in rods similarly to the lithium compounds, have a definite 2-D character in which anionic layers of $[Cu(oeo)]^{4-}$complex alternate with cationic layers of alkali metal and water molecules.

On the other hand, the crystal structure $Rb_4[Cu(oeo)]_2 \cdot 4H_2O$ **(22)** is the only hydrate that has been obtained with rubidium and $Cs_4[Cu(oeo)]_2 \cdot 5½H_2O$ **(23)** with caesium (see Chapter 7 and 8, respectively). However, if more time was devoted to the study of the Caesium and Rubidium salts and it is quite likely that other polymorphs and hydrates would be found. The crystal structure of **22** has also a layered structure where anionic layers of $[Cu(oeo)]^{4-}$ complex alternate with cationic layers of rubidium and water molecules. In **23**, the dimer packs in infinite rods which are linked through caesium ions and water molecules.

In some cases, more than one phase were grown in the same vial. For instance, the two potassium hydrates **19** and **20** were grown in the same vial, each one crystallising with different copper(II) amounts. Species **10b**, **10c** and **12** were also obtained in the same vial, crystallising the former in a chiral space group whereas the two others in a centrosymmetric space group. As in all other reaction mixtures, achiral reagents and achiral solvents were used. However, **10b** grew at the top of the vial crystallising in a chiral space group $P6_5$ whereas the other two enantiomeric species (**10c** and **12**) were

grown at the lower part of the vial. This evidences some differences in energy between interactions of the complex and the solvents.

These polymorphs and hydrates usually have clearly different habits, such as **19** and **20** (Figure 6.1, see Chapter 6), but they can also have almost indistinguishable morphologies making the sample characterisation more difficult, like **10c** and **12** (See Chapter 4). At first, when **10c** and **12** crystals were analysed using X-ray diffraction, we thought they were the same compound since their morphologies were alike and the cell parameters had very similar values except *a* and *b* cell edges, of which values were exchanged. However, careful studies showed they were new two hydrates. Therefore, we have to take into account that samples that have been analysed could had contain more than one phase that look very similar. In addition, it is noteworthy that the number of polymorphs and hydrates of dimeric copper(II) complex would probably increase if a wider range of temperatures and compositions of the reaction mixtures were investigated.

Furthermore, it could be observed that what happens on a "large" scale (crystals, mm) is also reflected in small scale (microcrystals, μm). A microcrystalline solid can also be made up of different hydrates and polymorphs, especially when different morphologies and habits can be observed (See Chapter 4). Several crystal morphologies and habits were observed when the microcrystalline solid was studied by SEM (Scanning Electron Microscopy) or using a microscope, suggesting also the formation of different pseudo-polymorphs or polymorphs. As a result, the exact composition of a microcrystalline solid remains undetermined since the amount of water molecules and copper can not be determined.

The main two variables to synthesise the different polymorphs and hydrates are the temperature, the composition and concentration of the reaction mixture; and the technique that was used to obtain the crystals. The range of temperatures in which crystals were grown was quite wide since the temperature in the laboratory was quite variable, typically between 10^{o}C and 30^{o}C depending on the time of the year and the moment of the day. On the other hand, the reactant mixtures from where the compounds were obtained were prepared using different proportions of copper(II) salt and ligand as well as variable amounts of solvents were used. Therefore, formation of the different

hydrates and polymorphs was probably affected by these changes, making the results very difficult to be reproducible.

Therefore, the building block $[Cu(oeo)]_2^{4-}$ shows quite complex structural chemistry as evidenced by the many structures that we have been determined. However, if the right conditions to obtain a single species are found, this copper(II) complex could be used as a "brick" in magnetochemistry.

11. 7 The partial occupancy of the copper(II) site

Another curious aspect of these crystal structures is the partial copper(II) occupancy in the copper sites of the dimer. Due to the structural morphology of the dimer, hydrogen bonds between the two chelating oxamato groups of the copper atom can be formed when the copper(II) site is vacant and thus maintain the dimeric structure. This is possible thanks to the distance between the two oxamato groups which is the right one for having hydrogen bonds between the carboxylate oxygen atoms and the amide hydrogen atoms of each group (See Chapter 3).

A wide range of copper(II) occupancies have been noted in the crystal structures, from species with a full occupancy to species with only 10% of copper. Even more, separate crystals obtained from the same reaction mixture but grown using different techniques have been found with essentially the same structure but having quite varied occupancies in the copper site. That is to say that essentially the same crystal structure can be achieved with different copper(II) occupancies although there are some slight changes in the distances around the metal site in these isomorphic structures.

The standard method that has been followed in the synthesis of the copper(II) dimer, $[Cu(oeo)]_2^{4-}$, has been the careful addition of a copper(II) solution with the later addition of a basic solution into an aqueous solution of the ligand $(oeo)^{4-}$. Then, deep blue crystals of the dimer were grown by slow evaporation of the solvent or slow diffusion of a solvent insoluble with the complex into the reaction mixture.

It seems that the amount of copper in the dimer does not follow a simple relationship between the amount of copper(II) added into the mixture and the final amount of copper(II) in the dimer, but it is related to the packing of the dimer in the crystal

structure. For instance, compound **23**, which the copper(II) site fully occupied, was obtained from a solution prepared adding 0.5 equiv of the copper(II) to the reaction mixture and the crystal has copper(II) site fully occupied (See Chapter 8). On the other hand, **19** and **20** were obtained from a reaction mixture in which 1 equiv of copper(II) was added and they both crystallised containing different occupancies in metal site, both less 100% (0.89 and 0.78%, respectively) (See Chapter 6). The probable reason for this difference between amounts of copper in the dimer is that particular structures or crystal packing may favour the formation of $[Cu(oeo)]_2^{4-}$ more than $[CuH_2(oeo)_2]^{4-}$. This is to say that in compound **23**, as well as in the lithium compounds, where the dimer packs in rods, the interaction between dimers is carried out through the copper(II) and thus it needs the metal site to be fully or almost fully occupied for the structure to be stable. On the other hand, in **19** and **20** there is no specific interaction between dimers through the copper(II) and there is a wide range of copper(II) occupancies. Structural correlations between the copper(II) occupancy and the packing of the $[Cu(oeo)]_2^{4-}$ dimer will be discussed in depth below.

Furthermore, three different occupancies have been observed in the three rubidium crystals that have been analysed. All three species are isomorphic structures with different amounts of copper(II) in the metal site although they were obtained from the same reaction mixture but grown using different techniques and time scales, of which the species with the higher occupancy was obtained by slow solvent evaporation (See Chapter 7). By contrast, crystals of the sodium copper(II) complex were grown by slow solvent diffusion from the same reaction mixture but using two different solvents. Two crystals were analysed (**16a** and **16b**) and they both contained the same amount of copper in the dimer (See Chapter 5). Therefore, the amount of copper(II) present in the dimer may differ depending on the technique that is used to grow crystals, although using different solvents can afford the same amount of copper(II) in the dimer. However, different occupancies can be found in different hydrates or polymorphs grown in the same vial.

It is possible that the crystals that grow at the top of the beaker may have different amount of copper(II) in the dimer than the crystals grown at the bottom. When a solution is under stirring, the solution has a homogeneous concentration. However, when a mixture is left standing in order to grow crystals, the solution remains unstirred

and the concentration may rather exist as a gradient and its composition would probably be reflected in crystals grown from this solution. Therefore, we may observe some difference in concentration of the metal depending on where in the beaker the crystal is picked up. Because of this, when one crystal is picked up from a sample and analysed by X-ray, we cannot assure that the crystal will be representative of the sample.

This wide range of copper occupancies as well as the variety of polymorphs and hydrates, evidences the complexity of the study of the chemistry copper(II) dimer. It makes more difficult to know the exact composition in a microcrystalline solid as different hydrates and polymorphs suggest different amount of copper(II) in the different species . It also suggests that the obtaining of a robust copper(II) dimer in which the addition of transition metal ions would give rise to the formation of polymetallic bis(oxamato) complexes might be too difficult a challenge as a result of the variable amount of copper(II).

11. 8 Structural correlations between packing of the copper(II) complex and the occupancy of the metal site

As stated above, a wide range of copper(II) occupancies have been obtained in the copper(II) site, from structures with 10% of copper to structures with the copper site fully occupied. Two types of packing have been generally noted in this system: a stack and a layered fashion. In the former, the $[Cu(oeo)]_2^{4-}$ dimer packs in infinite rods which are surrounded by counter ions. The dimers are connected within the rod through a Cu-O bond or weak Cu-N interactions between neighbouring dimers as well as the rods are connected in two dimensions through the surrounding cations. In the later, anionic layers of $[Cu(oeo)]_2^{4-}$ complexes alternate with anionic layers of the cations and water molecules. In this case, the complexes have no interaction between them but they are connected in the crystal lattice through the cations and water molecules.

It seems feasible that we can correlate general structural types with the space groups in which they are formed and with the occupancy of the metal site in the dimer. When the dimer packs in rods and crystallise in a non-chiral space group, they can crystallise in the $P\bar{1}$ space group (Compounds **11**, **21** and **23**) or in the $C2/c$ (Compounds **10a, 10c**, **12**). The rods are surrounded by the cations in all directions in the former, whereas in

the latter, the cations are only placed in certain positions and thus the packing is described as a layered structure where anionic layers alternate with the cationic layers. However, the anionic layer is built by rods of dimers which are alternated with infinite hydrophobic pockets. In all structures where the dimer packs in rods, there is an interaction between dimers within the rods and therefore they can only be observed in crystals with a very high copper(II) occupancy (>89%). On the other hand, when the occupancy of the copper(II) site is low, the layered packing with no interaction between dimers is observed.

As previously mentioned, the addition of a large amount of copper(II) to the reaction mixture does not guarantee the formation of crystals with high copper occupancies and thus, the formation of certain crystal packing. However, the synthesis of the copper(II) dimer using lithium as the counterion seems to guarantee the formation of species with almost fully occupied copper(II) sites. Probably, as a consequence of the small size of the lithium ion, lithium compounds crystallise in rods, which need high amounts of copper(II) to be stable, and in which the lithium ions are chelated by two oxamato groups of two different rods.

11. 9 The geometry around the copper site

We have seen that when copper(II) site is less than half occupied the expected bond length trend around the copper atom is not seen. This has been observed in the sodium crystal structures (**14** and **16**), in one species of the potassium structures (**18**) and in some of rubidium crystal structures (**22b** and **22c**).

As discussed in previous chapters, this is a consequence of the dominance of the hydrogen-bonded geometry of the oxamato groups in the crystal lattice. X-ray structure "sees" a superposition of two species in one site, weighted by their relative occupancies. Therefore when the amount of copper is high, the predominant species in the crystal lattice is the structure where the ligand, and thus the oxamato group, is coordinating the metal. However, when the copper occupancy is low the main species in the dimer is the one in which both ligands are hydrogen-bonded being reflected in the geometry around the copper(II) site (See Figure 3.5). In this species, the apparent Cu-N bond length is increased whereas the apparent Cu-O bonds length is decreased. It has been noted in the

rubidium copper(II) complexes that the less copper(II) present in the dimer, the shorter the distance between nitrogen and oxygen, giving some evidence of a tendency to lead to the right distances for a hydrogen bonded interaction (See Chapter 7, Table 7.2). As a result, an elongation of the thermal ellipsoid of the oxygen atom site is also observed due to the superposition of the two geometries: the hydrogen bonded geometry and the copper chelating geometry where the former geometry prevails.

In addition , a mononuclear bis(oxamato) copper(II) complex formed by one metal atom and two ligand molecules have been found **(25a)** (See Chapter 9). It was obtained using tetrabutylammonium as the counterion and, as in the copper(II) dimer, the copper atom is coordinated by two deprotonated amido nitrogens and two carboxylate oxygens of two oxamato groups giving rise to a *trans*-bis(H-*N,O*) arrangement around the metal ion. However, a mononuclear complex built with two ligand molecules was formed instead of the dimer, probably due to the bulkiness of the $[n\text{Bu}_4\text{N}]^+$ cations. In this compound it can be observed the ideal geometry of a copper(II) ion chelated by two oxamato groups.

11. 10 The chemistry of the $[\text{Cu(oeo)}]_2^{4-}$ complex solution

As previously discussed in Chapter 3, the repeated observation of dimeric coordination complex, and the absence of any other, such as the hypothetical essentially planar Cu(oeo)^{2-}, seems good evidence for the stability of this copper species, and its dominance in solution. However, neither UV-Vis spectra nor ^{1}H-NMR studies on the reaction mixtures can prove it.

In general, the $[\text{Cu(oeo)}]_2^{4-}$ complex is only stable in concentrated basic solutions since the dilution of the reaction mixture tends to the decomposition of the dimer to form coordination polymers. Also, at high temperatures the complex decomposes to form copper oxides and coordination polymers. However, we have seen that crystals of the dimer can still be formed after having the reaction mixture at high pressure and high temperatures, like in the *Teflon lined autoclave* in which the final solution had a low concentration and a neutral pH (See Compound **14**). This low concentration was reflected in the occupancy of the copper(II) site which was 5%.

11. 11 Cobalt (II) salts and Bimetallic compounds

Looking at the structure of the mononuclear copper(II) complex, **25a**, it can be observed that the flexidentate system has six *non*-coordinated chelating units (See Figure 9.2). Therefore, the addition of further transitions metals may give rise to heterometallic transition metal complexes. Quite a few attempts of formation of bimetallic transition metal complexes have been carried out and some bimetallic compounds were obtained. However, the low solubility of the solids and their partial crystallinity made the characterisation very difficult (See Chapter 11).

On the other hand, cobalt(II) salts of the diethyl ethylene-1,2-dioxamate have been obtained. Similarly to the copper(II) salt, **7c**, the crystal structure is formed by a dimeric structure built with two cobalt(II) ions, two doubly hydralised ligand molecules and two DMSO molecules, $CoH_2(oeo)\cdot DMSO$ **(8a)**. However, the transition metal salts have different structures (See Chapter 2). Also, the crystalline solid phase has been obtained although the exact composition of the compound could not be deretmined (See Chapter 11).

11. 12 Infrared studies of the ligand, precursors, and the Cu(II) complexes

For all the work done here we have followed the chemical transformation of the "oeo" compounds by IR spectroscopy, from the Et_2H_2oeo ligand, with the subsequent formation of the $M_2H_2(oeo)$ and $MH_2(oeo)$ salts until the achievement of the $M_4[Cu(oeo)]_2$ species. Firstly, the hydrolysis of the ester of $Et_2H_2(oeo)$ **(1)** afforded the salt of the ester, $M_2H_2(oeo)$ where M = alkali. Then, the transmetallation of the alkali salt was carried out with the addition of a transition metal, giving rise to the transition metal salt, $M'H_2(oeo)$ where M' = Cu and Co. Finally, the dimeric copper(II) complex, $M_4[Cu(oeo)]_2$ where M = alkali metals, was achieved with the addition of the corresponding alkali base and the consequent dissociation of the amide which then coordinates the copper ion. The mononuclear species of the copper(II) complex, $(Bu_4N)_4CuH_2(oeo)$ **(25a)**, was also obtained which could be considered the intermediate species between the dimer and the transition metal salts of the esters. All these changes can be correlated with the IR spectra of the different compounds (See Appendix A1).

The ligand is an oxamate of which the main bands corresponding to the amide and the ester can be recognized in all spectra of the products. The most distinct bands to recognise are the strong C=O stretching bands which appear around 1650cm^{-1}. The C=O stretching band of the amide (Amide I band) appears at lower frequencies than the ester due to the resonance form of the amide, which decreases the double character of the carbonyl group. At lower frequencies, the Amide II band, which is due to the N-H bending, appears around 1500-1600 cm^{-1}. In some cases, the overtone or combination band of the N-H bending can be observed approximately at 3080 cm^{-1}. In addition, the O-H and N-H stretching are located in the >3000 cm^{-1} region, the former being at higher frequencies and always showing association due to the hydrogen bonding. The N-H wagging is generally observed around 750 cm^{-1}. On the other hand, the Csp^3-H stretching appears below 3000 cm^{-1}, usually showing several bands, whereas the C-H bending is observed around 1450 cm^{-1}.

The IR spectrum of **1** (Spectrum 1) has the C=O stretching bands of the amide and the ester well differentiated around 1740 and at 1670 cm^{-1}, respectively. Looking at the crystal structure of **1**, the 3305 cm^{-1} band is consistent with an associated N-H stretching due to the intermolecular hydrogen bond between the amide hydrogen and the carbonyl oxygen of the oxamato groups.

Once the ester is hydrolysed by the addition of an alkali base the salt of the ester is formed, such as Li_2H_2(oeo) **(2)** and K_2H_2(oeo)·H_2O **(4a)**, and then the C=O stretching of the ester appears at lower frequencies as a shoulder of the amide's C=O stretching (Spectra 2 and 3, respectively). Similarly to the amides, this is probably a consequence of the electronic effect of the resonance forms of the carboxylate group, where the double character of the carbonyl group is distributed over two oxygens. However, in the transition metal salts, CuH_2(oeo)·$3H_2O$ **(7a)** and CoH_2(oeo)·DMSO **(8),** it appears more differentiated from the Amide I band (Spectra 4 and 5, respectively).

In addition, there are some other bands that are common in the IR of the salts of the ligand and can be used to identify them. These bands appear in the fingerprint region as they appear below 1500cm^{-1}. Firstly, a strong band at approximately 1380 cm^{-1}, then a couple of nearby bands around 1250cm^{-1} and a weaker one between them at about 1320 cm^{-1}; and lastly another weak one around 1050cm^{-1}. All these bands are difficult to

assign unambiguously since several bands appear in this region and they can show a wide range of frequencies depending of the molecule. However, two bands arising from the CO-O stretching of the ester are expected in this region, as well as the C-N stretching and O-H bending of the water molecules. The band at about 1380 cm^{-1} is usually quite strong in the salts whereas in the ester, **1**, it appears very weak. This change in intensity suggests a modification in the structure, which could be a result of the hydrolysis of the ester where the band appears broader and at higher frequencies due to the resonance forms of the carboxylate group. Moreover, the two nearby bands around 1250 cm^{-1}, which also appear in the spectrum of **1**, might be assigned to CO-O and C-N stretching.

In the O-H and N-H stretching region, all compounds show association of the amine groups, as well as association of the water molecules, except for **8** which only shows N-H stretching since it has DMSO molecules in the crystal packing instead of water molecules. On the other hand, in the crystal structure of **25a** it is observed a N-H which is not hydrogen bonded due to the bulky of the cation. This feature can be observed in the IR spectrum of the crystal (Spectra 6), where the two peaks at 3396 and 3382 cm^{-1} appear at higher frequencies of the associated N-H stretching. These bands are only seen in this spectrum and thus, this suggests that the bands are a result of the free N-H stretching. Also, it can be noted in the spectrum a vast enhancement of the C-H stretching as a consequence of the *n*-butyl groups.

The IR spectra of the dimeric copper(II) complex crystals, $M_4[Cu(oeo)]_2$ M = Li and K (Spectra 7 and 8, respectively), also show the common features previously stated. Nevertheless, it is worthy to mention the difference of the N-H bending band between the two spectra, which is affected by the copper(II) occupancy in the dimer. In compound α-$Li_4[Cu_{1.80}H_{0.40}(oeo)]_2 \cdot 6H_2O$ **(10a)**, it was seen that the occupancy in the copper(II) site is 90% whereas in $K_4[Cu_{0.33}H_{1.34}(oeo)]_2 \cdot 5H_2O$ **(18)** it is 33%. Therefore, the later compound has a large quantity of hydrogen bonds between the amide hydrogens and the carbonyl oxygens of the two oxamato groups that would be chelating the copper(II) atom. This is consistent with the IR spectra in which no Amide II band is observed in the spectrum of **10a** whereas in the spectrum of compound **18** shows a strong Amide II band at 1524 cm^{-1}. Lastly, the band at 3292 cm^{-1} is likely to be the N-H stretching.

This type of analysis can be useful to approximate the amount of copper(II) present in a solid of the copper(II) salt of which, as stated above, the amount of copper remains unknown. For instance, if we compare the spectrum of the solid of the reported potassium copper(II) complex, $K_4[Cu_xH_{(1-x)}(oeo)]_2 \cdot nH_2O$ **(17)** (Spectra 9) with the spectra of **18** and **10a** (Spectra 8 and 7, respectively), we can observe that a quite high amount of copper(II) is present in the solid as the mentioned features of the Amide II band and the N-H stretching are not observed. The same kind of approximation can be done when looking at the spectrum of $Na_4[Cu_xH_{(1-x)}(oeo)]_2 \cdot nH_2O$ **(15)** (Spectra 10), which, together with spectrum of **17**, is comparable with the spectrum of compound **10a**, of which occupancy of the copper(II) is above 90%. As stated above, the occupancy of the copper(II) in both solids (**15** and **17**) was expected to be higher than in the respective crystals as they both were obtained first. Crystals of the sodium and the potassium copper(II) complex (**16** and **18**) were grown from the same reaction mixture than the respective solids but after the precipitation of the solids (See Chapters 5 and 6).

11. 13 Final conclusions and forward look

The synthesis method and the description of the structures of a series of a new chiral bis(oxamato) copper(II) complex have been reported. These compounds were initially expected to become the building block for the obtaining of the so-called chiral molecule-based magnets but the subsequent exploration of the chemistry of these compounds evidenced that the conditions of synthesis and control of these products is more involved than their analogues. Chirality is a quite unexplored property in magnetic materials which, as a consequence of the non-centrosymmetric arrangement of the spin carriers, may affect the properties of the material and give rise to some new interesting behaviour such as magnetochiral dichroism.[5] For a chiral molecule-based magnet exhibiting high ordering temperature and spontaneous magnetisation, the chirality must be maintained in the entire crystal structure as well as on the high dimensionality of the extended arrays. However, this is not the case in our copper(II) dimeric system as the enatiopure chiral $[Cu(oeo)]_2^{4-}$ complex could not be obtained. All crystals crystallised in a racemic space group, except one which was grown as a twin of a chiral space group.

As previously stated, the standardised method for the preparation of polymetallic complexes is the step-wise incorporation of transition metal ions into aliphatic or aromatic group-substituted oxamato metal containing complexes as ligands (building

blocks). For that you need a well reproducible synthesis of the building block and the formation of a crystalline polymetallic system in order to be able to characterise it. None of these requirements were fulfilled in the present case. The reproducibility in the synthesis of the building block failed as a consequence of the uncontrolled varied occupancy of the copper(II) site that was obtained, even in crystals that were grown from the same batch.

In addition, the assortment of polymorphs and hydrates that could be afforded also from the same batch and the impossibility of assigning them when a microcrystalline solid is synthesised shows the difficulties for obtaining the building block in a well controlled manner. The presence of several *non*-coordinated units where the solvent molecules and the cations can interact with the anion, as well as the spherical nature of the $[Cu(oeo)]_2^{4-}$ complex, results in the presence of a range of polymorphs and hydrates of the copper(II) complex. This wide variety reflects the small energy differences between the different configurations in the arrangement of the solvent molecules and cations. Consequently, because of the presence of more than one phase in a microcrystalline solid and the diversity of occupancies of the copper(II) site, the exact composition of a microcrystalline solid a remains difficult to establish.

In order to obtain heterobimetallic bis(oxamato) complexes with interesting magnetic behaviour, it is needed a fully occupied copper(II) site for the different spin carriers interact with each other. It was observed in the crystal structures that only when Caesium and Lithium where used as the counterions, the copper(II) site was fully or almost fully occupied due to the packing of the dimers in the crystal lattice. Thus, the synthesis of the $[Cu(oeo)]_2^{4-}$ building block using these cations could guarantee the full occupancy of the copper(II) site. Moreover, it has been noted by IR analysis that the addition of an organic solvent to the reaction mixture of the copper(II) dimer with lithium afforded a microcrystalline solid with copper(II) site highly occupied. However, the presence of more than one morphology and habits in the solid evidenced the presence of more than one phases.

On the other hand, some derivations in the ligand of the building block as well as in cation would afford the synthesis of enantiomerically pure species. The synthesis of a copper(II) dimer starting from a chiral building block using a chiral aliphatic or

aromatic ligand such as 1,2-aminocyclohexane or derivates could result in the formation of chiral helicates and would provide some different solubility properties. The synthesis of enantiomerically pure species could also be achieved using a chiral cation like a chiral ammonium cation. It is also worth the study of the stability of the copper(II) complex in solution and its rate in the process of formation. The possible conversion of one enantiomer into another in solution and all the equilibria that this involves may affect the formation of the insoluble copper(II) complex (when the volume of the solution is drastically reduced) as well as the formation of insoluble bimetallic compounds. Thus, the study of the stability of the complex regards to dissociation of the complex and its racemization rate in solution might be useful to understand the chemistry of the complex.

Furthemore, the bimetallic bis(oxamato) copper(II) compounds that have been obtained could not be fully characterised. In general, the polymerisation reaction of our $[Cu(oeo)]_2^{4-}$ and $[CuH_2(oeo)_2]^{4-}$ building blocks with other transition metals was too fast to give a crystalline solid, even when slow diffusion techniques such as H-shaped tubes were used, as revealed by their X-ray powder diffraction patterns. Some crystalline solids could be achieved in which the presence of the ligand as well as the metal ions was observed. However, the difficulty to fully characterise these compounds prevent us to carry out in developing more these systems. If the formation of bimetallic bis(oxamato) compounds could be achieved in a slow and controlled manner using the $[CuH_2(oeo)_2]^{4-}$ building blocks, this may give rise to compounds with interesting magnetic properties as the starting building block guarantees a fully occupied copper(II) site.

[1] B. Cervera, J. L. Sanz, M. J. Ibañez, G. Vila, F. Lloret, M. Julve, R. Ruiz, X. Ottenwaelder, A. Aukauloo, S. Poussereau, Y. Journaux, M.C.Muñoz, *J. Chem. Soc., Dalton Trans.,* **1998**, 781
[2] P. Comba, S. P. Gavrish, Y. D. Lampeka, P. Lightfoot, A.Peters, *J. Chem. Soc*., *Dalton Trans*., **1999**, 4099
[3] J. C. Colin, T. Mallah, Y. Journaux, F. Lloret, M. Julve, C. Bois, *Inorg. Chem.*, **1996**, *35* (14), 4170
[4] Braga, D., Grepioni, F., *Chem. Soc. Rev.,* **2000**, *29*, 229
[5] E. Coronado, J. R. Galán-Mascarós, C. J. Gómez-García, A. Murcia-Martínez, *Chem. Eur. J*., **2006**, *12*, 3484

Appendix

A1 - Infrared Spectra

Spectrum 1 – $Et_2H_2(oeo)$ **(1)**

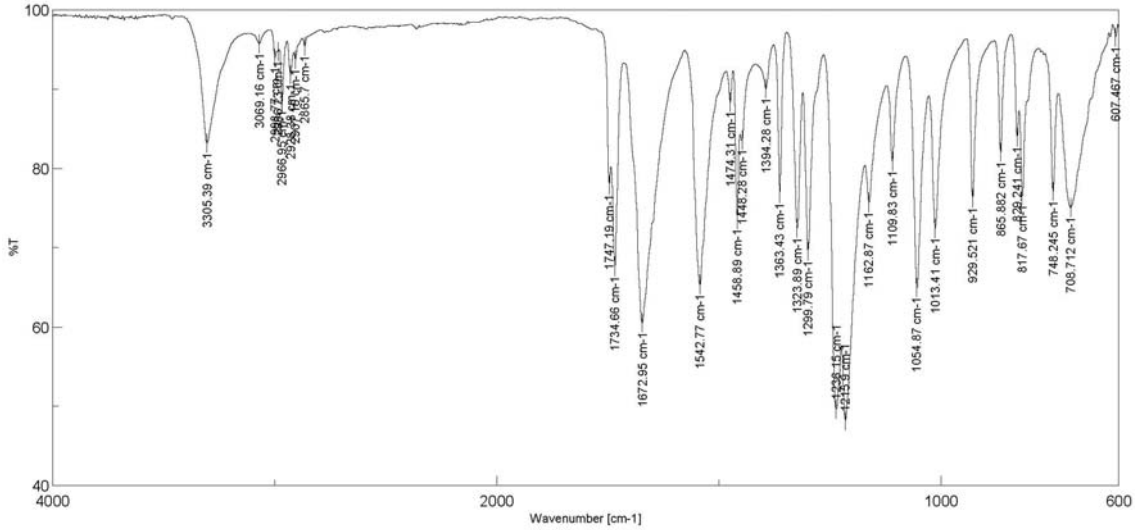

Spectrum 2 – $Li_2H_2(oeo)$ **(2)**

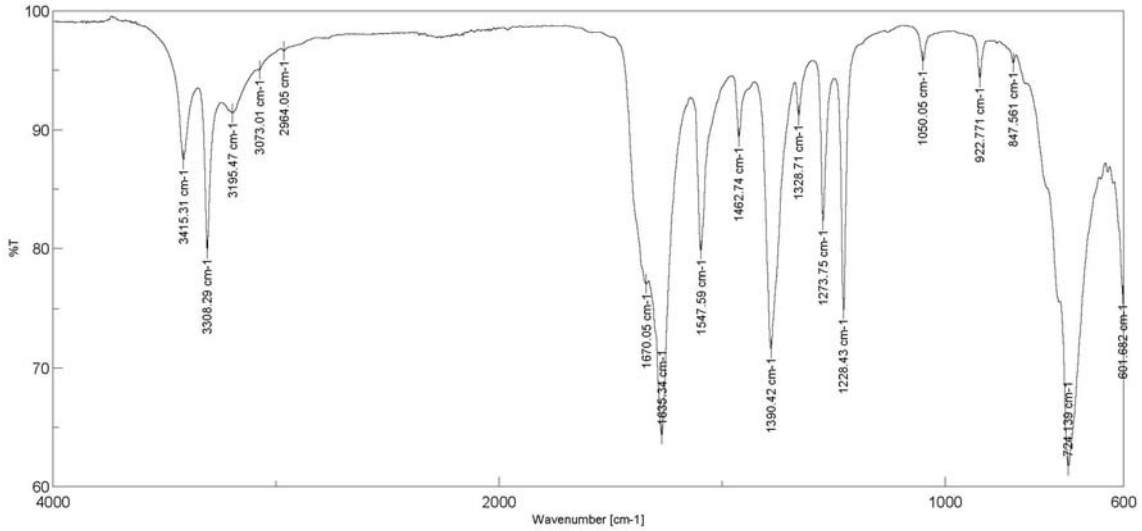

Spectrum 3 – $K_2H_2(oeo)\ H_2O$ **(4a)**

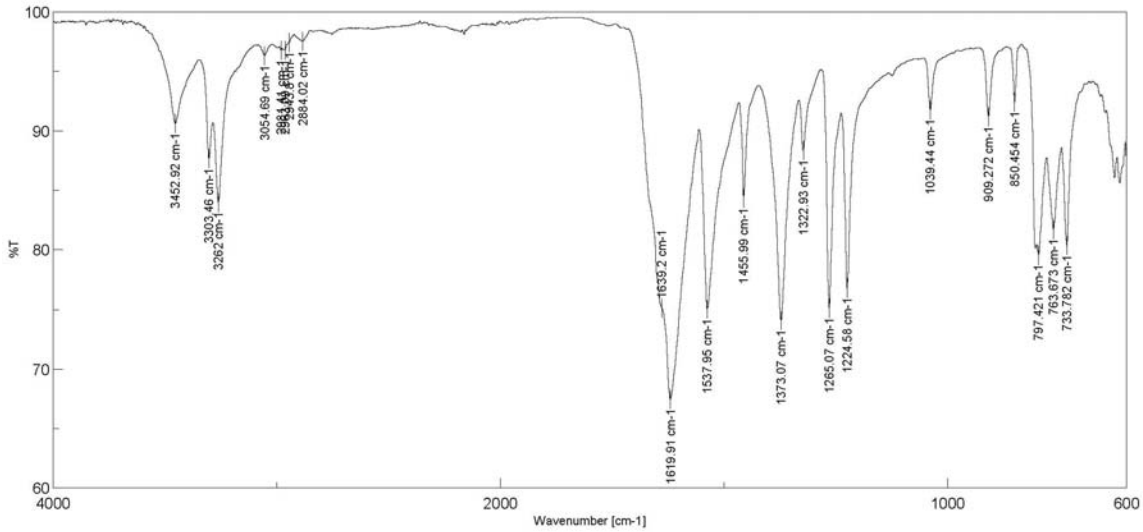

Spectrum 4 – $CuH_2(oeo)\cdot 3H_2O$ **(7a)**

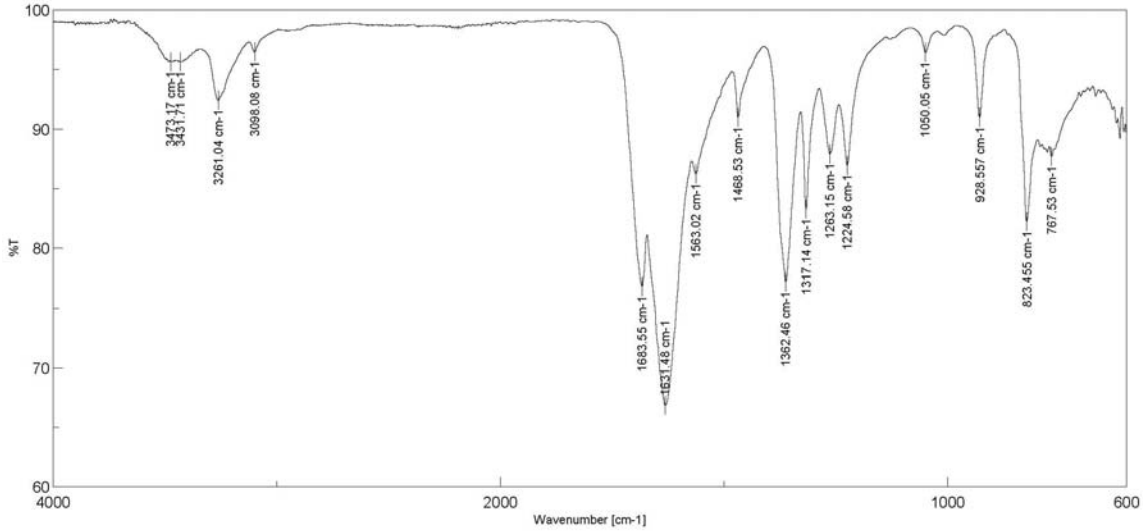

Spectrum 5 – $CoH_2(oeo)\cdot DMSO$ **(8)**

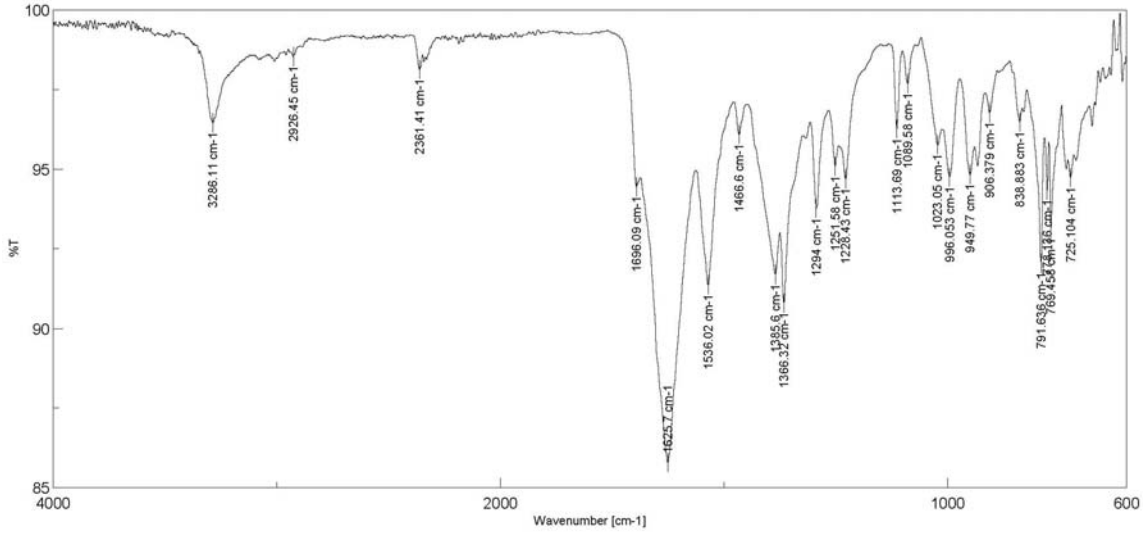

Spectrum 6 – $(Bu_4N)_4Cu(oeo)_2\cdot 4H_2O$ **(25a)**

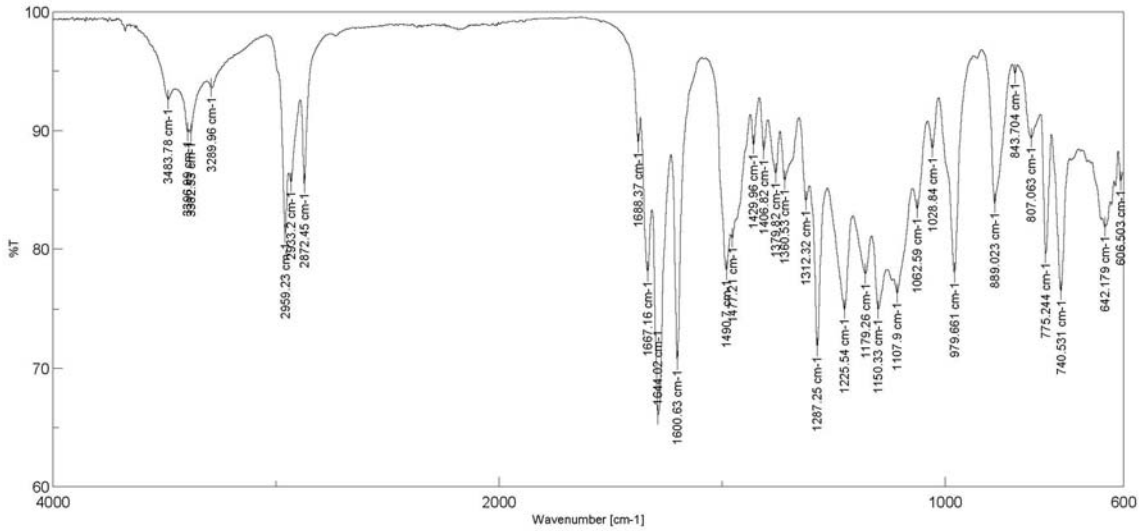

Spectrum 7 – α-$Li_4[Cu_{0.90}H_{0.20}(oeo)]_2 \cdot 6H_2O$ **(10a)**

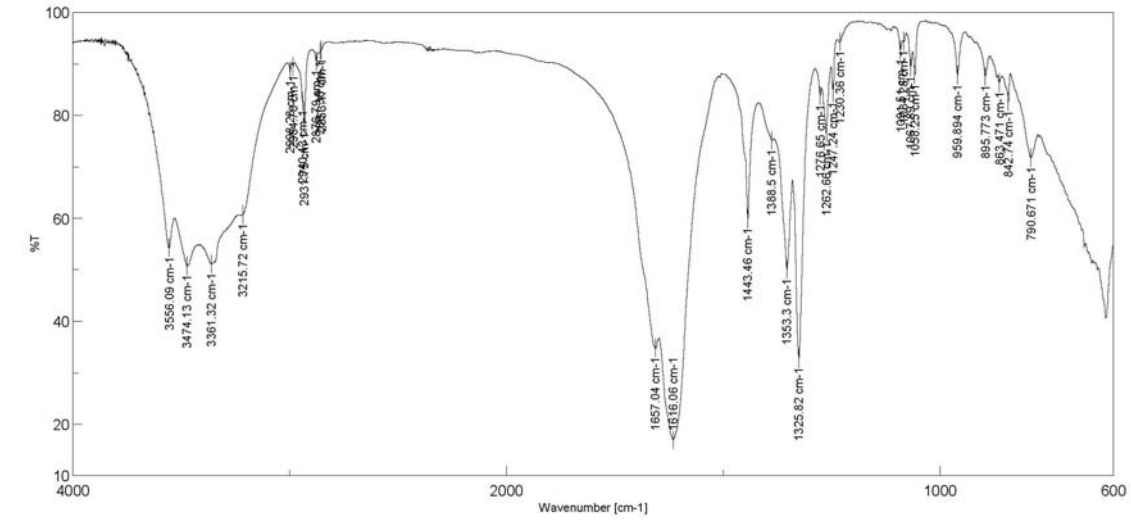

Spectrum 8 – $K_4[Cu_{0.66}H_{2.68}(oeo)] \cdot 5H_2O$ **(18)**

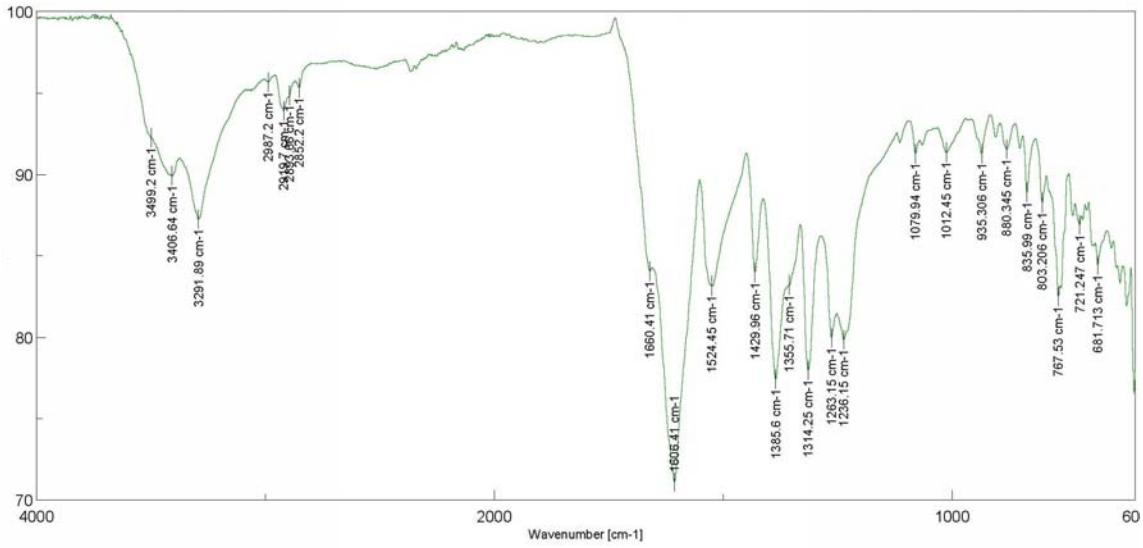

Spectrum 9 – $K_4[Cu_x(H_{(1-x)}oeo)]_2 \cdot nH_2O$ solid **(17)**

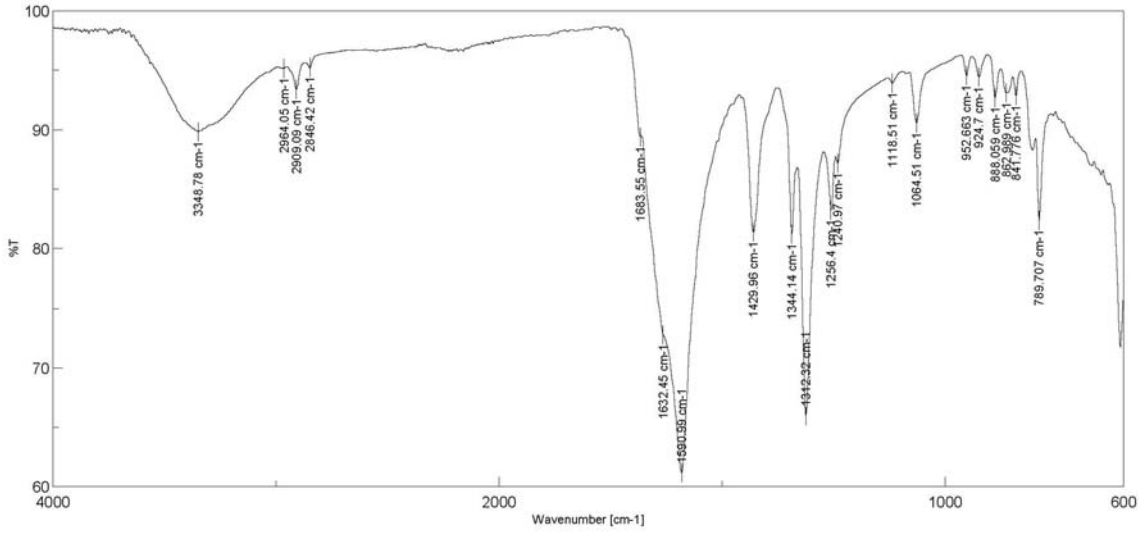

Spectrum 10 – $Na_4[Cu_x(H_{(1-x)}oeo)]_2 \cdot nH_2O$ solid **(15)**

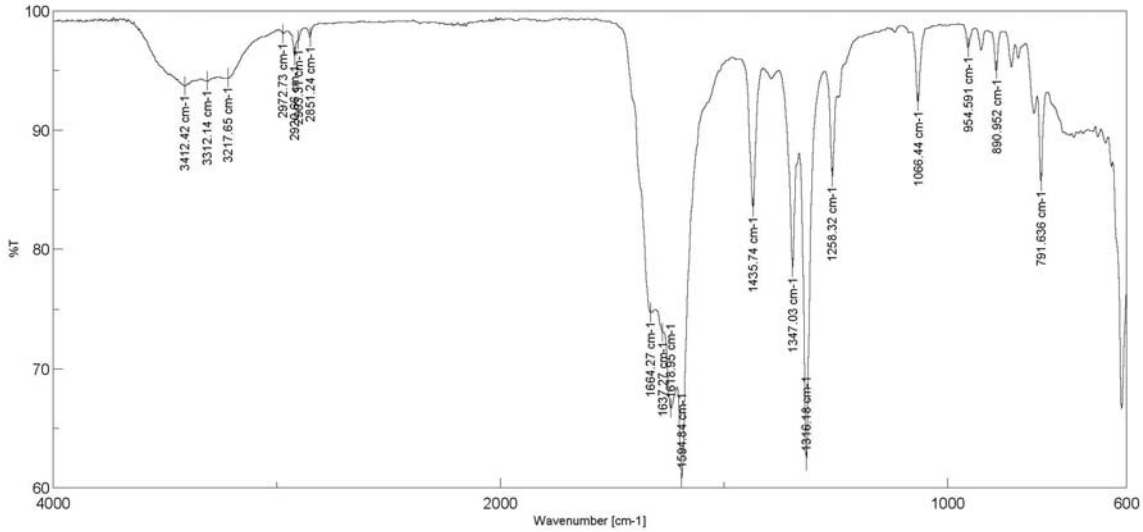

Spectrum 11 – $Co_x(H_yoeo)_2Cl(H_2O)_z$ **(26)**

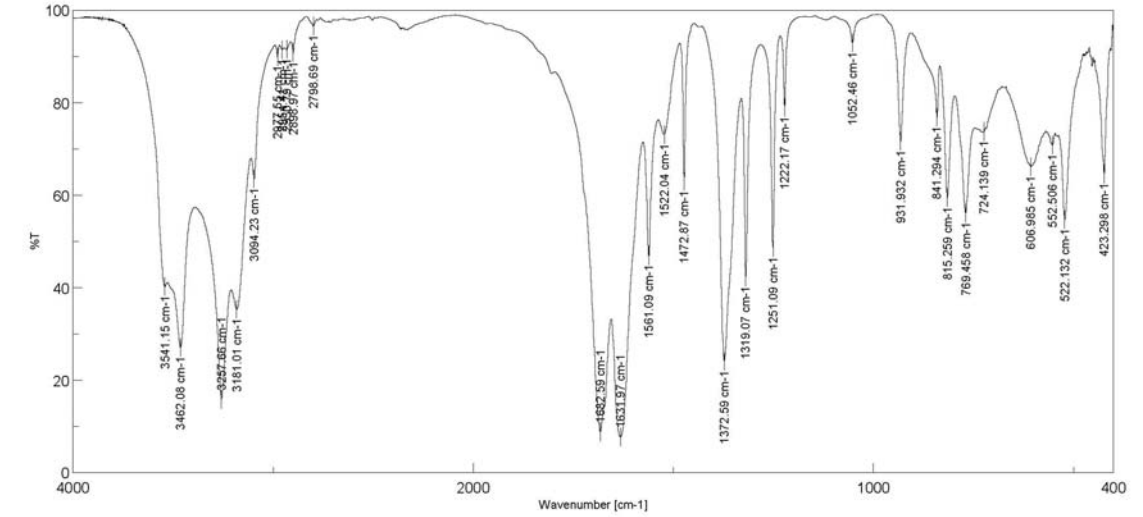

Spectrum 12 – $Co_xCu_y(oeo)(DMSO)(H_2O)_3$ **(29)**.

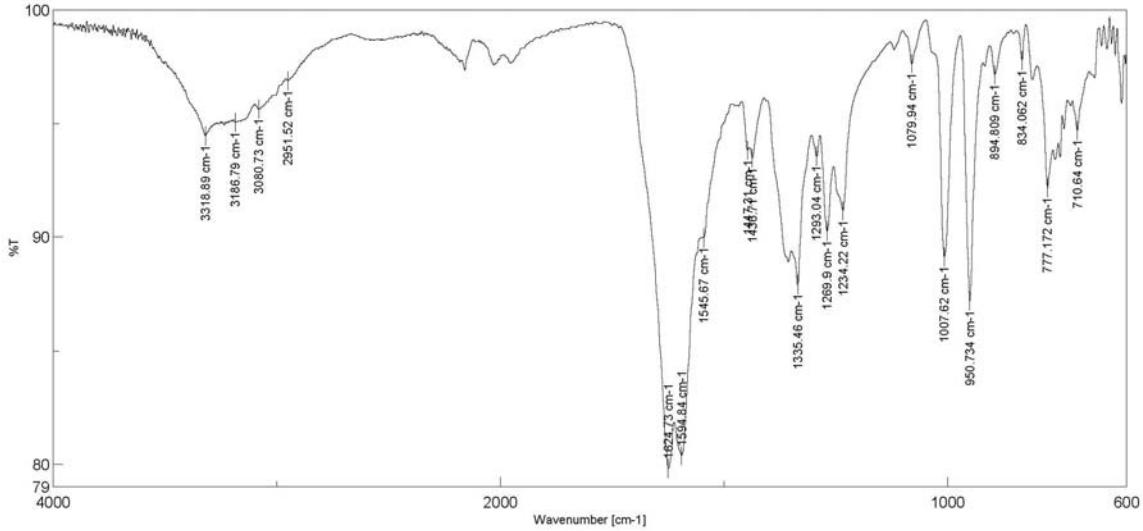

Spectrum 13 – **(30)**.

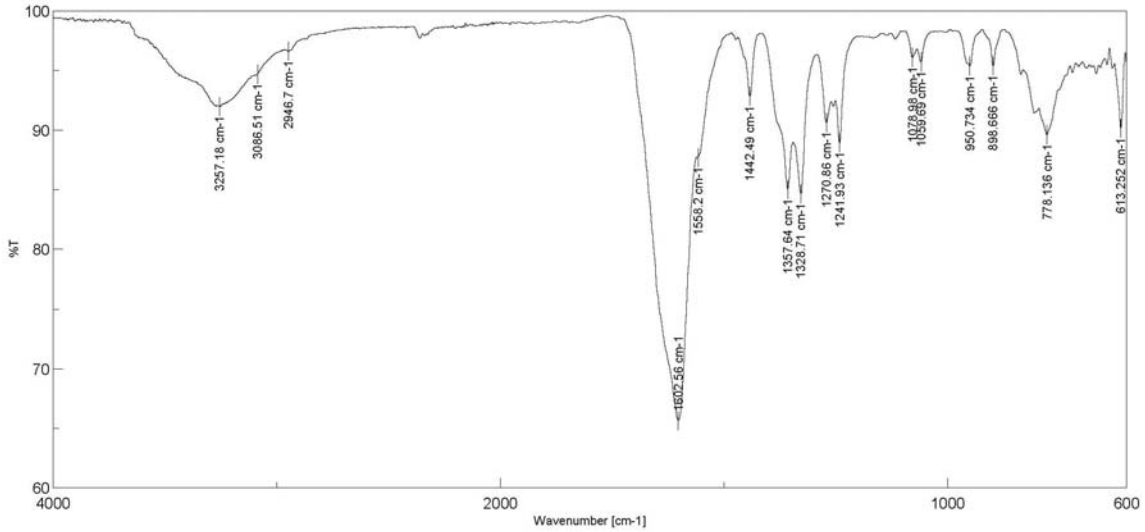

A2 - Synthesis and characterisation of (ebo)H_4 (31)

Ethyl oxamate (3.54 g, 29.7 mmols) was added to mixture of EtOH/H_2O (2:1, 60 ml) heated in a water bath at approximately 40^oC until the solid was dissolved. Then ethylenediamine (0.35 ml, 5.18 mmols) was added dropwise to the mixture and stirred for 48hrs at room temperature. The white solid that formed was filtered off and washed with EtOH. A second wash was carried out in hot EtOH being the mixture filtered in hot and the solid dried in air **(31)**. The ^{1}H-NMR measurement was run to the initial crop showing the presence of the ligand as well as the presence of ethyl oxamate as impurity. ^{1}H-NMR (400 MHz, $(CD_3)_2SO$, δ in ppm) **31**: 8.83 (s, 1H, *NH*), 8.24 (s, 1H, *NH_2*), 7.95 (s, 1H, *NH_2*), 3.26 (m, 4H, CH_2(*NH*)).

A3 - Crystallographic data of 16b

Empirical formula	$C_{12}H_{27.26}Cu_{0.37}N_4Na_4O_{20}$
Formula weight	662.95
Crystal system	Monoclinic
Space group	$P2_1/n$
a (Å)	11.2406(10)
b (Å)	10.5814(9)
c (Å)	21.245(2)
α (°)	90.00
β (°)	91.223(3)
γ (°)	90.00
V (Å^3)	2526.3(4)
T(K)	100(2)
ρ_{calc} (g/cm^3)	1.743
Z	4
F (000)	1368
Reflections collected	18647
Unique reflections	6051
Reflections observed [I>2σ(I)]	4490
R_{int}	0.0447
Parameters refined	441
Number of restraints	20
λ (Å); Mo Kα	0.71073
μ (mm^{-1})	0.515
θ Range (°)	1.92-27.99
Goodness-of-fit (GOF) on F^2	1.066
[a]R_1 [I>2σ(I)]	0.0441
[b]wR_2 (all data)	0.0953
Largest difference in peak and hole (e Å^{-3})	0.38 and -0.31
Crystal size	0.1×0.1×0.1
Crystal morphology	blue prism

[a]$R_1 = \Sigma(|F_o| - |F_c|)/ \Sigma|F_o|$

[b]$wR_2 = [\Sigma w(F_o^2 - F_c^2)^2]/\Sigma w(F_o^2)^2]^{1/2}$ where $w = 1/[\sigma^2(F_o^2) + (0.2P)^2$ and $P = [F_o^2 + 2F_c^2]/3$

A4 - Arrangements of the Potassium ions and water molecules in the cationic layer of $K_4[Cu(oeo)]_2 \cdot 6H_2O$ (21)

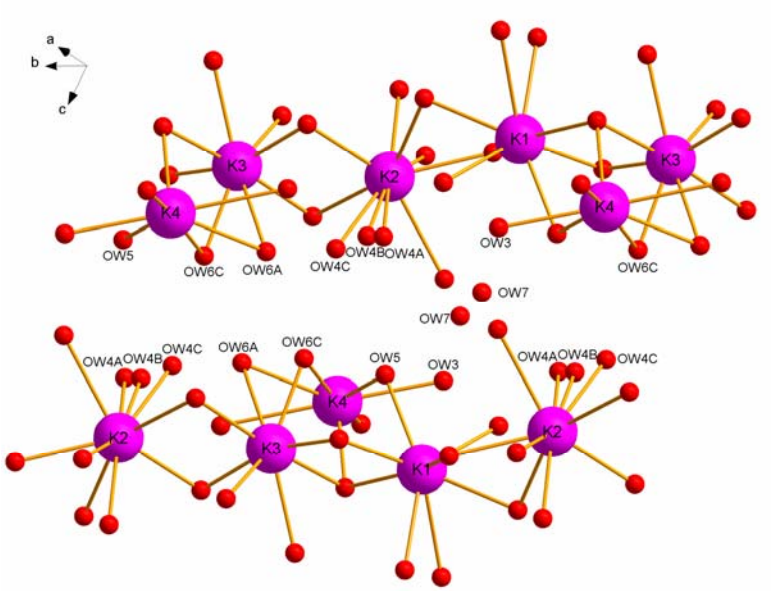

Figure A4. 1 Perspective view along the diagonal of the *ac*-plane of a section of the anionic layer showing the distribution of the potassium ions and the water molecules when K3 and K4 sites are filled.

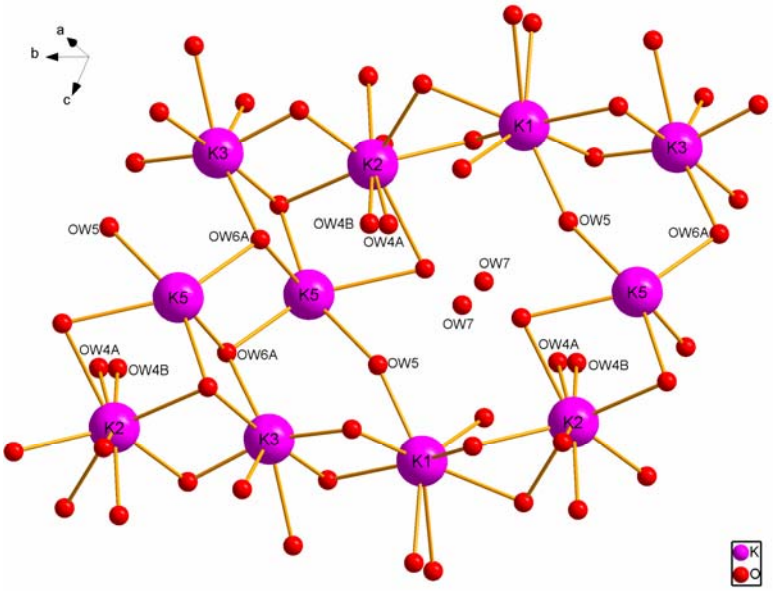

Figure A4. 2 Perspective view along the diagonal of the *ac*-plane of a section of the anionic layer showing the distribution of the potassium ions and the water molecules when K3 and K5 sites are filled.

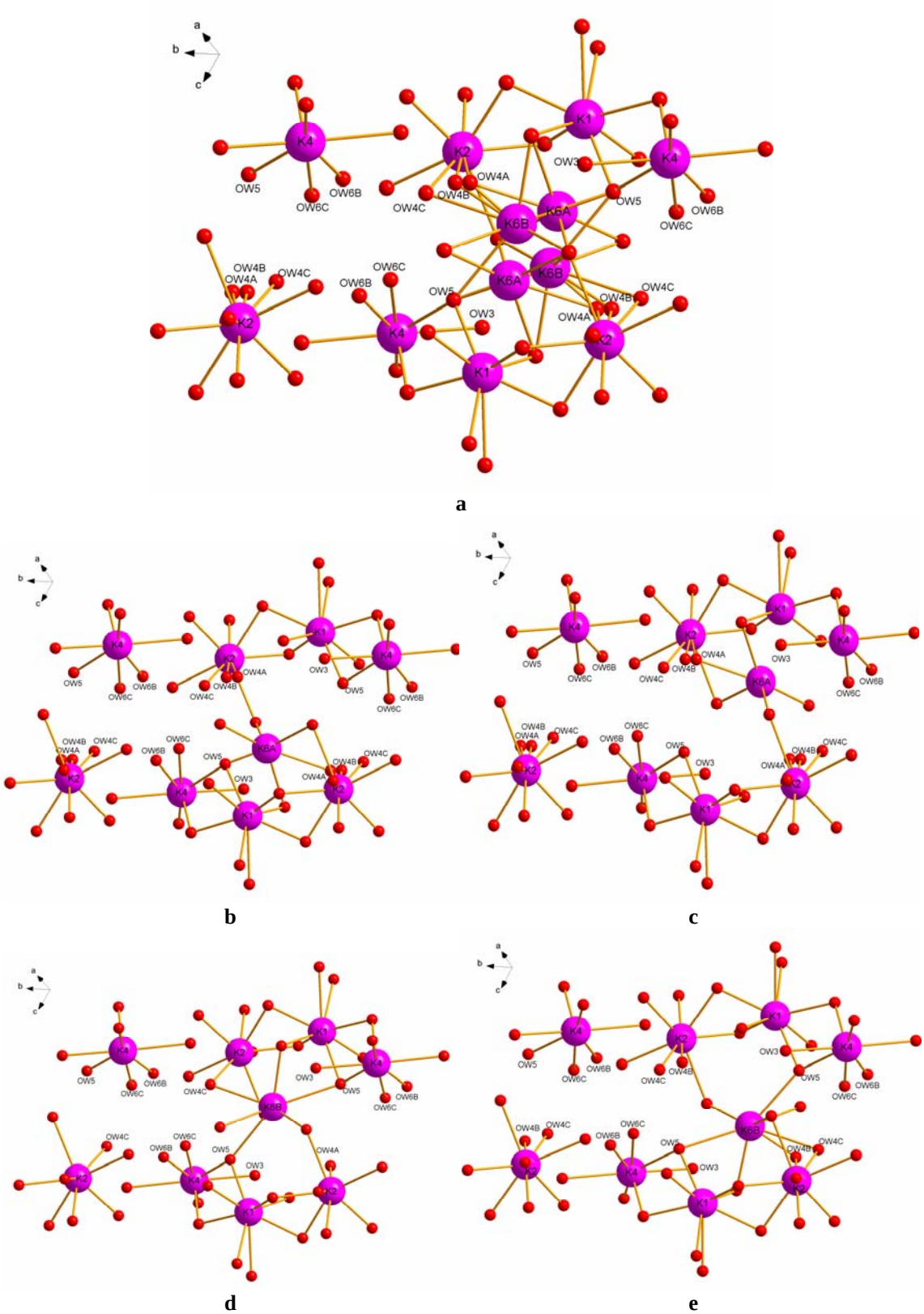

Figure A4. 3 Perspective view along the diagonal of the *ac*-plane of a section of the anionic layer showing the distribution of the potassium ions and the water molecules when K4 and all K6 sites are filled **(a)** and when K4 and one of the four possible K6 sites is filled **(b, c, d, e)**.

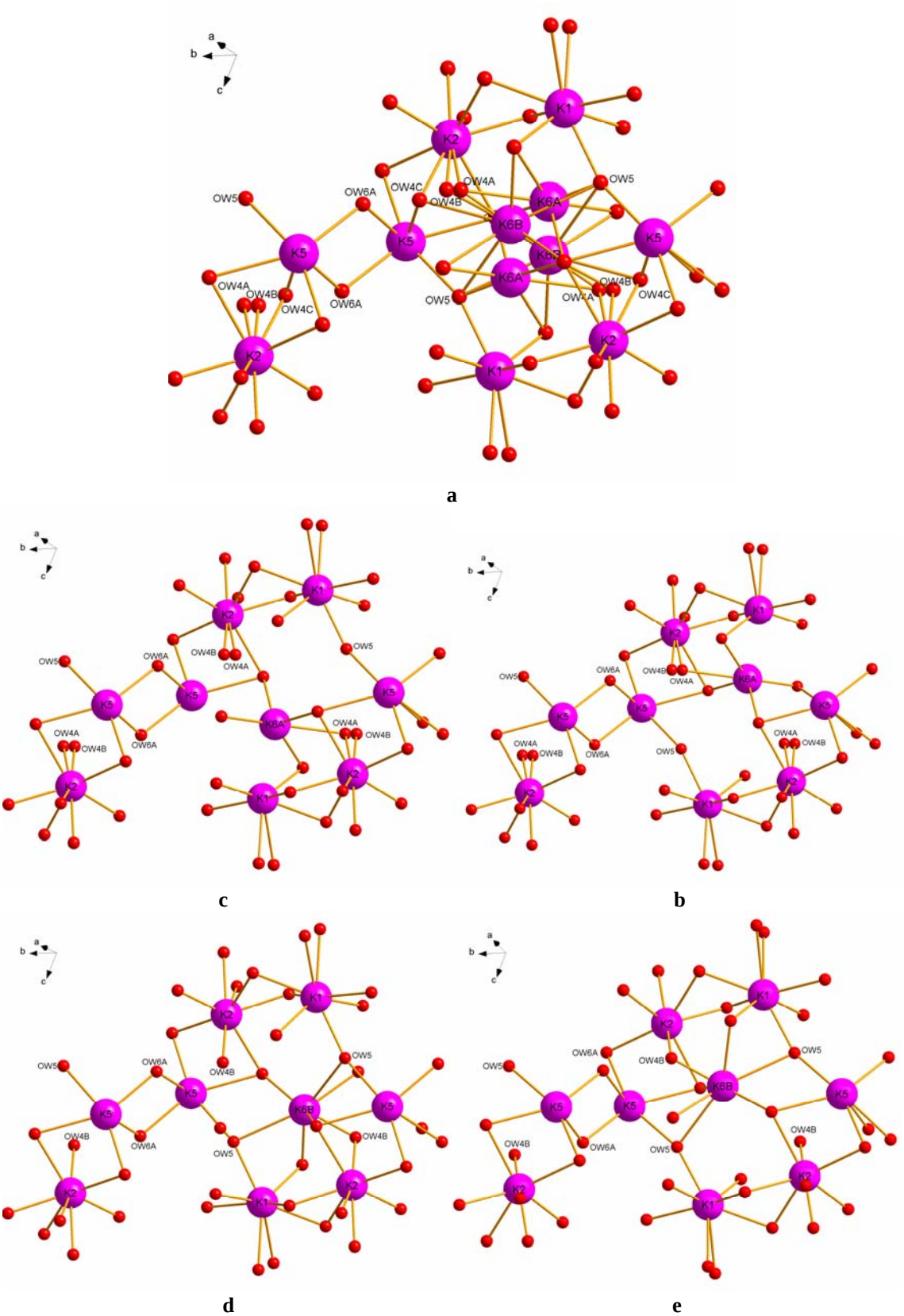

Figure A4. 4 Perspective view along the diagonal of the *ac*-plane of a section of the anionic layer showing the distribution of the potassium ions and the water molecules when K5 and all K6 sites are filled **(a)** and when K5 and one of the four possible K6 sites is filled **(b, c, d, e)**.

A5 -List of $M_4[Cu(oeo)]_2$ crystals

	Molecular Formula	**Solid Solution Composition**
10a	α-$Li_4[Cu_{0.90}H_{0.20}(oeo)]_2 \cdot 6H_2O$	$Li_4\{[Cu_2(oeo)_2]_{0.80}[Cu(Hoeo)_2]_{0.20}\}$
10b	β-$Li_4[Cu_{0.94}H_{0.12}(oeo)]_2 \cdot 6H_2O$	$Li_4\{[Cu_2(oeo)_2]_{0.89}[Cu(Hoeo)_2]_{0.11}\}$
10c	γ-$Li_4[Cu(oeo)]_2 \cdot 6H_2O$	$Li_4\{[Cu_2(oeo)_2]\}$
11	$Li_4[Cu_{0.93}H_{0.14}(oeo)]_2 \cdot 10½H_2O$	$Li_4\{[Cu_2(oeo)_2]_{0.79}[Cu(Hoeo)_2]_{0.21}\}$
12	$Li_4[Cu_{0.96}H_{0.08}(oeo)]_2 \cdot 5H_2O$	$Li_4\{[Cu_2(oeo)_2]_{0.92}[Cu(Hoeo)_2]_{0.08}\}$
14	$Na_4[Cu_{0.05}H_{1.90}(oeo)]_2 \cdot 4H_2O$	$Na_4\{[Cu(Hoeo)_2]_{0.10}[(H_2oeo)_2]_{0.90}\}$
16	$Na_4[Cu_{0.18}H_{1.64}(oeo)]_2 \cdot 8H_2O$	$Na_4\{[Cu(Hoeo)_2]_{0.37}[(H_2oeo)_2]_{0.63}\}$
18	$K_4[Cu_{0.33}H_{1.34}(oeo)]_2 \cdot 5H_2O$	$K_4\{[Cu(Hoeo)_2]_{0.66}[(H_2oeo)_2]_{0.44}\}$
19	$K_4[Cu_{0.89}H_{0.22}(oeo)]_2 \cdot 3H_2O$	$K_4\{[Cu(oeo)_2]_{0.88}[Cu(Hoeo)_2]_{0.22}\}$
20	$K_4[Cu_{0.78}H_{0.44}(oeo)]_2 \cdot 4.5H_2O$	$K_4\{[Cu(oeo)_2]_{0.57}[Cu(Hoeo)_2]_{0.43}\}$
21	$K_4[Cu(oeo)]_2 \cdot 6H_2O$	$K_4\{[Cu_2(oeo)_2]\}$
22a	$Rb_4[Cu_{0.80}H_{0.40}(oeo)]_2 \cdot 4H_2O$	$Rb_4\{[Cu(oeo)_2]_{0.60}[Cu(Hoeo)_2]_{0.40}\}$
22b	$Rb_4[Cu_{0.30}H_{1.40}(oeo)]_2 \cdot 4H_2O$	$Rb_4\{[Cu(Hoeo)_2]_{0.60}[(H_2oeo)_2]_{0.40}\}$
22c	$Rb_4[Cu_{0.18}H_{1.64}(oeo)]_2 \cdot 4H_2O$	$Rb_4\{[Cu(Hoeo)_2]_{0.36}[(H_2oeo)_2]_{0.64}\}$
23	$Cs_4[Cu(oeo)]_2 \cdot 5\ ½\ H_2O$	$Cs_4\{[Cu(oeo)]_2\}$

A6 - Powder X-Ray Diffraction Patterns

Pattern 1 – $Na_4[Cu_x(H_{(1-x)}oeo)]_2 \cdot nH_2O$ solid **(15)**

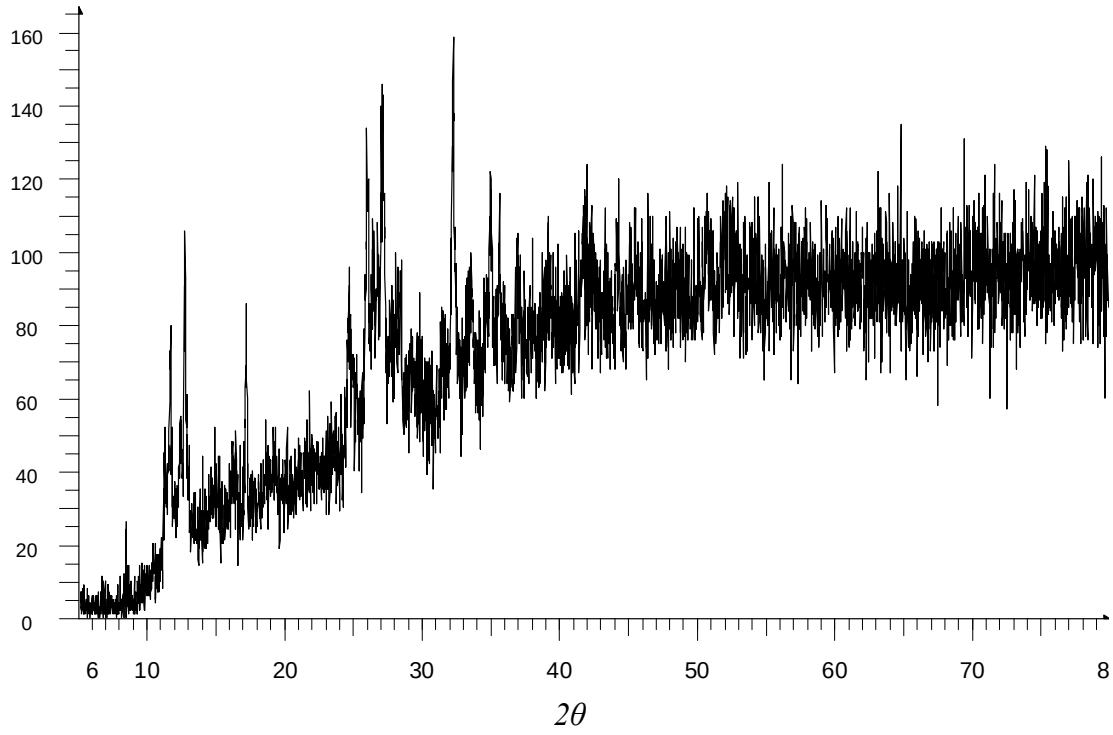

Pattern 2 – $Co_x(H_yoeo)_2Cl(H_2O)_z$ **(26)**

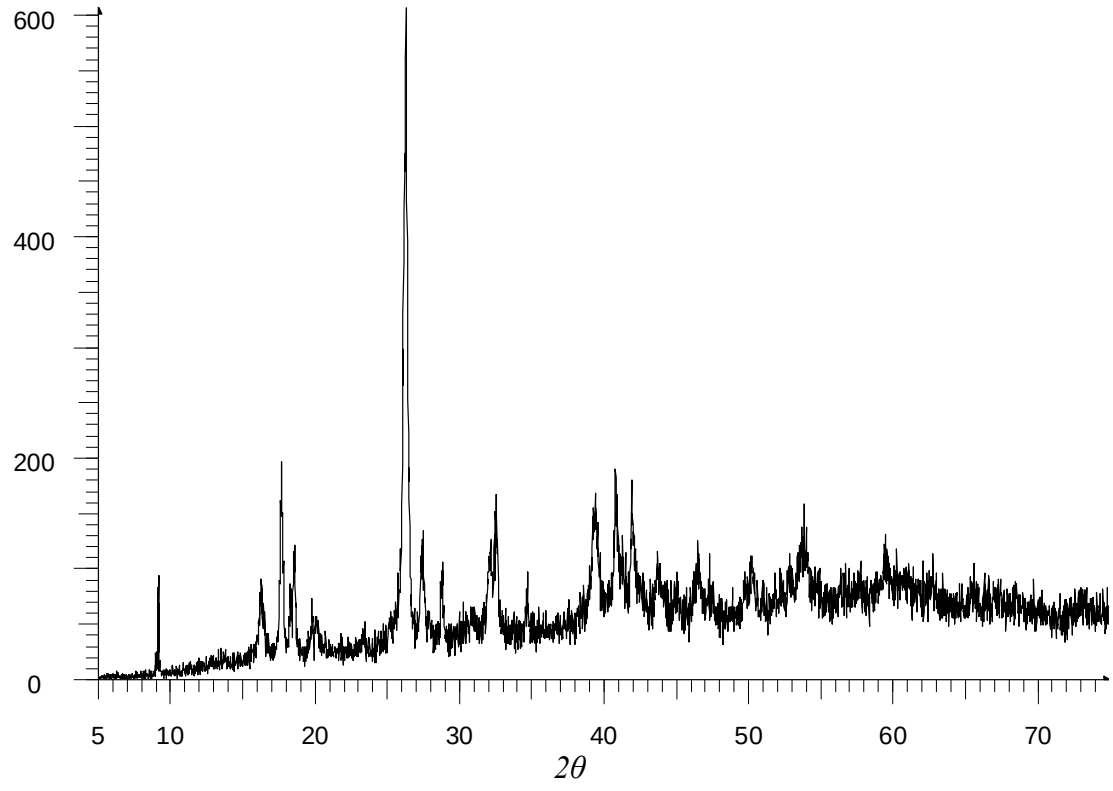

Pattern 3 – $Co_xCu_y(oeo)(DMSO)(H_2O)_3$ **(29)**.